

Modelling Safety Impacts of Automated Driving Systems in Multi-Lane Traffic

Mullakkal-Babu, Freddy

DOI

[10.4233/uuid:37c8ec51-59f0-4dec-a3fa-bdd3c69e09db](https://doi.org/10.4233/uuid:37c8ec51-59f0-4dec-a3fa-bdd3c69e09db)

Publication date

2020

Document Version

Final published version

Citation (APA)

Mullakkal-Babu, F. (2020). *Modelling Safety Impacts of Automated Driving Systems in Multi-Lane Traffic*. [Dissertation (TU Delft), Delft University of Technology]. TRAIL research school / School of transportation of SEU research school. <https://doi.org/10.4233/uuid:37c8ec51-59f0-4dec-a3fa-bdd3c69e09db>

Important note

To cite this publication, please use the final published version (if applicable).
Please check the document version above.

Copyright

Other than for strictly personal use, it is not permitted to download, forward or distribute the text or part of it, without the consent of the author(s) and/or copyright holder(s), unless the work is under an open content license such as Creative Commons.

Takedown policy

Please contact us and provide details if you believe this document breaches copyrights.
We will remove access to the work immediately and investigate your claim.

Modelling Safety Impacts of Automated Driving Systems in Multi-Lane Traffic

F.A. Mullakkal-Babu

Delft University of Technology, 2020



Modelling Safety Impacts of Automated Driving Systems in Multi-Lane Traffic

Proefschrift

ter verkrijging van de graad van doctor
aan de Technische Universiteit Delft,
op gezag van de Rector Magnificus prof.dr.ir. T.H.J.J. van der Hagen,
voorzitter van het College voor Promoties,
in het openbaar te verdedigen op maandag 16 March om 10:00 uur
door
Freddy Antony MULLAKKAL-BABU
Master of Technology in Transportation Systems Engineering,
Indian Institute of Technology, Mumbai, India,
geboren te Kerala, India.

Dit proefschrift is goedgekeurd door de promotoren:

Prof.dr.ir. B. van Arem

Dr.ir. R. Happee

Copromotor:

Dr.ir. M. Wang

Samenstelling promotiecommissie:

Rector Magnificus

Prof.dr.ir. B. van Arem

Dr.ir. R. Happee

Dr.ir. M. Wang

voorzitter

Technische Universiteit Delft, promotor

Technische Universiteit Delft, promotor

Technische Universiteit Delft, copromotor

Independent members:

Prof.dr. D. Cao

Prof.dr. R. Liu

Prof.dr.ir. E.C. van Berkum

Prof.dr.ir. J.W.C. van Lint

Prof.dr.ir. B. De Schutter

University of Waterloo

University of Leeds

Universiteit Twente

Technische Universiteit Delft

Technische Universiteit Delft, reservelid



Applied and
Engineering Sciences

This thesis is the result of PhD research supported by NWO Domain TTW, the Netherlands, under the project From Individual Automated Vehicles to Cooperative Traffic Management Predicting the benefits of automated driving through on-road human behaviour assessment and traffic flow models (IAVTRM)- TTW 13712.

TRAIL Thesis Series no. T2020/6, The Netherlands Research School TRAIL

TRAIL

P.O. Box 5017

2600 GA Delft

The Netherlands

E-mail: info@rsTRAIL.nl

ISBN: 978-90-5584-265-0

Copyright © 2020 by F.A. Mullakkal-Babu

All rights reserved. No part of the material protected by this copyright notice may be reproduced or utilized in any form or by any means, electronic or mechanical, including photocopying, recording or by any information storage and retrieval system, without written permission of the author.

Printed in the Netherlands

Acknowledgments

My direct interview for this PhD vacancy took place in Washington D.C, amidst an international conference. On the interview day, I had eye inflammation, and to make things worse, I accidentally overdosed the medicine. I was tired and sceptical about my chances of being selected. Fortunately, the interviewers- Bart and Riender - found something, beyond my red eyes and tired demeanour, and offered me the position. My doctoral tenure was one of the most satisfying phases of my life and I would like to thank everyone who was instrumental in making it so.

First my supervisors. Bart, thank you, for your genuine care about my well-being and for challenging me to take a broader perspective on my research. Your philosophies on science and your creative suggestions have guided the course of this thesis. Riender, thank you, for being an empathetic colleague, for your guidance in particular on my writing, and for your willingness to dive into the details of the method and its implementation when needed. Meng, thank you for patiently listening to me in my moments of confusion and for guiding me through the subtleties of research. My biweekly meetings with you, were an immense source of motivation and clarity. I tackled several hurdles by reflecting on your comments and questions during those meetings. In research, feedback is often an expression of care. I am indebted to my entire committee for their extremely quick, thorough, constructive and encouraging feedback on all of my manuscripts. I thank the IAVTRM project members for the insightful discussions at user-group meetings.

Apart from my committee, I was lucky to collaborate with a few inspiring researchers. Arthuro, Barys, Haneen and Wouter, thank you for your insights and tools. They were vital to the completion of this thesis.

I thank my officemates: Kai, Malvika, Meiqui, Peyman, Xiao and Yu, with whom I have shared my moments of anxiety and excitement. Our office was my second-home in Delft, and it used to be the last to switch-off lights on most days. Thank you for never complaining about my unique possessions, like the extra large Mayonaise bottle. Dehalaila, thanks for your assistance in all the travel and administrative procedures. Edwin, thanks for your help in IT-related issues. Conchita, thanks for your help in formatting and printing of this thesis.

Department of Transport and Planning offered me several warm moments to cherish. Thanks to Bernard, Florian, Hari, Jishnu, Konstanze, Lin, Maryna, Na, Nadjla, Niharika, Nikola, Panchamy, Pablo, Paul, Silvia, Tim, Xavi and Yu, for all the coffee corner chats, dinners and barbecues. Jork, thanks for your help on the Dutch translation of the thesis summary. I thank you for involving me in the on-road behaviour study in Amsterdam. Joining you in the preparation and execution of this study was a fruitful experience. Shubham and Maria, thanks for your enthusiasm in my research. I am lucky to have a close group of Indian friends, whom I could count on any day for an evening game, to answer my where-

to-find-tea-powder message and to urgently borrow a travel-bag. Thanks, Arun J, Arun M, Abhijeet, Anjana, Chirag, Gautam, Kamakshi, Lakshmi, Manu, Prashant, Ranjani, Syam and Vaishnavi.

I thank my father and mother for their persistent faith in my decisions and my ever-supportive sibling, Flemy. Nathan, my baby boy, the softness of your baby cheeks was enough to melt away all my final-year stress. Now you have learned to balance on your own feet. I hope you will choose the right path to walk, fall and run in your life. The last words go to my love Amy. I understand that the last four years with a preoccupied researcher (not always though) were not easy. But this thesis would not have been the same, if not for your evening visits to the university with dinner box, if not for your, "its OK" messages and if not for your hi-fives and hugs.

Freddy Antony Mullakkal-Babu,
Delft, March 2020.

Contents

Acknowledgments	v
1 Introduction	1
1.1 Background of vehicle automation	2
1.2 The societal problem of traffic safety	3
1.3 Overview of traffic safety assessment: metrics and tools	4
1.3.1 Safety metrics	5
1.3.2 Simulation tools	5
1.3.3 Research gaps in simulation-based safety assessment	6
1.4 Research objectives	8
1.5 Research scope	9
1.6 Contributions	9
1.6.1 Scientific contributions	9
1.6.2 Practical contributions	11
1.7 Thesis outline	11
2 Comparative assessment of safety indicators for vehicle trajectories on high-ways	13
2.1 Introduction	14
2.2 Literature review	14
2.3 Qualitative analysis	15
2.3.1 Desirable mathematical properties for a risk measure in multivehi- cle scenario	15
2.3.2 Risk factors and expected causal tendencies	16
2.3.3 Benchmarking the safety indicators with expected risk tendencies	17
2.3.4 Findings of the qualitative analysis	19
2.4 Simulation case studies	22
2.4.1 Case study 1	22
2.4.2 Case study 2	24
2.4.3 Findings of the simulation analysis	24
2.5 Discussion	26
2.6 Conclusions and future research	27
3 Probabilistic field approach for motorway driving risk assessment	29
3.1 Introduction	31
3.2 Modelling driving risk	33
3.2.1 On-road obstacles	34

3.2.2	Modelling the road boundary object as a risk field	35
3.2.3	Modelling the neighbouring vehicle as a risk field	36
3.2.4	Incorporating the vehicle geometry and motion constraints	38
3.2.5	Estimating risk over multiple time steps	40
3.3	Examples of the model applications	42
3.3.1	Risk assessment of near crash events	42
3.3.2	Road boundary crash avoided by corrective steering	43
3.3.3	Rear crash avoided by swerving	45
3.3.4	Rear-end crash avoided by braking	45
3.3.5	Risk estimation of path plans	47
3.4	Discussion	49
3.5	Conclusion	53
4	Empirics and models of fragmented lane changes	55
4.1	Introduction	56
4.2	Data extraction and classification of trajectory samples	58
4.3	Comparative analysis and models of LC execution	62
4.3.1	Comparision of kinematics during lane-changing	62
4.3.2	Models of lateral kinematics during LC execution	63
4.3.3	Performance evaluation	66
4.4	Comparative analysis and models of LC impact	66
4.4.1	Relative kinematics of ambient vehicles at the onset of lane change	68
4.4.2	Change in the relative kinematics by the end of lane change	69
4.4.3	Models of LC impact on the target-follower	70
4.5	Discussion	74
4.6	Conclusions	76
5	A hybrid submicroscopic/microscopic traffic flow simulation framework	79
5.1	Introduction	80
5.2	Model framework	82
5.2.1	Framework	82
5.2.2	Vehicle model	84
5.2.3	Formulating tactical functions	86
5.2.4	Formulating operational functions	86
5.3	Operationalisation of the framework with behavioural models	88
5.3.1	Models of tactical functions	88
5.3.2	Models of Operational Functions	90
5.4	Simulation experiments and results	92
5.4.1	Evaluating the modelling framework	92
5.4.2	Evaluating the traffic flow simulation	98
5.5	Discussion	100
5.6	Conclusion	102

6	Safety assessment of automated driving strategies at merges in mixed traffic	105
6.1	Introduction	107
6.1.1	Safety assessment approaches for ADS-equipped vehicles	107
6.1.2	Automated driving strategies to handle cut-in	108
6.1.3	Objective and structure	111
6.2	Model formulation	111
6.2.1	Acceleration models to follow the predecessor	112
6.2.2	Acceleration models with cut-in handling	113
6.2.3	Model for lane-changing	117
6.3	Safety metrics	118
6.4	Case study and results	120
6.4.1	Characteristics of lane changes	120
6.4.2	Aborted lane changes	122
6.4.3	Conflicts with neighbouring vehicles	124
6.4.4	Expected severity of crashes	124
6.4.5	Driving risk during cut-in	124
6.5	Sensitivity analysis	126
6.6	Conclusions and future work	128
7	Findings, conclusions and recommendations	131
7.1	Findings	131
7.2	Conclusions	133
7.3	Recommendations for practice	134
7.4	Recommendations for future research	135
A	Algorithm and calculations of Chapter 3	137
	Bibliography	139
	Samenvatting	153
	Summary	157
	Curriculum vitae	161
	TRAIL Thesis Series publications	165



List of Figures

1.1	Thesis structure and relations between chapters	12
2.1	Demonstration of safety field strength due to a moving vehicle. Blue colour indicates higher risk; unit of field strength is Newton	21
2.2	Visualisation of risk measures over the operational space using different safety indicators. Blue colour indicates higher risk	21
2.3	Results of case study 1: (a) when leader brakes and follower brakes to avoid a collision; (b) when leader brakes and follower changes lane via trajectory A (timely lane change); (c) when leader brakes and follower changes lane via trajectory B (late lane change).	23
2.4	Results of case study 2 (a) the leader cuts-in and follower brakes to avoid collision (b) the follower changes the lane to avoid collision	25
3.1	The variation of potential PDRF strength due to the road boundary object over lateral positions within the lane. The black line represents potential PDRF strength for different k and red represents the potential PDRF strength for different offsets of the road boundary object.	36
3.2	Collision likelihood contours around n , for a subject travelling at the same speed in forward direction: (a) n with longitudinal acceleration noise $\sigma_X = 0.7$ and lateral acceleration noise $\sigma_Y = 0.2$ prediction time step $\tau = 3$; (b) n with a relatively high longitudinal acceleration noise $\sigma_X = 1$; (c) n with a relatively high lateral acceleration noise $\sigma_Y = 0.4$; and (d) collision likelihood contours for a shorter prediction time step $\tau = 2$	39
3.3	Illustration of multi-step prediction scheme for vehicle n starting from the initial position $[0, 8]^T$ and an initial velocity $[20, 0]^T$. The black dots represent the entire set of predicted positions at each prediction time step; the green dots represent the expected positions of at each time step according to the acceleration plan and variability distribution; and the black line connecting the green dots represents the expected trajectory instance.	41
3.4	Risk estimates of an encounter in which the subject vehicle avoids a crash with the right lane boundary by corrective steering.	44
3.5	Risk estimates of an encounter in which the subject vehicle avoids a rear-end crash by swerving to its left.	46
3.6	Risk estimates of an encounter in which the subject vehicle avoids a rear-end crash by braking	48

3.7	Illustration of the hypothetical simulation scenario: lane marking represented a dashed line; the lane boundary marking represented as a solid line; initial states of the subject vehicle s , and the three neighbouring vehicles ($n1, n2, n3$).	48
3.8	The trajectory plans of the neighbouring vehicles $n1$ (a); $n2$ (b) and $n3$ (c) represented in terms of the expected acceleration ($\hat{A}_X(t_k)$) as square black markers and $\hat{A}_Y(t_k)$ red dots) and the error limits defined by the acceleration noise	50
3.9	The multi-step PDRF risk estimates for trajectory plans at a typical lane drop section. The probability and severity of a crash between s and $n1$ (a); s and $n2$ (b); s and the right lane marking (c); and the combined PDRF risk along the trajectory plans (d)	51
3.10	Generalised TTC calculated for the trajectory plans in lane drop section	51
4.1	Illustration of the influential neighbouring vehicles during a typical lane change manoeuvre	58
4.2	Illustration of the method to identify the LC fragments	59
4.3	Illustration of extraction and classification of observed lane-changing trajectories: (a) an observed CLC trajectory and (b) an observed FLC trajectory. The black dots depict the observed positions; the red circles represent the laterally active points, and the blue asterisk depicts the critical moments along during the lane change, the dashed line represents the lane boundary.	61
4.4	Illustration of steering sequence for CLC adapted from Hofmann et al. (2010)	63
4.5	Frequency distribution of duration: a) continuous lane-changing b) fragmented lane-changing	64
4.6	Illustration of the double sinusoidal lateral acceleration model for a fragmented lane change	66
4.7	Example of simulated and observed lane-changing trajectories of FLC (a, c, e) and CLC (b, d, f)	67
4.8	Estimates of initial and subsequent transition of the mean relative velocity: (a) Subject and Follower (b) Leader and Subject. In each figure, the velocity means are significantly different with $p < 0.01$	71
4.9	Temporal evolution of average τ for all the followers during anticipation; τ s are measured with respect to the lane-changers. On the x-axis, $t = 0$ s depicts the moment of lane change insertion.	73
4.10	Temporal evolution of average τ s for all followers (a) during continuous lane change; (b) during fragmented lane change.	74
4.11	Percentage of fragmented lane changes among total lane changes per 100 meters in each lane	75
4.12	Relationship between the characteristics of the follower and characteristics of the lane-changers (a) prior to the continuous lane change, (b) prior to the fragmented lane change	76
5.1	Framework for hybrid submicroscopic-/microscopic simulation, the red box indicates the scope of this work	83
5.2	The two coordinate systems and the motion variables	84

5.3	Flowchart of tactical planning	87
5.4	Control structure implemented in the framework	87
5.5	Step response of the vehicle model with varying model parameters	93
5.6	Simulated steering operation during curve negotiation	94
5.7	Simulated steering operation during corrective steering	94
5.8	Simulated lateral and longitudinal dynamics during a normal lane change to the slower lane	95
5.9	Simulated lateral and longitudinal dynamics during an aborted lane change	96
5.10	Simulated lateral and longitudinal dynamics during a fragmented lane change	96
5.11	Macroscopic traffic flow with varying density	99
5.12	Simulation results; blue lines indicate vehicle trajectories and black lines indicate lane boundaries	99
5.13	Distribution of front wheel steering angle with varying longitudinal velocity	100
6.1	Example illustration of cut-in events (a) cut-in detected by Predictive ADS and HV (b) cut-in detected by all vehicle types	114
6.2	Example illustration leader selection for yielding in the vicinity of motorway merge (a) i (Predictive ADS) selects g from set of adjacent vehicles a 's (b) i (human driver) selects g from set of adjacent vehicles a 's	115
6.3	Effects of ADS penetration on the spatial distribution of lane changes at low on-ramp demand (a),(b) and high on-ramp demand (c),(d)	121
6.4	Effects of ADS penetration rate on the velocity at the start of lane change	123
6.5	Effects of ADS penetration rate on the number of aborted lane changes at high on-ramp demands	123
6.6	Notations for the vehicles in the vicinity of the lane changer c	124
6.7	Effects of ADS penetration rate on the frequency of conflicts between the c (cut-in vehicle) and each of its neighbours $n \in \{f, r, p, t\}$ at low on-ramp demand (a),(c) and high on-ramp demand (b),(d)	125
6.8	Effects of ADS penetration rate on mean Delta-V at low (a) and high on-ramp demands (b)	125
6.9	Mean maximum PDRF risk with low on-ramp demand (a) and high on-ramp demand (b)	127
6.10	Evolution of risk during lane-changing in scenarios with ADS at low (a) and high on-ramp demands (b)	127
A.1	Geometric representation of the polygons Q , Z and their overlap O (area shaded in pink), used for the crash probability estimation in Algorithm A.1	138



List of Tables

1.1	SAE Classification of driving automation systems	2
2.1	Theoretical verification of safety indicators	20
4.1	Comparative analysis of trajectory kinematics	64
4.2	Summary of performance evaluation of the LC trajectory models	67
4.3	Summary of the comparative analysis of the ambient traffic state at the onset of two LC types	69
4.4	Summary of the comparative analysis of the transition of ambient traffic state in each LC type	70
4.5	Summary of calibration results of the LC impact models	75
5.1	Parameter values in the prototype traffic flow simulation	102
6.1	Review summary of cut-in handling functionalities in ADS	109
6.2	Parameter values in the simulation experiments	122
A.1	X Coordinate of corners of polygon Q and Z in spatial domain	138
A.2	Y Coordinate of corners of polygon Q and Z in spatial domain	138



Chapter 1

Introduction

This chapter outlines the purpose, objective and contributions of this thesis. Section 1.1 describes the different classes of automotive applications along with a brief history of their development. Section 1.2 draws attention to the societal problem of traffic safety and current knowledge on the impacts of novel automotive applications on it. Section 1.3 overviews the prominent methods, metrics and tools employed to assess traffic safety and highlights the relevance and potential of simulation-based safety assessment. Section 1.4 states the objectives that will be pursued in this research. Section 1.5 outlines the scope of research and Section 1.6 presents the scientific and practical contributions of this thesis. Finally, Section 1.7 briefly describes the chapters in this thesis and their relationships with each other.

1.1 Background of vehicle automation

The last three decades have witnessed the emergence of several automotive applications that enhance the convenience of on-road driving. A prominent class among them is formed by the driving automation systems. These systems are characterised by their functionality to perform one or more driving subtasks on a sustained basis. All subtasks that should be performed to operate a vehicle in real-time are collectively referred to as the Dynamic Driving Task (DDT). Examples of DDT subtasks are manoeuvre planning, signaling and gesturing, steering and acceleration control, and Object and Event Detection and Response (OEDR). The Society of Automotive Engineers (SAE, 2018) categorises driving automation into six discrete and mutually exclusive levels as shown in Table 1.1. The difference between these levels is the varying role of the human user and the system in operating the vehicle. According to this taxonomy, level 0 represents no driving automation, implying that the human user performs the entire DDT and is the only driver of the vehicle; level 5 represents full driving automation, implying that the system performs the entire DDT under any driving condition and the human is only a passenger in the vehicle. Active safety systems such as Automated Emergency Braking are classified as a level 0 feature as they merely provide momentary interventions and their interventions do not change the role of the human user.

Table 1.1: SAE Classification of driving automation systems

Level	Name	DDT		DDT fallback	ODD
		Sustained lateral and longitudinal vehicle control	OEDR		
Driver performs part or all the DDT					
0	No Driving Automation	Driver	Driver	Driver	n/a
1	Driver Assistance	Driver/System	Driver	Driver	Limited
2	Partial Driving Automation	System	Driver	Driver	Limited
ADS (System performs the entire DDT while engaged)					
3	Conditional Driving Automation	System	System	Fallback ready user becomes the driver	Limited
4	High Driving Automation	System	System	System	Limited
5	Full Driving Automation	System	System	System	Unlimited

The history of lower level automation (level 0-2) can be traced back to the 1950s. Such systems are currently deployed in approximately 10 per cent of the new cars in Europe and the US (Kyriakidis et al., 2015). A well known example of Level 1 feature is Adaptive Cruise Control (ACC), which controls the vehicle acceleration to regulate the velocity based on user-set speed or user-set time headway (Xiao & Gao, 2010). An example of Level 2 driving automation is the Autopilot feature available in cars such as Tesla Model 3, BMW

X5 and Mercedes Benz E class. This feature performs longitudinal and lateral vehicle control within its specified ODD, but the driver is expected to monitor and intervene when needed.

The two demonstrator vehicles VITA 2 and Vamp may be considered as the first successful prototypes of a system that can monitor and operate the vehicle in real traffic. They appeared in 1994 as a result of the European project PROMETHEUS (PROgramMme for a European Traffic of Highest Efficiency and Unprecedented Safety, 1987 — 1995). In 1986, a research and development centre on Advanced Transit and Highways was set up in the US: PATH (Partners of Advanced Transportation Technologies) Program (Shladover, 2007). Efforts towards a higher level of automation features gained momentum in early 2000s, following the success of three consecutive DARPA Grand challenges (in years 2004, 2007 and 2008) (Leonard et al., 2008; Urmson et al., 2008) and other European projects such as Cybercars focussing on low-speed urban (Naranjo et al., 2008), CityMobil and HAVEit (Resende & Nashashibi, 2010). By 2010, the research and development landscape of ADS became even more dynamic with the entry of companies such as Waymo, Uber and several other automotive manufacturers. The transition of fully automated driving from an idea to functional prototypes in the first decade of the 21st century was enabled by several technological breakthroughs, such as the emergence of low-cost sensing systems, accurate detection and interpretation algorithms based on artificial intelligence and electric actuators. Level 5 automation, by definition, means that the system can drive the vehicle anywhere and under any condition in which a human would be able to drive. This feature, as of 2019, faces several technological and institutional challenges and its deployment is still a distant target (Shladover, 2018).

Currently, vehicle driving is being gradually automated with systems replacing the human in driving loop, and the traffic fleet is mixed with human-driven and system-driven vehicles, and is expected to be so at least for the next decade (Sivak & Schoettle, 2015).

1.2 The societal problem of traffic safety

On-road accidents have been a major concern since the advent of automobiles. Currently, injuries from traffic accidents are the leading cause of death among children and young adults aged (5-29 years) (World Health Organization, 2018). In approximately 90% of the crashes, the underlying reasons are human-errors such as distracted driving and driving fatigue (Fagnant & Kockelman, 2015; Kyriakidis et al., 2019). Such errors can be reduced with in-vehicle safety systems featuring automation level 1-2 that assist the human driver with alerts, notifications, and even take over the vehicle control in dangerous situations. Such systems have been shown to improve safety both at the individual and traffic level (Jeong & Oh, 2017; Yue et al., 2018), and to reduce the number of insurance claims (Kockelman et al., 2016). However, the benefits of lower-level automation cannot be extrapolated to ADS features as the human is not part of the driving loop.

The prospect of ADS-equipped vehicles, accompanies a crucial question: What will be the impact of ADS functionalities on traffic safety? Reliable predictions on the safety of future traffic are of vital importance for road operators to judiciously arrange for the infrastructural requirements of ADS-equipped vehicles; for traffic planners to devise effective strategies to manage mixed traffic operations; for policymakers to formulate safety policies

and establish safety standards; for automotive developers to obtain feedback at an early concept development stage of their product; and in general, to facilitate informed discussions on the subject.

The impact of higher automation features on traffic safety is not yet known, and there has not been a consensus even on the directionality of the impact. ADS-equipped vehicles have the potential to enhance or detriment traffic safety. ADS could improve safety, as it can respond quicker than human drivers, with a relatively smaller response time; and it is free from the typical human-errors such as distracted driving and driving fatigue. The concern, however, is the performance of these systems under complex on-road situations characterised by uncertain information about the environment, ambiguity in the right of way, and conflicts with obstacles of diverse properties. The ability to react faster than human driver does not guarantee collision avoidance (Fraichard & Howard, 2012). For example, consider a vehicle heading towards the road median at high speed. This makes risk assessment a critical component of on-road manoeuvring. Risk assessment techniques employed by ADS vary in the level of robustness to uncertain traffic situations ranging from simple reactive schemes (Xia et al., 2010) to sophisticated schemes involving manoeuvre prediction of adjacent vehicles (Ardelt et al., 2012). ADS may also differ in the comprehensiveness of risk definition, ranging from simple metrics of temporal proximity to a crash (Time-To-Collision) to more comprehensive metrics accounting for consequence of the crash. According to Ibanez-Guzman et al. (2010), the use of TTC as a risk metric in motion planning caused a collision and several near-miss situations in DARPA challenges. If the vehicle is temporarily stationary, for instance at an intersection, TTC could be high even in a high risk situation. Another aspect of concern is the ADS' interaction with human-driven vehicles (Calvert et al., 2016). When the right of way is ambiguous, human-drivers take actions by simply relying on social conventions that they expect the other vehicles to respect (Spalanzani et al., 2012). A human driver may merge onto a motorway expecting the following vehicle to yield, even when the available gap is short. To resolve ambiguous situations on human-populated roads, ADS should respect and exploit such conventions. Another concern related to the level 3 ADS feature is that the human user might become over reliant on the system and may fail to react, or react more slowly to a DDT fallback request. Such effects on the human behaviour are typically known as behavioural adaptation (Rudin-Brown & Parker, 2004). However, this issue is not investigated in this thesis.

It is clear that the safety impacts of ADS cannot be generalised, as their common features such as quicker response and absence of human-like errors are not the only factors governing driving safety. ADS differ in terms of the level of robustness and comprehensiveness of risk assessment schemes and in the level of human-friendliness, and these differences may determine their impacts on traffic safety. In this context, the logical first step would be to investigate the relationship between ADS functionalities and their impact on traffic safety.

1.3 Overview of traffic safety assessment: metrics and tools

Traditionally, traffic safety studies relied on the records of reported vehicle crashes. Such studies have been effective to identify the factors influencing traffic safety (Young et al., 2014) and to draw realistic conclusions on the effectiveness of automotive applications such as Automated Emergency Braking and Forward Collision Warning (Yue et al., 2018). How-

ever, the dependency on crash records is a major limitation of this approach, as crashes are rare events and the records may not contain all information required for analysis. Moreover, this method cannot be applied to predict the safety impacts of ADS features that are yet to be deployed in the traffic. An alternative approach to safety assessment, that does not rely on crash records, is by computer simulation. In this approach, the traffic of the target road facility is simulated at high resolution and the simulations are post-processed to estimate the magnitude and frequency of one or more safety-metrics. The distributions of these metrics are then statistically analysed to draw conclusions about the level of traffic safety. There exist several statistical methods for such analysis, for example alternate hypothesis tests (Bagdadi, 2013; Morando et al., 2018), curve fitting (St-Aubin et al., 2011), probabilistic causal models (G. A. Davis et al., 2011; Kuang et al., 2015) and extreme value theory (Songchitruksa & Tarko, 2006). Currently, simulation-based safety assessment has been used to predict the traffic-safety impacts of automotive applications related to Intelligent Transportation Systems (Liu et al., 2017; Jeong & Oh, 2017; Dedes et al., 2011). Both safety metrics and the simulation tool influence the effectiveness of safety assessment and hence the remainder of this section overviews the prominent works on these topics.

1.3.1 Safety metrics

In a simulation-based assessment, safety is quantified by certain metrics that are estimated from the simulated vehicle trajectories. The variation of these metrics is analysed to interpret and explain the collective traffic safety within the studied road stretch. Such measures are known as Surrogate Measures of Safety (SMoS) since they characterise the initial conditions of a regular (non-crash) event as the "surrogate" for a crash event (Gettman & Head, 2003; Laureshyn et al., 2016). A prominent example is Time-To-Collision (TTC). These metrics indicate a potential conflict between two road users. The underlying hypothesis is that a crash process is a temporal sequence of events in which a conflict event (safety-critical situation) occurs prior to a crash event (vehicle accident) (Laureshyn et al., 2016). Defining the crash process this way provides theoretical credibility for traffic safety predictions. Since conflicts and crashes are aligned on the same continuum of events, the frequency of low-risk events (conflicts) can be used to predict the frequency of high-risk events (crashes) (Laureshyn et al., 2016). The literature on SMoS is rich and diverse and can be broadly classified into two categories. The metrics in the first category are based on spatial and temporal proximity to the collision. Examples of this include Post Encroachment Time (L. Zheng et al., 2014a), TTC and its derivatives, Potential Index for Collision with Urgent Deceleration (Bevrani & Chung, 2012), Deceleration Required to Avoid a Collision (Archer, 2005), Safety Field Strength (J. Wang et al., 2016). The second category includes metrics based on driver actions such as maximum braking, jerk rate (Bagdadi & Várhelyi, 2011), standard deviation of lateral position (Niezgoda et al., 2012) and acceleration noise.

1.3.2 Simulation tools

Simulation-based safety assessment relies on computer-simulated synthetic trajectories instead of actual pre-crash trajectories. Before describing the techniques to generate vehicle trajectories in a computer, let us look into the theoretical description of on-road driving. On-road driving can be described as a process by which the driver simultaneously performs

multiple interrelated tasks in order to traverse from a point of origin to destination. Michon (1985) proposed a hierarchical relationship between these tasks, classifying them into strategic, tactical and operational levels. The strategic level tasks include deciding on the destination and route of the trip. Tactical level tasks include detecting and tracking obstacles and events, and deciding and planning a manoeuvre appropriate for the local driving environment such as lane-changing, Car-Following (CF) or negotiating an intersection. Operational level tasks include generating control commands (steering and acceleration) to execute the manoeuvre. The strategic goals are typically updated at a time scale of minutes, tactical decisions in seconds and operational commands in milliseconds. This representation of driving is generic to both humans and driving automation systems.

The traffic simulators employed for safety assessment use mathematical models to mimic driving subtasks at the three levels, and thereby generate the trajectories of all the vehicles in a time-discrete form. Such simulators are termed as microscopic in traffic literature as they describe the motion of individual vehicles as a time-series of longitudinal and lateral coordinates, or as submicroscopic when using detailed vehicle dynamic models. In these models, actions of a driver pertaining to a driving subtask are formulated as the response to ambient vehicles and as a means to achieve his/her intrinsic driving objectives. Traffic simulators integrate a combination of featured driving models within a numerical framework. Few of the prominent traffic simulators are VISSIM (Barcelo, 2010), PARAMICS (Sykes, 2010), CORSIM (Brockfeld et al., 2004), SUMO (Krajzewicz, 2010), AIMSUN (Casas et al., 2010), MOTUS (Schakel et al., 2013) and OTS (van Lint & Calvert, 2018). Even though traffic simulators describe driving tasks in all the three levels, tactical and operational-level actions are directly related to safety, and therefore these tasks are of particular interest here. The drivers actions corresponding to these levels are typically modelled by a pair of longitudinal motion model and lane-changing model. Most of the longitudinal motion models describe the forward acceleration as an action in response to the preceding vehicle or to attain its desired velocity during unconstrained driving. The earliest microscopic longitudinal model was proposed in 1953 (Pipes, 1953), and was succeeded by several others (Bando et al., 1995; Kesting et al., 2007; Treiber et al., 2000). The lane-changing is typically described by a pair of Lane-Changing Decision (LCD) and Gap Acceptance (GA) models. The LCD model prescribes whether or not to switch lanes, and the GA model determines whether the available gap in the target lane is safe. Simulators may also describe explicit tactical-level behaviours which require planning within a spatial or temporal look-ahead horizon. For example, in MITSIM (Ben-Akiva et al., 2010), the driver plans the desired sequence of driving lanes to reduce travel time or effort; and in VISSIM (Barcelo, 2010), the driver plans the desired acceleration profile while approaching an intersection or a merging zone.

1.3.3 Research gaps in simulation-based safety assessment

In this section, we list the research gaps in the existing literature on safety metrics and simulation tools that are addressed in this thesis.

Regarding the safety metrics, we consider the following two research gaps to be critical for their usability in mixed traffic studies.

- G1 *Lack of a generic expression of crash risk:* Factors related to driver behaviour, infrastructure and interaction with surrounding vehicles can influence crash risk. Moreover,

they distinctively affect the aspects of driving risk, such as crash likelihood and crash severity (consequences of the crash). Surrogate measures of safety (SMoS) are typically formulated to describe the effect of one of these factors in a specific driving scene. For instance, TTC describes the temporal proximity of a crash with respect to the preceding vehicle, as a proxy for the crash likelihood. Even though relevant, they provide only a partial description of the risk. Several researchers have highlighted the necessity of a generic expression of driving-risk that is sensitive to the risk-contributing factors and incorporates both likelihood and severity of the crash (Laureshyn et al., 2010; Mahmud et al., 2017; Young et al., 2014).

G2 Lack of a numerical estimate for motion uncertainties applicable to safety estimation:

In most cases, the derivation of SMoS considers just one possible future vehicle motion, i.e. with unchanged velocity/acceleration. In reality, several stochastic factors, related to driver behaviour and control, influence the vehicle motion and there exist multiple possibilities of future manoeuvre. Hence the magnitude of uncertainty is an integral component of the crash risk. Several probabilistic approaches are available in the safety analysis literature to calculate SMoS while accounting for the motion uncertainty (Saunier & Sayed, 2009). Such methods typically require that the movement of vehicles in the given environment can be observed long enough. Thereby, machine-learning techniques are employed to estimate a set of prototype trajectories, exploiting the structure of the environment (Saunier & Sayed, 2009). However, this brings back the requirement of empirical observations. There have been efforts to estimate SMoS for a pair of road users whose motion predictions are sampled from pre-determined probability distributions (Mohamed & Saunier, 2013). However, a numerical expression of risk that aggregates the influence of more than one moving and non-moving road entity is missing.

The accuracy and quality of synthetic trajectories generated by traffic simulators determine the reliability of the safety results. The following three research gaps should be addressed to improve the reliability of simulation results used in safety assessment studies.

G3 Absence of closed-loop interconnections between the different levels of driving tasks in the simulation framework:

As discussed earlier, driving involves performing multiple tasks that are interconnected. The tactical and operational modules in ADS architectures function as a closed-loop (Ardelt et al., 2012; Nilsson et al., 2015; Resende & Nashashibi, 2010; Vanholme et al., 2013). This connection can also be observed in human driving. Lane change manoeuvres are often interrupted (Yang et al., 2015) or aborted during the execution (L. Zheng et al., 2014b) due to safety/efficiency concerns. Such manoeuvres reflect the interaction between the lane changing decision (tactical-level) and steering actions (operational-level). Even though state-of-the-art traffic simulators describe the functions of each level, they are often disconnected from each other. The interaction between the tactical and operational level is treated as an open-loop process. For example, the vehicle is propagated to the target lane upon a positive lane change decision, without any reconsideration while carrying out the lane change. Therefore, the current simulation frameworks deviate from the general ADS architecture and cannot generate manoeuvres with re-planning such as aborted lane changes and fragmented lane changes.

- G4 *Oversimplification of lateral vehicle dynamics model and steering control model in traffic simulation frameworks*: Microscopic models treat the vehicle as a floating-point-mass entity with bounded acceleration and velocity space ignoring the lateral vehicle dynamics and yaw motion. Such a vehicle model allows fast calculations with a limited number of parameters, but ignores the influence of vehicle geometry and mass, tyre properties on the lateral manoeuvre capability. A related issue is the lack of an explicit model for steering-control (Moridpour et al., 2009; Yang et al., 2015). Studies on human steering control conclude that lane-changing is a closed-loop control process in which the driver uses visual feedback to regulate the steering input (Salvucci & Gray, 2004). The steering-control technique implemented by the human driver or system have a direct impact on safety. For example, lack of control accuracy has been cited to be a factor contributing to the lane departure related accidents at highway curves and oversteering related secondary accidents (Staubach, 2009), thus creating a need for submicroscopic modelling taking into account the lateral vehicle dynamics.
- G5 *Deficiency of empirical insights into factors affecting lane-changing execution and their effects on adjacent vehicles*: Recent studies have revealed that the local traffic state can significantly influence the lane-changing trajectory, and that the lane-changing manoeuvres can influence the driving behaviour of adjacent vehicles. However, the exact factors and their influence on the lane changing trajectory are yet to be empirically identified. Similarly, the influence of the lane-changing execution characteristics on the driving behaviour of adjacent vehicles is unknown. Such insights are necessary to improve the accuracy of multi-lane traffic simulation.

Both metric-related and simulator-related limitations have so far restricted the applicability of simulation-based safety assessment approach in the following topic

- G6 *Lack of insights into the effects of key ADS design factors on the multi-lane motorway safety*: Several researchers have applied simulation-based approaches to analyse the safety of longitudinal conflicts on motorways; but very few studies analyse the safety of lateral conflicts, such as the one during a lane change, merging or overtaking. This is partially due to the research gaps in traffic simulation and risk estimation literature.

1.4 Research objectives

The objectives of this research address the research gaps presented in Section 1.3, and are defined as follows:

Objective 1: To formulate a metric for driving risk that contains information on crash-severity and crash probability and is sensitive to properties of conflicting on-road entities. (*related to G1 and G2*)

Objective 2: To develop a submicroscopic multi-lane traffic flow simulation framework that is generic to ADS equipped and human-driven vehicles incorporating the respective tactical-level functions, control-level functions, vehicle dynamics, and the interconnections between them. (*related to G3, G4 and G5*)

Objective 3: To demonstrate the application of the proposed risk metric and the traffic simulation framework and to identify the relations between the key ADS design parameters and the safety impacts on multi-lane motorway traffic. (*related to G6*)

1.5 Research scope

This thesis focusses on motorway operations with a fleet of Human driven Vehicles (HVs) and ADS-equipped vehicles (SAE level 3-5). We made this choice expecting the safety impacts of ADS to be prominent on motorways where vehicles move at high speeds and manoeuvre between lanes. Moreover, the first generation ADSs are likely to be featured on motorways due to their uniform and low complexity environment and behavioural homogeneity in traffic fleet.

Secondly, we focus on the decision- making and control strategies of ADSs, which determine their impact on traffic safety. However, we strongly idealise the sensing, perception and actuation techniques implemented in ADSs.

Thirdly, safety issues investigated in this thesis are restricted to motion safety. Even though the risk of system failure and governing factors are relevant aspects of vehicle safety (W. Wang et al., 2010), they are out of the scope of this work.

Fourthly, we do not study the situations involving control transition between the automation system and the human user. Accordingly, we omit the system failure events, when the control of level 3 ADS will be transferred to the fallback-ready user. Moreover, we assume that simulated road facilities are all within the ODD of the ADS in order to avoid system initiated take over requests.

Finally, all case studies in this thesis include solely passenger cars, as they represent the majority of vehicles on motorways. The other vehicle types such as trucks and motorcycles exhibit distinct driving behaviours and vehicle dynamics and are not considered in this thesis. Nevertheless, the safety assessment approaches developed in the thesis are not restricted to passenger cars.

1.6 Contributions

1.6.1 Scientific contributions

Qualitative and quantitative comparison of surrogate metrics of safety: This thesis compares five prominent safety metrics based on a set of qualitative and quantitative criteria and thereby demarcates their mathematical properties, identifies the appropriate scope of application, and reports their limitations.

A generic and probabilistic approach to assess the driving risk: This thesis presents a safety assessment approach named as Probabilistic Driving Risk Field based on field theory. The risk posed by a road entity is formulated as an artificial risk field. Any obstacle (neighbouring entity on the road) to the subject vehicle is treated as a finite scalar risk field that is formulated in the predicted configuration space of the subject vehicle. Thereby, the subject vehicle' driving risk at any given moment is the value of the risk field at the position of its centre of mass. This risk field is formulated as the product of two factors: expected crash energy (as an approximation of consequences) and the collision probability.

The collision probability with an immovable object is modelled as a decreasing function of relative spacing. The collision probability with a movable obstacle (vehicle) is estimated based on probabilistic motion predictions of the subject and neighbouring vehicle's possible positions at discrete future time steps. Compared to other surrogate safety metrics with context-specific definitions, this approach is generic for multiple reasons: 1) the risk posed by any entity: immovable objects on the road boundary or moving vehicles on the road can be formulated as distinct risk fields; 2) the formulation of risk field incorporates both the chances of a crash and the consequences of a potential crash; and 3) by adjusting the discretisation of motion predictions, this approach can be deployed to analyse traffic risk (one time-step) and as a risk estimate of path plans (multiple time-steps). This approach implements a numerical estimate for crash-probability based on characteristic acceleration distribution of the conflicting vehicles. Compared to existing sampling-based methods to account for motion uncertainty, the numerical approach is a computationally efficient and mathematically tractable alternative.

New empirical insights on lane-changing process and models thereof: We perform statistical analysis of an empirical trajectory dataset to reveal new insights on a less studied type of lane change: fragmented lane change, in terms of its execution, motivating factors, and the behavioural effects on the adjacent vehicles. Moreover, we present models to describe the trajectory and safety impacts of this type of lane-changing.

An enhanced framework to simulate vehicle motion within multi-lane and multi-class traffic: This thesis presents a submicroscopic simulation framework consisting of two coupled layers, an upper tactical level that generates manoeuvre plans; and a lower operational layer with explicit control module (steering and acceleration control) that operates in a closed loop with a bicycle model of vehicle dynamics. The framework depicts a hierarchical decision and control structure of vehicle operation.

This framework provides several methodological benefits compared to conventional microscopic simulators. First, the framework contains modules featuring driving sub-tasks that are common to both ADSs and human drivers, and thereby provides multi-class trajectories at a comparable level of detail. Secondly, the simulated trajectories account for lateral vehicle dynamics and yaw motion and provide additional variables such as vehicle orientation and steering commands, improving the realism of simulated trajectories. Finally, the framework provides a means to simulate a wider range of lateral vehicle manoeuvres such as curve negotiation, corrective steering, aborted lane-changing and fragmented lane-changing.

New insights into the relationship between ADS functionalities and the traffic safety: We apply the simulation-based approach to assess the safety impacts of ADS-equipped vehicles on lane-changing manoeuvres performed by human-driven vehicles. More precisely, we model two generic types of ADS' cut-in response: aided and not aided by a prediction algorithm, and compare their impact on traffic safety. The ADS's acceleration control is modelled by a Full-Range Adaptive Cruise Controller and its cut-in prediction by a rule-based logic. This study provides detailed predictions on traffic safety impacts and kinematic characteristics of the lane changes. The safety assessment approach presented in this thesis is one of the few approaches that can analyse multi-lane traffic safety considering lateral manoeuvres.

1.6.2 Practical contributions

For road traffic modelling and analysis, this thesis provides an innovative simulation framework with a hybrid and modular architecture. The framework is hybrid in the sense that it simulates the motion at a microscopic level when the vehicle is in car-following or unconstrained driving mode and switches to submicroscopic simulation (higher resolution) during lateral manoeuvres. This hybrid scheme enhances computational performance while providing a trajectory resolution suitable for safety assessment. The modularity of the framework allows the user to easily replace a featured driving-subtask with another one of interest.

For ADS designers, the insights in this thesis indicate that the level of anticipation of upcoming events and the principles underlying decision-making algorithms are the key determinants of driving safety on motorways. We find that a predictive control approach, of proactively responding to an incoming vehicle before it begins to cut-in, yields a safer interaction than a reactive approach. To ensure safety, the decision-making algorithms should not only pursue egoistic goals, but also consider the convenience of adjacent vehicles. For instance, our results show that ADS-equipped vehicles that do not yield to a merging vehicle can detriment individual and collective traffic safety and may create congestion in the on-ramp.

For road operators, the simulation-based safety assessment approach provides a framework to estimate the impacts of emerging ADS features and to evaluate design alternatives controlling for road alignment and properties of roadside barriers. Our results suggest that an increase in the acceleration lane length is a promising step to reduce the frequency of unsuccessful merges that may occur due to reactive automated vehicles on the main-lane. The driving risk metric, proposed in this thesis, accounts for crash severity. Thereby it enables policymakers to devise effective measures by identifying and mitigating the possibility of severe conflicts, which may cause more damage to life.

1.7 Thesis outline

Figure 1.1 depicts the seven chapters in this thesis as boxes. The black arrows between the boxes depicts the relationship between the chapters.

Chapter 2 and 3 deal with the metrics and methods for safety assessment. In Chapter 2, we review four prominent driving risk metrics and elaborate on the benefits and shortcomings of each of these metrics. Chapter 3 addresses the knowledge gaps identified in Chapter 2 by presenting a safety assessment approach based on field-theory: Probabilistic Driving Risk Field (PDRF). The approach is verified by applying it to describe risk of three near-crash scenarios documented in a public dataset and in hypothetical simulation case studies.

Chapter 4 and 5 identify and address the methodological deficiencies in the traffic simulation frameworks in the context of safety assessment. In Chapter 4, we investigate the empirical lane-changing trajectories to characterise and model two types of lane changes: Continuous Lane-Changing: when a vehicle move between two lanes without interruption and Fragmented Lane Changing (FLC): when the vehicle temporarily pauses its lateral movement during the manoeuvre. Chapter 5 presents the submicroscopic traffic simulation framework that provides trajectories at a higher level of detail than common microscopic

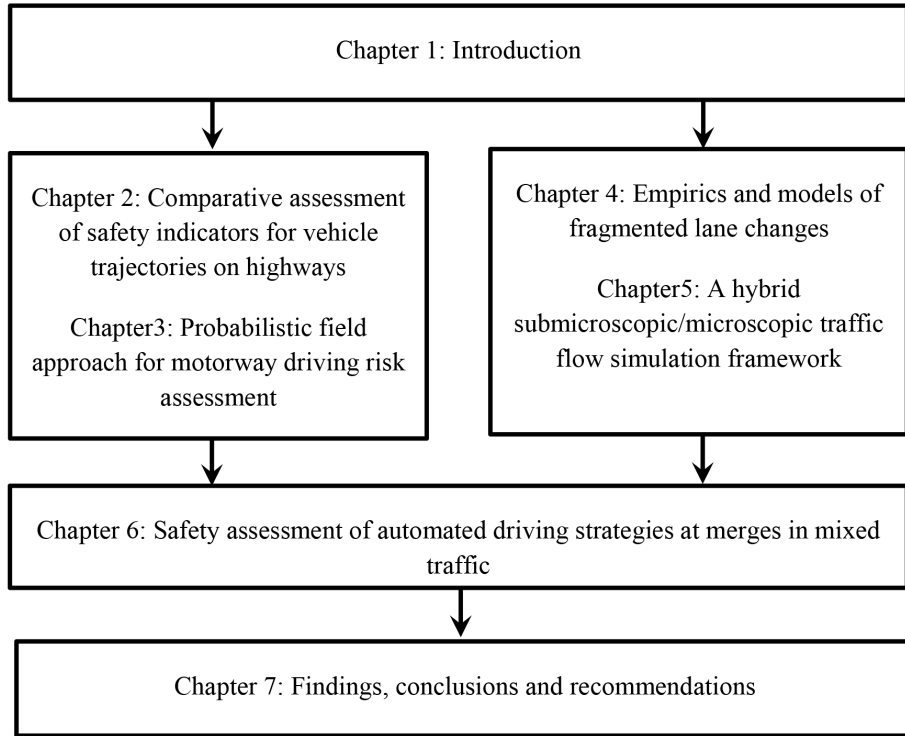


Figure 1.1: Thesis structure and relations between chapters

frameworks. Several simulation examples are provided to demonstrate the unique capabilities of the framework and its ability to reproduce typical traffic properties.

Chapter 6 presents an application of the simulation framework in Chapter 5 and safety assessment approach in Chapter 3. Here, we present the scenario case studies to evaluate the safety at a motorway merge section, when traffic consists of manual and varying share of ADS equipped vehicles. The safety metrics, including PDRF are analysed to quantify the safety impacts, delineate and compare the trends with an increasing share ADS-equipped vehicles in the traffic fleet. Finally, the findings, conclusions and recommendations of this thesis are summarised in Chapter 7.

Chapter 2

Comparative assessment of safety indicators for vehicle trajectories on highways

Abstract

Safety measurement and its analysis have been well researched topics in transportation. Conventionally, surrogate safety measures have been used as safety indicators in simulation models for safety assessment, in control formulations for driver assistance systems, and in data analysis of naturalistic driving studies. However, surrogate indicators give partial insights on traffic safety; that is, these indicators only indicate a predetermined set of possible precrash situations for an interacting vehicle pair. Recently, a safety indicator called the driving safety field, based on field theory, was proposed for two-dimensional vehicle interactions. However, the objectivity of its functional form and its validity are yet to be tested. In this chapter we provide a qualitative and quantitative comparison of different safety indicators to demarcate their mathematical properties and evaluate their usefulness in quantifying trajectory risk. Five prominent safety indicators were compared: inverse time to collision, post encroachment time, potential indicator of collision with urgent deceleration, warning index, and safety field force. Their formulations were mathematically analysed to yield qualitative insights and their values over simulated vehicle trajectories were evaluated to yield quantitative insights. The results acknowledge the limitations and demarcate the functional utilities of the selected safety indicators.

This chapter is an edited version of the following paper:

Mullakkal-Babu, F. A., Wang, M., Farah, H., van Arem, B., & Happee, R. (2017). Comparative Assessment of Safety Indicators for Vehicle Trajectories on Highways. *Transportation Research Record*, 2659(1), 127-136. <https://doi.org/10.3141/2659-14>

2.1 Introduction

Safety is a key performance indicator of any transportation system. Road safety research has received considerable attention owing to the enormous societal losses incurred in road accidents worldwide, with about 1.25 million fatalities, and between 20 and 50 million non-fatal injuries (World Health Organization, 2015). Recent efforts in safety research are primarily focusing on the use of Surrogate Measures of Safety (SMoS), as a proactive and cost efficient method to evaluate safety, acknowledging the limitations of using crash records (Archer, 2005) e.g. road safety assessment (Azevedo & Farah, 2015; Wilmink et al., 2007); ex-ante safety evaluation in driver assistance and automation systems (Kuang et al., 2015; M. Wang et al., 2015); and behaviour modelling of human drivers in safety critical scenario (Kiefer et al., 2006). The advent of intelligent vehicles has brought in uncertainties, especially with regard to vehicle interactions. The uncertainties stem from the fact that an intelligent vehicle possesses enhanced communication and control capabilities compared to a human-driven vehicle, but lacks in the spatial and temporal anticipative capabilities. Achieving an agreement on a set of objective safety indicators that are applicable in mixed traffic is a methodological challenge. Hence, the selection of a safety indicator has profound implications on the quality and agreeability of the safety research findings.

Essentially, a safety indicator is a measure of risk associated with a vehicle interaction. SMoS are the most common risk indicators used in safety studies. The risk delineated by SMoS could vary depending on their formulation and parameter consideration. More importantly, they are often discontinuous as their validity is limited to a prescribed set of interacting vehicle configurations. For example, time to collision is not defined in a car following situation with a faster leader. Recently, a safety model has been proposed that is capable of describing risk continuously over the vehicle path. This safety model is based on field theory and defines driving risk as a spatial field (J. Wang et al., 2015). However, the validity of its functional form is yet to be tested. Therefore, despite the wide range of safety indicators, selection of an appropriate indicator warranting validity and agreeable results is intricate.

Safety indicators are usually selected based on their study scope and methodological suitability, making it difficult to generalize their findings. Even though safety indicators have been extensively reviewed and empirically validated in the past, limited literature exists on the demarcation of their mathematical properties; representation of risk causal factors in their formulation; evaluation of their usefulness in quantifying trajectory risk. To that end, in this chapter, we compare relevant safety indicators for their qualitative and quantitative aspects. Their formulations are mathematically analysed to yield qualitative insights and their values over simulated vehicle trajectories are evaluated to yield quantitative insights. Our results acknowledge the limitations and demarcate the functional utilities of the selected safety indicators.

2.2 Literature review

Crash statistics have been traditionally used for road safety evaluation. Even though relevant, it has drawbacks such as the unavailability of sufficient crash data to derive statistically significant conclusions and inability to be used for ex-ante evaluation. These drawbacks

made researchers turn towards a complementary approach that uses SMOs. The characteristics of SMOs are that they are more frequent than crashes; they are observable in traffic; and they represent crash causality and crash mechanisms (Svensson, 1998).

SMOs have been critically and extensively reviewed over time (van Beinum et al., 2016; Gettman & Head, 2003; Kuang et al., 2015; Young et al., 2014; L. Zheng et al., 2014a). Generally, SMOs define the collision risk of an interacting vehicle pair as a function of their instantaneous kinematic states (acceleration, velocity and position) and depend on their spatial configuration. Hence, these indicators can be categorized into longitudinal and lateral indicators based on the location of the interacting vehicles. Longitudinal indicators have been widely used in forward collision warning systems, safety assessment of highways and human behavioural modelling in rear-end crash scenarios. Common longitudinal-SMOs are Time To Collision (TTC), inverse Time To Collision (iTTC), Time Exposed Time to collision (TET), Time Integrated Time to collision (TIT) (Minderhoud & Bovy, 2001), Deceleration Required To Avoid Collision (DRAC), Potential Indicator of Collision with Urgent Deceleration (PICUD) (van Beinum et al., 2016). Lateral-SMOs like Post Encroachment Time (PET) have been used as a risk measure in lane change controllers, safety assessment of intersections and lateral vehicle manoeuvres.

SMOs that are not intrinsically bounded to lateral or longitudinal interactions can be found in the literature. For instance, Crash Potential Index (CPI) and Aggregated Crash Index based on a predetermined set of probable set of evasive manoeuvres (Jula et al., 2000; Kuang et al., 2015). The functionality of these probabilistic indicators is restricted to certain driving regimes due to the difficulty of exhaustively listing all possible manoeuvres. Additionally, predictive risk maps have been proposed to estimate the future risk based on the predicted trajectories of interacting vehicles (Damerow & Eggert, 2014). Even though this approach is efficient for ex-ante safety evaluation in controllers, its performance inherently depends on the prediction modules and does not fall within the scope of this work. Recently, J. Wang et al. (2015) proposed an alternative risk assessment methodology for two-dimensional vehicle interactions based on field theory (J. Wang et al., 2015). They model risk as a vector field and incorporate road, vehicle and driver characteristics into a unified field formulation. In this study, we focus on five safety indicators: iTTC, PICUD, Warning Index (WI) (relevant longitudinal indicators with different parameter considerations), PET (relevant lateral indicator), and safety field force (two-dimensional safety indicator).

2.3 Qualitative analysis

Qualitative analysis of the selected indicators was performed with the following objectives: to evaluate the mathematical properties of their functional form in the multi-vehicle scenario; and to benchmark their formulation with expected causal tendencies of major risk contributing variables.

2.3.1 Desirable mathematical properties for a risk measure in multi-vehicle scenario

In this section we present the desirable mathematical properties of safety indicators to verify the applicability of selected safety indicators in multivehicle scenarios. Mathematical

measure theory has prescribed criteria for a function to be termed as a measure (L. C. Evans & Gariepy, 2015). Being a risk measure of vehicle interaction, it is desirable for safety indicators to adhere to these criteria as follows:

Let X be the set of all interacting vehicles V under consideration, and Σ be the collection of possible subsets of X . A risk measure $\mu : \Sigma \rightarrow R$ from Σ to the real number line R is a mathematical risk measure if the following conditions are satisfied:

Non-negativity: The risk measure μ of any vehicle V with index k in Σ is a non-negative value.

$$\mu(V_k) \geq 0 \quad (2.1)$$

This property is desirable considering that a negative risk value is non-intuitive and its use is ambiguous in multi-vehicle scenarios, i.e. it could cancel a positive risk value.

Countable additivity: The risk measure μ should indicate the union of risk values due to the interacting vehicles M in a multi-vehicle scenario. Wherein, the risk measure of a countable disjoint collection of vehicle $\{V_i\}_{i=1}^M$ is the same as the sum of all risk measures of each vehicle unit as follows:

$$\mu\left(\bigcup_{k=1}^M V_k\right) = \sum_{k=1}^M \mu(V_k) \quad (2.2)$$

This property simplifies the individual risk calculations for complex multivehicle interactions; and it allows the addition of individual risk measures to estimate the total societal/collective risk. However, this is not an essential property to indicate the risk associated with vehicle pair interaction like car following.

2.3.2 Risk factors and expected causal tendencies

In this section we detail the major contributing factors of risk and their expected causal tendencies. This expectation is based on reasoning and relationships that are reported in previous empirical and physics-based crash studies. Dynamics and causality of a crash are directly and indirectly influenced by various factors, and it would be farfetched to exhaustively list them. But few of these factors have been reported to have a causal relationship with vehicle collisions. Firstly, the probability of a collision between two road users is expected to increase with their approaching rate and decrease with the inter-vehicle spacing (shorter time for the driver to react; the lesser possibility of risk mitigation or evasive manoeuvre). Secondly, the collision impact is expected to increase with an increase in velocity (Aarts & Van Schagen, 2006) and mass (L. Evans, 1994) of the conflicting vehicles (with higher vehicular velocity, the driver should react more rapidly to avoid a collision; higher vehicular mass results in higher kinetic energy transferred and higher collision severity). Thirdly, the collision impact is reported to increase with delta-V or the change in vehicle velocity as the result of an impact (Laureshyn et al., 2016). Finally, the roadway characteristic like surface friction (Othman & Thomson, 2007) and driver characteristic like reaction time (Klauer et al., 2006) are expected to influence the collision risk.

2.3.3 Benchmarking the safety indicators with expected risk tendencies

In this section, we compare the expected risk tendency of a factor with the risk tendency as described by the partial derivative of the indicator with respect to the factor.

Time To Collision

TTC is defined as the time required for two vehicles to collide if they continue in their present velocity along the present path. $TTC = \frac{s_n}{\Delta v_n}$; $v_n > v_{n-1}$, where, v_n denotes the instantaneous velocity of the vehicle n ; $\Delta v_n = v_n - v_{n-1}$ and s_n denotes the relative velocity and forward spacing of vehicle n with respect to the front vehicle $n - 1$. iTTC is the inverse formulation of TTC and is widely used in controllers like adaptive cruise controller (Moon et al., 2009) and to assess human driver behaviour (Fancher et al., 2001). A higher value represents higher risk and the interaction risk is often captured with the minimum-TTC or maximum-its over the interaction period. It is formulated as follows

$$iTTC = \frac{v_n - v_{n-1}}{s_n}, \quad \text{if } v_n > v_{n-1} \quad (2.3)$$

$\frac{\partial iTTC}{\partial \Delta v} = \frac{\partial iTTC}{\partial v_n} = \frac{1}{s_n} > 0$ indicates that the risk increases with an increase in approaching rate. $\frac{\partial iTTC}{\partial s_n} = \frac{-\Delta v}{s_n^2}$ indicates that the risk decreases with an increase in the spacing of the slower leader. As shown in Table 2.1, both these indications are in agreement with the expected risk tendencies.

Potential Index for Collision with Urgent Deceleration

PICUD is defined as the forward spacing between two vehicles if both of them brake with a maximum deceleration (van Beinum et al., 2016) as follows:

$$PICUD = s_n + \frac{v_{n-1}^2 - v_n^2}{2a_{max}} - t_h v_n \quad (2.4)$$

where a_{max} denotes the maximum deceleration and t_h denotes the time delay of human response and smaller PICUD indicate higher risk. $\frac{\partial PICUD}{\partial \Delta v} = -\frac{v_n + v_{n-1}}{2a_{max}} < 0$, $\frac{\partial PICUD}{\partial v_n} = -\left(\frac{v_n}{a_{max}} + t_h\right) < 0$ and $\frac{\partial PICUD}{\partial t_h} = -v_n < 0$ indicates that the risk increases with an increase in approaching rate, vehicle velocity and human reaction time respectively. $\frac{\partial PICUD}{\partial s} = 1 > 0$ indicates that the risk decreases at a constant rate with an increase in spacing. As shown in Table 2.1, PICUD is in agreement with the expected risk tendencies.

Warning Index

Warning Index(WI) is a safety indicator used in collision warning algorithms (Moon et al., 2009). This indicator also includes factors like tire-road friction and system delay. A lower w represents higher risk and it is formulated as follows:

$$WI = \frac{s_n - d_{br}}{d_w - d_{br}} \quad (2.5)$$

$$d_{br} = \Delta v_n t_s + f(\mu) \left(\frac{v_n^2 - v_{n-1}^2}{2a_{max}} \right) \quad (2.6)$$

$$d_w = \Delta v_n t_s + f(\mu) \left(\frac{v_n^2 - v_{n-1}^2}{2a_{max}} \right) + v_n t_h \quad (2.7)$$

where, d_{br} denotes the required braking distance; d_w denotes the required warning distance; $f(\cdot)$ denotes the friction scaling function and μ is the estimated value of tire-road friction. t_s is the system delay and t_h is the delay of human response. The decreasing WI indicates an increasing risk. Considering this, $\frac{\partial WI}{\partial \Delta v} = -\frac{f(\mu)(v_n + v_{n-1})}{2a_{max}v_n t_h} - \frac{t_s}{v_n t_h} < 0$ and $\frac{\partial WI}{\partial t_h} = -\frac{w}{t_h} < 0$ indicates that the risk increases with an increase in approaching rate and human reaction time respectively. $\frac{\partial WI}{\partial s} = \frac{1}{v_n t_h} > 0$, indicates that the risk decreases with an increase in spacing. As shown in Table 2.1, WI is in agreement with the expected risk tendencies. However, there are some relations that contradict the expected risk tendencies. $\frac{\partial WI}{\partial v_n} > 0$ is subject to the condition $\frac{\Delta v_n t_s}{v_n^2 t_h} < \frac{s}{v_n^2 t_h} + \frac{f(\mu)}{2a_{max} t_h} + \frac{f(\mu)v_{n-1}^2}{2a_{max} t_h v_n^2}$ and $\frac{\partial WI}{\partial \mu} = \frac{v_n^2 - v_{n-1}^2}{2a_{max} v_n t_h} > 0$ is an increasing function of μ . This indicates that the risk increases with an increase in road friction coefficient while approaching a faster leader.

Post Encroachment Time

PET is used as a risk measure in scenarios involving lateral manoeuvres. PET denotes the time lapse between the end of the encroachment of the turning vehicle and the time when the vehicle actually arrives at the potential point of collision (L. Zheng et al., 2014a). The encroachment line x^e in case of a lane changing manoeuvre is defined as a virtual line perpendicular to the lane dividing marker and crossing the intersection point of the lane dividing marker, and the lane change trajectory. To understand the variation of PET chronologically, we predict the encroachment line and the corresponding PET at every time-step, using kinematic prediction with constant velocity assumption. In a situation where two vehicles pass the encroachment line one after the other, the PET definition as per the above assumption is as follows:

$$PET = \frac{x^e - x_j}{v_j} - \frac{x^e - x_i}{v_i} \quad (2.8)$$

where, x_j and v_j are the position and velocity of the first vehicle respectively; x_i and v_i are the position and velocity of the second vehicle respectively. x^e is the longitudinal position of the encroachment line. Since this formulation does not directly involve Δv , we do not further analyse the mathematical properties.

Driving Safety Field

Field theory has been used to model traffic flow (Ni, 2013). In this theory, moving road objects such as vehicles and non-moving road objects such as lane markings are represented as component fields and their union represents the total driving risk. Based on field theory, J. Wang et al. (2015) proposed a Driving Safety Field (DSF). DSF of a road object is a physical field that denotes its influence on driving safety. This influence is determined by the driver behaviour characteristics, road condition, attributes and kinematic state of the road object. The magnitude and direction of this influence are denoted by the field strength

vector. A vehicle in the aforementioned field experience a Safety field Force (SF) which denote its current driving risk. The proposed field strength and field force for two moving vehicles are given as follows:

$$\mathbf{E}_{cj} = kR_c M_c (1 + DR_c) e^{k_1 v_c \cos \theta} \frac{1}{|\mathbf{r}_{cj}|^{k_3}} \cdot \frac{\mathbf{r}_{cj}}{|\mathbf{r}_{cj}|} \quad (2.9)$$

$$\mathbf{F}_{cj} = E_{cj} \cdot R_j M_j (1 + DR_j) e^{-k_1 v_j \cos \theta} \quad (2.10)$$

where, \mathbf{E}_{cj} and \mathbf{F}_{cj} denote the safety field strength vector and the SF vector, respectively on vehicle j due to a moving vehicle c ; \mathbf{r}_{cj} denotes the radial distance vector from vehicle c to vehicle j . θ (clockwise positive) is the angle between directions v_c and \mathbf{r}_{cj} ; is the angle between directions v_j and \mathbf{r}_{cj} . k , k_1 and k_3 are the calibration coefficients. $DR_i : i \in \{c, j\}$ denotes the driver risk factor and is a dimensionless value between 0 (safe driver) and 1 (risk taking driver). $M_i : i \in \{c, j\}$ denotes the virtual mass of a moving or non-moving object, and is parameterized by its physical mass, vehicle type and velocity. $R_i : i \in \{c, j\}$ denotes the factor that influence the road condition and is parameterized by road-tyre friction coefficient, curvature, slope and visibility. In this study, we have used the values of parameters as suggested in (J. Wang et al., 2015). Figure 2.1 demonstrates the spatial distribution of the safety field strength caused by vehicle c . A larger \mathbf{F}_{cj} (blue colour) means a higher driving risk for vehicle j .

$\frac{\partial \mathbf{F}_{cj}}{\partial \Delta v} = k_1 \mathbf{F}_{cj} > 0$, indicates that the risk increases with an increase in approaching rate.
 $\frac{\partial \mathbf{F}_{cj}}{\partial r_{cj}} = -k_3 \mathbf{F}_{cj} |r_{cj}|^{k_3-1}$, indicates that the risk decreases with an increase in spacing.

The original paper (J. Wang et al., 2015) does provide a detailed formulation of R_i , DR_i and M_i . If R_i is defined as an increasing function of $f(\mu)$, \mathbf{F}_{cj} decreases with road friction coefficient. If DR_i is defined as an increasing function of t_h , \mathbf{F}_{cj} increases with human reaction time. If M_i is defined as an increasing function of v_n , \mathbf{F}_{cj} increases with vehicular velocity. This holds for vehicular mass as well. As shown in Table 2.1, the indications are in agreement with the expected tendencies.

2.3.4 Findings of the qualitative analysis

The theoretical verification of the five safety indicators described above reveals the following:

- the selected indicators have limited consideration of risk factors and the SF formulation incorporates the largest number of factors
- the selected indicators formulations represent the expected risk tendencies. However, a contradiction was found in the case of the WI (See Table 2.1)
- the selected SMOs do not account for vehicle mass in their formulation

Examination of the mathematical properties of the selected indicators reveals the following:

- none of the selected safety indicators can claim countable additivity property as they are defined for vehicle pairs. Even though the SF on a vehicle is additive, in its present vector formulation the risk due to the presence of multiple vehicles cannot be

Table 2.1: Theoretical verification of safety indicators

Aspects	Factors	Expected tendency	iTTC	PICUD	Warning Index	Safety Force
Proximity to collision point	relative velocity	increase	increase	increase	increase	increase
	spacing	decrease	decrease	decrease	decrease	decrease
Collision impact	vehicle velocity	increase	increase	increase	increase subject to condition	increase
	vehicle mass	increase	NA	NA	NA	increase
Roadway characteristics	surface friction	decrease	NA	NA	decrease subject to condition	decrease
human factors	reaction time	increase	NA	increase	increase	increase
Range	NA	NA	$(0, \infty)$	$(-\infty, +\infty)$	$(0, \infty)$	$(0, \infty)$

added. For example, forces acting in opposite direction tend to cancel out, but the risk measure due to two vehicles cannot cancel out.

- PICUD and PET can have a negative risk value which is undesirable in a multi-vehicle scenario (See Table 2.1).
- quantitatively, iTTC, WI and SF may go to infinity at limiting conditions (See Table 2.1). Even though theoretically plausible, this property violates the principle of countable additivity and necessitates an upper bound definition. For instance, a risk measure tending to ∞ is computationally undesirable for adaptive cruise control systems (Moon et al., 2009).

Figure 2.2 depicts the forward spacing vs relative velocity plot representing the vehicle operational space as suggested by (Fancher & Bareket, 1994). A vehicle trajectory can be visualised on this plot as a continuous line with a plausible direction of motion. The principle concerning the plausibility of the direction of motion is demonstrated using arrows in Figure 2.2(a). The risk measures, for a vehicle moving at 10 m/s, described by different safety indicators are depicted as color map on this plot. In this chapter, the parameters values for WI is $a_{max} = 3.3 \text{ m/s}^2$, $t_s = 0.5 \text{ s}$, $t_h = 1 \text{ s}$, $f(\mu) = 1$; and for PICUD are $a_{max} = 3.3 \text{ m/s}^2$ and $t_h = 1 \text{ s}$. We use this plot to visually examine the indicators for their validity and the risk variation along a trajectory. As shown in Figure 2.2(a), iTTC is not defined for the lower quadrant, which depicts a faster leader. PICUD and WI have smoother transition from safe-green to unsafe-blue than iTTC and SF. Moreover, the iTTC risk indication abruptly disappears in a transition from upper to lower quadrant of the plot.

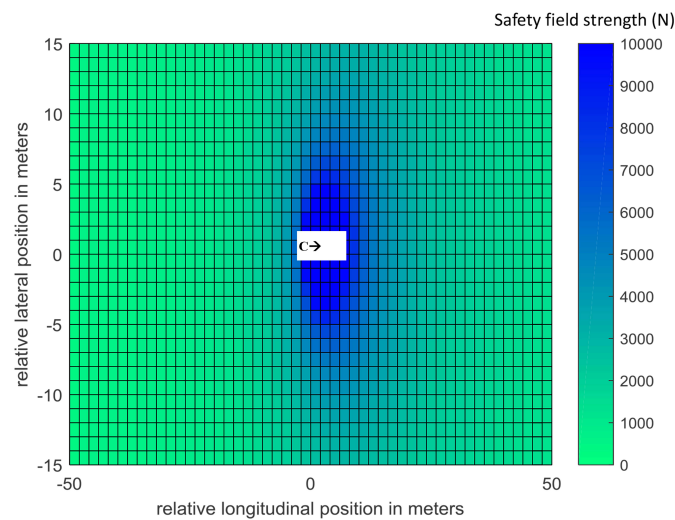


Figure 2.1: Demonstration of safety field strength due to a moving vehicle. Blue colour indicates higher risk; unit of field strength is Newton

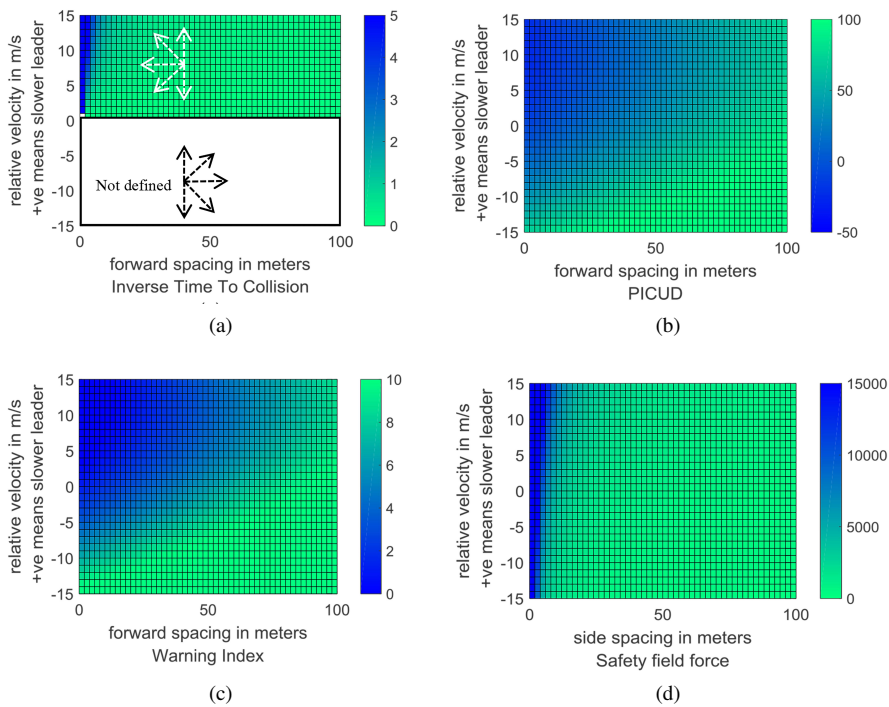


Figure 2.2: Visualisation of risk measures over the operational space using different safety indicators. Blue colour indicates higher risk

2.4 Simulation case studies

We extend our study from theoretical findings to simulation-based comparison of risk values associated with two-dimensional trajectories. In particular, we examine peaks of the risk measures, analyse the ability to represent the risk related to vehicle manoeuvres and inspect the continuity of the risk measure over typical trajectories.

Towards this, we defined two typical safety critical scenarios on highways (Hyden, 1987): emergency braking (case study 1) and cut-in (case study 2). The two case studies were performed as a numerical simulation (simulation time of 20 s and a time-step of 0.2 s) for a vehicle pair: a leader with a predefined trajectory to facilitate the scenario simulation and a follower. Longitudinal follower trajectories were simulated using the Intelligent Driver Model (IDM) with default parameters as in the original paper (Treiber et al., 2000). Another conservative simulation assumption used is that a vehicle would be identified as the leader only if it is ahead on the same lane. This implies that a cut-in will be detected only after the vehicle crosses the lane boundary. The safety indicators considered are iTTC (threshold 0.5 s^{-1}) (Moon et al., 2009), PET (threshold 0.45 s), PICUD (threshold 0 m) and SF. The above thresholds describe the safe ranges (Azevedo & Farah, 2015; Moon et al., 2009; Ni, 2013).

2.4.1 Case study 1

In this case study, we simulate a leader applying sudden braking (predefined) and three possible evasive manoeuvres of the follower vehicle. Here, the leader vehicle travelling at 5 m/s and a spacing of 10.5 m ahead of the follower suddenly brakes (-2.5 m/s^2) at 5 s and reaches a complete halt at 7 s.

Figure 2.3(a) shows the risk profiles calculated using various safety indicators when the follower brakes to avoid a collision as dictated by the car following model IDM. It can be seen that iTTC is defined only in the time interval when the leader is slower than the follower. All three indicators depict an increasing risk measure as the leader brakes. PICUD and iTTC show the highest risk when the leader reaches a complete halt and thereafter the risk decreases, whereas, SF indicates an increase in risk starting with the braking of the leader and reaches the maximum when the subject vehicle stops.

Trajectory planning systems often compare the risk levels of alternate trajectories to select the safer path (M. Wang et al., 2015). To verify if the selected indicators are capable of trajectory comparison, we simulate two evasive lane change trajectories A and B as possible alternative responses to the braking leader on a two-lane highway (one-way). Figure 2.3(b) shows the risk profiles calculated using various safety indicators when the follower adopts trajectory A. The follower trajectory A begins with deceleration at 5.2 s in response to the lead vehicle braking, followed by a left lane change beginning at 5.4 s and ending at 9.6 s when the vehicle reaches the left lane centre. Figure 2.3(c) shows the risk profiles calculated using various safety indicators when the follower adopts trajectory B (late lane change). The follower trajectory B begins with deceleration at 5.2 s in response to the lead vehicle braking, followed by a left lane change beginning at 6.4 s and ending centre of the left lane at 10.6 s. The lane change in two trajectories follows an S shaped path defined by a fifth degree polynomial parameterized by lane change duration of 4.3 s which is the typical value indicated in Samiee et al. (2016) and the lateral displacement 3.75 m which is the

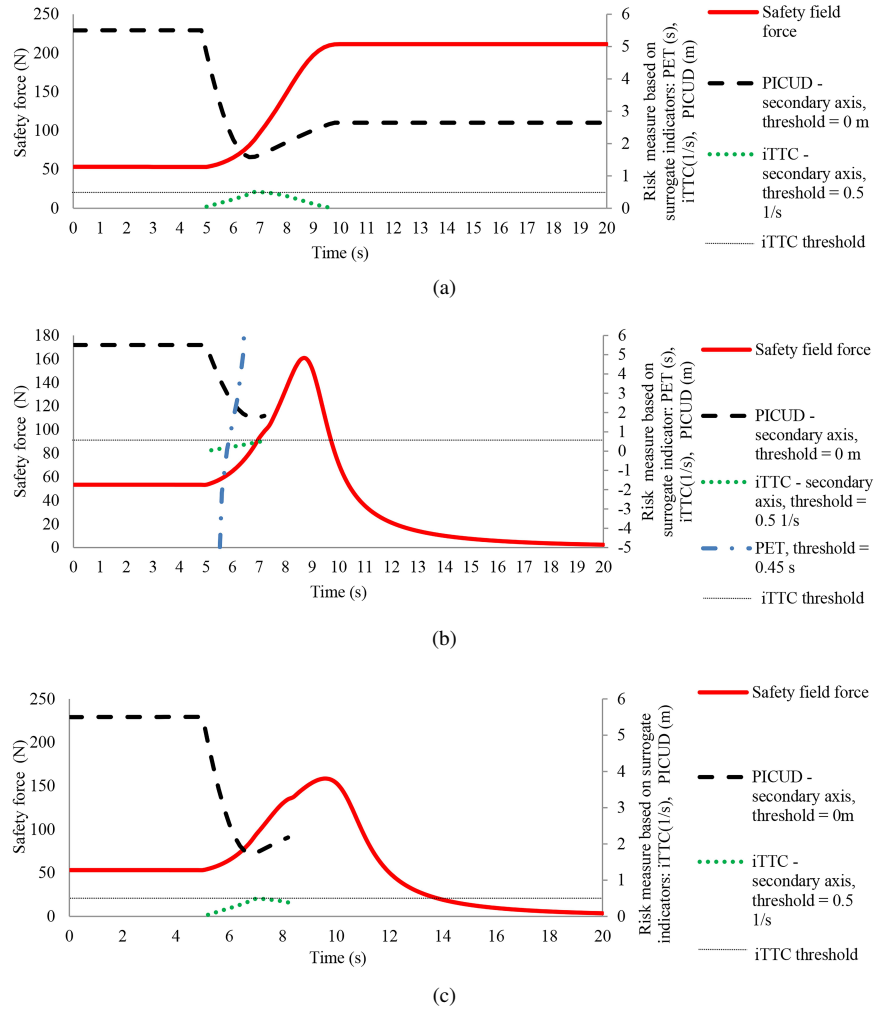


Figure 2.3: Results of case study 1: (a) when leader brakes and follower brakes to avoid a collision; (b) when leader brakes and follower changes lane via trajectory A (timely lane change); (c) when leader brakes and follower changes lane via trajectory B (late lane change).

typical lane width of a highway. The follower begins to accelerate once the lane boundary is crossed and finally passing the leader on the adjacent lane at 9 s (Trajectory A) and 10.2 s (Trajectory B). In both cases, PICUD and its show an increasing risk while approaching; however, they were discontinued after the lane change. PET shows a decreasing risk starting from the beginning of the lane change via Trajectory A. SF shows continuous risk variation throughout the evasive manoeuvre and indicates the highest risk corresponding to a passing manoeuvre (See Figure 2.3(b) and 2.3(c)). The SF indicates a lower risk peak for evasive lane change trajectory A compared to evasive braking (See Figure 2.3(a)). The total risk measure using SF (area under the plot) associated with trajectory B (late lane change) is higher compared to trajectory A (timely lane change). Note that the other indicators cannot be used for comparison as they are discontinuous over the simulated trajectory.

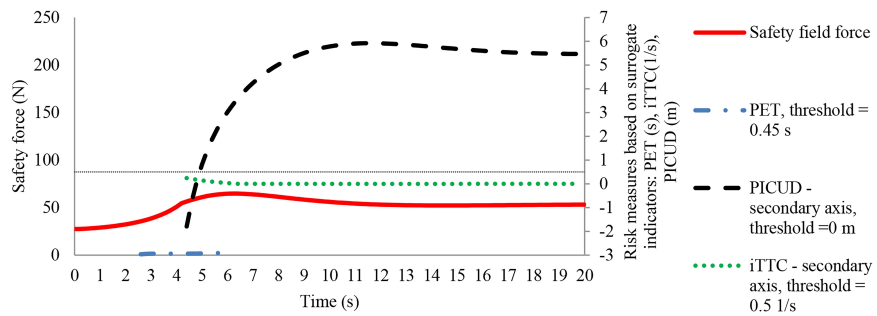
2.4.2 Case study 2

In this case study, we simulate a three-lane highway (one-way) with two vehicles (on the right and middle lanes) moving with a forward spacing of 10.5 m. The vehicle travelling ahead on the right lane starts to cut-in towards the middle lane at 2 s and reaches its centre at 6.2 s. We simulate the two possible evasive manoeuvres of the vehicle initially travelling behind in the middle lane. Risk profiles (using selected indicators) when the follower brakes are shown in Figure 2.4(a). PICUD and iTTC indicate the highest risk when cut-in is detected and decreases thereafter. PET indicates the highest risk earlier at the beginning of the cut-in and thereafter decreases. SF indicates risk from the beginning of cut-in; however the highest risk is indicated at a later point when the cut-in vehicle reaches the centre of the middle lane and thereafter decreases.

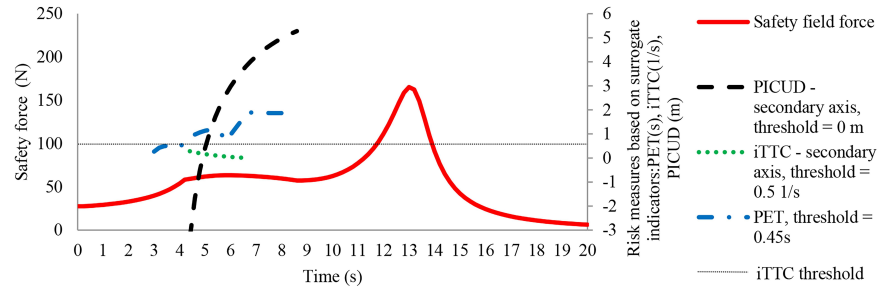
Risk profiles (in terms of selected indicators) when the follower performs evasive left lane change is shown in Figure 2.4(b). The follower begins to change lane at 6.4 s and reaches the left lane centre at 10.6 s. PICUD and iTTC indicate the highest risk as the leader cut-in is detected. However, they are not defined during the evasive lane change as there is no leader in the left lane. PET indicates increasing (yet below threshold) risk with leader cut-in. SF indicates the highest risk for passing manoeuvre (at 13.6 s) and reducing risk thereafter.

2.4.3 Findings of the simulation analysis

- The point in time corresponding to the highest risk for a manoeuvre differs with the risk measures. For example, PICUD and TTC indicate the highest risk corresponding to the point of cut-in whereas the SF indicates the point of passing to be the riskiest (See Figure 2.4).
- SMoS are defined for a collision course and hence have limited ability to capture the precautionary risk measure; on the contrary SF is able to indicate risk in the absence of a collision course, for example, a passing manoeuvre (See Figure 2.3 and Figure 2.4).
- SMoS are defined for the prescribed set of vehicle configurations and therefore indicate a sudden drop or rise in risk profile during a change in this vehicle configuration. For example, the risk measures by TTC and PICUD increase suddenly when a vehicle



(a)



(b)

Figure 2.4: Results of case study 2 (a) the leader cuts-in and follower brakes to avoid collision (b) the follower changes the lane to avoid collision

is detected ahead (See Figure 2.4(b) at 4.6 s). Additionally, from a control perspective, this is a false negative risk indication, i.e. the indicator wrongly suggests zero risk for a vehicle cutting-in ahead before being identified as a leader. We note that SF is free of this drawback as it is independent of vehicle configuration assumptions.

- Even though PET and SF describe the risk profile of lateral manoeuvres, the risk measures have limitations. The PET fluctuates throughout the manoeuvre (See Figure 2.4(b)) and does not discriminate near miss events where vehicle passes at a low lateral distance. On the contrary, in the present formulation of SF, inter-vehicle spacing hold a high weightage and therefore it consistently indicates the highest risk for lateral vehicle passing even if both vehicles follow their lane centre.

2.5 Discussion

As suggested in previous studies, the usefulness/validity of a safety indicator does not (only) depend on the extent to which expected accident numbers can be correctly estimated, but also on whether safety problems can be detected or not, and/or road safety countermeasures/treatments can be compared or evaluated (Laureshyn et al., 2016). In this study, we did not explore the empirical validity. We reviewed the indicators on the basis of their ability to theoretically represent the expected risk tendencies and to evaluate safety problems along simulated trajectories in critical highway situations.

From the perspective of vehicle control systems accounting for safety, it is of interest to have smooth and objective risk measures (Mullakkal-Babu et al., 2016). Simulation analysis showed that all the selected indicators are capable of delineating risk continuously in a one-dimensional interaction like car following. However, SMoS like iTTC, PET, WI and PICUD often display fluctuating or/and discontinuous values. For example, iTTC (and TTC) is undefined at $\delta v < 0$ (See Figure 2.2). The measured relative speed may oscillate from positive to negative due to sensing errors, and this will result in fluctuating risk measures and in turn the control signals based on them. Moreover, as shown in the simulation analysis, discontinuous risk measures cannot be used in trajectory planners to compare alternate trajectories. Secondly, these indicators do not possess mathematical properties that are desirable in a multivehicle scenario. Thirdly, benchmarking the safety level based on an indicator threshold value is difficult due to limited number of parameters considered by these indicators (Damerow & Eggert, 2014; Ni, 2013). This is because the threshold may vary with road characteristics, interacting vehicle type and driver reaction time. For example, a TTC that is considered safe on a high friction road could be deemed unsafe on a low friction or icy road. Moreover, most of the SMoS do not account for the conflict severity. Hence, the decision-making modules of intelligent vehicles using these indicators cannot identify the trajectory of lesser crash severity in an unavoidable collision situation. Finally, as shown in simulation analysis, indicators defined for a prescribed set of vehicle interaction configurations often lead to false negative risk measures.

Our findings also have implications in regard to the use of safety indicators for traffic safety assessment. The one-dimensional safety indicators yield partial insights in safety as they are only valid for a predefined set of vehicle interactions and do not account for collision severity. Additionally, these indicators cannot be used to estimate collective risk as

they do not possess the property of countable additivity. As reported in our simulation results, SMOs differ based on the threshold definition and underlying kinematic assumptions. This makes it difficult to reach an objective consensus on the safety impact. Finally the limitations of the lateral indicators like fluctuation (PET) and sensitivity to the spacing (SF) question the objectivity of safety assessments for multilane highways. SF can potentially be used to model precautionary measures taken by human drivers as it can describe risk despite a collision course.

All the studied safety indicators are based on underlying deterministic assumptions on the future kinematic state of the interacting vehicles, rather than acknowledging the uncertainty in vehicle movement. For example, consider a scenario where a vehicle follows a leader at a spacing of 1 m. This scenario would be deemed safe by a TTC indicator that is based on constant velocity assumption. However, this scenario cannot be regarded as safe if we consider the probability that the leader may brake. Even though the safety field approach does not depend on kinematic assumptions, it also does not explicitly account for uncertainties. Moreover, automated vehicles further contribute to the necessity of accounting vehicle uncertainty in the risk measures. Automated vehicles may attain more precise control as compared to manual driving, and may thereby safely pass at low distances; however the precision of automated vehicles will be affected by its perception quality. Therefore we note this inconsideration for uncertainties related to vehicle state is a drawback of these indicators.

Our study demonstrates the advantages of the safety field framework in depicting risk of two-dimensional vehicle interactions. Recently, J. Wang et al. (2015) demonstrated the use of an SF-based indicator for collision warning applicable in multivehicle scenarios (J. Wang et al., 2016). Moreover, if augmented with prediction paradigms, SF can be used for ex-ante safety evaluation in path planners. However, the formulation has to be fine-tuned or/and refined for practical applications. Unlike other SMOs, SF does not represent the collision causal mechanism, and therefore interpretation of the safety field risk measure could become ambiguous.

2.6 Conclusions and future research

In this study, we compared safety indicators based on their qualitative and quantitative aspects as a risk measure. Our results showed that all the selected indicators are capable of delineating risk continuously in a one-dimensional interaction like car following. Moreover, the selected safety indicators in general match the expected risk tendencies. However, in agreement with previous research (van Beinum et al., 2016; Gettman & Head, 2003; Kuang et al., 2015; Young et al., 2014; L. Zheng et al., 2014a) our findings acknowledge the mathematical limitations of selected safety indicators like discontinuity over the operational space, omission of uncertainty in vehicle state assumption and the inability to account for crash severity. We also note that all these indicators lack mathematical properties to account for multiple vehicles and the safety field framework is a promising approach that allows risk estimation in two-dimensional vehicle interactions. Our analysis could be further improved by verifying the findings using empirical accident data. Future research should also focus on defining a safety indicator addressing the limitations of existing indicators found in this study.



Chapter 3

Probabilistic field approach for motorway driving risk assessment

Abstract

We present an approach to assess the risk taken by an individual vehicle during on-road driving. The driving risk is defined as a Surrogate Measure of Safety characterising a conflict event: a safety-critical situation that occurs prior to a crash event. The assessment approach is developed within the framework of artificial field theory, envisioned for safety analysis and design of driving (support/automation) applications. Here, any obstacle (neighbouring entity on the road) to the subject vehicle is treated as a finite scalar risk field that is formulated in the predicted configuration space of the subject vehicle. The driving risk estimate is the strength of the risk field at the subject vehicles location. This risk field is formulated as the product of two factors: expected crash energy (as an approximation of consequences) and the collision probability. The collision probability with a movable obstacle (vehicle) is estimated based on probabilistic motion predictions. The subject and neighbouring vehicles possible positions at discrete future time steps are predicted. Thereby, the risk can be assessed for a single time step or over multiple future time steps, depending on the required temporal resolution of the estimates. The properties of the risk estimates are mathematically evaluated. We applied the single step approach to assess the driving risk in three near-crash situations selected from a naturalistic dataset. The risk description qualitatively reflects the narration of the situation. Additionally, we applied the multi-step approach to estimate the risk along four possible trajectories while approaching a lane drop section. The risk estimates along the trajectory plans clearly marked the safest trajectory. The results of both example sets show that the risk trends, in general, are consistent with Time To Collision (a prominent surrogate measure of safety). The proposed risk estimate provides a better basis to assess the driving safety of an individual vehicle by considering the uncertainty over the future ambient traffic state and magnitude of expected crash consequences. Therefore, the proposed driving risk model could potentially be used as a component of integrated vehicle safety applications and as a supplementary surrogate measure of safety.

This chapter is based on the following article, which is currently under review:

Mullakkal-Babu, F. A., Wang, M., van Arem, B., & Happee, R. (under review)
Probabilistic field approach for motorway driving risk assessment

3.1 Introduction

Safety analysis of observed interactions between road users has been a prominent subject of traffic research. Traffic safety analysis has identified several factors which correlate with crash statistics and yield useful insights on collective traffic safety. Currently, an increasing research attention is being put into model driving safety, i.e. the safety of an individual vehicle during on-road driving. Driving safety models are key components of various integrated vehicle driving applications such as collision warning/avoidance systems and advanced automated vehicle control systems. Modelling driving safety entails a detailed description of the subject vehicle and its environment, and careful consideration of the crash mechanism. Fortunately, safety analysts now have the means to scrutinise driving at a far more detailed level; thanks to the high resolution driving data provided by the modern sensing and communication technologies. However, the conventional methods of traffic safety analysis are often inadequate to examine safety at this level of detail. In this context, we explore the possibility of developing an assessment method for driving safety (converse risk). Such a method could be used to assess the risk of human driving, and to evaluate (and design) proactive safety systems and advanced vehicle control systems. Towards this, we survey the relevant literature from the safety analysis domain and review methods for modelling driving risk.

The risk faced by an individual vehicle during on-road driving can be described by measures used for traffic safety analysis. These measures indicate a conflict between two road users. The underlying hypothesis is that a crash process is a temporal sequence of events in which a conflict event occurs prior to a crash event (Laureshyn et al., 2016). Defining crash process this way provides theoretical credibility for traffic safety predictions. Since conflicts and crashes are aligned on the same continuum of events, the frequency of the low-risk events (conflicts) can be used to predict the high-risk events (crashes) (Laureshyn et al., 2016). Such measures are known as Surrogate Measures of Safety (SMoS) as they characterise the initial conditions of a regular (non-crash) event as a surrogate for the crash event.

During on-road driving, the surrounding traffic environment, i.e. neighbouring road users and their relative states, can vary dynamically. Therefore, to monitor the risk on a sustained basis, the driving risk should be estimated continuously in time. The SMoS, which are defined based on the predicted motions of interacting road users, are suitable for this purpose, i.e. they can be calculated at each moment during an encounter. Examples include Time To Collision (TTC), Time Headway, Time to Lane Crossing (TLC). There exists an extensive set of such SMoS, and among them, TTC has been employed widely as an ex-ante driving risk estimate in collision avoidance systems and collision warning systems (Kiefer et al., 2005; Moon et al., 2009). Besides, continuous risk measurement provides valuable information for safety analysis: the evolution and critical moments during the crash process. Yet, continuity does not always guarantee a finite risk measure. For instance, TTC (the ratio of spacing to the relative velocity between two interacting bodies) is undefined when the relative velocity is non-positive. This problem is tackled by combining multiple continuous measures for collision warning/avoidance applications (Moon et al., 2009) and for safety analysis (Laureshyn et al., 2010). Accordingly, the driving risk can be continuously estimated by combining multiple predictive SMoS.

The subject road user, is not certain about the future motion of its neighbouring road

users and consequent crash outcome. Uncertainty, therefore, is an inherent component of the driving risk estimate. Advanced vehicle control systems should consider this uncertainty over the future state of the surrounding traffic environment to find a robust risk mitigation plan. SMOs do not typically account for this uncertainty. They assume a deterministic future motion, i.e. motion with unchanged velocity/acceleration. There exist several probabilistic approaches in safety analysis literature to calculate SMOs while taking the motion uncertainty into account. The causal model treats crash probability as a mixture of the probability of multiple sets of initial conditions and the mixing probabilities are governed by the evasive action (G. A. Davis et al., 2011; Kuang et al., 2015). However, estimating the probability distributions for an exhaustive list of initial conditions and evasive actions is challenging, particularly while considering two-dimensional vehicle motion (Young et al., 2014). An alternate approach is to define a finite set of trajectories that the interacting road users could possibly follow, and assign a likelihood to each trajectory. Accordingly, Saunier & Sayed (2009) proposed a probabilistic approach in which the set of prototype motion patterns and their occurrence likelihood are generated by machine learning model. The model is trained over a set of road user trajectories observed from the roadside (Mohamed & Saunier, 2013; Saunier & Sayed, 2009). This approach is particularly beneficial at intersections, as the motion predictions reflect the situational context such as the turning movement. Collision avoidance theory provides an exhaustive approach to generate a set of motion predictions: as a tree of possible paths (Jansson, 2005). Here, the predicted time and acceleration space (control variable) are discretised. The vehicle is assumed to maintain a constant acceleration during a time step. Such an exhaustive prediction approach provides a powerful reference to evaluate the control designs offline. But a long prediction horizon is computationally inhibiting in online applications, as the number of trajectory predictions increases exponentially with the prediction horizon. Here, the likelihood of each predicted path is derived from the likelihood of an underlying sequence of acceleration signals. The probability function of acceleration typically takes the form of a normal distribution and its standard deviation is known as the acceleration noise. Remarkably, the acceleration variation has been found to be related to driving risk (Osafune et al., 2016). A driver who drives faster than the traffic stream exposes himself to a higher crash risk (Aarts & Van Schagen, 2006) and is observed to have a significantly higher acceleration noise (Herman et al., 1959) than a driver following the traffic stream. A congested traffic flow results in a higher frequency of traffic conflicts (Qu et al., 2015) and also increases the acceleration noise (Jones & Potts, 1962; J. Ko et al., 2010). Wind and sharp horizontal curves increase both the driving risk (Schneider et al., 2009) and the acceleration noise (Jones & Potts, 1962). Compared to sampling-based and machine learning methods, using a numerical estimate of uncertainty based on acceleration noise have benefits of control design: its distribution parameters can be estimated by monitoring the vehicle over a finite stretch (Jones & Potts, 1962) or logged by the vehicles onboard sensors (accelerometers) (Khattak & Wali, 2017; J. Ko et al., 2010); it is analytically tractable and allows mathematical evaluation.

The consequence of crash - crash severity - is another important factor constituting the driving risk. Advanced vehicle controllers can weigh possible evasive actions based on crash severity (Jansson, 2005). Even if a crash is unavoidable despite any possible evasive manoeuvre, it might still be possible to reduce the potential consequence, for instance, by reducing the speed (Jansson, 2005). Moreover, crash severity is important to traffic analysis: safety policies such as Vision Zero aim to eliminate not all but the most severe injury crashes

(Johansson, 2009). Crash severity, however, is typically not accounted by continuous SMoS. Therefore, safety analysis studies often segregate conflicts based on the type of involving road users: conflicts solely involving motor vehicles and conflicts involving vulnerable road users. Alternatively, the crash severity can be approximated using factors derived from the Newtonian model of crash mechanics. Delta-V (collision induced speed change) is a factor that is correlated with crash severity (L. Evans, 1994; Lareshyn et al., 2017; Shelby, 2011). Another such factor is the crash energy, which is expected in case of a collision (Damerow & Eggert, 2014). Alternatively, such factors can be integrated into the formulation of a surrogate measure of safety (Lareshyn et al., 2017).

The artificial potential field is a prominent paradigm used to tackle vehicle and robot navigation (Dunias, 1996). The attractive feature is that it allows the vehicle to autonomously navigate using only its location and local sensor measurements. In this paradigm, an obstacle to the vehicle is modelled as a repulsive potential field (or risk field). The vehicle can use the field gradient at its location to generate control actions to navigate while avoiding the obstacle. J. Wang et al. (2015) used the field paradigm to model driving risk accounting for the influence of driver, vehicle and road characteristics. Later, this model was extended and applied in a rear-end crash avoidance system (J. Wang et al., 2016). However, the model cannot be directly used for traffic safety analysis, as it is not objectively formulated using factors correlated to crash statistics. The artificial potential field theory, therefore, offers a paradigm to develop a generic driving risk assessment approach which could be applied for vehicle control and for traffic safety analysis (Mullakkal-Babu et al., 2017).

Using the paradigm of artificial field theory, in this work, we present an approach to assess the driving risk of an individual vehicle. The driving risk estimate constitutes a crash severity term and a collision probability term. To estimate the collision probability, the subject and neighbouring vehicles possible positions and associated probabilities at discrete future time steps are predicted. Thereby, the risk can be estimated for a single time step or over multiple future time steps, depending on the required temporal resolution. We illustrate the application of the single-step approach to assessing the safety of human driver interaction. Here we use sample trajectories from a public near-crash dataset. Additionally, we apply multi-step risk to evaluate the risk along four trajectory options to the subject vehicle while approaching a lane drop. This set of trajectory exemplifies the plans generated by an advanced vehicle controller.

3.2 Modelling driving risk

In this section, we develop the model for driving risk based on the artificial risk field theory. We first introduce the definition of driving risk, and thereafter present the models of the risk fields and their mathematical properties.

The risk is an abstract entity and requires a specific definition to be operationalised. Risk, in general, is defined as the magnitude of the consequences of an action that is taken in spite of uncertainty. In this study, we interpret this definition as follows: for an encounter between the subject vehicle and a road obstacle, driving risk is defined as the consequence to which the subject exposes itself by maintaining its present kinematic state in spite of the uncertainty that the obstacles future motion may (or may not) lead them to collide. Hereafter, driving risk will be simply be referred to as risk.

Any obstacle that the subject vehicle encounters while driving on the road is formulated as a risk field in the configuration space of the subject vehicle. The strength of the risk field at a spatial point around the obstacle can be formulated as the product of the crash severity and collision probability with the subject. The collision probability ranges from 0 - 1 and reflects the variation of risk field strength around the obstacle. It is determined by the initial states and the future motion of the subject and the obstacles. The crash severity determines the amplitude of the risk field strength, such that the crash severity posed by a heavy vehicle would be higher than that by a lighter car. The subject often encounters multiple obstacles in traffic such as vehicles and the road boundaries. Here, the net risk taken by the subject vehicle can be quantified as a single measure by adding the strengths of multiple risk fields (superposition). The risk field model, that operationalises the above risk definition, should meet the following functional specifications (Dunias, 1996): S1) the strength of the risk field around an obstacle should represent the severity of the crash, weighted by the probability of crash occurrence and should possess a finite maximum of risk (\bar{R}); S2) the risk field around an obstacle should possess a continuous gradient; S3) the risk field around an obstacle should exhibit no other maxima, except at the obstacles expected position; S4) the risk field should be restricted to a finite area; S5) the risk field should enclose the geometric shape of the obstacles.

3.2.1 On-road obstacles

In this study, the road space is considered as a flat Euclidian plane consisting of road surface markings. The axis X is in the direction of the vehicle movement and is aligned along the outer lane marking, and the axis Y is in the direction perpendicular (counter-clockwise) to the outer lane marking. We define two types of on-road obstacles: road boundary objects existing outside the driving lane such as medians, roadside barriers; and movable obstacles such as vehicles. This classification is similar to the one used by J. Wang et al. (2016). All the road boundary objects are treated as an immovable entity, and medians and barriers are modelled as finite line segments parallel to the X axis, and those such as roadside trees and poles are modelled as point masses. Vehicles are modelled as a rectangle with its length denoted as L and width denoted as W , and possess a finite physical mass. The dynamic state of a vehicle i is described in global coordinates by the position of its centre of mass $P = [X_i, Y_i]^T$ and velocity $V = [V_{Xi}, V_{Yi}]^T$ with V_{Xi} and V_{Yi} respectively denoting the longitudinal and lateral components of the velocity. A vehicle is treated as a control system whose state is manipulated by its controller. Accordingly, the state of the vehicle i is manipulated by the control input/variable which is acceleration $A = [A_{Xi}, A_{Yi}]^T$ with A_{Xi} and A_{Yi} respectively denoting the longitudinal and lateral components of the acceleration. In order to predict the evolution of the vehicle state, the dynamic behaviour of the vehicle is modelled as the following differential equation:

$$\frac{d}{dt} \begin{pmatrix} P \\ V \end{pmatrix} = \begin{bmatrix} 0 & 1 \\ 0 & 0 \end{bmatrix} \cdot \begin{pmatrix} P \\ V \end{pmatrix} + \begin{pmatrix} 0 \\ 1 \end{pmatrix} \cdot A \quad (3.1)$$

The vehicle motion is subject to physical constraints. We emulate them in the vehicle model as a set of constraints: $-0.17V_X \leq V_Y \leq 0.17V_X$ representing the non-holonomic behaviour of the vehicle. This condition assumes that the vehicle heading angle $\beta = \arctan\left(\frac{V_Y}{V_X}\right)$ is

bounded as $|\beta| \leq 10^\circ$, during motorway driving; 2) $V_X \geq 0$ representing the strictly forward movement; 3) $A_X^{\min} \leq A_X \leq A_X^{\max}$ representing the feasible acceleration range that is restricted by the engine power and brake torque limitations.

The risk fields presented in this work are named Probabilistic Driving Risk Field (PDRF). The road boundary objects are modelled as the potential PDRF and vehicles are modelled as the kinetic PDRF. The risk estimate is the strength of PDRF at the location of the vehicle under consideration, s . Accordingly, at a given moment s takes a total risk R which is comprised of potential risk (total potential PDRF strength) R_B from multiple road boundary objects and kinetic risk (total kinetic PDRF strength) R_N from multiple dynamic road objects as follows:

$$\begin{aligned} R &= R_B + R_N \\ &= \sum R_b + \sum R_n \end{aligned} \quad (3.2)$$

where b denotes an individual road boundary object and n denotes the individual vehicle. Based on the superposition property of fields, the total risk model of (3.2) combines risk posed by multiple road obstacles into a single measure. This implies that the risk posed by an obstacle is assumed to be independent of the risk posed by another obstacle. The risk model (3.2) will meet the specification S1 if R_b and R_n are formulated as the product of crash severity and collision probability. Vehicle crashes are not perfectly elastic (collision with no loss of net kinetic energy); and some part of the kinetic energy is dissipated as thermal energy, sound energy, and material deformation. Given a crash, the portion of dissipated energy that is spent on deforming s is termed as expected crash energy. We use expected crash energy as the approximation of crash severity. The collision probability will be specifically formulated for the two obstacle types.

3.2.2 Modelling the road boundary object as a risk field

The potential risk taken by s due to a fixed road boundary object b is modelled as follows:

$$R_{b,s} = 0.5kM(V_{s,b})^2 \cdot \max \left(e^{\left(\frac{-|r_{s,b}|}{D} \right)}, 0.001 \right) \quad (3.3)$$

where $R_{b,s}$ denotes the strength of the PDRF due to the road boundary object b ; M denotes the mass of s ; $r_{s,b}$ is a vector that denotes the shortest distance between s (point mass at the centre of mass) and b ; and $V_{s,b}$ denotes the velocity of s along $r_{s,b}$. The potential risk $R_{b,s}$ can be separated into two terms: a crash severity term and a collision probability term. The crash severity term, $0.5kM(V_{s,b})^2$ denotes the expected crash energy scaled by the parameter k , with range [0-1], representing the rigidity of the road boundary object. Accordingly, $k = 1$ when b is immovable with infinite mass; and $k = 0$ when b is very compliant and effectively dissipates the crash energy. Among road boundary objects, the cable barrier, in general, dissipates the highest amount of energy; followed by the guardrail, the concrete median and any fixed objects such as trees and roadside poles. The assumption that b dissipates a portion of the crash energy, lowering the crash severity is consistent with findings by

Zou et al. (2014). The collision probability term $e^{\left(\frac{-|r_{s,b}|}{D} \right)}$ ranges between [0-1], where the coefficient D determines the steepness of descent of the potential risk field. This term attains

the maximum of 1 at $r_{s,b} = 0$ and depicts a decrease in crash probability with an increase in $r_{s,b}$. This is intuitive; a road object further away offers more possibility for the driver to avoid the collision. This hypothesis is consistent with the empirical studies that demonstrate that an increase in the offset of the road object reduces the odds of collision (Zou et al., 2014).

Therefore, the model of R_b in (3.3) meets S1. The gradient $\frac{dR_b}{dr_{s,b}} = -0.5kM(V_{s,b})^2 \cdot \frac{e^{\left(\frac{-|r_{s,b}|}{D}\right)}}{D}$ is a continuous and a decreasing function of $r_{s,b}$; and the risk reaches a finite maximum $R_b = 0.5Mk(V_{s,b})^2$ solely at the position of b when $r_{s,b} = 0$. The influence of R_b is restricted to a finite area by two means. First, we truncate the function of (3.3) at the lower value of 0.001. Second, we set $D = (\text{Lanewidth})/14$ meaning that collision probability term attains a marginal value ($0.00091 \approx 0.001$) at the lane centre. It can be seen that R_b satisfies all the functional specifications. Figure 3.1 illustrates the sensitivity of the parameter k and the offset of b on the potential risk.

3.2.3 Modelling the neighbouring vehicle as a risk field

The kinetic risk taken by s due to a neighbouring vehicle is modelled as follows

$$R_{n,s} = 0.5M_s\beta^2|\Delta V_{s,n}|^2 \cdot p(n,s) \quad (3.4)$$

where $R_{n,s}$ denotes the strength of the kinetic PDRF due to the vehicle n ; $|\Delta V_{s,n}| = |V_s - V_n|$ denotes the counteracting velocity between s and n ; $\beta = \frac{M_n}{M_s + M_n}$ denotes the mass

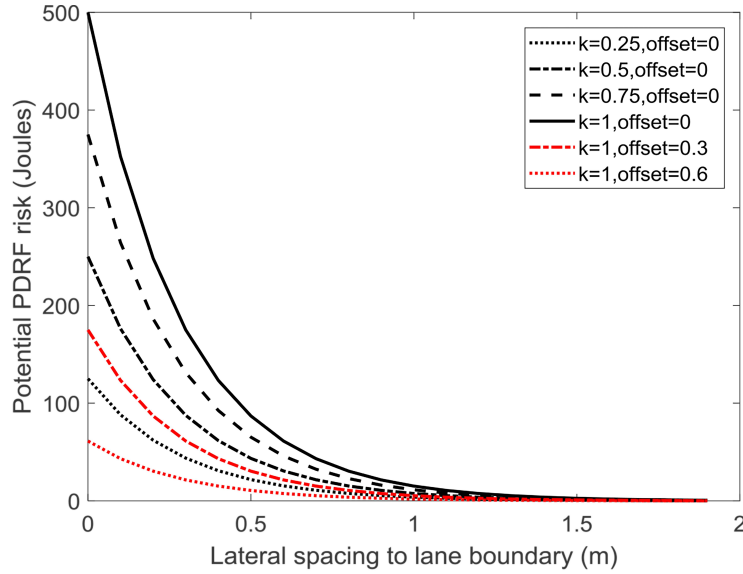


Figure 3.1: The variation of potential PDRF strength due to the road boundary object over lateral positions within the lane. The black line represents potential PDRF strength for different k and red represents the potential PDRF strength for different offsets of the road boundary object.

ratio. The kinetic risk, $R_{n,s}$ can be separated into two terms: a crash severity term and a collision probability term. The crash severity term: $0.5M_s\beta^2|\Delta V_{s,n}|^2$ describes the portion of expected crash energy that has to be absorbed by s if it collides with n . The collision process is assumed to be inelastic where both the vehicles move together after their first contact. Here, the division of crash energy is inversely proportional to the individual mass. Therefore a lighter vehicle will dissipate more energy than a heavier vehicle. The second term $p(n,s)$ with range $[0, 1]$ denotes the crash probability. According to the model of (3.4), when $p(n,s) = 1$, $R_{n,s}$ attains a finite maximum $R_{n,s} = 0.5M|\Delta V_{s,n}|^2$, i.e. expected crash energy.

A vehicle, unlike a road boundary object, is a movable entity and therefore the collision probability term in Eq.(3.4) takes account of the dynamic nature of the interaction. We operationalise the risk definition as follows: risk is the consequence of s maintaining its state (single motion prediction assuming an acceleration signal, $A = 0 \text{ m/s}^2$), despite the unknown motion of n (a continuous range of acceleration signals $A \in \{A^{\min}, A^{\max}\}$). Earlier studies have used constant acceleration heuristics to calculate TTC along a single motion prediction (Happee et al., 2017); but here we consider a range of motions possible to n .

Given the above future motion of s and n , we now estimate the probability of collision. To illustrate the estimation approach, we initially treat vehicles as floating point masses. Two point mass vehicles collide if they appear in the same position at a given time. In this work, we estimate the collision probability at a single future time instant; therefore the collision probability is merely related to the chances of a spatial overlap. Accordingly, we use the prediction time step τ as an estimation parameter, and $p(n,s|\tau)$ denotes the probability of collision (spatial overlap) between n and s at a future time $t_0 + \tau$. To estimate $p(n,s|\tau)$, we only use the predicted position of s and the range of predicted positions of n at $t_0 + \tau$. This predicted approach can be viewed as the simplest case in the tree of possible paths: with a single time step τ which is also the prediction horizon. Note that this collision probability estimate is conceptually different from SMOs such as TTC, which approximates the probability of a spatial and temporal overlap. A human driver requires a finite duration commonly referred to as the reaction time (Treiber et al., 2006) to sense, perceive, decide and act to stimuli. Therefore, s is unaware and unresponsive to the action of n within this reaction time. It must be noted that s cannot perceive kinetic risk estimated for τ shorter than its reaction time.

The probability of motion predictions is attributed to the underlying acceleration signal. The probability functions of acceleration variability can be estimated by treating acceleration signals as a random variable (Wagner et al., 2015). We assume acceleration variability to follow a normal distribution (J. Ko et al., 2010). Accordingly, the expected motion (i.e. The vehicle motion, assuming the acceleration signal equal to the mean of the acceleration variability distribution, typically 0 m/s^2) is associated with the highest probability, and those motions, assuming acceleration signals that are three standard deviations away from the mean, are associated with a probability less than 0.001. The parameters of this distribution can be estimated as follows:

$$\mu_A = \frac{1}{T} \int_0^T A(t) \cdot dt; \sigma_A^2 = \frac{1}{T} \int_0^T [A(t) - \mu_A]^2 \cdot dt \quad (3.5)$$

where μ_A denotes the mean acceleration; σ_A denotes the standard deviation of the acceleration (acceleration noise) and T denotes the sampling time duration. The acceleration noise when a vehicle is stopped in traffic is zero, which might distort its estimated value; therefore the acceleration noise should be measured only while the vehicle is moving (Jones & Potts, 1962). The absolute probability of a continuous random variable to take a particular value is 0, and it can only be determined for a particular range, which will be defined in the next section by accounting for the vehicle geometry. However, in this section, we express each vehicle as an infinitesimally small point mass, for illustrating the concept and evaluating the mathematical properties. Here, the value of the acceleration variability distribution for a particular value of acceleration is interpreted as the relative likelihood of occurrence. We tentatively consider collision likelihood defined as the relative likelihood of n applying acceleration: $A_{X,n} = \frac{\Delta X - \Delta V_X \cdot \tau}{\tau^2}$ and $A_{Y,n} = \frac{\Delta Y - \Delta V_Y \cdot \tau}{\tau^2}$. Considering $A_{X,n}$ and $A_{Y,n}$ as random variables, the collision likelihood p_L can be defined as follows:

$$p_L(n, s | \tau) = \mathcal{N}\left(\frac{\Delta X - \Delta V_X \cdot \tau}{0.5 \cdot \tau^2} \middle| \mu_X, \sigma_X\right) \cdot \left(\mathcal{N}\frac{\Delta Y - \Delta V_Y \cdot \tau}{0.5 \cdot \tau^2} \middle| \mu_Y, \sigma_Y\right) \quad (3.6)$$

where \mathcal{N} is the probability density function, and its parameters μ denotes the mean and σ denotes the standard deviation of the distribution; $\Delta X = X_s - X_n$ and $\Delta Y = Y_s - Y_n$ denotes the relative spacing, and $\Delta V_X = V_{X,s} - V_{X,n}$; $\Delta V_Y = V_{Y,s} - V_{Y,n}$ denotes the relative velocity in longitudinal and lateral directions. By substituting for $p(n, s)$ in in Eq.(3.4) with p_L in Eq.(3.6), we obtain a specific form of $R_{n,s}$. Thereby, $\frac{dR_n}{d\Delta X_{s,n}}$ and $\frac{dR_n}{d\Delta Y_{s,n}}$ are continuous and decreasing functions of $\Delta X_{s,n}$ and $\Delta Y_{s,n}$ respectively for $\tau > 0$. According to the model of (3.4), the kinetic risk attains finite maximum $R_{n,s} = 0.5M_n\beta|\Delta V_{s,n}|^2$ solely when $\frac{\Delta X - \Delta V_X \cdot \tau}{\tau^2} = \mu_{A_X}$ and $\frac{\Delta Y - \Delta V_Y \cdot \tau}{\tau^2} = \mu_{A_Y}$, i.e. the future position of s and the expected position of n overlaps. Thereby, R_n satisfies S1, S2 and S3. The contours in Figure 3.2 represent the relative positions of s around n where the collision likelihood is the same. As described in the introduction, the acceleration noise can be impacted by road, traffic state and driver-related factors. It can be seen that the PDRF approach relates an increase in acceleration noise to an increased region of risk; the region of high collision likelihood widens with an increase in the acceleration noise (See Figure 3.2(b) and (c)). Furthermore, it can be seen that the collision likelihood is sensitive to the parameter τ (See Figure 3.2(d)).

3.2.4 Incorporating the vehicle geometry and motion constraints

We introduced the kinetic PDRF field based on the estimates of collision likelihood between point mass vehicles, treating the acceleration signal as a continuous random variable. However, the vehicle possesses a finite geometry and the probability of continuous random variable can only be estimated over a range. In this section, we specify the collision probability of the vehicle model specified in section 3.2.1 (rectangular geometry and constrained motion). Imposing the motion constraints in section 3.2.1, the boundary of the reachable state of n at time $t_0 + \tau$ can be represented as quadrilateral polygon Q . Using the predicted position of s at $t_0 + \tau$ along with the geometry of the two vehicles, we define the potential collision zone: Z . Thereby, the collision probability is non zero if there exists an overlap in Q and Z . The overlapping region is another polygon denoted by O defined in the spatial domain. The calculation of Q , Z and O are provided as an implementable algorithm in the appendix A.

The overlap O in the spatial domain has to be converted to acceleration domain denoted A^O for probability estimation by using the following relation.

$$A_X^c = \frac{(X^c - X_n(0)) - V_{X,n}(0) \cdot \tau}{0.5 \cdot \tau^2}, A_Y^c = \frac{(Y^c - Y_n(0)) - V_{Y,n}(0) \cdot \tau}{0.5 \cdot \tau^2} \quad (3.7)$$

where X^c, Y^c denotes the corner positions of O , and A_X^c, A_Y^c denotes the corresponding corners of A^O . Eq 3.7 specifies a linear relationship between acceleration coordinates and the spatial coordinates, and therefore A^O is also a quadrilateral polygon. Then the collision probability can be obtained by integrating the joint acceleration variability distribution over A^O as follows:

$$p(n, s | \tau) = \mathcal{N}(dA_X \cdot dA_Y) \quad (3.8)$$

By bounding the reachability of based on motion constraints and incorporating the vehicle geometry we ensure that R_n satisfies the specifications S4 and S5.

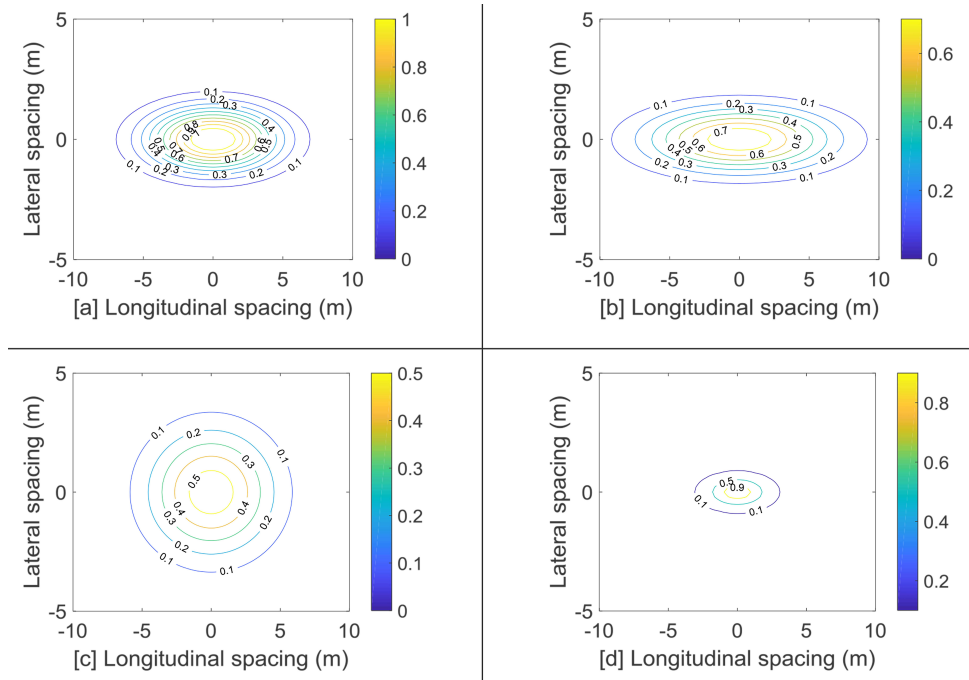


Figure 3.2: Collision likelihood contours around n , for a subject travelling at the same speed in forward direction: (a) n with longitudinal acceleration noise $\sigma_X = 0.7$ and lateral acceleration noise $\sigma_Y = 0.2$ prediction time step $\tau = 3$; (b) n with a relatively high longitudinal acceleration noise $\sigma_X = 1$; (c) n with a relatively high lateral acceleration noise $\sigma_Y = 0.4$; and (d) collision likelihood contours for a shorter prediction time step $\tau = 2$

3.2.5 Estimating risk over multiple time steps

In the previous sections, we described the procedure to estimate risk based on collision probability for one fixed time step. Such a risk estimate is intended to assess the driving safety of human drivers from observed vehicle interactions; and to be used as a trigger for collision warning/avoidance systems. However, advanced vehicle control systems plan the vehicle trajectory as a function of future time step. Therefore, risk estimates over a sequence of future time steps are necessary to create and to evaluate such trajectory plans. The single-step PDRF approach is inadequate for this purpose, and therefore, we extend the definition of the PDRF model. The total risk taken by s at each time step t_k is $R^T(t_k)$ which is defined as follows:

$$\begin{aligned} R^T(t_k) &= R_B^T(t_k) + R_N^T(t_k) \\ &= \sum R_b^T(t_k) + \sum R_n^T(t_k) \end{aligned} \quad (3.9)$$

where $R_B^T(t_k)$ denotes the potential risk (total potential PDRF strength) at time t_k due to the presence of road boundaries; and $R_N^T(t_k)$ denotes the kinetic risk (total kinetic PDRF strength) at time t_k due to the presence of neighbouring moving objects. $R_b^T(t_k)$ is the potential risk due to the individual road boundary object b and is equivalent to R_b (modelled in (3.3)) calculated at t_k using the expected conditions at the time t_k . For path planning purposes, in addition to the road boundary objects that can inflict physical crash energy, it might be of interest to formulate virtual road objects such as lane marking as artificial risk fields. This can be achieved by adjusting the value of the scaling parameter k to match the subjective level of risk attached to the lane marking type.

In order to extend the model (3.2) towards generating risk estimates over multiple time steps as in Eq. (3.9), three questions must be answered: 1) How to predict the possible motions of over multiple time steps? 2) How to determine the probability of these motion predictions? 3) How to estimate the collision probability under a probabilistic setting? The answer to the third question can be obtained from the work of Saunier et al. (2010). They illustrated a procedure to identify the collision points along a pair of motion predictions, and thereby to express collision probability as the discrete sum over a finite number of collision points. Whereas, questions one and two can only be answered by considering the envisaged application.

The multi-step prediction is envisaged to estimate the safety of trajectory plans. Trajectory planning is done when the subject vehicle s is operated by an advanced vehicle control system. The motion possibilities of neighbouring vehicles are predicted by a scheme which employs two functions. 1) an acceleration plan which is defined as the discrete time series of expected acceleration signals that spans for a finite prediction horizon. 2) the spread of the acceleration signal at each time step along the discrete time series. The acceleration signal at each time step is considered as a random variable whose variability distribution is parameterised by the expected acceleration and its spread. The horizon of an acceleration plan determines the length of the trajectory prediction and spread determines the spatial spread of the predicted trajectory set. In this work, the multi-step approach is used to assess the risk of trajectory plans. However, an advanced vehicle control system can use this approach to evaluate the safety of its candidate trajectory plans. For this, the system should predict the acceleration plan of n (using manoeuvre prediction algorithms) and the spread in acceleration signals (using on-board measuring and estimation systems).

We answer the first question by describing the approach to predict the motion of n over

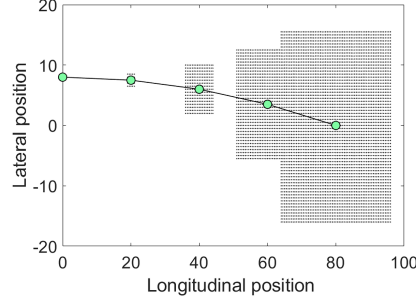


Figure 3.3: Illustration of multi-step prediction scheme for vehicle n starting from the initial position $[0, 8]^T$ and an initial velocity $[20, 0]^T$. The black dots represent the entire set of predicted positions at each prediction time step; the green dots represent the expected positions of at each time step according to the acceleration plan and variability distribution; and the black line connecting the green dots represents the expected trajectory instance.

multiple time steps. According to the risk definition, if s maintains its trajectory plan and would be exposed to the consequence of the uncertain motion of n (a finite set of trajectory predictions). The trajectory of a road user i is denoted as $T_i(t) = (X_i(t), Y_i(t))$. $\hat{T}_s^H(t_k) \forall k \in 0, 1, \dots, H$ is the single trajectory plan of s in time discrete form, with k as the prediction time instance and H as the total number of prediction time steps; $\{\hat{T}_{n,m}^H(t_k)\} \forall k \in 0, 1, \dots, H; m \in 0, 1, \dots, M$ denotes the finite set of possible trajectories of n , where m denotes the trajectory instance and M denotes the total number of predictions. The motion possibilities of n are predicted as a tree of possible paths (Jansson, 2005). To predict one trajectory instance, a pair of the acceleration signal (A_X, A_Y) is assigned to n at the beginning of each time step, and thereafter it is propagated using the assigned acceleration during the time step. In this study, we use a set of 25 unique pairs of acceleration inputs, i.e. all possible combination among the 5 values (with an interval of 1 m/s²) of A_X and A_Y . At each time step, all the previous end states are assigned this set of accelerations and they are further updated. This process is done iteratively at each time step till the end of the prediction horizon ($H = 4$ s in this work) and results in a set of 390625 trajectories. After that, we impose motion constraints to the predicted trajectory set to eliminate the infeasible trajectories.

Now we answer the second question by describing the method to assign a probability to each trajectory instance within the finite set of predictions using the acceleration probability distribution. Since the trajectory predictions are finite, we convert the continuous probability density function to discrete probability mass function. The discretisation interval is 1 m/s², corresponding to the acceleration interval used for motion prediction. Thereby, the probability assigned to each trajectory prediction is the scalar product of individual probabilities of the underlying sequence of acceleration signals. Figure 3.3 provides an example illustration of this prediction scheme. The initial position of n is $[0, 8]^T$ and the velocity is $[20, 0]^T$. The acceleration plan of n is $\hat{A}_X(t_k) = 0 \forall k \in \{1, 2, 3, 4\}$ and $\hat{A}_Y(t_k) = -1 \forall k \in \{1, 2, 3, 4\}$. The acceleration variability distributions follow a discrete normal distribution as follows: $A_X^d(t_k) = \mathcal{N}^d(\hat{A}_X(t_k), 0.7) \forall k \in \{1, 2, 3, 4\}$ and $A_Y^d(t_k) = \mathcal{N}^d(\hat{A}_Y(t_k), 0.7) \forall k \in \{1, 2, 3, 4\}$

We now deploy the approach proposed by Saunier & Sayed (2009) to estimate the crash probability for a finite set of trajectory predictions. Towards this, we first define collision event as the function $Proximity(A, B)$ defined for a given spacing d and spacing threshold ψ as follows:

$$Proximity(A, B) = \begin{cases} 1: d(A, B) \leq \psi \\ 0 \end{cases} \quad (3.10)$$

In order to calculate the collision probability, we need to identify those trajectories that will lead to a collision and sum up their probability. Upon checking for the condition $Proximity(\hat{T}_s^H, \hat{T}_{n,m}^H) = 1$ over all the time steps and trajectory instances, we can identify the time instances called Collision Points (CP) that satisfy the condition. More precisely, for a given trajectory instance $\hat{T}_{n,m}^H$, $CP(n, m)$ is the first time instant satisfying the proximity condition. Let g_k be a function defined over CP specific to t_k that returns all the trajectory predictions of n those lead to the collision. The crash probability can then be estimated as follows:

$$p(s, n|t_k) = \sum_{1 \leq c \leq C_k} p(g_k(CP_c)) \quad (3.11)$$

where C_k is the total number of collision points at t_k . Now $R_n^T(t_k)$ is a time series of R_n calculated at t_k using the expected conditions at time t_k and $p(s, n|t_k)$

3.3 Examples of the model applications

In this section, we illustrate the applicability of the risk assessment approach and evaluate its performance. First, we apply the single step PDRF model to generate risk estimates along vehicle trajectories observed during three near-crash events. These events will be selected from a naturalistic dataset. This will reveal if the risk descriptions match the event narration and if it could provide insights into the risk evolution in terms of safety-critical moments during the event. As seen in section 3.2 (See Figure 3.2(d)) the risk measure is influenced by the prediction time step τ . Therefore, we will use this experiment to evaluate the sensitivity of τ . In the next step, we will apply the multi-step approach to estimate the risk of four possible trajectories that the subject could pursue while approaching a typical motorway lane drop section. This will reveal if the estimates are reasonable and how they compare to a standard safety indicator: generalised TTC. Besides, we will use this experiment to illustrate the application of the motion prediction scheme to calculate the generalised TTC proposed by Saunier et al. (2010).

3.3.1 Risk assessment of near crash events

The sample trajectories are obtained from the public dataset provided by the 100 vehicles naturalistic study (Neale et al., 2005). The study employed volunteering drivers with instrumented vehicles to collect large-scale naturalistic driving data. The vehicle is instrumented with a system of data collection equipment including video cameras, front and rear radars; GPS positioning system and vehicle motion sensors. This database provides a detailed record of 761 near-crash situations in terms of annotated event video; textual narration of the incident. In addition, the data set provides time-stamped vehicle state of the subject vehicle and its spacing (range) and relative longitudinal velocity (range rate) with the front and

rear vehicles (maximum 7 vehicles). The dataset includes situations labelled as near-crash, meaning a conflict situation requiring a rapid, severe evasive manoeuvre to avoid a crash (Neale et al., 2005). The presence of an evasive action indicates that the driver considered the situation to be risky, and therefore these situations can be regarded as examples of conflicts characterising true risk. We selected 3 scenarios to meet the experiment objective: 1) road boundary crash that was evaded by corrective steering; 2) rear end near-crash that was evaded by swerving to the left; 3) rear-end crash that was evaded by braking. The trajectory samples were extracted via the following steps: 1) identify the safety critical neighbouring vehicle in the encounter, based on the textual narration of the event; 2) extract the trajectory of the subject and the safety critical neighbouring vehicle; 3) estimate the lateral velocity (longitudinal acceleration) from the difference in lateral position (longitudinal velocity) between two consecutive time records. The lateral velocity and longitudinal accelerations were found to be highly noisy, and therefore we applied a moving average filter with a time span of 1 s.

3.3.2 Road boundary crash avoided by corrective steering

We consider the near crash event during trip number 8299 in the study dataset. The subject vehicle is in the entrance/exit only lane, trying to get into the left lane. The subject inadvertently drifts towards the concrete barrier on the right side of the road. She applied corrective steering to bring the vehicle back to the lane centre. We calculate the total risk R taken by the subject. According to Eq. (3.2), $R = R_b$ where b is the concrete barrier. Since the offset of the concrete barrier from the lane boundary is unknown, we consider the barrier to be at an offset of 0 m. We set the value of scaling factor k to 0.61 (the odds of injury ratio with a concrete barrier wall measured by Zou et al. (2014)). Additionally, we calculate the Time to Lane Crossing (TLC, the ratio of lateral spacing to the lateral velocity of the subject in the direction of the barrier). The lateral dynamics of the subject are described in Figure 3.4 (a), (b). Both TLC and PDRF risk descriptions qualitatively reflect the event narration in the dataset. During the initial phase of the encounter (time 0 s – 2 s), both PDRF and TLC risk estimates remained marginal. Thereafter, the subject drifted towards the right barrier which increased the chances of crashing onto the right boundary; this unsafe development is indicated as a rise in the PDRF risk description (See Figure 3.4 (d) at 2 s); and as a descent in the TLC description. Realising the impending hazard, the subject applied a corrective steering (See Figure 3.4 (d) at 3.2 s) to bring the vehicle back to the lane centre; the success of evasive action is indicated as a descent in PDRF risk description from a maximum (See Figure 3.4 (d) at 3.2 s) to a marginal value (See Figure 3.4(d) at 3.6 s); and as an ascend in TLC description. Figure 3.4(c) describes the variation of the crash probability term in PDRF risk as given in Eq.(3.4). As expected from its formulation, the term correlates with the lateral position (See Figure 3.4 (a) and Figure 3.4). It can be seen that the PDRF approach provides continuous risk estimates with relatively smooth variations, and therefore it could clearly mark critical moments during the encounter. The risk was first seen to appear at 2 s (in Figure 3.4 (d)). This provides an approximate time point to investigate for driver actions or circumstances that lead to the event. Secondly, the risk estimate attained the maximum at 3.2 s (See Figure 3.4 (d)). The maximum risk provides a representative risk measure for the entire encounter.

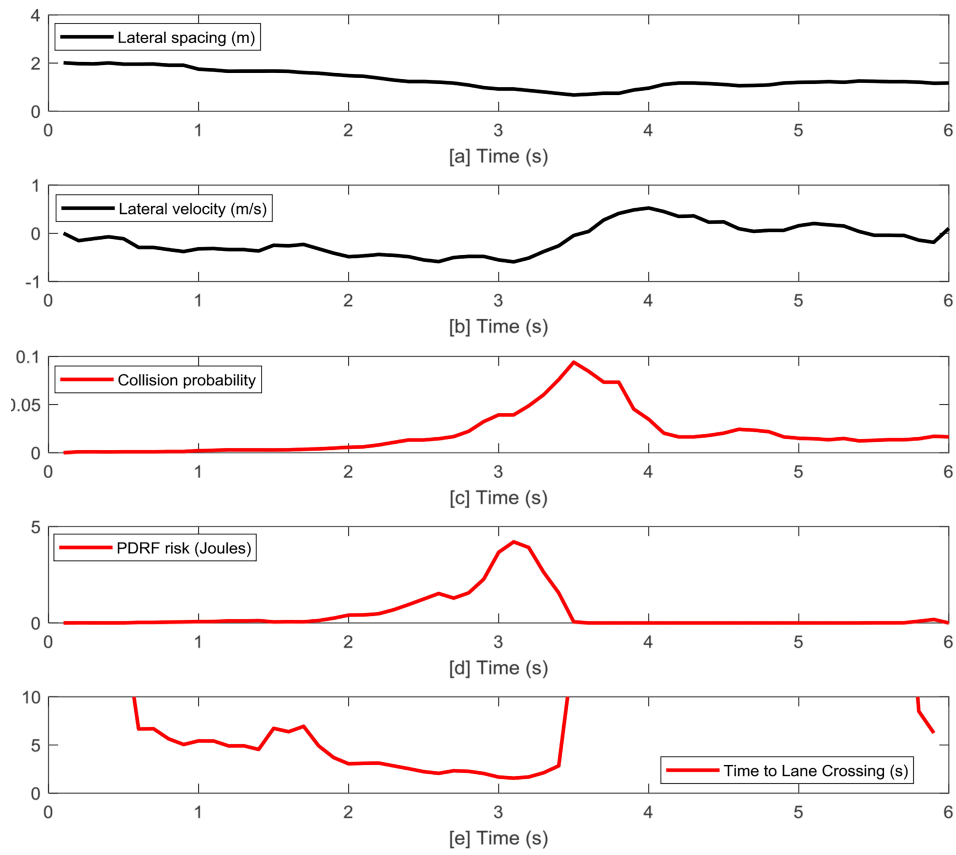


Figure 3.4: Risk estimates of an encounter in which the subject vehicle avoids a crash with the right lane boundary by corrective steering.

3.3.3 Rear crash avoided by swerving

We consider the near crash event during trip number 8450 in the study database. The preceding vehicle brakes and slows down on the interstate. The subject vehicle is fairly far behind the preceding vehicle, but the preceding vehicle decelerates at a faster rate than the subject driver is initially aware of, so the subject has to brake and steer left to avoid hitting the preceding vehicle in the rear. We calculate the total risk R taken by the subject. According to Eq. (3.2), $R = R_n$, where n is the preceding vehicle. The trajectory of n was not available long enough to estimate the distribution of acceleration. Therefore, we used a standard set of parameters to define the acceleration variability of n as $\mathcal{N}(A_X|0, 0.7)$ and $\mathcal{N}(A_Y|0, 0.2)$. Another estimate of risk employed here is the Time To Collision defined as $TTC = \left(\frac{X_n - L - X_s}{V_{X,s} - V_{X,n}} \right)$. The evasive manoeuvre undertaken by the subject can be seen from its lateral movement in Figure 3.5 (a); and the applied braking in Figure 3.5 (f).

Both TTC and PDRF risk estimate qualitatively reflected the event narration. During the initial phase of the encounter (time 0 s – 60 s) the subject vehicle was far behind suggesting a safe following. During this phase, both PDRF risk (See Figure 3.5 (d)) and TTC (See Figure 3.5 (e)) estimate depicted a marginal risk. Thereafter, the preceding vehicle suddenly decelerates at a fast rate; this unsafe development is described as a steep descent in TTC (8–10 s) and as a steep and temporally adjacent rise in the PDRF risk descriptions ($\tau = 4, 3$ and 2 s).

It can be seen that the PDRF approach provided continuous risk estimates with relatively smooth variations (See Figure 3.5 (d)) within a finite range; and the crash probability and crash severity varied independently (See Figure 3.5 (b) and (c)). As expected, the prediction time step (τ), influenced the risk estimates, more specifically the collision probability term. Therefore the PDRF risk descriptions differed temporally and quantitatively (See Figure 3.5 (d)).

However, evaluating the multiple descriptions of risk (See Figure 3.5 (d)) and crash probability (See Figure 3.5 (c)) provides information about the evolution of risk during the encounter. The peak in crash probability with $\tau = 2$ s indicates high chances of an imminent crash at 2 s. Moreover, subsequent and comparable risk peaks ($\tau = 2$ and 3 s) around 90 s suggest that the evasive braking, which started around 80 s is not sufficient to avoid the danger. In combination, these observations indicate a growing urgency for an effective evasive action. This could provide an explanation as to why the subject swerved to its left (at approximately 90 s) instead of merely braking. Moreover, the absence of crash probability with $\tau = 1$ s indicates the collision was successfully avoided at least until the end of the observation. Notably, the PDRF risk with $\tau = 3$ s attained the highest estimate and its moment of maximum risk is closer to the moment when the subject begins the evasive manoeuvre: swerve with hard braking around 90 s (See Figure 3.5 (a), (f)).

3.3.4 Rear-end crash avoided by braking

We consider the near crash event during trip number 8427 in the study database. The subject vehicle is following the lead vehicle fairly closely on a 2-lane road when the preceding vehicle slows down to stop. Subject vehicle brakes to avoid hitting the preceding vehicle in the rear. Similar to the previous experiment, we calculate R_n and TTC estimates. Both TTC and PDRF risk estimates qualitatively reflect the event narration. During the initial

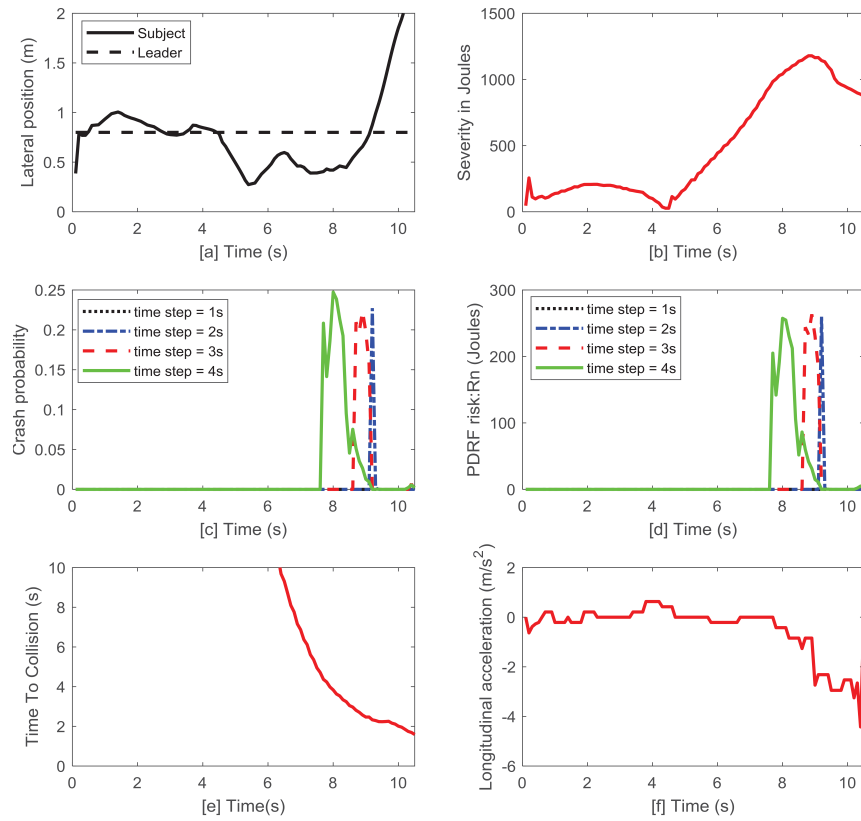


Figure 3.5: Risk estimates of an encounter in which the subject vehicle avoids a rear-end crash by swerving to its left.

phase (0–4 s), the subject was closely following the preceding vehicle indicating an unsafe interaction. During this phase, both PDRF risk (See Figure 3.6 (d), $\tau = 4$ s) and TTC (See Figure 3.6 (e)) estimate depicted the existence of risk. Thereafter the preceding vehicle slows down to stop; this unsafe development is described as a gradual descent in TTC (time 4 - 6 s) and as a temporally adjacent rise in the PDRF risk descriptions ($\tau = 4, 3$ and 2 s).

Evaluating the multiple descriptions of risk (See Figure 3.6 (d)) and crash probability (See Figure 3.6 (c)) reveals how this situation differs from the previous one in terms of risk evolution. The low peak in crash probability with $\tau = 2$ s indicates marginal chances of an imminent crash (i.e. at the next 2 s). Moreover, a high-risk peak with $\tau = 3$ s around 5.6 s and a subsequent lower risk peak with $\tau = 2$ s suggest that the evasive braking, which started around 5 s, is sufficient to evade the danger. In combination, these observations indicate that the braking was effective to evade the danger. The absence of risk with $\tau = 1$ s indicates the collision was successfully avoided at least until the end of the observation. Similar to the previous example, the PDRF risk with $\tau = 3$ s attained the highest estimate and its moment of maximum risk (See Figure 3.6 (c)) is closer to the moment when the subject begins the evasive braking around 5 s (See Figure 3.6 (f)). It can be seen that the PDRF risk model could qualitatively reflect the event narration, and its risk description was consistent with that by TTC. The prediction time step influenced the PDRF risk descriptions. When evaluated together, the risk descriptions with distinct prediction time steps could provide information about the risk evolution of the encounter. However, each of these descriptions differ in their qualitative properties. For example, a peak in crash probability with $\tau = 1$ s cannot be used to detect near-crashes; as it did not appear in the two near-crash examples. Similarly, a peak in crash probability with $\tau = 4$ s cannot be regarded as an accurate indicator of near crash; such peaks occurred multiple times during a single encounter. Notably, in both the examples, the PDRF risk estimate with $\tau = 3$ s yielded a single peak; attained the maximum value; and was temporally closest to the moment when the driver initiated the evasive manoeuvre.

3.3.5 Risk estimation of path plans

In this section, we apply the multi-step PDRF to estimate the risk of four trajectory plans while approaching a typical lane drop section. The situation involves four vehicles: s (the subject vehicle), $n1$, $n2$, $n3$ (neighbouring vehicles). The initial states are shown in Figure 3.7. Here, the controller of s makes four trajectory plans: T1, T2, T3 (lane change trajectories) and T4 (forward trajectory). All the lane change trajectory plans span over a duration 4 s and imply a constant lateral velocity of 1 m/s. Even though these trajectory plans are similar in terms of lateral movement, they differ in the prescribed longitudinal dynamics: T1 represents a constant velocity of 20 m/s; T2 represents a decreasing velocity with a constant deceleration of -2 m/s^2 , T3 represents a decreasing velocity with a milder constant deceleration of -0.7 m/s^2 . T4 represents moving forward at 20 m/s in the original left lane. In this experiment, we set the trajectory plans $\hat{A}_X(t_k)$ and $\hat{A}_Y(t_k)$ of neighbouring vehicles as shown in Figure 3.8. The acceleration plan of $n3$ implies that it will continue to accelerate at 1 m/s^2 (See Figure 3.8 (c)); $n1$ and $n2$ according to the Intelligent Driver Model (See Figure 3.8 (a)); and $n2$ will move to the middle lane (See Figure 3.8 (b)). The acceleration variability distribution is set as follows: $A_X^d(t_k) = \mathcal{N}^d(\hat{A}_X(t_k), 1) \forall k \in \{1, 2, 3, 4\}$ and $A_Y^d(t_k) = \mathcal{N}^d(\hat{A}_Y(t_k), 0.1) \forall k \in \{1, 2, 3, 4\}$.

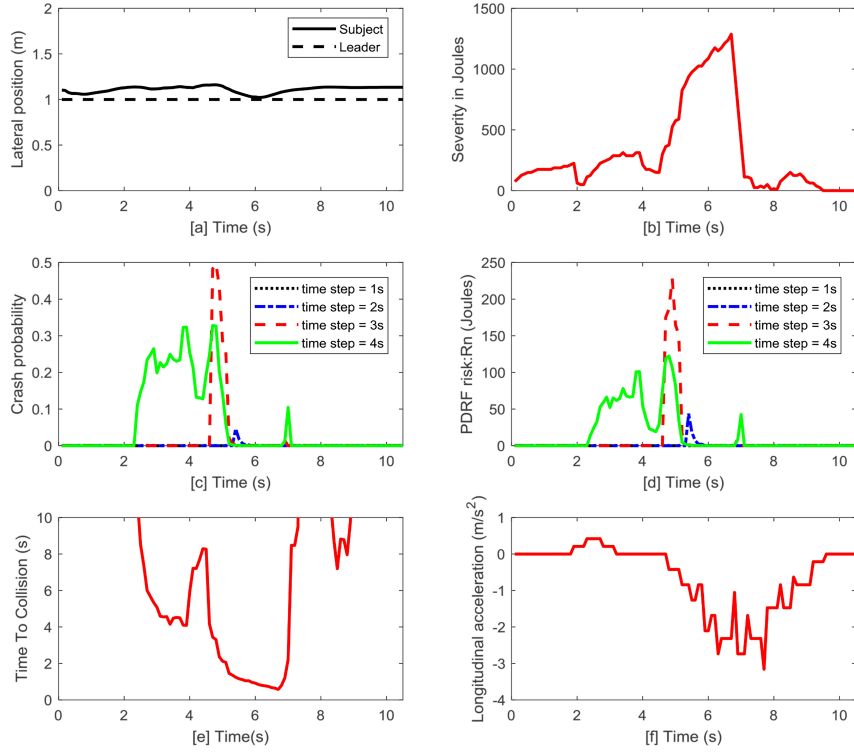


Figure 3.6: Risk estimates of an encounter in which the subject vehicle avoids a rear-end crash by braking

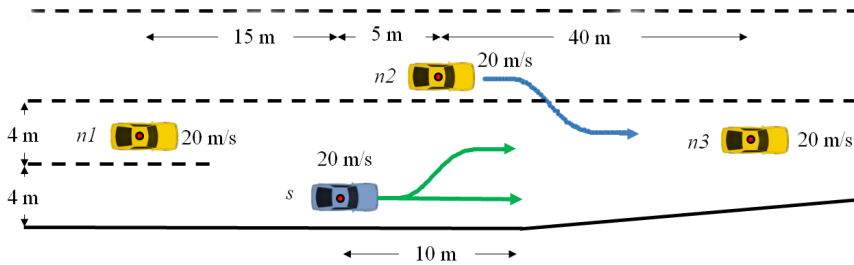


Figure 3.7: Illustration of the hypothetical simulation scenario: lane marking represented a dashed line; the lane boundary marking represented as a solid line; initial states of the subject vehicle s , and the three neighbouring vehicles ($n1, n2, n3$).

According to the PDRF model, the risk of a crash between s and $n1$ is highest along T2 (lane change with hard braking); both in terms of collision probability and crash severity (See Figure 3.9 (a)). Whereas, in the encounter between s and $n2$, the crash probability is highest along T1 (lane changing at constant velocity) (See Figure 3.9 (b)). The risk description indicates a significantly high risk along T2; and lowest along T4 (See Figure 3.9 (d)). This means that objectively the safest trajectory is T4; however, if the subject decides to change the lane, it should avoid T2, and choose between T1 and T3. Figure 3.9 (d) shows that even though the maximum risk values along T1 and T3 are comparable (T3 slightly lesser than T1), the danger is more imminent along T3 (at 3 s) than along T1 (at 4 s). The experiment shows the applicability of multi-step PDRF to generate ex-ante risk estimates in order to differentiate the trajectory plans. To compare our approach, we describe an additional metric generalised TTC proposed by (Saunier et al., 2010). By this generalised definition of conflict, TTC is the time required for two vehicles to collide, following the predicted trajectories. The generalised TTC for the set of trajectory predictions is defined as follows:

$$TTC(s, n) = \frac{\sum_{TTC=1}^H p_{TTC} \cdot TTC}{\sum_{TTC=1}^H p_{TTC}} \quad (3.12)$$

Figure 3.10 describes the generalised TTC values along the four trajectory plans. p_{TTC} is the aggregated collision probability for a given t_k , according to 3.2.5, which can also be interpreted as the TTC. Figure 3.10 shows the generalised TTC, with $H = 4$, along the four trajectory plans. The trend shown by the generalised TTC values reflects the temporal proximity of a crash along the trajectories. Both generalised TTC and PDRF estimates suggest that T4 is the safest trajectory. Notably, the riskiest trajectory is T3 as per generalised TTC estimates (Figure 3.10), whereas it is T2 as per PDRF (See Figure 3.9 d). This is due to the absence of severity dimension in generalised TTC. It can be seen that the high crash severity is the factor that differentiates T2 for encounters with $n1$ and $n2$ (See Figure 3.9 (a) and See Figure 3.9 (b)). Even though generalised TTC is an effective and simple approach to detect critical interactions, multi-step PDRF risk contains the crash severity information, which is vital to differentiate risk level trajectory plans.

3.4 Discussion

In this introductory work, we have relied on several simplifying assumptions to operationalise the framework. One should be cautious about the implications of these assumptions while using the approach and interpreting the results.

The crash severity is expressed solely as the expected crash energy, an important characteristic of the crash process. But the outcome of a crash is influenced by several other factors such as vehicles material stiffness at the point of impact, the presence of passive safety systems such as seat belts; and the material property of crash bumpers that are designed to partially dissipate the crash energy. Considering these elements in the crash severity quantification will improve the accuracy of the model. The crash between two vehicles is assumed to be inelastic, where the vehicles move together

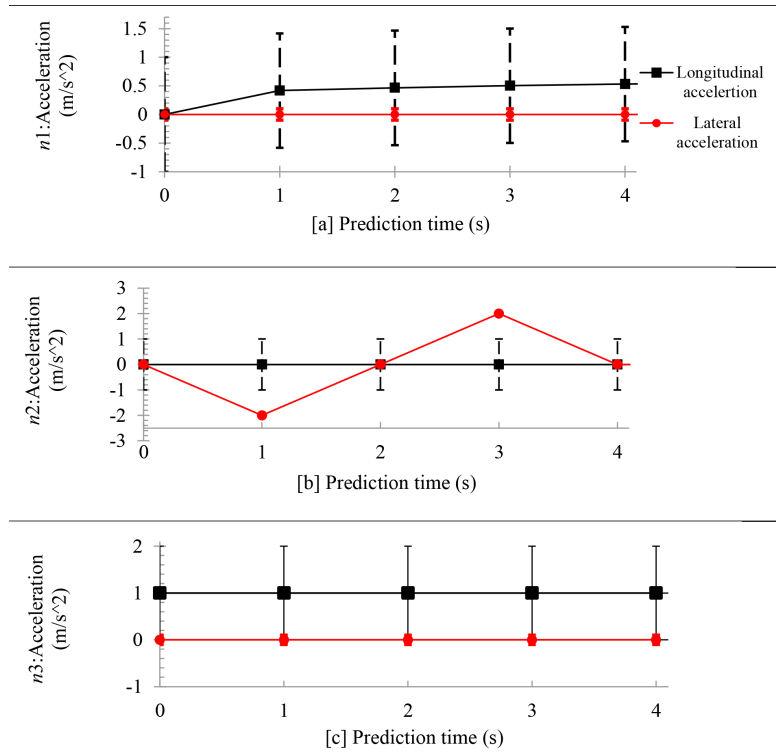


Figure 3.8: The trajectory plans of the neighbouring vehicles n1 (a); n2 (b) and n3 (c) represented in terms of the expected acceleration ($\hat{A}_X(t_k)$) as square black markers and $\hat{A}_Y(t_k)$ red dots) and the error limits defined by the acceleration noise

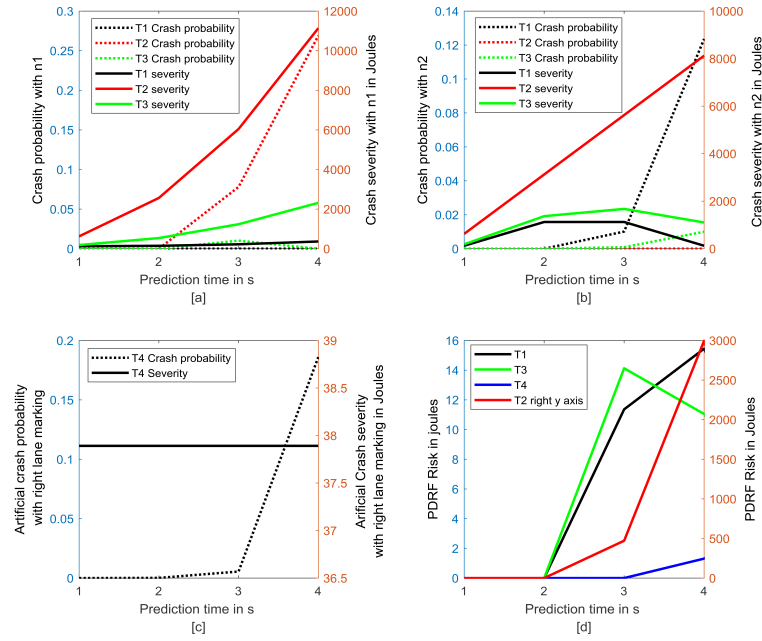


Figure 3.9: The multi-step PDRF risk estimates for trajectory plans at a typical lane drop section. The probability and severity of a crash between s and $n1$ (a); s and $n2$ (b); s and the right lane marking (c); and the combined PDRF risk along the trajectory plans(d)

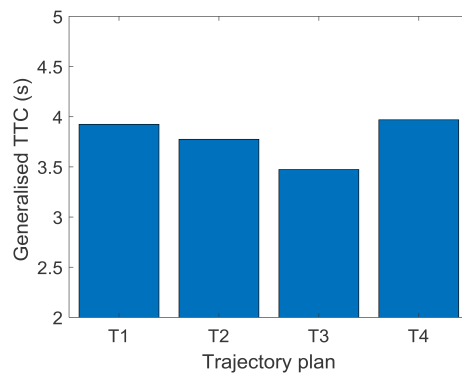


Figure 3.10: Generalised TTC calculated for the trajectory plans in lane drop section

after the first contact. However, in reality, vehicle crashes involve some amount of elasticity, where vehicles rebound from each other. A scaling coefficient can be introduced to capture this effect.

The acceleration variability distributions in the forward and lateral direction were assumed to be independent. However, they can be correlated during manoeuvres such as lane changes. If such a correlation is detected while estimating the parameters, then variability should be modelled as a joint distribution.

The crash probability estimation is based on the assumption that the subject vehicle maintains its current state; however, it might not do so during a system failure. The probability of system failure is a critical dimension of the risk measure. This dimension can be incorporated in the present framework treating the future motion of the subject vehicle as a stochastic feature that is related to the probability of a system failure. The probability of system failure is influenced by various factors such as hardware faults, software failures, which can be modelled as a fault tree (W. Wang et al., 2010).

The additivity property of the artificial field is constructed under the condition that driving risk with two distinct road objects is independent. This condition is not met, in a conflict involving multiple vehicles when the mutual vehicle interactions could influence each others motion. However, such events are less prevalent than crashes between a vehicle pair.

The proposed approach cannot be used to assess the driving risk posed by obstacles within the driving lane such as work zone equipment and potholes. Given a representative geometry of these obstacles, the crash probability can be modelled by treating them as stationary vehicles, (i.e. a kinetic field with acceleration noise = 0). However, the crash severity term needs to be adapted specifically to the crash process. Such in-lane obstacles, however, are less ubiquitous than the road boundary obstacles.

For illustrative purpose, the risk measures in this chapter were generated using parameter values selected from the literature. The accuracy of the risk measure can be improved by estimating them directly from a trajectory dataset or via test experiments as follows,

The parameter k , in potential PDRF, can be estimated in multiple ways. An objective approach is based on the relationship between k and the coefficient of restitution e_{res} as follows: $k = (1 - e_{res}^2)$. The coefficient of restitution can be measured from vehicle crash tests with the specific road object (Noon, 1994). Some studies report that e_{res} increases exponentially with the impact velocity (Noon, 1994). However, identifying e_{res} for multiple combinations of the vehicle (at different velocity ranges) and boundary objects that appear in the dataset would be practically strenuous. Another, rather subjective, approach is to use the odds of injury (Zou et al., 2014) as the value of k . Such an approach can loosely capture the influence of the energy dissipation capacity of boundary objects on crash severity.

The parameters of acceleration variability distributions can be estimated from the acceleration samples of a vehicle during a finite duration according to Eq.(3.5). The acceleration samples of a vehicle can be extracted from its trajectory data (simulated

or video based naturalistic data) or can be acquired directly from the vehicles data log. The sampling horizon should be small enough to capture the local traffic conditions and long enough to ensure statistical validity. Further research is needed to find an optimal sampling horizon. The acceleration noise when a vehicle is stopped in traffic is zero, which might distort its estimated value. Therefore, the acceleration noise should be measured only while the vehicle is moving. Furthermore, manoeuvres such as lane changing, turning and evasive braking are expected to feature distinctive sets of parameters, which require further study.

3.5 Conclusion

We presented an approach to assess driving risk, which employs a probabilistic motion prediction scheme, within the framework of artificial potential field theory. The approach was designed to yield a continuous risk estimate and to account for important aspects of the driving risk: the crash severity and motion uncertainty. As a proof of concept, we illustrated the application of the approach with examples of safety assessment problems. Firstly, we applied the approach to analyse the risk of three near-crash situations selected from a naturalistic dataset. Here, we employed the risk estimate that describes the risk of a crash at a finite future time step. It was observed that the risk description qualitatively reflects the document narration of the situation; the evolution of risk in the situation. Secondly, we applied the model to estimate the risk of four possible trajectories that the subject could pursue while approaching a typical lane drop section. Here we employed the multi-step risk estimate that describes the risk of a crash at a sequence of multiple future time steps. It was observed that the risk estimates of the trajectory plans are plausible and clearly mark the safest trajectory, which is consistent with the well known Surrogate Measure of Safety: generalised TTC.

Both sets of illustrations demonstrated certain properties of the driving risk estimate. The risk descriptions vary within a finite intuitive range, i.e. between 0 and the expected crash energy. The results of both example sets showed that the risk trends described by the PDRF model, in general, were consistent with the prominent SMoS: Time To Collision. However, the risk measure (strength of PDRF) contained additional information: crash severity, which was seen to be the factor that differentiates the risk levels of trajectories. Based on the exhibited properties, and the relevance of the component aspects in characterising the driving risk, the proposed approach can be applied in analysing the safety of vehicle interactions and as a risk estimate in path planning algorithms. As part of the assessment approach, we presented a probabilistic motion prediction scheme, which employs a distribution of acceleration variation to approximate the motion uncertainty. The use of acceleration variability makes the prediction scheme analytically tractable. The parameters of the distribution could be measured by monitoring the vehicle for the finite duration; and they are known to be sensitive to factors relevant to safety analysis such as road geometry, driver aggressiveness and traffic congestion.

The examples presented in this work are illustrative. The single step approach should be tested with large-scale naturalistic data (including crash, near-miss and regular driving) to evaluate its effectiveness in detecting risky situations. Such a test is also necessary to identify the optimal value of τ that provides the highest number of accurate detections.

Similarly, the effectiveness of the multi-step approach as an ex-ante risk estimate should be evaluated by employing it in an advanced vehicle control design. Our future research will focus on the above-mentioned aspects.

Chapter 4

Empirics and models of fragmented lane changes

Abstract

Existing microscopic traffic models represent the lane-changing manoeuvre as a continuous and uninterrupted lateral movement of the vehicle from its original to the target lane. We term this representation as Continuous Lane-Changing (CLC). Recent empirical studies find that not all lane-changing manoeuvres are continuous; the lane-changer may pause its lateral movement during the manoeuvre resulting in a Fragmented Lane-Changing (FLC). In comparison to a CLC, this study investigates the distinction of an FLC in terms of its execution and its effects on neighbouring vehicles. We find that during the execution of an FLC, the lane-changer exhibits distinct kinematics and takes a longer duration to complete the lane-changing. We propose a trajectory model to describe the lateral kinematics during an FLC. Additionally, we find that the FLC induces a distinct effect on the follower in the target lane, and propose a model to describe the transient behaviour of the target-follower during an FLC. The modelling results suggest that the accuracy of traffic flow models can be improved by deploying lane change execution and impact models that are specific to FLC and CLC. Besides, this study identifies a set of factors that might be related to the decision-making process behind FLC: an average driver executes an FLC when the preceding and following vehicles in the target lane are slower, and when the follower in the target lane is closer than those observed during the onset of a CLC. Our findings suggest that FLC is motivated by an increased necessity to change lane such as during a mandatory lane change.

This chapter is based on the following article, which is currently under review:

Mullakkal-Babu, F. A., Wang, M., van Arem, B., & Happee, R. (under review) Empirics and models of fragmented lane changes

4.1 Introduction

Lane-changing manoeuvres have profound impacts on the traffic flow (L. Zheng et al., 2014b) and therefore receive extensive research attention. In order to change-the-lane, the driver must perform at least two tasks: 1) decide if and when to initiate the manoeuvre; 2) operate the steering and acceleration to execute the manoeuvre. We refer to the first task as lane-changing decision and the second task as lane-changing execution. The process of lane-changing may also be depicted in more than two steps (Balal et al., 2016; Keyvan-Ekbatani et al., 2016). Besides, lane-changing impacts other vehicles in the vicinity, which we refer to as lane-changing impact. Therefore a complete description of lane-changing (LC) entails models for its decision, execution and impact.

Existing studies primarily focus on the LC decision and the impact (Moridpour et al., 2010b; M. Rahman et al., 2013; L. Zheng et al., 2014b). The LC decision is typically modelled based on two considerations: the drivers preference for the target lane; and assessment of the safety of the available target gap. Accordingly, LC decision models typically consist of a lane preference model and a complementary gap acceptance model (Gipps, 1986; Kesting et al., 2007; Moridpour et al., 2009; Schakel et al., 2012; Toledo et al., 2007). The common set of explanatory factors used to describe LC decision are relative space headway and relative velocity of the lane-changer w.r.t. three vehicles: the rear (or following) vehicle in the target lane, the preceding vehicle in the target lane and the preceding vehicle in original lane (Moridpour et al., 2010b). On the other hand, LC impact models capture the impacts induced by lane changes. The impacts refer to the macroscopic traffic flow characteristics and microscopic behaviours induced by lane changes. At the macroscopic level, lane changes have a direct influence on phenomena such as traffic breakdowns (Cassidy & Rudjanakanoknad, 2005) and traffic stop-and-go oscillations (Ahn & Cassidy, 2007). Besides, lane changes might destabilise the traffic flow in both original and target lanes, and thereby hurt traffic safety (Z. Zheng et al., 2010). At the microscopic level, an LC temporarily changes the longitudinal behaviour of the lane-changer, the rear vehicle in the original lane and the following vehicle in the target lane. Several studies report a process known as relaxation by which the target-follower accepts short-spacing to facilitate the lane change and relaxes to equilibrium spacing after the lane change (Duret et al., 2011; Leclercq et al., 2007; Z. Zheng et al., 2013). Z. Zheng et al. (2013) identified another process known as anticipation by which the target-followers longitudinal behaviour changes upon noticing the lane change intention.

Compared to LC decision and impact, studies on lane change execution are rare. Existing studies on LC execution indicate that the human driver uses visual feedback to adjust the steering-control actions (van Winsum et al., 1999). Salvucci and Gray (2004) modelled steering-control as a closed-loop process. The above-mentioned studies are performed in a driving simulator, which provides detailed measurements to analyse the steering-wheel angle and the brake pedal position during the LC execution. However, the artificial setting in a driving simulator is different from the on-road driving environment and might detriment the transferability of the findings. Alternatively, researchers analysed LC execution as observed from the LC trajectory. The trajectory samples can be extracted from road-side traffic observations. Li et al. (2018) derived the steering pattern of the lane changes from trajectory samples. Toledo & Zohar (2007) analysed and modelled the LC duration. Q. I. Wang et al. (2014) implemented a heuristic-based approach to filter out abnormal trajectories and to

define the start and end of an LC trajectory. They identified that a normal LC can be approximately depicted by fifth-degree polynomials. Similarly, several researchers have modelled the lane-changing trajectories (Moridpour et al., 2010a; Yang et al., 2016, 2015; Yao et al., 2012). Recently, Yang et al. (2015) observed two types of lateral movement during LC. We term them as Continuous lane-changing (CLC) and Fragmented lane-changing (FLC). During CLC, the vehicle uninterruptedly moves to the target lane; whereas, during FLC, it exhibits a temporary pause in the lateral movement before the completion of LC. Apart from the apparent difference in lateral movement, so far, it is not clear if FLC trajectories represent a distinct type of lane-changing.

Fragmented lane changes present a methodological challenge to current behavioural models, which rely on a normative representation of LC. The current models describe the LC decision as a choice between changing the lane and remaining in the current lane, treating lane change execution as an open-loop process. But the driving-simulator-based studies suggest that LC execution is a closed-loop process (van Winsum et al., 1999) and the driver might revise the LC decision during the execution: for instance the driver might abort a pre-initiated lane change for safety reasons. Similarly, the intermediate pause of lateral movement during an FLC implies a non-typical LC execution. The current LC impact models represent the duration of LC as a fixed value; typically the mean or mode of observed sample distribution (Laval & Leclercq, 2008). Using a fixed value is inaccurate, as the lane change durations spread over a wide interval of 1-14 s (Toledo et al., 2007). Furthermore, Yang et al. (2015) report that FLCs are considerably longer than CLCs. The use of summary statistics is only reasonable to represent unimodal distributions, i.e. if all the data points come from a single type of lane-changing. We did not find any study that tests the unimodality of lane change duration samples.

To gauge the implications of FLCs to traffic flow modelling, the first step is to examine if they represent a distinct LC execution and induce a distinct impact. The realism of LC execution and impact models influences the validity of model predictions. The metrics to quantify the safety of the lane-changing are calculated directly from the trajectories simulated using LC execution models (Mullakkal-Babu et al., 2017). Models of LC impact, determine the accuracy of macroscopic and microscopic impact predictions (Z. Zheng et al., 2013). If FLC indeed represents a distinctive LC execution and induce a distinct impact, models thereof can potentially improve the realism of traffic modelling.

The objective of this work is to investigate if FLC represents a distinct type of lane-changing in terms of the lane change execution and lane change induced impact and to propose models to describe the lateral kinematics and the microscopic impact induced by FLC on the target-follower. Towards this, we develop a method to identify the start, pause and end of the LC and thereby classify the trajectories. The analysis results provide strong evidence of FLC being a distinct type of LC in terms of execution and impacts. The modelling results suggest that separate execution and impact models of FLC and CLC improve the accuracy of the traffic flow models.

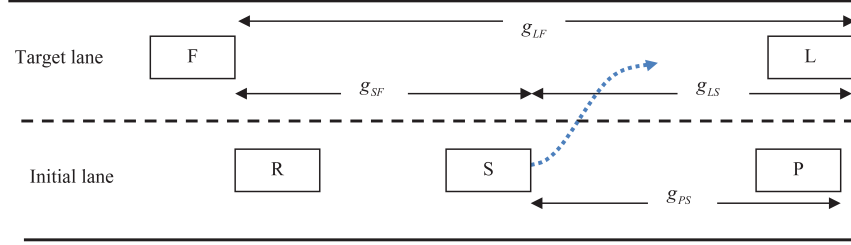


Figure 4.1: Illustration of the influential neighbouring vehicles during a typical lane change manoeuvre

4.2 Data extraction and classification of trajectory samples

This section describes the dataset and the algorithm to extract and classify the LC trajectory samples. This study uses trajectory dataset collected by the FHWA's Next Generation Simulation (NGSIM) program. Several researchers have previously used this dataset to analyse and model the lane-changing behaviour (Laval & Leclercq, 2008; Yang et al., 2015; Z. Zheng et al., 2013). The vehicle trajectories were extracted from the video images of northbound traffic on I-80 in Emeryville, California. The study site is approximately 500 m long. The vehicle positions were recorded every 0.1s from 4.00 p.m. to 4.15 p.m. and from 5:00 p.m. to 5:30 p.m. on April 13, 2005.

In order to identify and classify the observed lane-changing manoeuvres, the vehicle trajectories logged in the NGSIM dataset have to be processed. Towards this, we develop a systematic method which is presented in Algorithm 4.1. Figure 4.1 illustrates the vehicles involved in the lane change: F (follower in the target lane), L (leader in the target lane), P (preceding vehicle in the initial lane), and R (follower in the initial lane).

Algorithm 1 consists of two major loops. The first loop identifies the LC instances and corresponding insertion time t_{LC} from the NGSIM dataset. Here, t_{LC} denotes the insertion point, i.e. the time instant at which centre of the vehicles front edge crosses the lane boundary marking. This approach is similar to previous studies (Yang et al., 2015; Z. Zheng et al., 2013). Secondly, it filters out LC instances in which the subject vehicles trajectories are not observable for at least a $T \in [t_{LC} - 7, t_{LC} + 7]$. The time interval of 14 s was found to be long enough to entirely cover all lane change executions (Toledo et al., 2007). Thereafter, it logs the trajectories of the subject and neighbouring vehicles, for the selected LC instances.

The second loop of Algorithm 1 identifies the start and end of the lane change. The lane-changers trajectory between the start and the end of the lateral displacement (larger than a threshold) is typically identified as the CLC trajectory (Toledo et al., 2007). In the case of an FLC, a marginal lateral movement might only indicate an intermediate pause and does not necessarily mean that the LC is complete. The procedure to determine the LC duration is illustrated in Figure 4.2. First, it identifies all the time instances when the subject vehicles average lateral displacement is larger than a threshold. An averaging interval shorter than 0.3 s yields indiscriminately large number of time points within T and longer interval detracts the accuracy of temporal bounds. Moreover, the threshold should

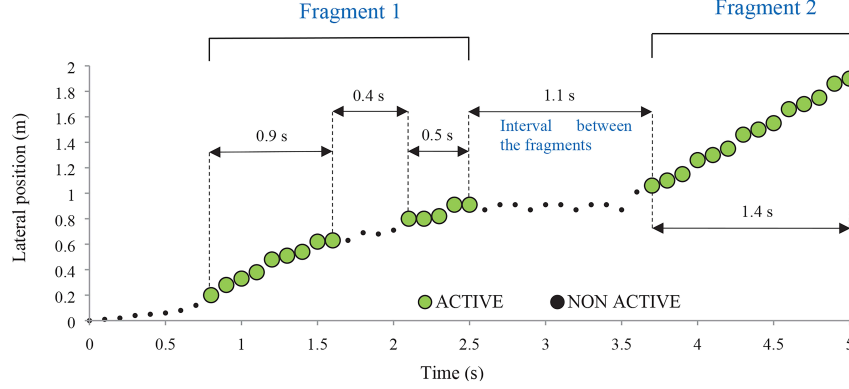


Figure 4.2: Illustration of the method to identify the LC fragments

discriminate between the lateral activity exhibited during active lane-changing and that during lane-keeping or an intermediate pause. Accordingly, a vehicle is identified as laterally active, i.e. $d^*(t) = 1$, if it exhibits an average lateral displacement larger than 0.1 m over the previous 0.3 s, where $d^*(t)$ is defined as

$$d^*(t) = \begin{cases} 1 & \text{if } |y(t) - y(t - 0.3)| \geq 0.1 \\ 0 & \text{if } |y(t) - y(t - 0.3)| < 0.1 \end{cases} \quad (4.1)$$

where y denotes the global lateral coordinate of the vehicles front-centre. The second step is to identify one or more series of lateral active points that represents continuous lateral movement or LC fragment. An LC fragment is defined as a sequence of at least 5 laterally active points; or a combination of such sequences that are separated by an interval of not more than 1 s. Here, 1 s threshold implies that during the interval between the fragments the vehicle did not move more than 0.33 m laterally, i.e. approximately 0.15 times the vehicle width.

Algorithm 1 classifies the LC trajectories based on the number of fragments. The lane change trajectory with a single fragment is classified as Continuous Lane Change trajectory, and that with two fragments is classified as Fragmented Lane Change trajectory. Finally, Algorithm 1 determines the temporal bounds of LCs. The timestamp of the first active-point of the first fragment is labelled as t^{start} denoting the lane change start point, and the timestamp of the last active point of the last fragment is labelled as t^{end} denoting lane change endpoint. The interval between t^{start} and t^{end} is labelled as D denoting the lane change duration. In case of an FLC, the timestamp of last active point of the first fragment is labelled as t^{start_p} denoting the start of the intermediate pause and the timestamp of the first active-point of the second fragment is labelled as t^{end_p} denoting the end of the intermediate pause. Figure 4.3 shows example trajectories of an FLC and a CLC as extracted by the algorithm.

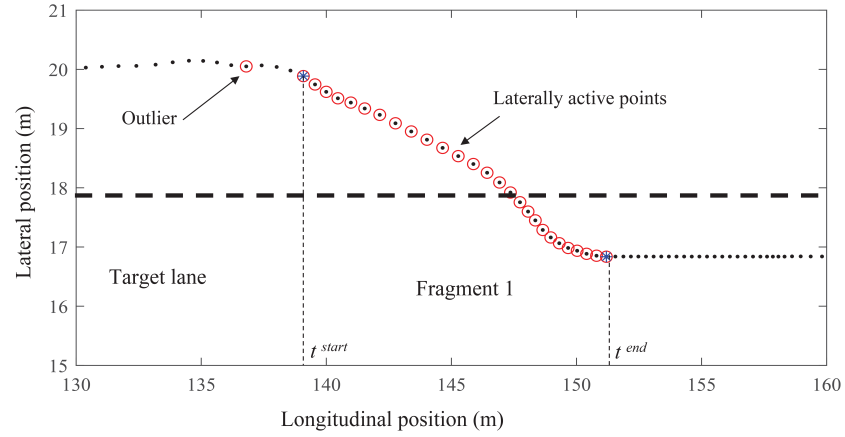
Lane change samples extracted by the algorithm were filtered before further analysis. To avoid non-typical trajectories, lane changes by heavy vehicles or those in which the lane-changer made two or more subsequent lane changes were excluded. We found that the lateral coordinates of certain locations (probably at the junction of the frame's bound-

Algorithm 4.1 Pseudo algorithm to extract and classify the lane-changing trajectories in NGSIM dataset

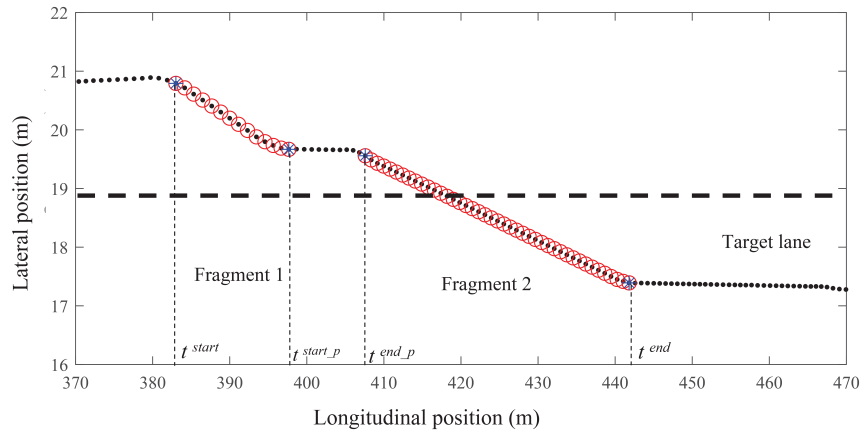
```

1: Data: NGSIM trajectory data log consisting of the following elements: row number (
    $k$ ), observation time ( $t$ ), vehicle ID,  $x$  coordinate,  $y$  coordinate, lane number, preceding
   vehicle ID, rear vehicle ID
2: Result: Trajectory of the subject vehicle  $S$  and neighbouring vehicles  $F, R, L, P$  during
   lane-changing
3: Result: Critical time points of the lane change trajectory:  $t_{LC}, t_{start}, t_{end}, t_{start_p}, t_{end_p}$ 
4: while  $k < \text{length}(\text{datalog})$  do
5:   if vehicle ID ( $k$ ) = vehicle ID( $k+1$ ) AND lane number ( $k$ )  $\neq$  lane number ( $k+1$ )
   then
6:     begin
7:     lane change instance  $LC(i) = k; t_{LC} = t(k)$ 
8:     if trajectory of  $S$  available for  $T$  then
9:       begin
10:       $R \leftarrow$  rear vehicle ID ( $k$ ),  $P \leftarrow$  preceding vehicle ID ( $k$ )
11:       $F \leftarrow$  rear vehicle ID ( $k+1$ ),  $L \leftarrow$  preceding vehicle ID ( $k+1$ )
12:      Neighbours ( $i$ )  $\leftarrow S, R, P, F, L$  during  $T$ 
13:       $i = i+1$ 
14:     end
15:   end
16: while  $j < \text{length}(LC)$  do
17:   begin
18:   Calculate  $d^*(t)$  of  $S$  and identify the laterally active points based on Eq. (4.1)
19:   Apply rules to identify fragments
20:   if number of fragment = 1 then
21:      $LC \text{ type}(i) \leftarrow \text{CLC}$ 
22:   if number of fragment = 2 then
23:      $LC \text{ type}(i) \leftarrow \text{FLC}$ 
24:   else
25:     remove
26:   Identify  $t_{start}, t_{end}, t_{start_p}, t_{end_p}$ 
27:   end

```



(a)



(b)

Figure 4.3: Illustration of extraction and classification of observed lane-changing trajectories: (a) an observed CLC trajectory and (b) an observed FLC trajectory. The black dots depict the observed positions; the red circles represent the laterally active points, and the blue asterisk depicts the critical moments along during the lane change, the dashed line represents the lane boundary.

aries of NGSIM recording cameras) are skewed. The lane changes at these locations were omitted. Accordingly, we obtained 794 CLC and 270 FLC samples. The velocity and acceleration were estimated from the vehicle positions every 0.1 s. In the analysis, we will use the extremes of these variables such as maximum lateral velocity and maximum lateral acceleration. However, extremes are directly affected by the noise in the dataset. In order to avoid such extremes, we smoothened these variables by employing a double-sided moving average filter proposed by Savitzky & Golay (1964). The velocity was smoothened with a time window of 1 s, and the acceleration with a time window of 2 s. The smoothening procedure and time span were chosen based on the recommendations in Thiemann et al. (2008).

As the first step, we test the assumption of unimodality of LC duration samples. This assumption forms the basis of normative representation of LC in the existing behavioural studies. We use the dip test for unimodality developed by Hartigan and Hartigan (1985). This test is widely used for the purpose due to its robustness (Freeman & Dale, 2013). The test result reveals that the lane change duration distribution exhibits a strong bimodality: $p = 0.005 < 0.01$; Hartigan's dip = 0.0185. The bimodality suggests that the sampled lane change trajectories are not the outcome of more than one process. Additionally, this finding strengthens the motivation to investigate if FLC represents a distinct type of lane changing.

4.3 Comparative analysis and models of LC execution

This section compares the lane change execution of FLCs and CLCs. Towards this, we first perform a comparative analysis of LC execution as observed from the two types of LC trajectories. Thereafter, we present a model of lateral kinematics during FLC execution.

4.3.1 Comparison of kinematics during lane-changing

Lane change execution consists of acceleration and steering operation. The steering operation during a typical CLC can be distinguished into two sequential phases of steering submovements as shown in Figure 4.4. This analysis approach has been used in previous studies (van Winsum et al., 1999). During the first phase, the steering wheel is turned to a maximum angle; and during the second phase, the steering wheel turns in the opposite direction. The second phase ends when the steering wheel angle reaches a second peak. Since this steering operation cannot be directly observed in the trajectory dataset, we define observable kinematic variables based on the above description of steering execution. The first and second steering angle peaks induce extremes in lateral acceleration due to the dynamics of vehicle movement as shown in Figure 4.4. The maximum triggering acceleration $a_{y,S}^t$ denotes the absolute maximum lateral acceleration in the first steering phase, and maximum stabilizing acceleration $a_{y,S}^s$ denotes the absolute maximum lateral acceleration in the second phase. We choose the absolute value of acceleration as it allows to jointly analysing the left and right lane change trajectories. The peak in the heading angle is accompanied by the maximum lateral velocity $v_{y,S}^{\max}$ (Rajamani, 2012). The acceleration operation during LC execution is analysed in terms of $a_{x,S}^{avg}$ denoting the average longitudinal acceleration. To summarise, we analyse LC execution using the following set of kinematic variables: D , $v_{y,S}^{\max}$, $a_{y,S}^t$ and $a_{y,S}^s$. To compare the FLC and CLC executions, we test the null hypothesis

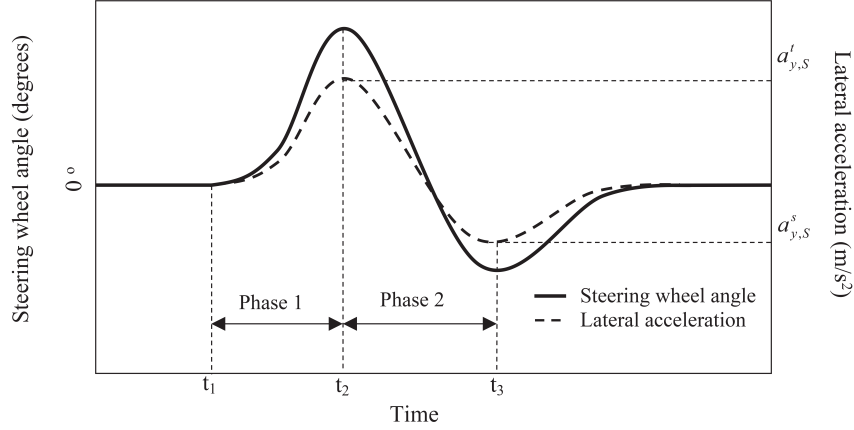


Figure 4.4: Illustration of steering sequence for CLC adapted from Hofmann et al. (2010)

that the mean of kinematic variables observed is equal between the two LC types, with two-tailed independent sample t-test. We reject the null hypothesis if the p -value is less than the significance level of 0.05. The test results presented in Table 4.1 suggest that LC execution of the FLC is different from a CLC. On average, the FLC spans a duration of 7.91 s, which is significantly longer than that of CLC 4.67 s as shown in Figure 4.5. This might be a possible reason for the bimodality of LC duration samples reported in Section 4.2. The vehicles performing CLC accelerates (0.05 m/s^2) more compared to FLC (-0.03 m/s^2). The larger longitudinal acceleration observed during a CLC might be related to the lane-changers attempt to adapt to higher velocity in the target lane. However, this hypothesis will be tested in the next section. For both types of LCs, the maximum triggering acceleration is significantly larger than the maximum stabilising acceleration. Such an asymmetry might be due to the underlying steering profile (Hofmann et al., 2010). The first peak in steering angle (corresponding to $a^s_{y,S}$) is typically higher than that of the second peak (corresponding to $a^s_{y,S}$). Salvucci & Gray (2004) attribute this asymmetry to the closed-loop steering process based on visual feedback. More precisely, the human driver controls the steering during the LC based on updated visual information on vehicle course and the target road region. Between the two types of LCs, a vehicle performing CLC is observed to have larger maximum triggering acceleration $a^s_{y,S}$ than an FLC; whereas maximum stabilising acceleration $a^s_{y,S}$ does not differ significantly. A possible explanation is that the drivers preparation for the lane change is primarily reflected in the first steering phase. The second phase consists of steering movement based on visual feedback to stabilise the vehicle on the trajectory (Hofmann et al., 2010). To summarise, the results confirm that the fragmented and continuous lane change trajectories are outcomes to two distinct processes of LC execution and agree with the existing notion that LC execution is a closed-loop process.

4.3.2 Models of lateral kinematics during LC execution

In this section, we propose a model of lateral kinematics along FLC trajectory and evaluate its fit with the observed trajectories. The functional form of the model should meet two

Table 4.1: Comparative analysis of trajectory kinematics

Parameter	LC TYPE (sample size)	Mean (Std. Error)	Difference (Std. Error)	t	Sig (2-tailed)
Average forward acceleration (m/s^2)	CLC (794)	0.05 (0.02)	0.09	2.58	0.01
	FLC (270)	-0.03 (0.02)	-0.03		
Maximum triggering acceleration (m/s^2)	CLC (794)	1.13 (0.03)	0.19	3.36	<0.001
	FLC (270)	0.94 (0.04)	-0.05		
Maximum stabilising acceleration (m/s^2)	CLC (794)	-0.53 (0.02)	0.06	1.33	0.181
	FLC (270)	-0.60 (0.03)	-0.05		
Maximum lateral velocity (m/s)	CLC (794)	1.02 (0.01)	0.04	1.87	0.062
	FLC (270)	0.98 (0.01)	-0.02		
Lane change duration (s)	CLC (794)	4.67 (0.07)	-3.23	-22.3	<0.001
	FLC (270)	7.91 (0.13)	-0.14		

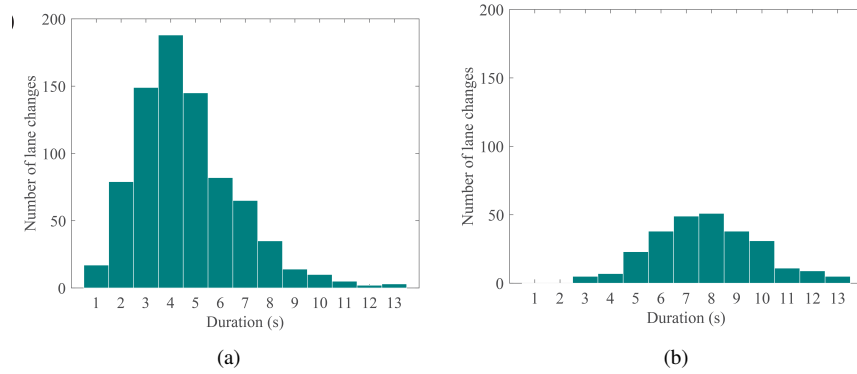


Figure 4.5: Frequency distribution of duration: a) continuous lane-changing b) fragmented lane-changing

requirements. First, the functional form should be differentiable at least until the second order. This is to ensure that the velocity and acceleration variables can be derived from the model. Secondly, the functional form should allow the distinctive lateral kinematic constraints of the FLC trajectory: 1) the vehicle laterally moves from the centerline of original to that of target lane during LC, i.e. $|y(t^{start}) - y(t^{end})| = W$; 2) the vehicle does not move laterally at the onset and end of LC, i.e. $v_y(t^{start}) = v_y(t^{end}) = 0$; $a_y(t^{start}) = a_y(t^{end}) = 0$ and 3) the vehicle does not move laterally during the pause between the two LC fragments, i.e. $v_y(t) = a_y(t) = 0 : t \in [t^{start-p}, t^{end-p}]$ where W denotes the total lateral displacement during a lane change.

Existing literature contains several models to describe an LC trajectory. The simplest and prominent representation of LC trajectory is the Linear Trajectory Model (LTM) described as follows:

$$y(t) = y(t_0) + \frac{W}{D} (t - t^{start}) \quad (4.2)$$

However, the LTM implicitly assumes constant lateral velocity and cannot represent the variation in acceleration. Therefore, this model does not meet the first functional requirement. Several other functional forms overcome this limitation such as polynomial models (Q. I. Wang et al., 2014); trapezoidal acceleration model (Soudbakhsh et al., 2013); linear acceleration model (Yang et al., 2015); hyperbolic tangent model (Zhou et al., 2017) and the Sinusoidal lateral Acceleration Model (SAM). Since empirical studies on human lane change trajectory show that lateral acceleration profiles during LC can be represented as a sinusoidal function (Salvucci & Liu, 2002), we select the SAM for further evaluation. This model has been widely used to describe the LC trajectory (Jula et al., 2000; Salvucci & Liu, 2002; J. Wang et al., 2015). The SAM expresses the lateral position during LC (the second derivative of the lateral acceleration) as:

$$y(t) = y(t^{start}) + \frac{-W}{2\pi} \sin\left(\frac{2\pi(t - t^{start})}{D}\right) + \frac{W(t - t^{start})}{D} \quad (4.3)$$

However, SAM does not meet the second functional criteria. Therefore, we propose a new model: Double Sinusoidal lateral Acceleration Model (DSAM). Among the FLC samples, the mean (standard error) duration of the first fragment is 2.58 s (0.9 s) and that of the second fragment is 2.69 s (0.1 s). This suggests that the average duration of the two fragments were approximately equal. Similarly, during the pause between the fragments the lane-changer is close to the lane marking; with a mean (standard error) lateral position error of 0.15 m (0.7 m). Based on these findings, this model assumes that a vehicle moving along an FLC trajectory achieve the total lateral displacement in two equal phases. Accordingly, the trajectory consists of two equal cycles of lateral sinusoidal accelerations, separated by a brief pause as illustrated in Figure 4.6. The DSAM can be expressed in terms of the lateral position as:

$$y(t) = \left\{ \begin{array}{l} y(t^{start}) + \frac{-W}{4\pi} \sin\left(\frac{2\pi(t - t^{start})}{d}\right) + \frac{W(t - t^{start})}{2d}; \\ \text{if : } t^{start} < t \leq t^{start} + d \\ y(t^{start}) + \frac{W}{2}; \text{if : } t^{start} + d < t \leq t^{start} + d + t_w \\ y(t^{start}) + d + \frac{-W}{4\pi} \sin\left(\frac{2\pi(t - t^{start} - d - t_w)}{d}\right) + \frac{W(t - t^{start} - d - t_w)}{2d}; \\ \text{if : } t^{start} + d + t_w < t \leq t^{start} + 2d + t_w \end{array} \right\} \quad (4.4)$$

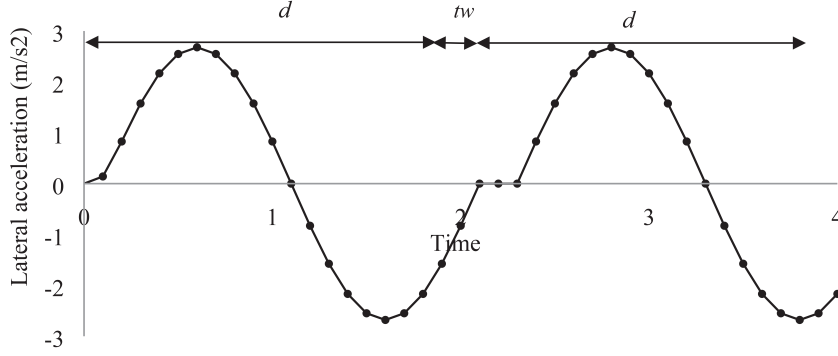


Figure 4.6: Illustration of the double sinusoidal lateral acceleration model for a fragmented lane change

where $t_w = t^{end-p} - t^{start-p}$ denotes the duration of the intermediate pause in seconds, $d = \frac{D-t_w}{2}$ denotes the duration of each lateral acceleration cycle.

4.3.3 Performance evaluation

We evaluate the performance of the DSAM model in representing the lateral kinematics of observed FLC trajectories and compare it with LTM and SAM (a more reasonable approximation of CLC). The model parameters: D, W, t_w were estimated for each sampled observation of lane-changing trajectory by Algorithm 1 as illustrated in Figure 4.2. To match the observed trajectory sampling interval, the lateral positions of the vehicle were modelled at an interval of 0.1 s. The lateral velocity and lateral acceleration of the artificial trajectories were numerically estimated from simulated vehicle positions every 0.1 s. Figure 4.7 shows examples of modelled and observed LC trajectories. We evaluate the modelling accuracy of four variables: y , $v_{y,S}^{\max}$, $a_{y,S}^t$ and $a_{y,S}^s$. As shown in Table 4.1, these variables reflect the distinction in the FLC trajectory. The performance of the three models was compared in terms of the MeanAbsoluteError(MAE) = $\frac{1}{N} \sum_{i=1}^N |X_{observed} - X_{simulated}|$. Here, N denotes the total number of trajectory samples. The MAE values in Table 4.2 indicate that trajectories produced by the DSAM describe the observed FLC trajectories more accurately than the SAM and LTM. Interestingly, the simple LTM is able to describe lateral positions during FLC with a comparable level of accuracy and is even better than the SAM model. However, DSAM provides a significant increase in the estimation accuracy of $v_{y,S}^{\max}$, $a_{y,S}^t$ and $a_{y,S}^s$ and therefore can be regarded as the best approximation of FLC trajectory. The results suggest that SAM indeed provides a better representation of a CLC trajectory than LTM.

4.4 Comparative analysis and models of LC impact

This section compares the microscopic impacts induced by FLCs and CLCs. First, we analyse the change in kinematic states of ambient vehicles during each type of LC. Towards this, we compare the relative kinematic state of neighbouring vehicles at the onset (Section 4.1)

Table 4.2: Summary of performance evaluation of the LC trajectory models

LC Type	Trajectory model	MAE values [% error reduction w.r.t. LTM]			
		y in m	$v_{y,S}^{max}$ in m/s	$a_{y,S}^t$ in m/s ²	$a_{y,S}^s$ in m/s ²
FLC	LTM	0.36	0.6	N.A	N.A
	SAM	0.42 [-17 %]	0.25 [57 %]	0.42	0.54
	DSAM	0.35 [2 %]	0.22 [62 %]	0.34	0.42
CLC	LTM	0.27	0.51	N.A	N.A
	SAM	0.21 [20 %]	0.23 [55 %]	0.54	0.48

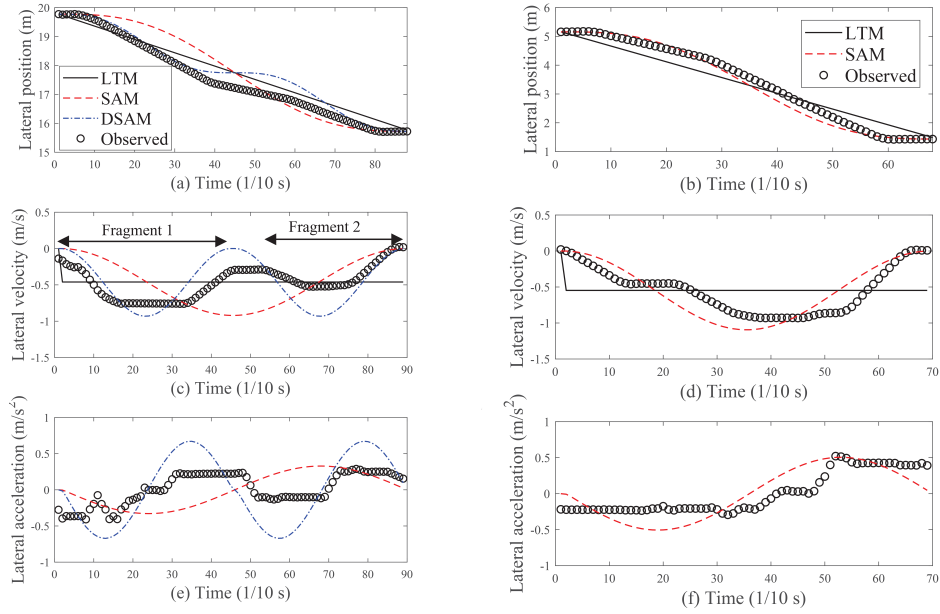


Figure 4.7: Example of simulated and observed lane-changing trajectories of FLC (a, c, e) and CLC (b, d, f)

and at the end of the lane change (Section 4.2). Secondly, we propose models to describe the effect of each type of lane change on the behaviour of the target-follower (Section 4.3).

4.4.1 Relative kinematics of ambient vehicles at the onset of lane change

As depicted in Figure 4.1, the lane change by S is influenced by neighbouring vehicles F , L and P . We use the space headway and relative velocity as explanatory variables (EV) to characterise the relative kinematics of neighbouring vehicles. This set of variables has been used in previous studies to explain the LC decision (Balal et al., 2016; Moridpour et al., 2010b,a). For each LC, the values of explanatory variables were calculated at $t - 0.2, t - 0.1, t, t + 0.1, t + 0.2$, and the average value during instances was used as the representative value in this study. The approach reduces the error caused by instantaneous measurements in NGSIM data (Balal et al., 2014). To examine the traffic conditions at the onset of the two LC types, we compare the distribution of their EV. Towards this, we test the null hypothesis, $H_0 : \mu_{EV_CLC}(t^{start}) = \mu_{EV_FLC}(t^{start})$, i.e. the mean EV of the two LC types are equal. Here, $EV \in \{g_{SF}, g_{LS}, g_{PS}, g_{PF}, \Delta v_{SF}, \Delta v_{LS}, \Delta v_{PS}, \Delta v_{PF}\}$. g_{ij} denotes the space headway of i w.r.t j and is calculated as $v_i - v_j$. The NGSIM data log contains only those vehicles which have transversed the stretch during the observation period. Therefore, trajectories of neighbouring vehicles were occasionally incomplete in lane change instances that occurred at the boundary of the test site. Such LC instances were filtered out from the analysis.

Table 4.3 summarises the test results. We reject the null hypothesis if the p value is less than the significance level of 0.05. It can be seen that the mean g_{SF} and g_{PS} are significantly different between the two LC types: in comparison to CLC, the FLC emerges when lane-changer is closer to F ; and farther away from P . Both these observations can be explained intuitively: the lower g_{SF} prevents the driver from quickly entering the target lane, and the higher g_{PS} allows the driver to remain longer in the original lane and to complete the LC relatively slower. Secondly, the mean Δv_{SF} and Δv_{LS} are significantly different between the two LC types: the FLC emerged when lane-changer is at higher velocity (on average) relative to F and L ; whereas a CLC emerged when the lane-changer is at a lower velocity (on average) relative to F and L . Assuming that the initial conditions of CLC as the standard, an average driver exhibits a preference for FLC when confronted with the relatively slower vehicles on the target lane including a closer follower, and a distant preceding vehicle. These results reveal the distinct traffic conditions related to the emergence of FLC. Additionally, the results in Table 4.3 shed light on the determinants of the choice of LC type. The EVs, underlying most of the LC decision models, are computed at the lane change insertion (t_{LC}). On the contrary, EVs listed in the present study are observed at the start of the LC. This approach is appropriate to analyse the determinants of FLC decision-making. First, EVs observed at t_{LC} is influenced by the anticipation behaviour following vehicles, and might not represent the relative kinematic state that the driver considers during the decision-making. Secondly, the choice of the FLC is made prior to lane change execution as it requires a pre-calculated steering profile. Therefore, EV observed at the start of the lane manoeuvre: t_{LC}^{start} could describe the decision-making process more accurately.

Table 4.3: Summary of the comparative analysis of the ambient traffic state at the onset of two LC types

EV	LC TYPE (sample size)	Mean (Std. Error)	Difference (Std. Error)	t	Sig (2-tailed)
$g_{SF}(m)$	CLC (762)	16.83 (0.48)	3.18	2.76	0.006
	FLC(263)	13.64 (1.04)	-1.02		
$g_{LS}(m)$	CLC (781)	12.37 (0.41)	-0.19	-0.22	0.819
	FLC(267)	12.54 (0.78)	-0.84		
$g_{PS}(m)$	CLC(647)	18.60 (0.45)	-2.3	-2.04	0.042
	FLC(184)	20.91 (1.03)	-1.13		
$g_{LF}(m)$	CLC(748)	28.90 (0.54)	2.39	1.78	0.075
	FLC(257)	26.51(1.22)	-1.34		
$\Delta v_{SF}(m/s)$	CLC (762)	-0.19 (0.09)	-0.99	-5	<0.001
	FLC(263)	0.79 (0.18)	-0.19		
$\Delta v_{LS}(m/s)$	CLC (781)	0.80 (0.09)	1.07	5.74	<0.001
	FLC(267)	-0.26 (0.17)	-0.19		
$\Delta v_{PS}(m/s)$	CLC(647)	-0.63 (0.08)	-0.09	-0.534	0.593
	FLC(184)	-0.54 (0.15)	-0.17		
$\Delta v_{LF}(m/s)$	CLC(748)	0.59 (0.07)	-0.1	-0.785	0.432
	FLC(257)	0.48 (0.11)	-0.13		

4.4.2 Change in the relative kinematics by the end of lane change

In order to evaluate the impact induced by the lane change, we compare the change in relative kinematics during each of the LC types. More precisely, we compare the change in the mean EV between the start and end of the LC, denoted as $\Delta EV = EV(t^{end}) - EV(t^{start})$: $EV \in \{g_{SF}, g_{LS}, \Delta v_{SF}, \Delta v_{LS}\}$. Towards this, we test the null hypothesis, $H_0 : \mu_{\Delta EV, CLC} = \mu_{\Delta EV, FLC}$, and the results are summarised in Table 4.4. To interpret the change, we use the ambient traffic state at the start of LC (Table 4.3) as the reference. Certain variables exhibited significantly different transitions. First, the mean transition of g_{SF} is significantly different. An average vehicle performing FLC gained a larger headway with F ($\Delta g_{SF} \approx 4.55$) by the end of LC than an average vehicle performing CLC ($\Delta g_{SF} \approx 0.38$). Note that at the start of the lane change, vehicles performing FLC had significantly shorter g_{SF} than vehicles performing a CLC (See Table 4.3).

Secondly, Table 4.4 shows that Δv_{SF} and Δv_{LS} exhibits a significantly different transition between the two LCs as shown in Figure 4.8. Table 4.3 shows that an average FLC (CLC) vehicle had higher (lower) velocity than the two vehicles in the target lane (See Figure 4.8). The results in Table 4.4 suggest that the speed difference was reduced during both types of LCs, and the transition was directed towards neutralising their initial values. Figure 4.8(a) and (b) show this trend clearly. More precisely, by the end of LC, an average FLC / CLC vehicle is at a smaller velocity difference with respect to F and L . In order to evaluate the role of each vehicle in the transition, let's first consider the interaction between S and L . In this interaction, L does not play an active role and therefore the transition is directly related to S . The respective transition of Δv_{LS} implies that an average FLC (CLC) vehicle reduces (increases) its relative velocity during lane change execution. This is consistent

Table 4.4: Summary of the comparative analysis of the transition of ambient traffic state in each LC type

EV	LC TYPE	Mean (Std error)	Difference (Std error)	t	Sig(2-tailed)
$[g_{SF}(t^{end})]$	CLC (762)	0.38 (0.40)	-4.16	-4.05	<0.000
$-g_{SF}(t^{start})$ in m	FLC (263)	4.55 (0.94)	-0.88		
$[g_{LS}(t^{end})]$	CLC (781)	-4.61 (2.05)	-3.75	-1.008	0.593
$-g_{LS}(t^{start})$ in m	FLC (267)	-0.85 (2.12)	-3.72		
$[\Delta v_{SF}(t^{end})]$	CLC (762)	0.39 (0.09)	0.84	4.15	<0.001
$-\Delta v_{SF}(t^{start})$ in m/s	FLC (263)	-0.44 (0.19)	-0.2		
$[\Delta v_{LS}(t^{end})]$	CLC (781)	-0.70 (0.09)	-1.14	-5.38	<0.001
$-\Delta v_{LS}(t^{start})$ in m/s	FLC (267)	0.43 (0.19)	-0.21		
$g_{SF}(t^{end})$ in m	CLC (762)	17.22 (0.33)	-0.97	-1.43	0.15
	FLC (263)	18.20 (0.60)	-0.69		
$\Delta v_{SF}(t^{end})$ in m/s	CLC (762)	0.20 (0.06)	-0.14	-1.17	0.24
	FLC (263)	0.34 (0.10)	-0.12		
$\Delta v_{LS}(t^{end})$ in m/s	CLC (781)	0.10 (0.06)	-0.06	-0.58	0.56
	FLC (267)	0.17 (0.09)	-0.11		

with the observation reported in Section 4.3.1 that the vehicles performing an FLC (CLC) exhibit a negative (positive) value of average acceleration: -0.03 m/s^2 (0.05 m/s^2). Now let's consider the interaction between S and F , in which both the vehicles play an active role. The identified action of and the anticipatory behaviour of F effect the transition of Δv_{SF} . More precisely, the reduction (increase) in velocity by an average FLC (CLC) vehicle and the anticipatory response of the F together reduce the speed difference between them. Figure 4.8(a) and (b) show this trend clearly. Therefore the results in Table 4.4 suggest that the FLC distinctly impact the follower in the target lane during LC. The mean g_{SF} , Δv_{SF} and Δv_{LS} are significantly different at the onset (See Table 4.3), but not at the end of LC (See Table 4.4). This suggests that both LC types ultimately result in similar local traffic conditions.

4.4.3 Models of LC impact on the target-follower

In the previous section, we identified that FLC induces a distinct transition on the follower in the target lane. The existing LC impact models describe the relaxation behaviour and anticipation behaviour, without differentiating the LC types. The relaxation process during the LC has been successfully modelled by (Laval & Leclercq, 2008). This model was conceived from a microscopic car following model incorporating the macroscopic lane change model. Z. Zheng et al. (2013) showed that this model can describe the entire transition process: anticipation and relaxation. However, none of the existing models distinguishes the impacts of FLC and CLC. We revise the model in (Z. Zheng et al., 2013) to capture the entire transition process induced by specifically by the LC types. The transition model proposed by Z. Zheng et al. (2013) is built on the assumption that vehicles obey Newell's car-following model. This model provides the speed function of a vehicle corresponding to the triangular fundamental diagram. In this model, the trajectory of a vehicle i is identical

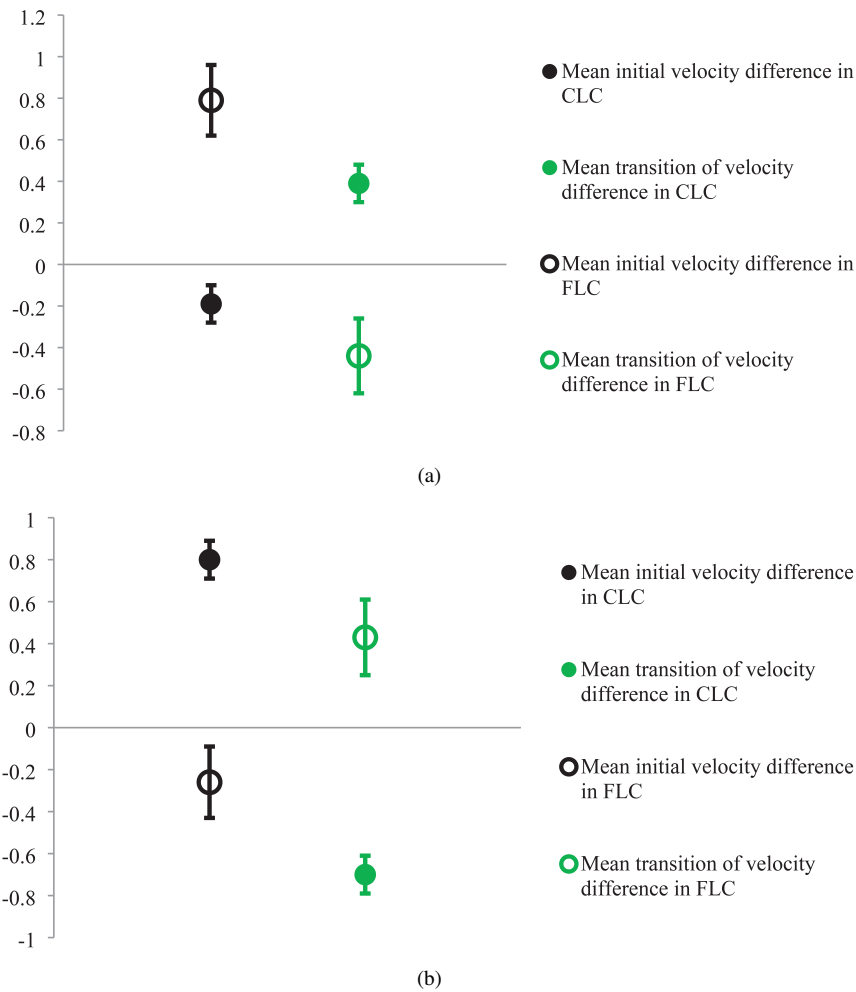


Figure 4.8: Estimates of initial and subsequent transition of the mean relative velocity: (a) Subject and Follower (b) Leader and Subject. In each figure, the velocity means are significantly different with $p < 0.01$

to that of the preceding vehicle $i + 1$ with a spatial shift d and a temporal shift τ . Thus d represents the minimum spacing and τ represents the time vehicle i waits until it responds (by manipulating its velocity) to a change in the velocity of the preceding vehicle $i + 1$. The followers transition process during a lane change is thereby modelled using a variation of its car-following parameter τ , i.e. this parameter temporarily deviates from the equilibrium value and gradually converges back. The formulation of the model is as follows:

$$\tau^i(t) = \tau^i(0) + \frac{\varepsilon}{\beta} \ln \left(1 + \frac{\beta t}{w + v^{i+1}(0)} \right) \quad (4.5)$$

where $\tau^i(t)$ is the response time of the vehicle i at the time t , $\tau^i(0)$ is its initial response time at the start of the transition, ε is the speed difference that i is willing to accept, β is a constant acceleration rate of the lead vehicle $i + 1$, w is the average velocity of kinematic waves and $v^{i+1}(0)$ is the initial speed of the vehicle $i + 1$.

Observing the transient behaviour of the target-follower

We measure the target-followers response time τ as proposed by Z. Zheng et al. (2013). Here, τ 's are measured along the set of kinematic waves propagating backwards in space with a velocity w . The process starts with the lane-changer signalling the intention to change the lane at a time t_0^{i+1} , thereby emanating the first kinematic wave. The wave moves upstream and arrives at the vehicle i at the time t_0^i . Then τ along the first wave is computed as $t_0^i - t_0^{i+1}$.

As the results in Section 4.2 show that FLC imposes a different impact on the follower in the target lane, we expect a difference in the anticipation process prior to FLC. To examine this, we filtered the pairs of lane-changers and immediate followers, those could be observed prior to the insertion, i.e. during $[t_{LC} - 10s, t_{LC} + 1s]$. A follower can be expected to exhibit the anticipation process only if its response time is shorter than the equilibrium car following response time (1.4 s). Hence, only the vehicle pairs with followers $\tau < 1.4$ s during $[t_{LC} - 10s, t_{LC} - 5s]$ are included in the analysis. Accordingly, we identified 168 vehicle pairs involved in CLCs and 75 vehicle pairs involved in FLCs. Figure 4.9 shows the temporal evolution of τ observed during CLCs and FLCs. The insertion point t_{LC} is marked as $t = 0$ s, thereby separating the anticipation phase ($t < 0$) and the relaxation phase ($t \geq 0$). The insertion point t_{LC} has been considered to be a good approximation of the time instant when the follower switches from anticipation to relaxation (Z. Zheng et al., 2013). During the anticipation phase, among the CLC samples, the average τ appears to be continuously increasing from -10 s. On the contrary, among the FLC samples, the evolution of average τ follows a different profile: it remains approximately constant for a finite time period initially (-10 s to -6 s). This could be because the follower is not yet certain that the lane-changer would cut-in, and therefore maintains its current τ . The response time is seen to steadily increase from -6 s, similar to the CLC. At the insertion time, followers (of both sets) exhibit a response time much below the equilibrium value (≈ 1.4 s) and follow a similar trend. Figure 4.9 depicts the different anticipation profile of F when confronted with FLC: follower maintains a short τ for a finite time period, and thereafter increases τ to the equilibrium value.

To observe the entire transition process of the follower: anticipation and relaxation, the vehicles should be observed for a longer period, i.e. $T^+ \in [t_{LC} - 10s, t_{LC} + 25s]$ (Duret et al.,

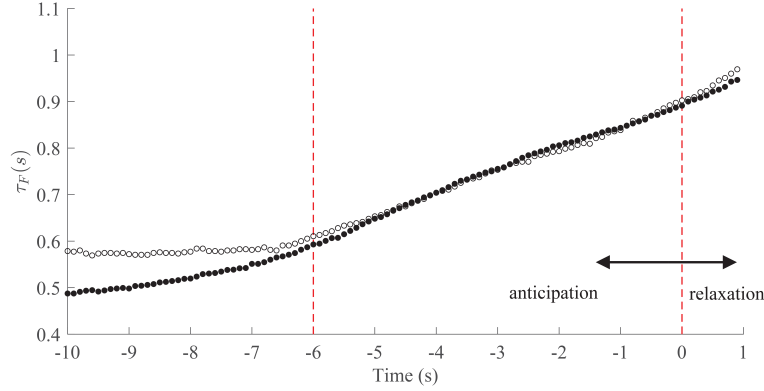
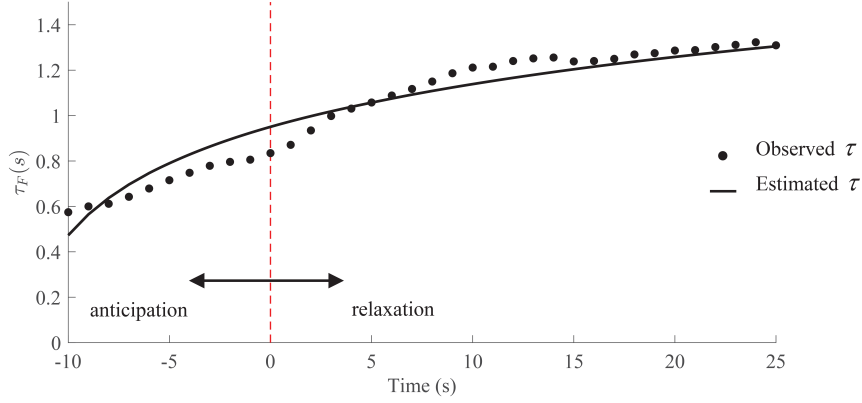


Figure 4.9: Temporal evolution of average τ for all the followers during anticipation; τ s are measured with respect to the lane-changers. On the x-axis, $t = 0$ s depicts the moment of lane change insertion.

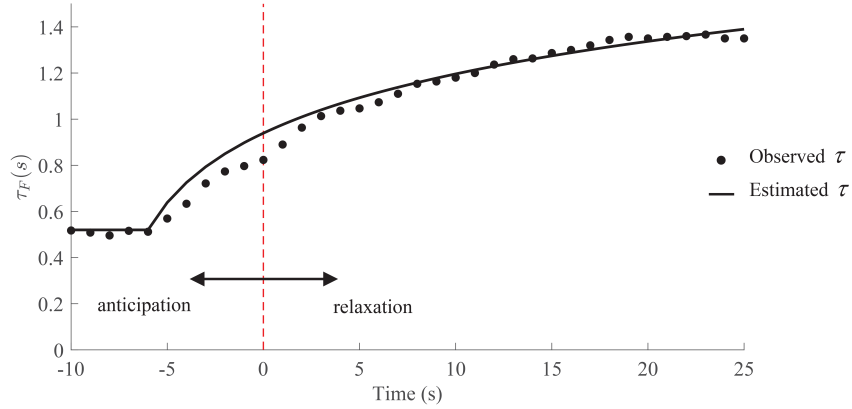
2011; Z. Zheng et al., 2013). A follower can be expected to exhibit the relaxation only if its response time deviates from the equilibrium value. As the equilibrium τ is approximately 1.4 s, only those followers with $\tau < 1$ s at $t - LC$ is considered in the analysis (Duret et al., 2011). Additionally, the follower and lane-changer must not perform any other lane change than the one of our interests. This is to avoid the effects of multiple transition processes. Accordingly, we identified 52 vehicle pairs involving a CLC and 30 vehicle pairs involving an FLC. In order to capture the entire dynamic transition process, τ s are measured along successive waves with an interval of 1 s, i.e. one out of ten τ samples is used for the modelling. This is consistent with the previous work by Z. Zheng et al. (2013). The temporal evolution of average of all followers is plotted in Figure 4.10(a) (for CLC samples) and 4.10(b) (for FLC samples). It can be seen that in both cases the followers attain a post relaxation equilibrium at around 15 - 17 s which is consistent with the study by Duret et al. (2011).

Model calibration and performance evaluation

As seen in the previous section, among the FLC samples, the mean value of τ s did not exhibit an increasing trend during the initial phase of anticipation; instead, they remain approximately constant till 6 seconds prior to insertion. To capture this observation, we model the anticipation process of the follower in response to an FLC as $\tau^i(t) = \tau^i(0) : t \in [-10, -6]$. We adopt the same calibration procedure as in the previous studies on the same dataset (Duret et al., 2011; Z. Zheng et al., 2013), and use the same values of the parameter: $w = 5$ m/s and $v^{i+1}(0) = 5$ m/s. For each lane change sample, we simultaneously calibrate $\tau^i(0)$, ε and β by minimizing the root mean squared error between observed and predicted τ values of F with respect to the lane-changer. We used unconstrained optimisation with the Quasi-Newton algorithm for minimising the RMSE error. The mean parameter values and their 95 % confidence intervals are detailed in Table 4.5. The RMSE value for the LC impact model of CLC is 0.059 and that of the FLC is 0.047, demonstrating good calibration performance. These results suggest that the follower undergo both anticipation and relaxation process ir-



(a)



(b)

Figure 4.10: Temporal evolution of average τ s for all followers (a) during continuous lane change; (b) during fragmented lane change.

respective of the lane change type it confronts. However, during the anticipation process for an FLC, the follower maintains its response time constant initially and increases thereafter.

To summarise, compared to CLC, FLC emerges under distinct traffic conditions. Moreover, FLC induces a distinct impact on the driving behaviour of the follower in the target lane, particularly during the anticipation process. We show that this distinct response of follower to FLC can be captured by a simple extension of an existing model (Z. Zheng et al., 2013).

4.5 Discussion

Compared to typical CLCs, this study revealed that FLCs represent a distinct type of lane change execution and induce a different impact on the ambient traffic. We performed two additional analyses to examine the role of the necessity of lane change and driver character-

Table 4.5: Summary of calibration results of the LC impact models

	Model of LC impact due to CLC		Model of LC impact due to FLC	
	Mean	95% CI	Mean	95% CI
$\tau^i(0)$	0.472	(0.34,0.60)	0.52	(0.35,0.68)
ε	1.061	(0.63,1.48)	1.435	(0.95,1.91)
β	3.186	(1.18, 5.18)	4.441	(2.08,6.79)
RMSE	0.059		0.047	

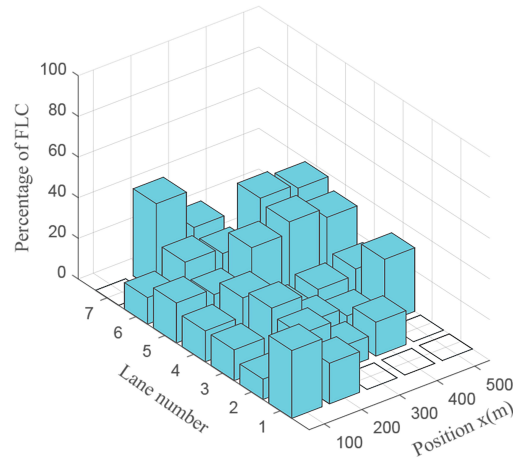


Figure 4.11: Percentage of fragmented lane changes among total lane changes per 100 meters in each lane

istics in the choice of LC type.

Figure 4.11 depicts the percentage of FLC among total lane changes originating from every 100 meters of the study stretch. In the figure, Lane 6 is the rightmost lane and Lane 7 is the on-ramp lane that merges onto the motorway. It can be seen that the share of the FLCs increase up to 40 percent downstream of the merge on lanes 5, 6 and 7. In these locations, lane changes are typically performed either to merge onto the motorway or to move to the middle lane from the rightmost lane (Balal et al., 2016). This increased necessity to change lane might also explain why the driver performs FLC despite the lower velocity of the vehicle in the target lane as reported in Section 4.1. We investigated if the characteristics of the driver such as being timid or aggressive influenced the choice LC type. The parameter has been used in several earlier studies to characterise driver behaviour (Chen et al., 2014; Z. Zheng et al., 2013). We investigate the driver characteristics of the F and S prior to the lane change. The driver characteristic is represented by the deviation in τ at $t = -10$ s from the average $\bar{\tau}$ in $t \in [-10, -15]$. A driver is classified as timid if and as aggressive if $\tau > \bar{\tau}$ and as aggressive if $\tau < \bar{\tau}$. Figure 4.12 plots the characteristics of the follower against that of the subject prior to each type of lane change. Among the follower-subject pairs, we did not find a statistical difference in the distribution of driver aggressiveness between those involved in

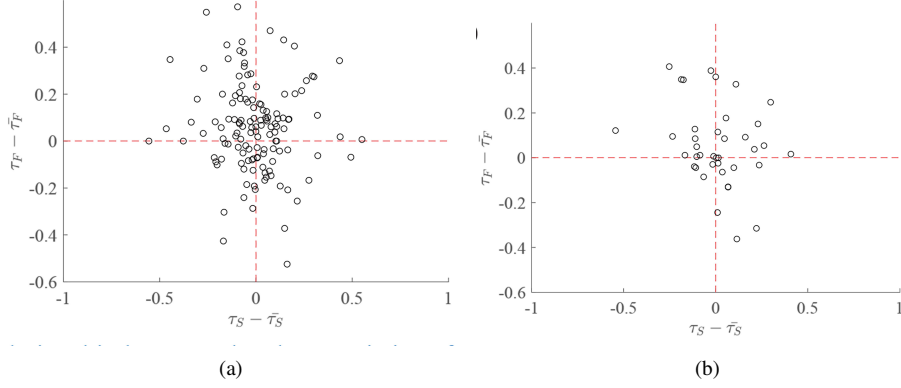


Figure 4.12: Relationship between the characteristics of the follower and characteristics of the lane-changers (a) prior to the continuous lane change, (b) prior to the fragmented lane change

the two LC types. The above two findings suggest that the choice of LC type is influenced by the necessity of lane change and not by the characteristics of the involved drivers. The results presented in this study are focused on LC of cars, as LC samples of other vehicle types were much less in the dataset. Therefore, it remains unknown if other vehicle types implement FLC. Compared to CLC, FLCs are less frequent events and hardly observed in small data sets. This study was performed on a single data set that provided a sufficient number of FLC samples. However, the findings and models are yet to be cross-validated from datasets from different locations.

4.6 Conclusions

The study employs a rule-based algorithm to systematically identify and classify the lane-changing trajectory samples from NGSIM dataset. We find that FLCs constitute a considerable proportion ($\approx 30\%$) of lane changes, thereby confirming the finding by Yang et al. (2015). We show strong evidence that FLCs are performed by a distinct execution process. A vehicle moving along the FLC trajectory exhibits a statistically different lateral and longitudinal kinematics, and longer lane change duration (≈ 7.9 s). We propose Double Sinusoidal Acceleration based model to describe the lateral kinematics of FLC trajectory. With just an additional parameter, this model describes an FLC trajectory better than the other selected models.

Regarding the impact of FLC on the potential follower, we find that an FLC induces a distinct behavioural transition of the follower in the target lane, in terms of longitudinal kinematics. The follower exhibits a different anticipation process during an FLC: it maintains the response time constant initially and increases thereafter. We presented models to describe the transient behaviour of the follower in the target lane induced by the two LC types. We find that a minor extension to the existing transition model by Z. Zheng et al. (2013) with no additional parameters improves the accuracy of the LC impact model. Additionally, this study reveals a set of factors potentially related to the choice of LC type. The

ambient traffic state at the onset of FLCs is different from that of a CLC: the follower on the target lane is spatially closer; the preceding vehicle is further away; and follower and leader in the target lane are relatively slower. Besides, the proportion of FLCs increases up to 40% under mandatory lane change conditions (at the vicinity and downstream of the acceleration lane). These two results suggest that a higher necessity to change lanes is one of the main factors motivating the driver to execute an FLC.

The insights and models presented in this the work have several applications. Describing the distinct impacts and execution of FLC can improve the accuracy of traffic flow models. The results reinforce the closed-loop nature of human steering process (Hofmann et al., 2010; Salvucci & Gray, 2004). Therefore, the conventional representation of LC execution as an open-loop process is restrictive to realistically model the LC and to describe manoeuvres such as FLC. The future work will focus on the above-mentioned aspects.



Chapter 5

A hybrid submicroscopic/microscopic traffic flow simulation framework

Abstract

Current microscopic traffic simulators combine car-following and lane changing logic to describe the vehicle motion on multi-lane road segments. However, there is no guarantee that the simulated lateral manoeuvres are physically possible, and this may detriment the accuracy of simulation results. We propose a hybrid framework consisting of an explicit vehicle model and depicting the hierarchical decision and control structure of vehicle operation. The resulting trajectories account for lateral and longitudinal dynamics and provide additional variables such as vehicle heading and steering commands. The framework adopts a modular architecture to allow implementing and testing of independent models specific to various driving sub-tasks. The resulting framework consists of two coupled layers, an upper tactical level that generates manoeuvre plans; and a lower operational layer with explicit control module (steering and acceleration control) that operates in a closed loop with the bicycle model of vehicle dynamics. The driving task addressed in each module is operationalised using specific behavioural models which have been empirically validated. Case study results provide a proof-of-concept demonstration of the power of the framework to include lateral manoeuvres such as curve negotiation, corrective steering, lane change abortion and fragmented lane changing. The framework is operationalised to model multi-lane traffic flow consisting of human-driven vehicles. At the macroscopic level, the multi-lane traffic flow simulation can reproduce phenomena such as capacity drop. Thus the framework preserves the properties of the component models and at the same time describes the planar movement of vehicles.

This chapter is based on the following article, which is currently under review:

Mullakkal-Babu, F. A., Wang, M., van Arem, B., Shyrokau, B., & Happee, R. (under review) A hybrid submicroscopic-/microscopic traffic flow simulation framework.

5.1 Introduction

Traffic models aim to describe the movement of individual vehicles in traffic. Microscopic models for longitudinal vehicle dynamics mostly use follow-the-leader logic. Such models describe the longitudinal vehicle motion as an outcome of dynamic interaction with the preceding vehicles (Hoogendoorn & Bovy, 2001). They have been applied to analyse the properties of single-lane traffic flow such as motorway capacity and platoon stability. In a multi-lane traffic environment, vehicles perform a planar motion (longitudinal, lateral and yaw motion). Therefore a longitudinal model must be combined with a counterpart lateral model to describe manoeuvres such as lane-changing and lane-keeping. Microscopic models of lateral movement mostly focus on the lane change decision (LCD). LCD models describe the decision-making process as an outcome of interactions with ambient traffic and that of a driver's intrinsic preferences (Kesting et al., 2007; Schakel et al., 2012). A typical microscopic traffic simulator for multi-lane traffic integrates a longitudinal car-following model and a lateral lane-change decision model to generate 2-D vehicle trajectories. It employs a simplified vehicle model to efficiently simulate a large number of vehicles necessary to test traffic management strategies and to evaluate the traffic flow impacts of longitudinal automation systems such as Adaptive Cruise Control. The simplified vehicle models employed by microscopic simulators, however, do not necessarily yield plausible trajectories of lateral manoeuvres, during which the dynamic constraints of vehicle motion come to play. Considering that the lateral manoeuvres such as lane changes are frequently observed on multi-lane motorways, realistically modelling them is relevant to ensure accurate results, especially regarding traffic safety (Mullakkal-Babu et al., 2017; So et al., 2015).

The simplified representation of lateral vehicle dynamics reflects four methodological deficiencies. Firstly, an explicit vehicle model is not included in the modelling framework; instead, the driver and vehicle are treated as a single unit (Barcelo, 2010). Hence, such simulators do not ensure that the driver-vehicle unit respects the nonholonomic constraints of the vehicle motion (So et al., 2015). Moreover, they do not differentiate the motion behaviour of vehicles based on physical properties such as mass and inertial properties. The second deficiency is the absence of a steering angle which is an essential control variable for lateral manoeuvres such as lane-changing. Alternatively, most of the simulators interpolate the lateral vehicle position during the lane change event, which is typically treated as an instantaneous event (Hidas, 2005) upon which the vehicle jumps from one lane to the other or as a fixed-duration process within which the vehicle achieves a lateral displacement (Fellendorf & Vortisch, 2010; So et al., 2015). Considering that the number of positive lane change decisions depends explicitly on the simulation time-step and the lane change duration, this approach can influence the number of simulated lane changes. Moreover, this treatment regards lane-changing as an open-loop process. Once a lane change decision is made, neither the lane change decision nor the movement is re-evaluated. On the contrary, behavioural studies on human-steering control report that lane changing is a closed-loop process in which driver uses visual feedback to regulate the steering operation (Li et al., 2018; Salvucci & Gray, 2004). The major problem with this approach, however, is that the dependency between lateral and longitudinal vehicle state variables is not accounted for.

The aforementioned deficiencies restrict or detriment the applicability of such simulators for safety assessment of traffic involving lateral vehicle manoeuvres. Safety metrics such as the surrogate safety measures are directly quantified from the simulated trajec-

ries (Mullakkal-Babu et al., 2017; So et al., 2015). If the trajectories are unrealistic, the safety assessments are prone to be inaccurate. Besides, lateral manoeuvres such as aborted lane changing and interrupted lane changing cannot be described by existing microscopic simulators, as they involve feedback between the steering operation and the lane change decision. Inaccurate modelling of lane changes can detriment the validity of estimation of lane change-induced impacts. Moreover, current microscopic simulators, which lack a steering angle description, do not allow direct modelling of steering controllers and are not suitable to assess their impacts.

Recently, modelling frameworks that integrate an explicit vehicle dynamic model with microscopic models have been proposed. Due to their detailed description of vehicle dynamics, they are known as submicroscopic or nanoscopic models (Hoogendoorn & Bovy, 2001; Ni, 2003). Compared to microscopic simulators, submicroscopic simulators improve the realism of simulated trajectories. Kumar et al. (2014) proposed a multi-level modelling framework based on bond-graphs incorporating detailed longitudinal dynamics. Dedes et al. (2011) proposed a framework that integrates the vehicle dynamics and GNSS-INS errors. Traffic simulators such as MIXIC (van Arem et al., 1997) and PELOPS (Rehder et al., 2019) allow detailed modelling of longitudinal vehicle dynamics. Such submicroscopic models, however, do not explicitly model vehicle dynamics in the lateral manoeuvre. So et al. (2015) proposed an approach to generate more realistic lateral manoeuvre trajectories. In this approach, targeted for traffic safety assessment, lateral trajectories from a microscopic model are post-processed by a high-fidelity commercial vehicle model (So et al., 2015, 2018). However, this approach is not adequate to analyse the effects of lateral manoeuvres on traffic flow characteristics. Kaths & Krause (2016) proposed a co-simulation framework wherein a single test vehicle is modelled by a high fidelity commercial vehicle model, and the surrounding vehicles are simulated by the microscopic model. None of the reviewed works attempts to model the multi-lane traffic flow wherein all the simulated trajectories respect vehicle dynamic constraints.

The objective of this work is to propose and operationalize a framework to model multi-lane traffic flow with 2D trajectory descriptions of vehicles by integrating driving-task-specific models (decision-making and operation) with an explicit vehicle model. Such a framework is envisioned to improve the accuracy of the traffic safety assessment. The framework adopts a modular architecture to allow implementing and testing of independent models specific to various driving sub-tasks. This chapter focuses on modelling human-driven vehicles, while future publications will address mixed traffic with human driven and automated vehicles. The resulting framework consists of two coupled layers: an upper tactical level that generates dynamic manoeuvre plans; and a lower operational layer with explicit control module (front road-wheel steering and acceleration control) that operates in a closed loop with the bicycle model of vehicle dynamics. The simulator employs a hybrid scheme to reduce the computational load. To enhance the computational efficiency, it activates the manoeuvre planning and steering control only during lateral manoeuvres such as lane changing and curve negotiation, and performs as a microscopic simulator otherwise.

In this work, we propose a method to integrate lateral vehicle dynamics into the traffic simulation framework. In comparison to the typical simulation approaches, the presented framework has three advantages: 1) The proposed framework captures the effects of vehicle model parameters on lateral dynamics and yaw motion by incorporating the bicycle model for lateral dynamics in traffic simulation, and thereby improves the realism of the simula-

tion 2) the framework can model a wider set of vehicle manoeuvres: the steering control module allows modelling curve negotiation, corrective steering; and closed-loop interconnection between tactical and operational layer allows modelling aborted and fragmented lane changes 3) the submicroscopic variables such as front road-wheel steering and vehicle heading angle allow examining the feasibility of the behavioural sub-models.

5.2 Model framework

In order to meet the research objective the framework design should meet three requirements: 1) it should be generic to include human-driven and automated vehicles; 2) it should be modular to allow testing of multiple models that independently focus on specific driving tasks, such as lane change decisions or car following; 3) it should be able to describe front road-wheel steering and acceleration variables subject to vehicle dynamics.

5.2.1 Framework

The framework consists of two coupled layers: an upper *tactical plan* layer and a lower *operational control* layer as shown in Figure.5.1. The constituent layers were conceptually proposed by Michon (1985). The proposed framework complements the conceptual framework by laying a solid mathematical foundation that operationalizes on-road driving tasks accounting for feedback in and between different layers. Besides, this framework is consistent with the decision and control system architecture applied for highly automated vehicles (Ardelt et al., 2012) and therefore satisfies requirement 1.

To meet requirement 2, the framework adopts a modular architecture. The influence of strategic plans such as route and destination choices is beyond the current research scope and therefore the strategic plan layer is omitted. The upper tactical layer generates dynamic decisions and plans pertaining to the vehicle manoeuvres. For the longitudinal driving task, the tactical layer sets the parameters such as desired velocity and desired time headway to desired values. The dynamic decision pertaining to lateral manoeuvres is the desired lane which is generated by the *desired lane* module. The vehicle performs a lane change manoeuvre if a lane other than the current lane is desired. In this case, the *reference trajectory* module generates the reference plan to facilitate the lane-changing manoeuvre. This can be a static plan over a time horizon or a dynamic plan updated at each time step. For lane-changing, the horizon is in the order of few seconds (typically < 10 s). Additionally, the tactical commands governing the lane change should ensure the safety of a prospective lane change. Most of the behavioural lane change decision models serve this purpose as they include a safety check prior to accepting a gap in the desired lane. In automated vehicles, this safety check is typically performed by the reference trajectory module.

The operational layer generates control commands (i.e. acceleration and front road-wheel steering angle), respecting the tactical decisions, to operate the vehicle along the reference trajectory. This layer consists of a *steering control* module and an *acceleration control* module which generates the frontage road-wheel steering and acceleration commands, respectively. Thereafter the vehicle state is updated subject to the dynamic behaviour described by the *vehicle model* module. The operational control commands are usually updated at the fraction of one second, a frequency much higher than the tactical

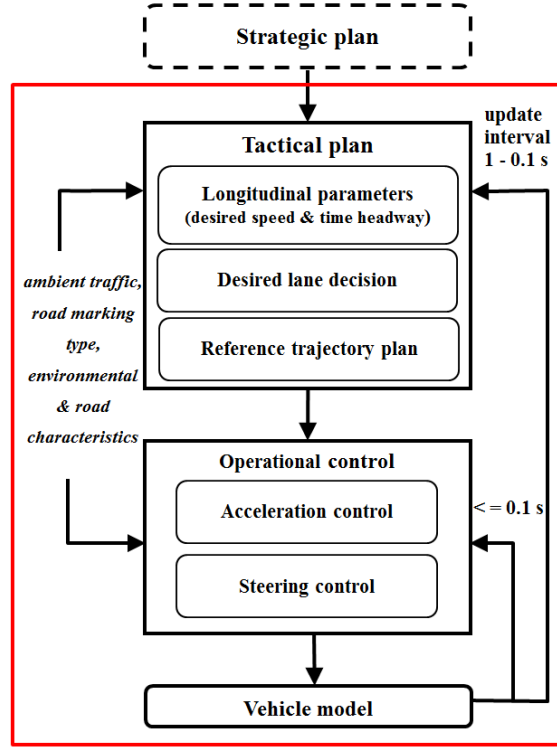


Figure 5.1: Framework for hybrid submicroscopic-/microscopic simulation, the red box indicates the scope of this work

layer decisions. The tactical and operational functions will be specifically formulated later in this section.

In this framework, the information is circulated between the two control layers and the vehicle system (represented by the system dynamics model) in order to model the revisions in manoeuvre plans, e.g., trajectory replanning or aborting a lane-change. The tactical plan is updated at a time-step Δt^u and the operational actions are updated at time-step Δt^l such that $\Delta t^u \geq \Delta t^l$. The kinematic states and properties of ambient traffic entities such as vehicles, road markings, and road characteristics enter the framework as environmental inputs at the tactical and operational layers.

The presented framework differs from most microscopic frameworks on two aspects: 1) the existence of an explicit vehicle model and steering control, 2) the existence of a feedback mechanism between the tactical and operational layers. The component modules in the framework allow modelling the lateral and longitudinal dynamics and yaw motion of individual vehicles in multi-lane traffic flow. Even though the two-layered structure is a well-known conceptual framework, in this contribution, we establish the component modules and construct the relationship between the component modules. This allows the modelling of driver-vehicle behaviours that cannot be captured in the microscopic framework such as dynamic trajectory planning and manoeuvres such as curve negotiation, corrective

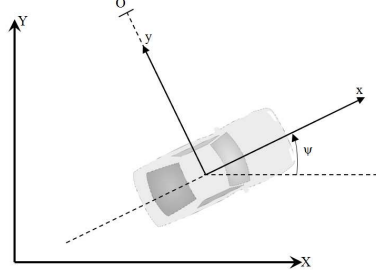


Figure 5.2: The two coordinate systems and the motion variables

steering, fragmented lane change and lane change abortion. We demonstrate the operations of the framework as a prototype simulator for human-driven vehicles.

5.2.2 Vehicle model

In this section, we specify the vehicle model used in the framework. The vehicle motion is modelled as a loosely coupled combination of two linearized models describing the longitudinal; and lateral and yaw motion.

Model for Longitudinal Vehicle Dynamics

Let (x) denote the longitudinal position of the vehicle based coordinate system as shown in Figure 2, then its longitudinal dynamics can be expressed as

$$m\ddot{x} = F_T - F_A - F_G - F_D \quad (5.1)$$

where m denotes the physical mass of the vehicle, F_T denotes the traction force, F_R denotes the aerodynamic drag, F_G denotes grade resistance and F_D denotes the mechanical drag. The longitudinal dynamics expressed in (5.1) can be modelled in a linear form by employing exact linearization. We refer to M. Wang (2018) for its detailed mathematical derivation. The following set of differential equations describe the linearized longitudinal model

$$\frac{d}{dt} \begin{Bmatrix} x \\ \dot{x} \\ \ddot{x} \end{Bmatrix} = \begin{Bmatrix} v_x \\ a_x \\ \frac{u_x - a_x}{\tau} \end{Bmatrix} \quad (5.2)$$

where v_x denotes the longitudinal velocity and a_x denotes the actual longitudinal acceleration. The longitudinal motion is controlled by the desired acceleration command u_x . The desired acceleration is executed with a lag: τ representing the finite time needed by the engine actuators to generate the desired acceleration. The physical limitations of vehicle motion are implemented as a set of constraints: we model strictly forward motion and feasible velocity limit by setting $0 < v_x < v^{max}$; we bound the acceleration representing the powertrain limitations and braking systems as $-a_{brake} \leq a_x \leq a_{acc}$.

Model for Lateral Vehicle Dynamics

The classical dynamic bicycle model (Rajamani, 2012) is chosen to model the lateral vehicle dynamics. This linear time-invariant model has been widely used in the design of steering controllers (Hatipoglu et al., 2003; Luo et al., 2016) and has been shown to demonstrate a good modelling accuracy (Smith & Starkey, 1995). First, the equation for the translational motion of the vehicle can be derived from Newton's second law of motion as follows

$$m(\ddot{y} + \dot{\psi}v_x) = F_{yf} + F_{yr} \quad (5.3)$$

where m denotes the mass of the vehicle. The inertial acceleration of the vehicle's centre of gravity in the y -direction (see Fig. 5.2) is the algebraic sum of the acceleration \ddot{y} along the y -axis and the centripetal acceleration $\dot{\psi}v_x$; ψ is the heading angle of the vehicle in the global X-Y coordinate system. The two front wheels and the two rear wheels are represented by a single front and rear wheel, and F_{yf}, F_{yr} are the lateral tire forces of the figurative single front and rear wheels respectively. The equation for yaw dynamics is obtained by the moment balance about the z -axis as

$$I_z \ddot{\psi} = l_f F_{yf} - l_r F_{yr} \quad (5.4)$$

where I_z denotes the moment of inertia about the z -axis; l_f, l_r denotes the respective distances of the front and rear axles from the center of gravity. The lateral tire forces in (5.3) are approximated by linear functions of slip angles (Rajamani, 2012) as

$$F_{yi} = 2C_i(\alpha_i), i \in \{f, r\} \quad (5.5)$$

where f and r denote the front and rear axle respectively, C_i is the cornering stiffness of lumped tires for the axle i , and α_i is the slip angle of lumped tire i . At small angles, α_i can be approximated as

$$\alpha_f = \theta_f - \frac{\dot{y} + l_f}{v_x}, \alpha_r = \frac{l_r - \dot{y}}{v_x} \quad (5.6)$$

where θ_f is the front road-wheel steering angle. The small angle approximation is reasonable for typical highway operating conditions. Substituting (5.5) and (5.6) into (5.4) and (5.3), the state space model for lateral motion can be written as

$$\dot{\mathbf{s}}_y = \mathbf{A}\mathbf{s}_y + \mathbf{B}\theta_f \quad (5.7)$$

where

$$\mathbf{s}_y = \begin{bmatrix} y \\ \dot{y} \\ \psi \\ \dot{\psi} \end{bmatrix}, \mathbf{B} = \begin{bmatrix} 0 \\ \frac{2C_{\alpha f}}{m} \\ 0 \\ \frac{2l_f C_{\alpha f}}{I_z} \end{bmatrix}$$

$$\mathbf{A} = \begin{bmatrix} 0 & 1 & 0 & 0 \\ 0 & -\frac{2C_{\alpha f} + 2C_{\alpha r}}{mv_x} & 0 & -v_x - \frac{2l_f C_{\alpha f} - 2l_r C_{\alpha r}}{mv_x} \\ 0 & 0 & 0 & 1 \\ 0 & -\frac{2l_f C_{\alpha f} - 2l_r C_{\alpha r}}{I_z v_x} & 0 & -\frac{2l_f^2 C_{\alpha f} + 2l_r^2 C_{\alpha r}}{I_z v_x} \end{bmatrix}$$

According to this model, the lateral vehicle position y and the heading angle ψ is con-

trolled by the front road-wheel steering input θ_f .

5.2.3 Formulating tactical functions

In this section, we specify the tactical functions and formulate models to represent them. Figure 5.3 depicts the tactical planning process in the framework. The function of the tactical layer is to generate the reference input vector $\mathbf{R} = (v^d, T^d, \xi(t), k(t))^T$. The first two elements are longitudinal reference inputs: v^d denotes the desired velocity during unconstrained driving. The second input, T^d denotes the desired time gap with the preceding vehicle on the desired lane σ^* . Here, v^d and T^d are dynamic variables that are revised to describe the temporary behavioural changes. For instance, v^d is revised to reflect the change in speed limit or T^d is reduced to reflect acceptance of shorter time headways during lane-changing. We select these two variables as the tactical reference signals governing the longitudinal motion, as they are commonly present in a wide range of phenomenological car following models (Treiber & Kesting, 2013) and longitudinal control systems such as Adaptive Cruise Control (Mullakkal-Babu et al., 2016).

The third and fourth elements are the lateral reference inputs. $\xi(t)$ denotes the direction of lane change, i.e. $\{-1, -0.5, 0, 0.5, 1\} := \text{change to the centre of the left lane, move to left boundary, no change, move to the right boundary, change to the centre of the right lane}$. Here, $\xi(t) = \pm 0.5$ represents the drivers decision to temporally pause the lateral manoeuvre by driving roughly along the lane boundary. Such fragmented manoeuvres are executed by human drivers (Yang et al., 2015) and are applied as a lane change strategy in highly automated driving systems (Ardelt et al., 2012). For human driven vehicles, the $\xi(t)$ can be modelled by existing lane change decision models, and their detailed review can be found in (Z. Zheng, 2014). $k(t)$ denotes the curvature of the reference trajectory plan as follows

$$k(t) = \begin{cases} k_\sigma & , \text{if: } \xi(t) = 0 \\ k(t) \forall t_0 \leq t \leq t_0 + \bar{D} & , \text{if: } \xi(t) \neq 0 \end{cases} \quad (5.8)$$

where k_σ is the curvature of the center line of the current lane, σ ; t_0 is the current time, \bar{D} is the lane change duration. The models to describe the aforementioned tactical inputs will be specified in Section 5.3.

5.2.4 Formulating operational functions

The function of the operational layer is to generate front road-wheel steering θ_f and acceleration commands u_x . The block diagram of the adopted control structure is shown in Fig. 5.4. The control problem is divided into two subproblems and we deploy two interconnected controllers to solve each problem. The longitudinal controller generates the acceleration command u_x to track the longitudinal reference input and lateral controller accounts for the velocity change induced by the longitudinal control and generates front road-wheel steering command to regulate the vehicle to track the reference path specified by the reference curvature input.

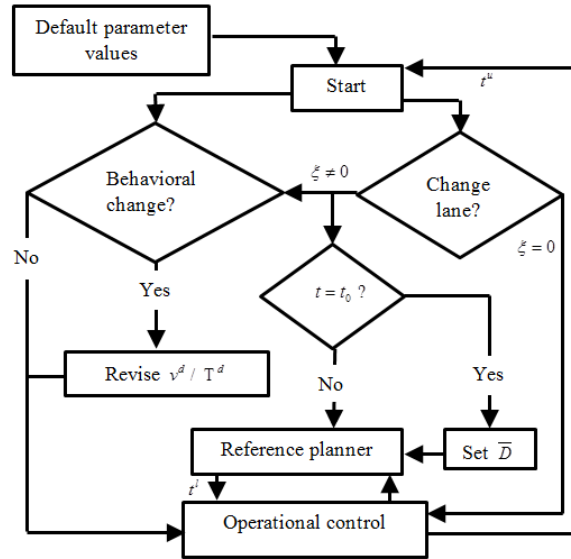


Figure 5.3: Flowchart of tactical planning

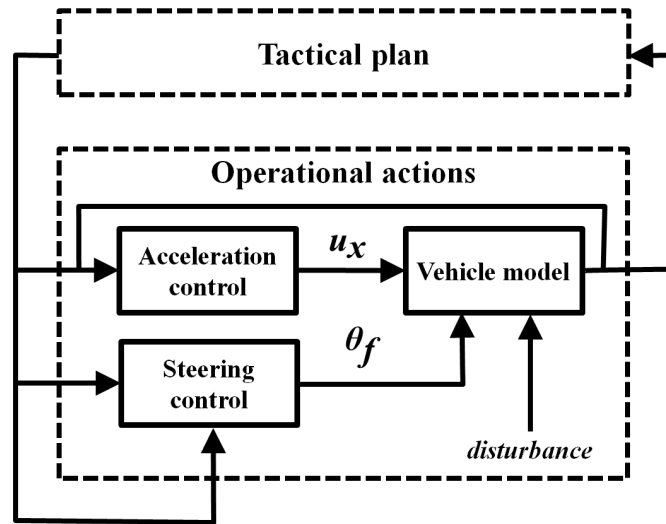


Figure 5.4: Control structure implemented in the framework

5.3 Operationalisation of the framework with behavioural models

In this section, we operationalize the framework to describe the trajectories of human-driven vehicles on a multi-lane road stretch. Towards this, we select a set of established behavioural models to be applied as component modules of the framework.

5.3.1 Models of tactical functions

This section details the chosen behavioural models to describe tactical reference inputs.

Longitudinal Parameters

The two tactical inputs governing the longitudinal dynamics are: v^d denoting the desired speed and T^d denoting the desired time headway. The value of v^d is fixed for each driver and is bounded by the maximum feasible speed v^{max} . Similarly, T^d is a fixed value, and is temporarily adjusted during a mandatory lane change. During a mandatory lane change, the lane-changing vehicle (c) and the following-vehicle in the target lane (f) accepts a shorter headway to facilitate the lane change and subsequently relaxes to the normal headway within a finite time horizon (Laval & Leclercq, 2008). In this work, the variation of T^d during the relaxation horizon is modelled as a linear rise (Schakel et al., 2012).

Lane Change Decision

The lane change decision is described by the model: Minimising Overall Braking Induced by Lane changes (MOBIL). The model description and validation can be found in (Kesting et al., 2007). This model specifies compact rules that govern the lane-change decisions of human drivers. This model derives the utility and risk of a lane change from a car-following model and is compatible with a wide range of car-following models. This model accounts for the car-following acceleration of three vehicles: the lane changing vehicle c , follower vehicle in the current lane o and potential follower in the target lane f . In this model, the utility of a lane change is defined as

$$U = \tilde{A}_c - A_c + p [\tilde{A}_f - A_f + \tilde{A}_o - A_o] \quad (5.9)$$

where A_c is the acceleration of c in the current lane and \tilde{A}_c is its acceleration after the prospective lane change. Similarly, the current and prospective accelerations of the original follower o and potential follower f are included in the model. The parameter p denotes the politeness parameter representing the degree of cooperation while considering a lane change: $p = 0$ implies egoistic behaviour without considering the implication to neighbouring vehicles and $p > 1$ implies an altruistic one. The lane change decision is then made based on the following rule

$$\xi(t) = \begin{cases} +1 : U_{right} > \Delta A_{th} - A_{bias} & \& U_{right} \geq U_{left} \\ -1 : U_{left} > \Delta A_{th} + A_{bias} & \& U_{left} > U_{right} \\ 0 : \text{otherwise} \end{cases} \quad (5.10)$$

where A_{bias} implements the keep-right directive on lane usage, A_{th} the threshold of overall acceleration gain.

Reference Plan for a Lane Change Trajectory

In order to generate $k(t)$ when $\xi(t) \neq 0$, a reference trajectory planner should be deployed. Since the tactical layer operates in a closed loop with the operational layer, the reference trajectory plan should allow dynamic updates. We use a time-based polynomial function to formulate the reference trajectory. This function has been used to formulate reference plans in automated lane change control systems (Luo et al., 2016). The reference trajectory is planned as an independent time series of the vehicle global lateral and longitudinal positions as follows

$$\begin{aligned} Y(t) &= a_5 t^5 + a_4 t^4 + a_3 t^3 + a_2 t^2 + a_1 t + a_0 \\ X(t) &= b_2 t^2 + b_1 t + b_0 \end{aligned} \quad (5.11)$$

The reference lateral trajectory is chosen to be a quintic polynomial as it allows a continuous curvature and is differentiable to the third degree. The reference longitudinal trajectory is chosen to be a quadratic polynomial so as to represent the constant longitudinal acceleration generated by the longitudinal controller. The above functions include nine unknown coefficients which can be determined by solving for the boundary conditions of the lane change process in (5.12), thereby smoothly connecting the preceding and following driving period.

$$\begin{aligned} X(t) &= X_0, \quad \dot{X}(t) = V_{X,0}, \quad \ddot{X}(t) = A_{X,0} \\ Y(t) &= Y_0, \quad \dot{Y}(t) = V_{Y,0}, \quad \ddot{Y}(t) = A_{Y,0} \\ Y(D) &= Y_D, \quad \dot{Y}(D) = 0, \quad \ddot{Y}(D) = 0 \end{aligned} \quad (5.12)$$

where $X_0, V_{X,0}, A_{X,0}$ are the current global longitudinal position, velocity and acceleration; $Y_0, V_{Y,0}, A_{Y,0}$ are the current global lateral position, velocity and acceleration; Y_D is the final lateral position and D is the remaining time duration to complete the lane change. Applying the boundary conditions in (5.12) to (5.11), the nine unknowns can be formulated as a function of D and Y_D . The curvature of the reference trajectory can be derived as a function of time as follows

$$k(t) = \frac{\ddot{Y}(t)\dot{X}(t) - \ddot{X}(t)\dot{Y}(t)}{\dot{X}(t)^3 \left(1 + \left(\frac{\dot{Y}(t)}{\dot{X}(t)} \right)^2 \right)^{\frac{3}{2}}} \quad (5.13)$$

The tactical variation in desired lane change direction $\xi_i(t)$ governed by (5.10) will be reflected in Y_D as follows: $Y_D(t) = Y_\sigma + W\xi_i(t)$, where Y_σ is the lateral position of the centerline of the current lane, σ ; W is the lane width; and as we model lane changes as fixed duration manoeuvres, we set $D = \bar{D} - t$.

Lane Change Duration

The duration of each lane change event is treated as a variable that is derived from the traffic conditions at the start of the lane change. We choose the model proposed by Toledo & Zohar (2007) to describe the lane change duration of a vehicle. This model guarantees a non-negative lane change duration, but does not constrain its maximum value. Therefore,

the lane change duration is restricted to a maximum value D^{\max}

$$\bar{D}_n = \min(e^{\beta E_n}, D^{\max}) \quad (5.14)$$

where E_n denotes the vector of explanatory variables including traffic density and relative kinematic states of the subject vehicle with respect to the follower and leader in the target lane. β is a vector consisting of the weights assigned to each explanatory variable.

5.3.2 Models of Operational Functions

This section details the chosen behavioural models to describe the acceleration and front road-wheel steering commands.

Acceleration Control

To describe the acceleration control of human drivers, we employ the behavioural model: Intelligent Driver Model (Treiber et al., 2000) with descriptive parameters. The IDM acceleration of a vehicle is a continuous function of space gap and velocity difference of n with the preceding vehicle $n - 1$.

$$u_x = a \left[1 - \left(\frac{\dot{X}_n}{v^d} \right)^4 - \left(\frac{s^*(\dot{X}_n, \Delta \dot{X}_n)}{s_n} \right)^2 \right] \quad (5.15)$$

where a denotes the maximum acceleration, v^d is the desired velocity obtained as the reference command, $s_n = X_{n-1} - X_n - L$ denotes the space gap, L denotes the length of the $n - 1$, $\Delta \dot{X}$ denotes the velocity difference of n with respect to the preceding vehicle $n - 1$. s^* denotes the desired minimum gap as follows

$$s^* = s_0 + \dot{x}T^d + \frac{\dot{x}}{2\sqrt{ab}} \quad (5.16)$$

where T^d is the desired time headway that is obtained as the reference signal from tactical layer, s_0 denotes the minimum space gap, and b is the comfortable braking.

Steering Control

We choose a steering controller with state feedback to describe the steering control (Rajamani, 2012). The controller regulates the front road-wheel steering angle by tracking the error: \mathbf{e} described as follows

$$\mathbf{e} = \begin{bmatrix} e_1 \\ e_2 \end{bmatrix} \in e_1 = y - y_{ref}; e_2 = \Psi - \Psi_{ref} \quad (5.17)$$

where y_{ref} is the vehicle based lateral coordinate of the reference trajectory (during lane changing) or the centerline of the current lane (during lane keeping), Ψ_{ref} is the reference heading angle which is the angle between the horizontal axis and the tangent of the reference path at y . The front road-wheel steering signal is obtained by a state feedback vector \mathbf{K}

in combination with a feedforward term θ_{ff} providing feedforward control of the desired curvature as follows:

$$\theta_f = -\mathbf{K}\mathbf{e} + \theta_{ff} \quad (5.18)$$

where θ_{ff} is derived from the steady state steering angle for zero lateral position error as given in (Rajamani, 2012). By inserting the steering control law to the vehicle dynamics model in (5.7), we can derive the closed loop state feedback system as:

$$\frac{d}{dt} \{\mathbf{e}\} = [\mathbf{A}^c - \mathbf{B}_1^c \mathbf{K}] \{\mathbf{e}\} + [\mathbf{B}_2^c] \dot{\psi}_{ref} + [\mathbf{B}_1^c] \theta_{ff} \quad (5.19)$$

where $\dot{\psi}_{ref}$ is the reference yaw rate is derived from the reference curvature command from (5.13) using the relationship $\dot{\psi}_{ref} = v_x k$. \mathbf{A}^c , \mathbf{B}_1^c , \mathbf{B}_2^c are the closed loop system matrices parameterized by the vehicle static vehicle parameters as follows

$$\mathbf{A}^c = \begin{bmatrix} 0 & 1 & 0 \\ 0 & -\frac{2C_{\alpha f} + 2C_{\alpha r}}{mv_x} & \frac{2C_{\alpha f} + 2C_{\alpha r}}{m} \\ 0 & 0 & 0 \\ 0 & -\frac{2l_f C_{\alpha f} - 2l_r C_{\alpha r}}{I_z v_x} & \frac{2l_f C_{\alpha f} - 2l_r C_{\alpha r}}{I_z} \\ 0 & -\frac{2l_f C_{\alpha f} - 2l_r C_{\alpha r}}{mv_x} & 1 \\ 0 & -\frac{2l_f^2 C_{\alpha f} + 2l_r^2 C_{\alpha r}}{I_z v_x} & 0 \end{bmatrix} \quad (5.20)$$

$$\mathbf{B}_1^c = \begin{bmatrix} 0 \\ \frac{2C_{\alpha f}}{m} \\ 0 \\ \frac{2l_f C_{\alpha f}}{I_z} \end{bmatrix}, \mathbf{B}_2^c = \begin{bmatrix} 0 \\ -v_x - \frac{2l_f C_{\alpha f} - 2l_r C_{\alpha r}}{mv_x} \\ 0 \\ -\frac{2l_f^2 C_{\alpha f} + 2l_r^2 C_{\alpha r}}{I_z v_x} \end{bmatrix}$$

Applying the optimal state feedback vector \mathbf{K} in (5.18) minimises the performance index J defined as

$$J = \sum_{K=0}^{\infty} \mathbf{e}^T(\mathbf{K}) \mathbf{Q} \mathbf{e}(\mathbf{K}) + \theta_f^T(\mathbf{K}) \mathbf{R} \theta_f \quad (5.21)$$

where J is a quadratic measure of future behaviour with origin as the target. Here, \mathbf{Q} is the weight of deviation of the state from the target and \mathbf{R} is the weight of the control activity. The optimal feedback \mathbf{K} in (5.21) is derived from \mathbf{S} which is solution of the associated algebraic Ricatti equation by setting

$$\mathbf{K} = \mathbf{R}^{-1}(\mathbf{B}_1^c \mathbf{S}) \quad (5.22)$$

The solution of \mathbf{K} in (5.22) is obtained by a Linear Quadratic Regulator algorithm. The global coordinates of the vehicle can be estimated as $X = \int_0^t v_x \cos(\psi_{ref}) dt - e_1 \sin(e_2 + \psi_{ref})$ and $Y = \int_0^t v_x \sin(\psi_{ref}) dt + e_1 \cos(e_2 + \psi_{ref})$ (Rajamani, 2012).

5.4 Simulation experiments and results

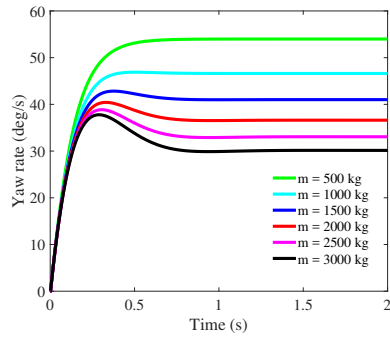
The framework and the selected formulations of the component models of the prototype simulator were presented in the previous section in a continuous time form. In this section, we numerically implement the hybrid framework using discrete time simulations. The tactical layer is updated at $\Delta t^u = 0.1$ s and the operational layer is updated at $\Delta t^l = 0.01$ s. To reduce the computational load, the acceleration commands are estimated at an interval of 0.1 s. We evaluate the performance of the integrated framework and prototype traffic flow simulation by two separate sets of simulation experiments performed in MATLAB. In the first set, the modelling framework is evaluated based on the simulation results of scenario case studies consisting of few vehicles. In the second experiment, the prototype is evaluated by simulating the human-driven traffic flow comprised of 2000 vehicles on a two-lane freeway section with an on-ramp bottleneck.

5.4.1 Evaluating the modelling framework

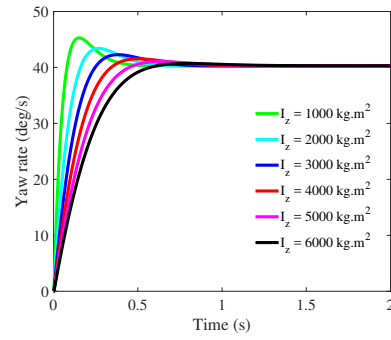
To verify the performance of the modelling framework, we designed three test cases. First, we evaluate the sensitivity of uncontrolled lateral vehicle dynamics towards the vehicle model parameters. In the second test, we evaluate the steering operation in two scenarios: curve negotiation and corrective steering. Finally, in the third test, we evaluate lane change trajectories, including dynamic reference replanning such as aborted lane change and fragmented lane change. The default vehicle model parameters are set as follows: $m = 1573$ kg; $I_z = 2873$ kg.m²; $C_{\alpha f} = C_{\alpha r} = 80000$ N/rad; $l_f = 1.1$ m; $l_r = 1.58$ m. These values correspond to a passenger sedan [11]. The results are compared to a similar experiment reported in (Mondek & Hromcik, 2017).

Evaluating the Sensitivity of the Vehicle Model

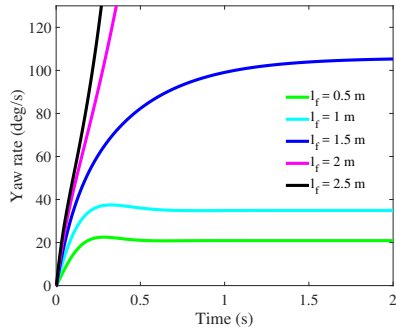
Figure 5.5 depicts the vehicle yaw dynamics under an initial steering input $\theta_f = 0.1$ rad. This illustrates the sensitivity of the vehicle yaw dynamics to the vehicle parameters of mass, the moment of inertia, the centre of mass and velocity. An increase in the mass of the vehicle reduces the steady-state yaw rate and reduces its damping in transient response (see Figure 5.5(a)). Thereby, this model will represent heavier vehicles as less steerable, which is intuitive. An increase in the moment of inertia increases the settling time indicating a slower time response (see Figure 5.5(b)). This behaviour is also intuitive, for example, sports cars are designed with a low moment of inertia for faster time response. As the centre of mass moves toward the vehicle front, the time response is seen to be quicker (see Figure 5.5(c)). Finally, the forward velocity is a key parameter that influences the vehicle handling (see Figure 5.5(d)). The steady-state vehicle yaw rate increases with an increase in velocity until a critical point (around 40 m/s for the selected vehicle parameters), and the steady state response decreases with an increase in the velocity beyond the point. The modelled behaviour is consistent with empirical observations and with previous studies (Mondek & Hromcik, 2017). The selected parameters are capable of modelling a representative vehicle operating at freeway conditions.



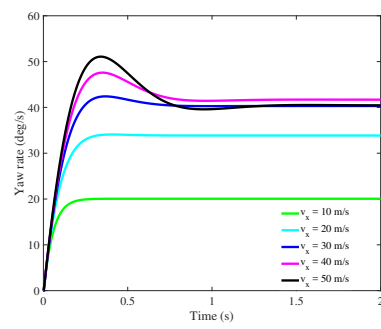
(a) Model response to varying vehicle mass



(b) Model response to varying moment of inertia



(c) Model response to shifting the center of gravity away from the front wheel



(d) Model response to varying velocity

Figure 5.5: Step response of the vehicle model with varying model parameters

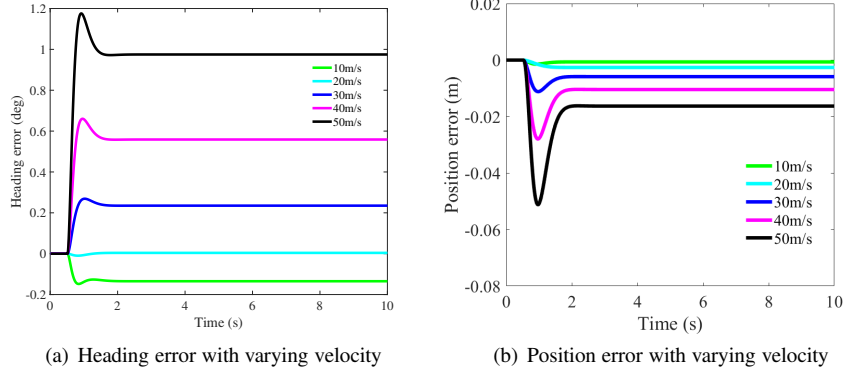


Figure 5.6: Simulated steering operation during curve negotiation

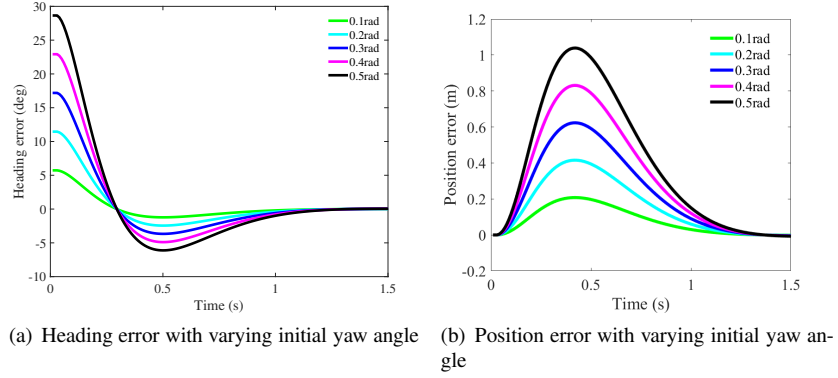


Figure 5.7: Simulated steering operation during corrective steering

Evaluating the Performance of the Operational Layer

Inaccurate steering control is a major factor contributing to single-vehicle accidents on motorway horizontal curves, and corrective oversteering can lead to vehicle crashes (Salvucci & Gray, 2004; Staubach, 2009). Even though this aspect has been reported in accident studies, conventional microscopic traffic simulation models are incapable to capture them. In this context, we evaluate the ability of the framework to model control related errors. In this experiment, we simulate two distinct steering operational tasks: curve negotiation and corrective steering. The tactical reference vector for the curve negotiation is as follows $v^d = 30 \text{ m/s}$; $k(t) = \begin{cases} 0 & 0 \leq t < 0.5 \\ 1/750 & t \geq 0.5 \end{cases}$. The change in reference curvature $k(t)$ reflects the change in road geometry: from a straight stretch to a horizontal curve of radius 750 m when $t \geq 0.5 \text{ s}$. The initial vehicle state is as follows: $X(0) = Y(0) = 0$; $V_X(0) = 30$; $V_Y(0) = 0$; $\psi(0) = 0$; $\dot{\psi}(0) = 0$.

The simulation results in Figure. 5.6 show that the operational model is able to capture the control related error while negotiating a horizontal curve. It can be seen, that negotiating

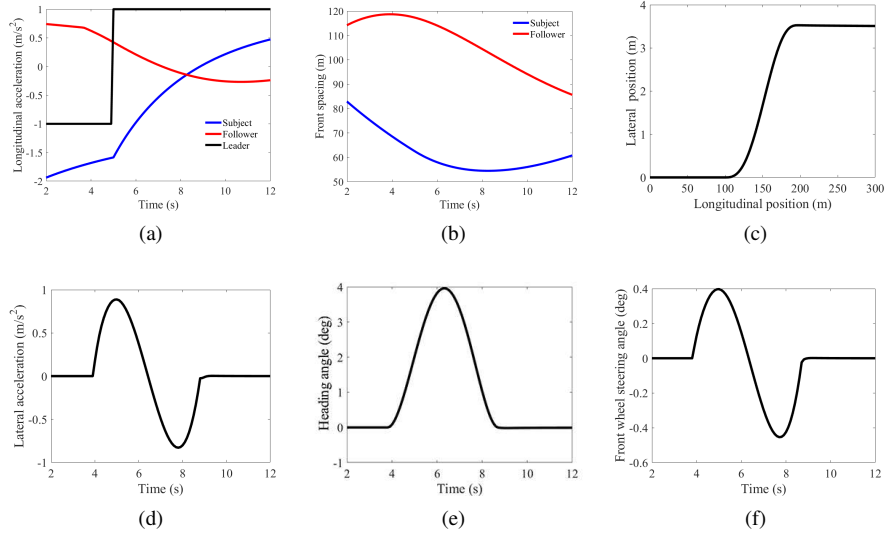


Figure 5.8: Simulated lateral and longitudinal dynamics during a normal lane change to the slower lane

the curve at higher velocities induces a larger position error (see Figure. 5.6(a)) and heading angle error (see Figure. 5.6(b)) defined in (5.17). Therefore, the modelled curve negotiations at high velocity results in a larger tracking error, which is consistent with the empirical observation that over-speeding is common characteristic underlying single vehicle accidents at motorway curves (Li et al., 2005; Staubach, 2009; Schneider et al., 2009).

The corrective steering is the manoeuvre undertaken when the vehicle has (perhaps inadvertently) disoriented itself with the road centre line and has to steer back in order to realign with the road centerline. Here, we consider a straight road stretch and vehicle's tactical reference input is $v^d = 30$ m/s. The initial state of the vehicle, except for the heading angle (varied) is as follows: $X(0) = Y(0) = 0$; $V_X(0) = 30$; $V_Y(0) = 0$; $\psi(0) = 0$. The initial heading angle is varied from 0.1 to 0.5 rad.

The simulation results in Figure. 5.7 show that steering amplitude and the settling time (see Figure. 5.7(a)) increase with initial heading error. This is consistent with human corrective steering performance examined in driving simulators (Salvucci & Gray, 2004).

Evaluating the Lane Change Simulation

The ability of the framework to model lane changes, is evaluated by three different scenario simulations resulting in different types of lane change execution. All three scenarios involve a subject vehicle (right lane), leader and preceding vehicles (left lane).

The first scenario describes a normal lane change to a slower lane. Initially, the subject vehicle moves at 30 m/s and the two neighbouring vehicles are at 20 m/s. The leader in the target lane applies a constant deceleration of -1 m/s² till 5 s. Meanwhile, the subject vehicle initiates a lane change at 4 s, simultaneously decelerating to follow the leader (see Figure. 5.8(a) and Figure. 5.8(b)). It can be seen that the vehicle successfully completes the

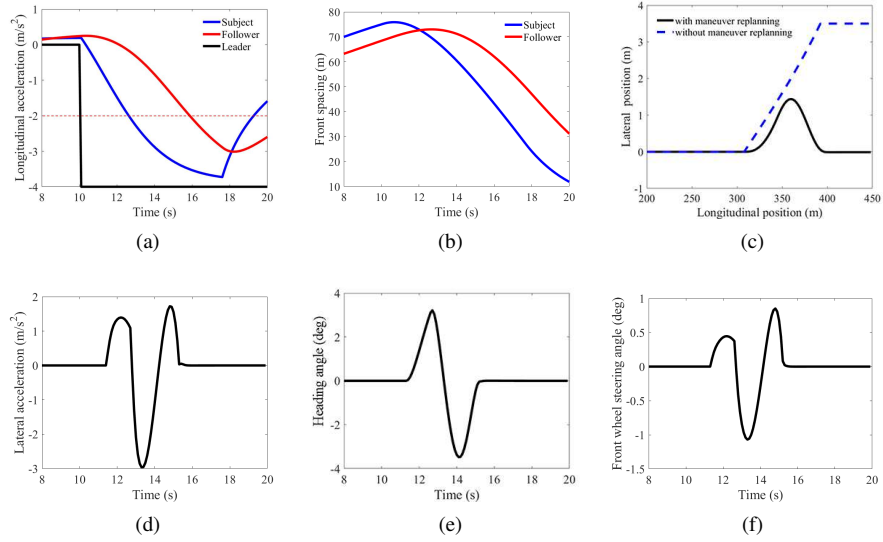


Figure 5.9: Simulated lateral and longitudinal dynamics during an aborted lane change

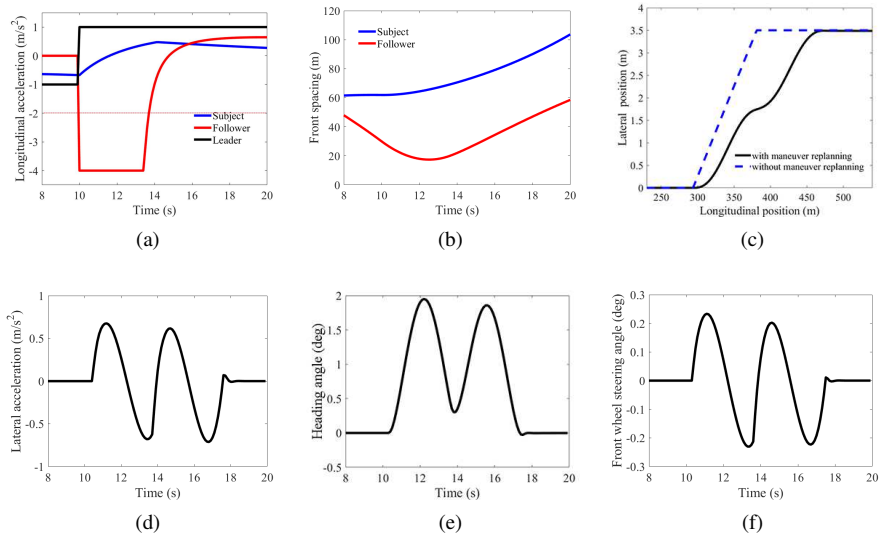


Figure 5.10: Simulated lateral and longitudinal dynamics during a fragmented lane change

lane change in the next 5 s (see Figure. 5.8(c)), re-align with the target lane ($\psi = 0$ from 9 s in Figure. 5.8(e)), to continue driving on it (see Figure. 5.8(d) and Figure. 5.8(f)).

The second and third scenarios describe an aborted lane change and a fragmented lane change respectively. These manoeuvres present interesting examples of manoeuvre replanning by human drivers (Yang et al., 2015). To meet the objective of this test, we define exemplary rule-based decision-making logic that allows to abort or interrupt a pre-initiated lane change as follows

$$\xi_i(t) = \begin{cases} \xi_i(t_0) & \text{if } : A_{X,i}(t), A_{X,i+1}(t) > A^* \\ 0.5\xi_i(t_0) & \text{if } : A_{X,i+1}(t) < A^* \\ 0, & \text{if } : A_{X,i}(t) < A^* \end{cases} \quad (5.23)$$

where $\xi_i(t_0)$ is the desired lane change direction of the vehicle i at the start of the lane change, i denotes the lane changing vehicle, $i + 1$ and $i - 1$ denotes the rear and leading vehicle in the target lane respectively. $A_{X,i}(t)$ is the acceleration signal provided by the longitudinal controller of i to follow $i - 1$, and $A_{X,i+1}(t)$ is the acceleration signal generated by the longitudinal controller of $i + 1$ to follow i , A^* denotes the deceleration threshold which is set as -2 m/s^2 . The logic of the rule (5.23) is as follows: if the longitudinal acceleration input of both i and $i + 1$ remain in the comfortable range ($> A^*$), then the lane change is sustained uninterrupted; if longitudinal acceleration input of $i + 1$ drops lower than the comfortable range ($\leq A^*$) at some point, then i temporarily pauses the lateral manoeuvre and waits for $i + 1$ to cooperate by decelerating, and proceeds with the lateral manoeuvre when the demanded $A_{X,i+1}(t)$ is comfortable; if the longitudinal acceleration input of i drops lower than the comfortable range at some point, the manoeuvre is aborted and i returns to its original lane. Besides, when the lane changing is temporarily paused, i.e. $\xi_i(t) = \pm 0.5$, the \bar{D} has to be extended to \bar{D}^* in order to accommodate the intermediate delay, where $\bar{D}^* = \bar{D} + t^p$. Here t^p denotes the intermediate pause time.

In the second scenario, we consider an aborted lane change. Initially, all three vehicles move at 30 m/s. The leading vehicle in the target lane applies an abrupt deceleration of -4 m/s^2 starting after 10 s (see Figure. 5.9(a) and Figure. 5.9(b)). The subject vehicle initiates the lane change at 11.5 s; however, as its longitudinal acceleration drops below A^* at 12.7 s (see red dotted line in Figure. 5.9(a)), its tactical layer commands to abort the lane change based on (5.23) and consequently swerves back to the original lane. Figure. 5.9 shows the detailed description of the manoeuvre provided by the proposed framework. It can be seen that the vehicle moves back to the original lane (see Figure. 5.9(c)), re-aligns with the original lane ($\psi = 0$ from 15 s in Figure. 5.9(e)), to continue driving on it (see Figure. 5.9(d) and Figure. 5.9(f)). In a typical microscopic simulator, the lane-changing vehicle moves with constant lateral velocity of 1 m/s without dynamic manoeuvre replanning. This would result in the blue-dashed trajectory in Figure. 5.9(c). It can be seen that without manoeuvre replanning, the simulation outcome of this situation would be different, and the lane-changer would end up in the target lane. Moreover, the lateral acceleration along this trajectory is discontinuous at the start and endpoint of the lane-changing due to a step-change in lateral velocity.

In the third scenario, we consider fragmented lane changing. Initially, all three vehicles move at 35 m/s. Initially, the leader applies constant deceleration of -1 m/s^2 till 10 s and thereafter applies an acceleration of 1 m/s^2 . Additionally, we set the following vehicle

acceleration as 0 m/s^2 till 10 s, implying that it does not react to the deceleration of the subject vehicle till that point. Thereafter its longitudinal controller is engaged and it begins to follow the subject vehicle (see Figure. 5.10(a) and Figure. 5.10(b)). Meanwhile, the subject vehicle initiates the lane change at 10.5 s. As the desired acceleration of the follower is below A^* , its tactical layer commands a temporary pause in lane change based on (5.23). After a pause of 3.3 s, the desired acceleration of the follower is above A^* at 13.7 s (see red dotted line in Figure. 5.10(a)), and the tactical layer commands to resume the manoeuvre to the right lane based on (5.23). Figure. 5.10 shows the detailed manoeuvre description. It can be seen that the vehicle reaches the target lane (see Figure. 5.10(c)), aligns with the target lane ($\psi = 0$ from 18 s in Figure. 5.10(e)) and continues driving on it (See Figure. 5.10(d) and Figure. 5.10(f)). Figure. 5.10(c) shows the simulation of this situation without manoeuvre replanning. As the time consumed by the intermediate pause cannot be modelled, the lane changer ends up in the target lane earlier, similar to a continuous lane change.

5.4.2 Evaluating the traffic flow simulation

In this section, we evaluate the prototype traffic flow simulation specified in section 5.3. To this end, a two-lane road section of 9.2 km long with open boundary conditions was simulated. The inflow at the upstream boundary was kept constant at 1,600 vehicles/h/lane. The lane width is 3.5 m, a standard for Dutch motorways. Furthermore, the road stretch consists of an on-ramp (merging length 200 m) at the location $x = 7.2 \text{ km}$ with a constant inflow of 800 vehicles/h. In order to simplify the analysis, we omit heavy vehicles in the simulation which can introduce distinct effects on traffic flow characteristics. As specified in section 5.3, the modules in the prototype traffic flow simulation are described by existing behavioural models, which have been empirically validated. The prototype does not include models for aborted and fragmented lane changes. The simulation period is 1800 s. The parameter values used in the simulation are listed in Table 5.1. The vehicle parameter values are the same as detailed in section 5.4.1. To reduce the computational load, the prototype traffic flow simulation, employs a hybrid scheme, wherein the trajectory planning and steering control modules (updated at a high frequency of 0.01 s) are activated only when a lane change is initiated, otherwise, it functions as a normal microscopic simulation.

Macroscopic Variables

Figure. 5.11 shows the simulated macroscopic flow characteristics. The flow and density were calculated using Edie's definitions (Edie, 1961) for a stretch of 1 km and time interval of 30 s. The diagram captures well known macroscopic traffic flow properties. Figure. 5.11 shows both the free flow regime and congested traffic state. It can be seen that the traffic on the road stretches downstream (green dots in Figure. 5.11) and further upstream of the bottleneck (green circles in Figure. 5.11) are in a free flow state. The stationary congested traffic occurs around the bottleneck and stop and go waves propagate upstream with a velocity of -14 km/hr . This is observed in road stretches in the upstream vicinity of the bottleneck (black dots and circles in Figure. 5.11). The transition from free flow state to congested state occurs approximately at 20 veh/km, which can be considered as the critical density. The values of stop and go wave velocity and critical density are consistent with empirical observations (Treiber & Kesting, 2013). It can be seen in Figure. 5.11 that near the

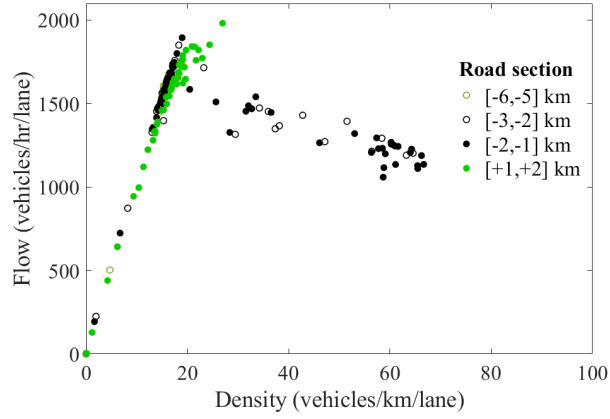


Figure 5.11: Macroscopic traffic flow with varying density

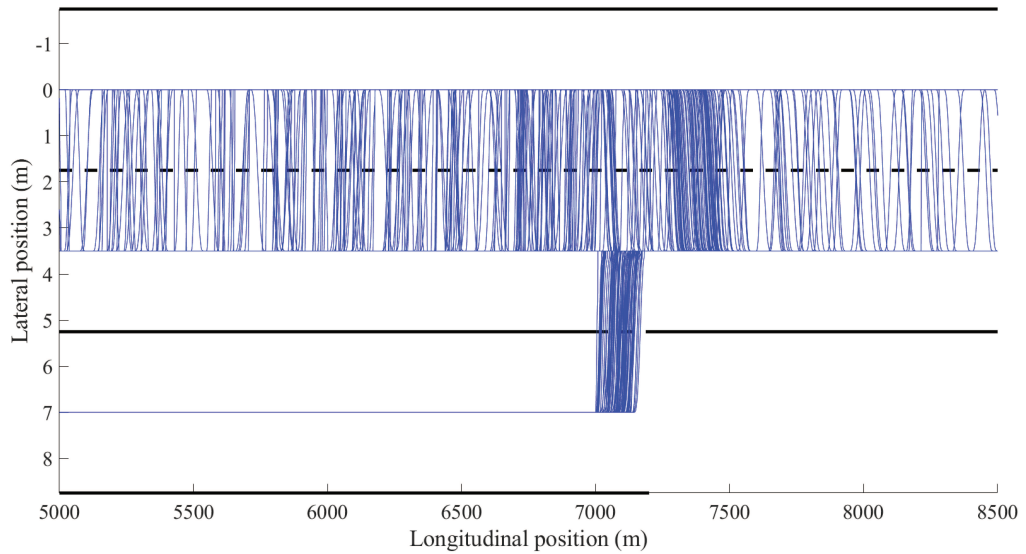


Figure 5.12: Simulation results; blue lines indicate vehicle trajectories and black lines indicate lane boundaries

maximum flow the points are arranged in the shape of an inverse λ , implying the existence of both free and congested states around the critical density. The corresponding reduction in the maximum flow is around 10% and is consistent with the empirical observations of 5 - 20% (Cassidy & Bertini, 1999; Treiber & Kesting, 2013).

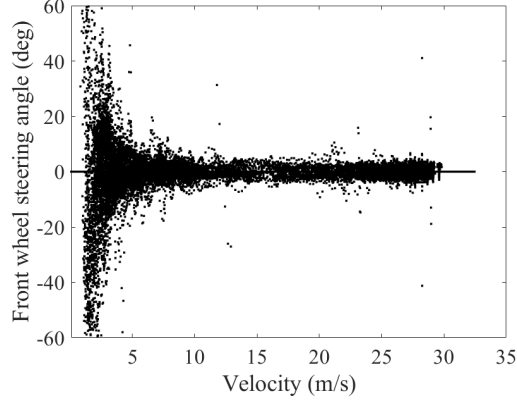


Figure 5.13: Distribution of front wheel steering angle with varying longitudinal velocity

Microscopic and submicroscopic variables

The vehicle trajectories near the onramp section are shown in Figure. 5.12. The simulation resulted in 1178 lane changes. It can be seen that the number of lane changes increases in the vicinity of the onramp entrance (7000 - 7200 m). The number of lane changes is relatively higher on the road segment immediately downstream (7200 - 7500 m) of the bottleneck, caused by vehicles moving to the right lane after the bottleneck. This could be the result of right lane bias implemented in the lane change decision model. The number of lane changes is relatively lower on the road segment further away from the merge (7500 - 8500 m) as the traffic here is predominantly in the free flow state (see Figure. 5.11).

Figure. 5.13 shows the distribution of steering angle with varying longitudinal velocity. It can be seen that at high-velocity regimes the front wheel steering angle remains within $\pm 10^\circ$ and at lower velocity, distribution of steering angles scatters to higher value.

5.5 Discussion

We presented the framework to model human-driven traffic flow by operationalizing the component modules with existing behavioural models. The longitudinal vehicle dynamics was described using the IDM car-following model. This model has been empirically validated in (Treiber et al., 2000). In order to preserve the properties of the behavioural car-following model, the actuator lag τ was set to zero. This parameter may be assigned a finite value to represent the vehicle motion by automated acceleration controllers such as Adaptive Cruise Control (Mullakkal-Babu et al., 2016; Rakha et al., 2012).

Few lane change trajectories in the simulation were found to be infeasible, i.e. $\theta_f > \pm 70^\circ$. These trajectories were observed when the longitudinal velocity dropped to 0 - 1 m/s. Since the safety concerns at this velocity range are marginal, such lane change trajectories were overridden with linear interpolations of lateral positions during the lane change duration. A possible reason is that the lane change duration used in the reference plan is estimated from a behavioural model that does not explicitly account for the trajectory fea-

sibility. Moreover, the steering commands were not explicitly constrained. This highlights the necessity for further empirical research on path planning by the human drivers at such low velocities.

The present framework can be improved by adding behavioural parameters characterizing the human drivers such as (variable) response time and perception error (Treiber et al., 2006). van Lint & Calvert (2018) proposed a theory to model the perception and response processes at tactical and operational layer. They implemented this theory to car-following dynamics. Z. Zheng et al. (2013) modeled the changes in car-following behaviour induced by lane changing. The presented framework describes lateral interactions during the lane-changing. However, interactions that span over a longer horizon such as during weaving and merging manoeuvres in congested traffic (Hidas, 2005; Schakel et al., 2012) can be incorporated in the framework by extending the planning horizon and reformulating the tactical planner with corresponding models.

Even though detailed trajectory descriptions are beneficial for traffic applications, the high computational demand is a major obstacle to its real-time application. In this study, we reduced the demand by employing a hybrid scheme, wherein the high-frequency update was only performed during lane changing. Besides we selected linear models for lateral and longitudinal dynamics. Thereby, the simulator could operate at real-time speed (run-time = 1 s, meaning that the simulator takes 1 second to simulate 1 second of traffic flow) with up to 100 active vehicles on the road. The run-time increased to 5 s with 440 active vehicles and further up to 10 s with 900 active vehicles. The run-time can be lowered by operating the simulator in a parallel or distributed computing system. Another possible step is to restrict the submicroscopic simulation to complex segments such as crossroads or merging sections.

In this study, the parameters of the component models were selected from their original papers. However, the parameters should be calibrated based on the simulator application. The level of detail to be considered in the calibration should depend on the objective of the analysis. In a safety assessment study, the surrogate safety metrics are extracted directly from the simulated trajectories and therefore the calibration might be restricted to microscopic variables (Mullakkal-Babu et al., 2017). High resolution trajectory datasets such as the one by Wagner et al. (2015) provide opportunities for such calibration attempts. On the contrary, if one is interested in the performance evaluation of a steering control system, then the parameters related to submicroscopic variables should be calibrated in more detail.

The presented simulation framework has several potential applications: 1) Assessing the safety impacts of driving applications such as Automated Lane-Changing Systems and Automated Lane Keeping Systems. This can be done by formulating the tactical planner and operational control with respective modules of the systems. 2) Investigating the effects of lateral vehicle control on traffic characteristics, such as the capacity drop at motorway horizontal curves. This can be done by operationalising the steering control module with a human steering model which can be developed from driving simulator experiments (Salvucci & Gray, 2004). 3) Examining the relationship between road design parameters and traffic safety at traffic facilities such as motorway discontinuities and intersections which are typically characterised by frequent lane changes including fragmented and aborted lane changes (Yang et al., 2015). 4) Comparing the performance of alternative crash-avoidance applications in different vehicle types in uncontrolled traffic situations involving dynamic vehicle interactions.

Table 5.1: Parameter values in the prototype traffic flow simulation

Parameter (description)	Value
a (IDM maximum acceleration)	1 m/s ²
b (IDM comfortable braking)	1.5 m/s ²
v^{max} (IDM maximum speed)	160 km/hr
v^d (IDM desired velocity)	108 km/hr
T^d (IDM desired time headway)	1 s
s_0 (IDM minimum space gap)	2 m
D^{max} (maximum lane change duration)	8 s
τ (actuator lag)	0 s *
A_{bias} (MOBIL bias parameter)	0.2
p (MOBIL politeness parameter)	0.15
ΔA_{th} (MOBIL acceleration threshold)	0.2

* $\tau = 0$ to preserve the behavioural properties of IDM

5.6 Conclusion

Compared to microscopic simulation, the proposed submicroscopic environment contains more vehicle model parameters and variables (front road-wheel steering angle and vehicle heading), and is hence termed as submicroscopic. A well-known limitation of submicroscopic simulation is its computational demand. To reduce the computational time, we hybridise the simulation with a manoeuvre-based scheme to switch between microscopic and submicroscopic resolution. The results indicate the possibility of real-time simulation with a hybrid scheme. Moreover, the existing submicroscopic frameworks entail connecting multiple commercial simulation packages through a custom interface. In contrast, we provide the detailed mathematical formulations of the component driving subtasks featuring prominent behaviour models and control techniques; and a numerical scheme to interconnect them.

The results of simulation case studies provide evidence to the performance and benefits of the framework. At the macroscopic level, the multi-lane traffic flow simulation can reproduce well-known traffic flow properties such as critical density and phenomena such as a capacity drop. Simulation examples demonstrate the limitation of typical simulation approaches to describe lateral manoeuvres involving dynamic trajectory replanning. In contrast, the proposed framework is able to simulate such lateral manoeuvres: curve negotiation, corrective steering, fragmented and aborted lane-changing. Thus the framework preserves the properties of the component models and at the same time describes the 2D planar movement of vehicles.

As detailed in the discussion section, there exist multiple prospects to improve the

framework, such as incorporating the behavioural aspects of human-driven vehicles and devising an appropriate computational paradigm to allow real-time simulation. Our future work will focus on the aforementioned tasks.



Chapter 6

Safety assessment of automated driving strategies at merges in mixed traffic

Abstract

We present a microscopic-simulation-based approach to assess the safety impacts of deploying vehicles equipped with Automated Driving Systems (ADS) in traffic consisting of Human-driven Vehicles (HV) as well. Specifically, we compare two generic longitudinal strategies of ADS to handle a cut-in: reactive and predictive, and identify their distinctive effects on the safety of cut-in manoeuvres of adjacent human-driven vehicles. The traffic scenarios in this study comprise of HVs that can change lane and ADS-equipped vehicles that move solely in the forward direction. We employ a microscopic traffic flow simulator that describes the lane changing process with high detail, accounting for the vehicle interaction and consequent trajectory updates. These high-resolution trajectories are post-processed to estimate a set of relevant surrogate measures of safety. By analysing these measures, we find that the predictive approach significantly outperforms the reactive one in aspects such as temporal proximity to crash, expected crash severity and the driving risk (combining the two aspects). The negative safety impacts of reactive ADS-equipped vehicles become prominent at the penetration rate $> 10\%$ and grow with an increase in the penetration rate. The major difference between the two approaches appears in the dynamics of risk during the lane changing. When a vehicle cuts in ahead of Reactive ADS, the risk peaks approximately halfway through the manoeuvre; whereas with Predictive ADS the risk remains marginal throughout. This effect is also reflected in the instances of lane change abortion when Reactive ADSs are being cut in. This work demonstrates the potential of simulation-based safety assessment approach to differentiate the safety impacts of automation functionalities at an early stage of product development.

This chapter is based on the following article, which is currently under review:

Mullakkal-Babu, F. A., Wang, M., van Arem, B., & Happee, R. (under review)
Comparative safety assessment of automated driving strategies at highway merges in mixed traffic

6.1 Introduction

Automated Driving Systems (ADSs) have been a prominent subject of research and development during the past three decades. An ADS, when engaged, drives the vehicle without human intervention or monitoring (SAE, 2018). Market trends indicate that ADS features will be technologically feasible in the near future (Chan, 2017) and the road-traffic will be *mixed* with ADS equipped and human-driven vehicles for at least a decade (Sivak & Schoettle, 2015). According to the standard taxonomy, engaged ADS should perform all the driving tasks necessary to operate the vehicle, in real-time on a sustained basis (SAE, 2018). The driving tasks at tactical-level include event detection, manoeuvre decision-making and at operational level include acceleration and steering control. The impacts of ADS-equipped vehicles on traffic safety cannot be generalised as ADSs differ in their tactical-level and operational-level functionalities to tackle on-road conflicts. In this context, identifying the relationship between the ADS strategies and traffic safety has gained increased research attention.

6.1.1 Safety assessment approaches for ADS-equipped vehicles

Safety of vehicle applications has been assessed either at the vehicle-level, based on their potential to reduce the number of crashes or at the traffic-level based on their potential impacts on collective traffic safety.

Yue et al. (2018) provide an exhaustive review of vehicle-level studies that focus on the crash-reduction potential of vehicle applications. Such studies estimate the effectiveness of an application based on the crash involvement rate of the equipped vehicle. The crash recordings may be derived directly from empirical sources such as accident records (Cicchino, 2017) or from in-lab experiments by reconstructing a set of pre-crash scenarios that are identified from empirical sources (Perez et al., 2011). Empirical crash records provide valuable insights into the safety performance of a given vehicle application, but crash data of ADS-equipped vehicles are rare and often confidential. In-lab crash reconstruction experiments, mostly comprise a standard set of traffic situations where the behaviour of neighbouring vehicles is predefined. Such a setting is not representative of on-road situations, as it does not account for the interactions with the adjacent vehicles (Salvucci & Liu, 2002), and the consequent variations in the trajectory of the vehicles. These interactions are fundamental to the dynamics of multi-lane traffic flow, and the performance of these systems in laboratory experiments may not reveal their actual impact on traffic.

Traffic simulators are potential tools to evaluate the safety impacts of a vehicle application at the traffic-level. The simulated trajectories (of equipped and non-equipped vehicles) are post-processed to derive metrics known as Surrogate Measure of Safety (SMoS). These metrics are analysed to find safety impacts. The majority of traffic safety studies focussed on the connected vehicle applications and their results consistently suggest that connectivity, if realised will improve the traffic safety (M. S. Rahman et al., 2019; Letter & Elefteriadou, 2017; Papadoulis et al., 2019; Yue et al., 2018). However, connectivity technology is not yet mature to be utilised by ADSs and their prospects are determined by the number of vehicles that can communicate (Menendez-Romero et al., 2018). On-board sensors remain the primary source of information for ADSs. Notably, the safety impacts of non-connected ADSs have been less studied compared to their connected counterparts (Bahram, Ghandeharioun,

et al., 2014; Jeong & Oh, 2017).

Most of the simulation-based studies, irrespective of the assumption on connectivity, express safety as the reduction in the likelihood of rear-end crashes, based on metrics such as Time-To-Collision (Bahram, Ghandeharioun, et al., 2014; Papadoulis et al., 2019; M. S. Rahman et al., 2018, 2019; Zhao et al., 2017) with very few exceptions (Guériau et al., 2016; Jeong & Oh, 2017) where lateral conflicts are evaluated. Recently, S. Wang & Li (2019), based on the crash record of vehicles with level 3/4 automation, identified that crashes caused by equipped vehicle are likely to be more severe (property damage) than those of non-equipped vehicles, and that equipped vehicle crashes are more severe on motorways. Besides, in comparison to intersections, an equipped vehicle on a motorway is more likely to be involved in angular and sideswipe crashes (mostly related to lane-changes). These findings highlight the need to examine motorway lateral conflicts involving ADS equipped vehicles in more detail.

Lateral conflicts on a motorway is a challenging subject for safety assessment, particularly those involving ADS-equipped vehicles. This is due to simulator-related and assessment-related challenges. In most of the traffic simulators, the lane change execution is represented as an open-loop process, disregarding the vehicle's interaction with adjacent vehicles during lane-changing execution. In reality, the lane-changing vehicle may dynamically update its lane-changing trajectory and may even abort the manoeuvre in unsafe situations. However, such instances of lane change abortion cannot be modelled in typical traffic simulators. Second, simulators often do not allow the accessible and flexible framework to model an ADS architecture. Several previous works modelled ADS by adjusting the default behavioural model of the simulators such as VISSIM, CORSIM and SUMO (Guériau et al., 2016; Letter & Elefteriadou, 2017; Park et al., 2011). But these approaches may fail to capture the differences between ADS-equipped and conventional vehicles with respect to sensing, decision-making and vehicle control. The resulting trajectory simulations are oversimplistic and therefore restricted to safety analysis. For instance, lane-changing is typically simulated as an event during which the vehicle jumps/drifts between two lanes, being unresponsive to the actions of adjacent vehicles. Such a synthetic trajectory does not provide realistic variables such as lateral position and lateral velocity necessary to estimate relevant SMoS. Mullakkal-Babu et al. (2017) identify that realistic simulation of lateral kinematics and appropriate selection of SMoS are necessary preconditions to compare the level of safety of two-dimensional trajectories.

6.1.2 Automated driving strategies to handle cut-in

One of the critical events that an ADS should handle while operating on a multi-lane motorway, is a cut-in, i.e. when an adjacent vehicle pulls in ahead by merging into its lane (Calvert et al., 2016). When a vehicle is cut in by an adjacent one, its intervehicle spacing decrease approximately by half. If a vehicle fails to brake effectively when being cut in, it could crash with the merging (cut-in) vehicle. This can be a major concern on motorway merging sections, where cut-ins are more frequent. Najm et al. (2007) report that approximately 10% of light vehicle crashes involve a lane-changing vehicle. To effectively respond to a cut-in, the ADS should be informed in real-time of the cut-in manoeuvre: intention, start and end of the manoeuvre.

To handle a cut-in event, the ADS should perform two tactical tasks: detect (predict)

Table 6.1: Review summary of cut-in handling functionalities in ADS

Functionality	Reactive handling	Predictive handling
Cut-in detection/prediction (tactical-level)	radar-based detection (Zhao et al., 2017)	turn signal-based intend prediction (W. Ko & Chang, 2018) learning-based intend prediction (Carvalho et al., 2016; Menendez-Romero et al., 2018; Rehder et al., 2019) bayesian statistics-based intend prediction (Schlechtriemen et al., 2014; Wei et al., 2013)
Motion prediction for adjacent vehicles (tactical-level)	N.A	constant velocity (Bahram, Wolf, et al., 2014) constant acceleration (Carvalho et al., 2016; Menendez-Romero et al., 2018; Wei et al., 2013) interaction-aware prediction (Bahram et al., 2016)
manoeuvre decision (tactical-level)	follow the cut-in vehicle (Moon et al., 2009; Mullakkal-Babu et al., 2016; Zhao et al., 2017)	follow the virtual leader (W. Ko & Chang, 2018) rule-based yielding (L. C. Davis, 2007; Hara et al., 2018; Park et al., 2011) expected utility-based manoeuvre planning (Bahram, Wolf, et al., 2014; Carvalho et al., 2016; Menendez-Romero et al., 2018; Wei et al., 2013) game theory-based manoeuvre planning (Bahram et al., 2016)
Acceleration control (operational-level)	feedback gain based control (Moon et al., 2009; Mullakkal-Babu et al., 2016)	feedback gain based control (W. Ko & Chang, 2018) optimal control (Bahram, Wolf, et al., 2014; Carvalho et al., 2016)

the vehicle that cut in (the intention of an adjacent vehicle to cut-in); decide the appropriate response. ADS' response to a cut-in is typically operationalised by its submodule: Adaptive Cruise Control (ACC). ACC system commands the acceleration to regulate the vehicle's velocity to follow the preceding vehicle with a safe spacing and desired speed. Table 1 describes the two generic approaches adopted by an ADS to handle a cut-in: reactive control and predictive control. In reactive control, the equipped vehicle identifies a cut-in when it detects another vehicle in its lane at a closer spacing than the preceding vehicle it was originally following. Thereafter, the component ACC system generates commands to follow the cut-in vehicle. Several ADS designs adopt the reactive approach (Mullakkal-Babu et al., 2016; Moon et al., 2009). But the disadvantage of this approach is that the sudden drop in intervehicle spacing often results in hard braking, which is uncomfortable for the driver (Moon et al., 2009; Mullakkal-Babu et al., 2016). Larsson et al. (2014) provide empirical evidence to show that the behaviour of the vehicle with ACC-engaged during cut-in, often scares the driver, forcing him/her to take back the control.

In the predictive control, the system predicts the cut-in intentions of the adjacent vehicles and identifies the adjacent vehicle which is most likely to cut-in. Several methods to predict the cut-in have been proposed as listed in Table 1: turn signal-based (W. Ko & Chang, 2018); learning-based approaches (Carvalho et al., 2016; Menendez-Romero et al., 2018; Rehder et al., 2019); Bayesian statistics-based approaches (Schlechtriemen et al., 2014; Wei et al., 2013). Upon cut-in prediction, the most appropriate manoeuvre is calculated taking into account the predicted future motion of the cut-in candidate. Table 1 summarises the prominent methods for manoeuvre decision-making, such as following the virtual leader (W. Ko & Chang, 2018), rule-based (L. C. Davis, 2007; Hara et al., 2018; Park et al., 2011), utility-based (Bahram, Wolf, et al., 2014; Carvalho et al., 2016; Menendez-Romero et al., 2018; Wei et al., 2013) and game theory-based (Bahram et al., 2016). The underlying motion prediction logic can be kinematic extrapolations based on constant velocity (Bahram, Wolf, et al., 2014); constant acceleration (Carvalho et al., 2016; Menendez-Romero et al., 2018; Wei et al., 2013); or model-based predictions accounting for vehicle interactions (Bahram et al., 2016). Predictive control allows early evoking of the response to cut-in, providing a temporal margin to smoothly regulate the vehicle's velocity to approach the cut-in vehicle. However, the implementation of the predictive approach entails additional computational expense and sensing requirements. Therefore, understanding the safety implications of these systems will facilitate an informed choice between the two approaches.

The ADS' cut-in handling functionalities have been typically tested based on crash-reduction potential by simulation and/or by test vehicles. The results show that they could decrease the number of events with hard-braking and reduce the average Time-To-Collision (Bahram, Ghandeharioun, et al., 2014). Few attempts have been found to estimate their impact on traffic safety. At the traffic level, Ioannou & Stefanovic (2005) found that ACC systems with a conservative target time-headway (≥ 1.2 s), may result in more spacing between vehicles and thereby invite more cut-in. Bahram, Ghandeharioun, et al. (2014) simulated ADS with a reactive approach. They found that such systems create more risky situations, but the risk is dispensed faster than human-driven vehicles. Moreover, they suggested that few crashes in the simulation could have been avoided if these systems had prediction capability. Similarly, L. C. Davis (2007) showed that the rule-based cooperation between equipped vehicles could improve the safety at merging sections. But none of these studies examine the impacts of cut-in handling functionalities on the safety of lateral

conflicts and the consequences of the vehicle interaction during the cut-in manoeuvre.

6.1.3 Objective and structure

The objective of this work is to present a simulation-based safety assessment methodology to assess the impacts of ADS's longitudinal functionality on the safety and characteristics of lateral manoeuvres by adjacent human-driven vehicles on the motorway. In this work, we apply this methodology to compare the reactive and predictive cut-in handling by ADS to facilitate an informed choice between them. Towards this, we employ a microscopic traffic simulator that provides continuous two-dimensional vehicle trajectories capturing dynamic lane-change re-planning. The simulated vehicle trajectories are post-processed to estimate surrogate metrics of safety characterising the conflicts with adjacent vehicles, expected crash severity and dynamics of the driving risk. In addition, we identify the change in lane change characteristics in terms of the frequency of non-successful lane changes, spatial distribution and average velocity. Based on simulations of several traffic scenarios, we delineate and compare the distinct trends in the safety metrics and lane changing characteristics under the increasing share of two types of ADSs.

The simulation framework, notations and mathematical formulation of the distinct cut-in handling approaches employed by ADS-equipped vehicles and Human-driven Vehicle (HV) are described in Section 6.2. In section 6.3, a set of metrics for safety analysis are selected. Section 6.4 presents the results of the case study. Finally, Section 6.5 discusses the limitations, conclusions and outlines future research.

6.2 Model formulation

This section presents three distinct models for cut-in handling and describes the model for manual lane-changing. To meet the research objective, two requirements were imposed on the microscopic traffic simulator: 1) it should describe both HV and ADS-equipped vehicle and their specific tactical-level and operational-level functions; 2) it should describe the two-dimensional lane-changing trajectory accounting for dynamic manoeuvre re-planning during a lane change.

The dynamic state of a vehicle i (point mass) is described by its position vector \mathbf{p}^i defined as $\mathbf{p}^i = [x^i, y^i]^T$, where x^i denotes longitudinal position, and y^i denotes lateral position; and velocity vector \mathbf{v}^i defined as $\mathbf{v}^i = [v_x^i, v_y^i]^T$, where v_x^i denotes longitudinal velocity, and v_y^i denotes lateral velocity. The control unit of vehicle i dynamically manipulates its state implementing an acceleration as the input vector \mathbf{a}^i defined as $\mathbf{a}^i = [a_x^i, a_y^i]^T$, where a_x^i denotes longitudinal acceleration and a_y^i denotes lateral acceleration. The dynamic relation of this system can be expressed in the state space form as

$$\frac{d}{dt} \begin{pmatrix} \mathbf{p} \\ \mathbf{v} \end{pmatrix} = \begin{bmatrix} 0 & 1 \\ 0 & 0 \end{bmatrix} \cdot \begin{pmatrix} \mathbf{p} \\ \mathbf{v} \end{pmatrix} + \begin{pmatrix} 0 \\ 1 \end{pmatrix} \cdot \mathbf{a} \quad (6.1)$$

The physical limitations of the vehicle motion are implemented as a set of feasibility constraints in the model. The velocity is constrained by $-0.17v_x \leq v_y \leq 0.17v_x$, to depict the nonholonomic behaviour of motor vehicles (Nilsson et al., 2015), and additionally by $v_x \geq 0$ assuming the vehicles move strictly in the forward direction. The mechanical limitations of

the vehicle are modelled by bounding the acceleration $a_{min} \leq a_x \leq a_{max}$, where a_{max} denotes the maximum and a_{min} the minimum feasible acceleration. In a cut-in event, the vehicle that is being cut in, performs two tactical-level tasks: cut-in event detection denoted by ζ , yield decision denoted by γ and employs a_x to operationalise the decision. The vehicle, that cuts in, performs tactical-level lane change decision denoted by ξ and employs \mathbf{a} to operationalise the decision. The following are the key assumptions in the study,

- 1 The ADS-equipped vehicle operates only in the longitudinal direction and does not change lane. Modelling the sustained automation of the longitudinal driving task is sufficient to meet the objective of this study.
- 2 The human-driven vehicle can change lane and can estimate the acceleration of adjacent equipped and non-equipped vehicles and thereby calculate the utility of a prospective lane change.

6.2.1 Acceleration models to follow the predecessor

The longitudinal acceleration behaviour of HV and ADS-equipped vehicle are differentiated by modelling them with distinct control laws.

Acceleration model of ADS-equipped vehicle

The longitudinal acceleration implemented by an ADS-equipped vehicle to follow a leader is formulated by the ACC law proposed by Mullakkal-Babu et al. (2016). This control law integrates both ACC and collision avoidance control in a single non-linear formulation, and yield smooth acceleration behaviour in a cut-in or when the leader brakes hard. The longitudinal acceleration input by the ACC law a_{ACC}^i is formulated as

$$a_{ACC}^i(\alpha) = \begin{cases} K_1 s_e - K_2 \Delta v_x^i(\alpha) R(s^i(\alpha)), & \text{if } s^i(\alpha) > r_f \\ K_3 (v^d - v_x^i), & \text{if } s^i(\alpha) \leq r_f \end{cases} \quad (6.2)$$

where α is the vehicle (ADS-equipped or Human driven) preceding i , v^d is the desired velocity of i , $s^i = x^\alpha - x^i - l$ is the space gap available to i with l denoting the length of the α , $\Delta v_x = v_x^i - v_x^\alpha$ is the velocity difference of i with respect to the vehicle α , r_f is the detection range of i 's forward sensor, K_1 , K_2 and K_3 are the control gains. The s_e is the spacing error defined as

$$s_e = \text{MIN} \{ s^i - s_0 - v_x^i \cdot t_d, (v_0 - v_x^i) \cdot t_d \} \quad (6.3)$$

where t_d is the desired time headway, s_0 is the minimum space gap. $R(s^i)$ is a sigmoidal function in s^i that enables collision avoidance, by evoking a strong braking response when approaching the leader at short space gap and a milder response when the leader is further away. $R()$ is defined as

$$R = \frac{-1}{1 + Qe^{-\left(\frac{s^i}{J}\right)}} + 1 \quad (6.4)$$

where Q and J are parameters determining the aggressiveness of the response.

Model for manual car-following

The longitudinal acceleration implemented by a human driver during to follow a predecessor is formulated by the Intelligent Driver Model (Treiber et al., 2000). IDM is a behavioural model in which the acceleration is a continuous function of the space gap and velocity difference of i w.r.t α . This model has been widely used to describe manual acceleration behaviour and to replicate emergent traffic phenomena such as capacity drop and congestion waves. The longitudinal acceleration input by IDM a_{IDM}^i is formulated as

$$a_{\text{IDM}}^i(\alpha) = \bar{a} \left[1 - \left(\frac{v_x^i}{v_d} \right)^4 - \left(\frac{s^*(v_x^i, \Delta v_x^i(\alpha))}{s^i(\alpha)} \right)^2 \right] \quad (6.5)$$

where \bar{a} denotes the maximum acceleration. s^* denotes the desired minimum space gap as follows

$$s^* = s_0 + v_x^i t_d + \frac{\Delta v_x^i(\alpha)}{2\sqrt{ab}} \quad (6.6)$$

where b is the comfortable braking.

6.2.2 Acceleration models with cut-in handling

In the previous section, we presented the models of a_x^i when the sole objective of i is to follow one leader α . In a cut-in, i confronts two vehicles: the preceding vehicle $i+1$ and the merging vehicle c . It should gradually transition from following-the-leader to following-the-merging-vehicle, meanwhile avoiding a crash.

First, we present the notations used to describe cut-in handling and label the relevant vehicles. Let σ^i be a discrete variable denoting the current lane number as $\sigma^i \in \{1, 2, \dots, L\}$, with 1 denoting the leftmost lane and L denoting the total number of lanes. Let ξ^i be a discrete variable denoting the lane change direction of vehicle i with $\xi^i \in \{+1, 0, -1\} := \{\text{move to the right lane, remain in the current lane, move to the left lane}\}$. Let ζ^i be a binary variable with $\zeta^i \in \{1, 0\}$ such that $\zeta^i = 1 := i$ is being cut in if there exists a vehicle c defined as

$$\zeta^i = \begin{cases} 1, & \text{if } \exists c, \text{ s.t. } x^{i+1} \geq x^c \geq x^i \\ & \text{and } \sigma^i - \sigma^c = \xi^c \\ 0, & \text{otherwise} \end{cases} \quad (6.7)$$

where c is the vehicle that cut in i , and $i+1$ is the vehicle preceeding i in its lane.

In the remainder of this section, we formulate three models for cut-in handling: reactive and predictive (for ADS-equipped vehicle) and manual (for HV). These models differentiate between the vehicles at tactical-level and control-level: 1) the forward and backward distance on the adjacent lane that can be sensed by i denoted by r_a^i symmetric in both directions (tactical-level); 2) the logic of an additional leader from the adjacent vehicles that are likely to cut in (tactical-level); 3) the logic to decide whether or not to yield to the cut-in vehicle (tactical-level) 4) the acceleration control employed to handle a cut-in (control-level). The manual cut-in handling differs from ADS cut-in handling at both levels. Among ADS-equipped vehicle models, the reactive and predictive differ in all except the first feature. They have the same sensing range of $r_a = 200$ m. The cut-in handling models are generic

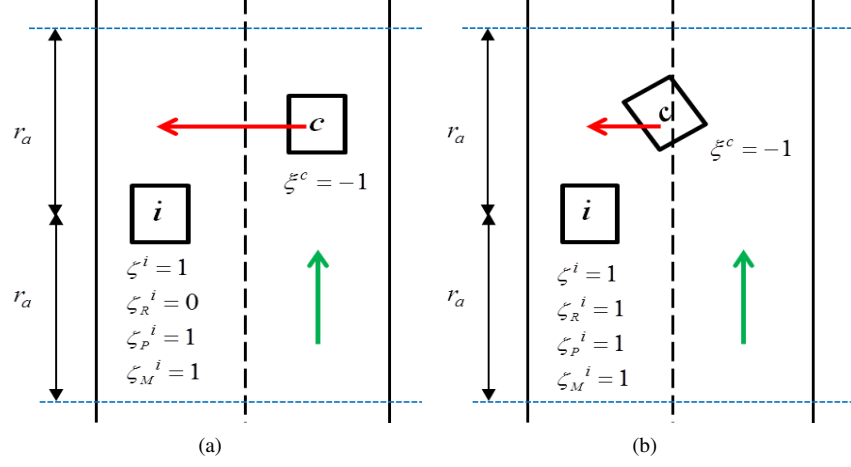


Figure 6.1: Example illustration of cut-in events (a) cut-in detected by Predictive ADS and HV (b) cut-in detected by all vehicle types

extensions of the respective acceleration models formulated in Section 6.2.1, with additional variables to switch to a new leader or include an additional leader in the control law or even switch between two control laws to handle a cut-in. In the remainder of the chapter, we refer ADS-equipped vehicle that employs reactive control simply as Reactive ADS and that which employ predictive control as Predictive ADS.

Model with reactive cut-in handling

A Reactive ADS detects a cut-in only when the cut-in vehicle crosses the target lane boundary. The binary variable ζ_R^i with $\zeta_R^i \in \{1, 0\}$ denotes whether the cut-in is detected, such that $\zeta_R^i = 1 := i$ detects the cut in, based on the conditions formulated as

$$\zeta_R^i = \begin{cases} 1, & \text{if } \zeta^i = 1 \text{ and} \\ & x^c \leq x^i + r_a \text{ and } |\Delta y(i, c)| \leq W \cdot 0.5 \\ 0, & \text{otherwise} \end{cases} \quad (6.8)$$

This formulation includes two conditions: 1) The cut-in should occur with the sensing range of i , represented as $x^c \leq x^i + r_a$; 2) the center of mass of c should cross the boundary of σ^i represented as $|\Delta y(i, c)| \leq W \cdot 0.5$, where W denotes the lane width. The detection condition ζ_R^i is then added to the control law to model the generic acceleration a_{RH} with reactive cut-in handling as

$$a_{RH}^i = \text{MIN} \{ a_{ACC}(i+1), \zeta_R^i \cdot a_{ACC}(c) \} \quad (6.9)$$

where $i+1$ is the vehicle preceeding i in its current lane and c is the cut-in vehicle.

Model with predictive cut-in handling

Compared to a reactive system, the predictive system possesses enhanced detection capabilities. Let ζ_P^i be a binary variable with $\zeta_P^i \in \{1, 0\}$, denotes whether the cut-in is detected,

such that $\zeta_P^i = 1 := i$ detects the cut in, based on the conditions formulated as

$$\zeta_P^i = \begin{cases} 1, & \text{if } \zeta^i = 1 \text{ and } x^c \leq x^i + r_a \\ 0, & \text{otherwise} \end{cases} \quad (6.10)$$

This formulation includes only a single condition that cut-in should occur within i 's sensing range. The distinction in the moments (during cut-in) when the event is detected by reactive and predictive ADS-equipped vehicle is illustrated in Figure 6.1. At the moment depicted in Figure 6.1(a), the cut-in event is not detected by reactive ADS-equipped vehicle, whereas at the moment in Figure 6.1(b) the event is detected.

Besides cut-in detection, a predictive system possesses additional functionalities. While approaching a motorway merging section on the rightmost lane, the predictive ADS-equipped vehicle selects an adjacent vehicle that is likely to merge and switches its acceleration control to yield for the selected vehicle within its predicted time of entry in the acceleration lane.

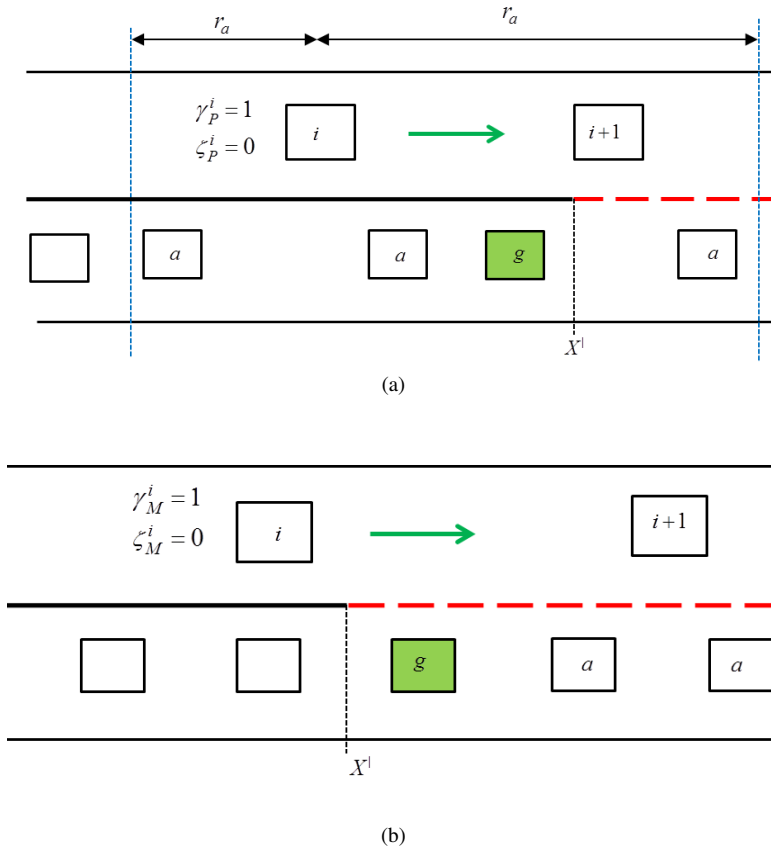


Figure 6.2: Example illustration leader selection for yielding in the vicinity of motorway merge (a) i (Predictive ADS) selects g from set of adjacent vehicles a 's (b) i (human driver) selects g from set of adjacent vehicles a 's

Let \mathbb{O} be the set of vehicles $o \in \mathbb{O}$ present on the on-ramp with $\mathbb{O} : o \in \mathbb{O} | \sigma^o = \sigma^{ramp}$, with σ^{ramp} denoting the lane number of on-ramp. A predictive ADS-equipped vehicle considers a set of adjacent vehicles \mathbb{A}_P on the on-ramp $\mathbb{A}_P \subset \mathbb{O}$, within its sensor range, i.e. $\mathbb{A}_P \ni a | x^i + r_a^S \geq x^a \leq x^i - r_a^S$. Thereafter, it selects a vehicle g from \mathbb{A}_P based on the selection rule: $g \in \mathbb{A}_P | x^{i+1} \geq x^g$ and $s(i, g) = \text{MAX} \{s(i, a) | a \in \mathbb{A}_P\}$. This rule prescribes that g should be i 's far most adjacent vehicle which is behind $i + 1$. Figure 6.2(a) illustrates the selection of g in an example traffic situation.

The future state of g depicted as $\{x^{g*}, v_x^{g*}\}$ are predicted at discrete time steps as $\mathbf{x}^{g*} = (x_1^{g*}, x_2^{g*}, \dots, x_P^{g*})^T$ and $\mathbf{v}_x^{g*} = (v_{x,1}^{g*}, v_{x,2}^{g*}, \dots, v_{x,P}^{g*})^T$ where P is the finite prediction time horizon. The following sets of equation are used to predict the future states of g over the discrete time instances k .

$$\begin{aligned} x^{g*}(k+1) &= x^{g*}(k) + v_x^{g*}(k) \cdot \Delta k \\ v_x^{g*}(k+1) &= v_x^{g*}(k) + a_{comf} \cdot \Delta k \end{aligned} \quad (6.11)$$

a_{comf} denotes comfortable acceleration, which is the constant acceleration input, Δk is the discrete prediction time step. Let γ_P^i be a binary variable with $\gamma_P^i \in \{1, 0\}$, denoting i 's decision to yield such that $\gamma_P^i = 1 := i$ decides to yield, and is defined as

$$\gamma_P^i = \begin{cases} 1, & \text{if } \exists g \in \mathbb{A}_P \ \& \ [x^i \geq X^| \ - r_a^S] \ \& \ [v_x^i \geq 5] \\ & \ \& \ [x_P^{g*} \geq X^|] \ \& \ [v_x^i - v_e^* \geq 0.5 \cdot v_x^i] \\ 0, & \text{otherwise} \end{cases} \quad (6.12)$$

where $X^|$ is the start of the acceleration lane. This model includes four conditions: 1) the start of the acceleration lane should be within the detection range of i ; 2) $v_x^i \geq 5$ to prevent i from reaching a complete stop in the process of yielding; 3) g should be predicted to enter the acceleration lane, represented as $[x_P^{g*} \geq X^|]$; 4) yielding should not entail major loss of speed to i , represented as $v_x^i - v_e^* \geq 0.5 \cdot v_x^i$.

Thereafter, the prediction \mathbf{x}^{g*} is inspected to find the discrete prediction instance k^* when g encroaches the acceleration lane, i.e. $x_k^{g*} \geq X^|$. Let v_e^* be the corresponding predicted velocity, i.e. $v_e^* = v_{x,k^*}^{g*}$. The objective of the yielding control law is to regulate the v_x^i to achieve the safe spacing $s^i = s^0 + v_x^i \cdot t_d$ at the predicted moment of cut-in. Therefore, the acceleration to yield a_{YLD} in order to achieve this safety condition is derived as

$$a_{YLD} = \frac{x^g(k^*) - x^i(0) - s(0) - l - v_x^i(0)(k^* \Delta k + t_d)}{0.5(k^* \Delta k)^2 + t_d k^* \Delta k} \quad (6.13)$$

By inserting the tactical commands γ_P^i and ζ_P^i , and a_{YLD} in the control law, the acceleration with predictive cut-in handling a_{pH}^i is modelled as

$$a_{pH}^i = \text{MIN} \{a_{acc}(i+1), \zeta_P^i \cdot a_{acc}(c), [\gamma_P^i - \zeta_P^i] \cdot a_{YLD}(g)\} \quad (6.14)$$

Model with manual cut-in handling

The manual cut-in handling is modelled based on two assumptions: 1) the human driver can detect a cut-in at any distance, $r_a^M = \infty$, hence $\zeta_M^i = \zeta^i$; 2) the human driver will yield to an adjacent vehicle on the acceleration lane. The second assumption is based on empirical observations that the human driver yield to adjacent vehicles before a cut-in (Z. Zheng et al., 2013).

The human driver considers a set of vehicles $\mathbb{A}_M \subset \mathbb{O}$ such that $A_M^i : a \in \mathbb{A}_M | x^a \geq X^i$. Thereafter it selects a vehicle g from \mathbb{A}_M , such that $g \in \mathbb{A}_M | x^{i+1} \geq x^g \geq x^i$ and $s(i, d) = \text{MIN}\{s(i, g) | a \in \mathbb{A}_M\}$. This rule prescribes that g should be i 's nearest adjacent vehicle which is behind $i + 1$. Figure 6.2(b) illustrates the selection of g by human driver in a traffic situation. Let the binary variable γ_M^i denote i 's decision to yield with $\gamma_M^i \in \{1, 0\}$ such that $\gamma_M^i = 1 := i$ decides to yield and is defined as

$$\gamma_M^i = \begin{cases} 1, & \text{if } \exists g \in \mathbb{A}_M \text{ and } v_x^i \geq 5 \\ 0, & \text{otherwise} \end{cases} \quad (6.15)$$

By inserting the tactical commands γ_M^i and ζ_M^i to the control law, the acceleration with manual cut-in handling a_{MH}^i is modelled as

$$a_{MH}^i = \text{MIN}\{a_{\text{IDM}}(i + 1), \zeta_M^i \cdot a_{\text{IDM}}(c), [\gamma_M^i - \zeta_M^i] \text{MAX}\{a_{\text{IDM}}(g), a_{\text{gap}}\}\} \quad (6.16)$$

where a_{gap} is the minimum acceleration that an HV would apply in order to yield.

6.2.3 Model for lane-changing

The lane change process of HV is modelled as two steps: lane-changing decision and lane-changing execution.

Lane change decision

We formulate the manual lane-changing decision by the model: Minimising Overall Braking Induced by Lane changes (MOBIL) proposed by Kesting et al. (2007). This model has been widely used to describe the lane-changing decision of HVs. MOBIL specifies the manual lane-changing decision as a set of compact rules, under the assumption that the human driver can estimate the acceleration of its neighbouring vehicle (HV or ADS-equipped vehicle). It derives the utility and risk of a lane change from the acceleration model of three vehicles: the lane-changing vehicle (c), following vehicle in the current lane (r) and potential follower in the target lane (f). In this model, the utility of a lane change is defined as

$$U = \tilde{a}^c - a^c + p [\tilde{a}^f - a^f + \tilde{a}^r - a^r] \quad (6.17)$$

where a^c is the acceleration of c in the current lane and \tilde{a}^c is its acceleration after the prospective lane change. Similarly, the current and prospective accelerations of the original follower o and potential follower f are included in the model, and p is a model parameter representing the politeness of c . The lane-changing decision is modelled as a dynamic

variable by following rule,

$$\xi(t) = \begin{cases} +1 : \tilde{a}_{right}^f(t) \geq b_{safe} \ \& \ U_{right} > \Delta a_{th} \ \& \ U_{right} \geq U_{left} \\ -1 : \tilde{a}_{left}^f(t) \geq b_{safe} \ \& \ U_{left} > \Delta a_{th} \ \& \ U_{left} > U_{right} \\ 0 : \text{otherwise} \end{cases} \quad (6.18)$$

a_{th} the threshold of overall acceleration gain. Note that $\xi(t)$ is a dynamic variable which can be modified during the lane-changing. Thereby, this formulation allows a lane change to be aborted if the prospective acceleration of the follower is beyond the safe limit, b_{safe} .

Lane-changing re-planning and trajectory

The lane-changing trajectory is modelled as time-based polynomial function that is dynamically updated. Polynomial functions have been widely used to model empirical lane-changing trajectories (Q. I. Wang et al., 2014) and as reference paths for Automated steering control systems for lane-changing (Luo et al., 2016). The two polynomial functions representing the independent time series of lateral and longitudinal position during the lane-changing is given as

$$\begin{aligned} y(t) &= a_5 t^5 + a_4 t^4 + a_3 t^3 + a_2 t^2 + a_1 t + a_0 \\ x(t) &= b_2 t^2 + b_1 t + b_0 \end{aligned} \quad (6.19)$$

The above functions include nine unknown coefficients which can be determined by solving for the boundary conditions of the lane change process. Accordingly, all these unknowns can be formulated as a function of longitudinal acceleration, a_x^c ; lane-changing duration, D ; and target lateral displacement by lane change, approximated by the lane width, W . During the lane change, c follows the preceding vehicles in the original l and target lanes p , and $a_x^c = \text{MIN}\{a_{IDM}(p), a_{IDM}(l)\}$. The duration of each lane-changing is estimated at the start of the manoeuvre by the model of (Toledo & Zohar, 2007). This model estimates D as a function of traffic density and relative kinematics of ambient vehicles, such as spacing and relative velocity. The lane change duration given by the model is not inherently bounded. Therefore, in the simulations, the range of D is bounded as $2 \leq D \leq 8$ within the empirically observed values (Z. Zheng et al., 2013). The lane-changing is initiated when $\xi(t) = \pm 1$. In case of a lane change abortion, i.e if $\xi(t) = 0$ during an ongoing lane change execution, the target lateral displacement is updated to bring the vehicle back to its original lane.

6.3 Safety metrics

This section presents a set of SMoS to comprehensively evaluate the cut-in manoeuvres covering aspects such as crash likelihood, crash severity and risk dynamics. The selected safety metrics are Post Encroachment Time (PET) to identify the conflicts with neighbouring vehicles, Delta-V as a crash severity estimate, and Probabilistic Driving Risk Field strength that measures the driving risk as a dynamic variable combining both crash likelihood and crash severity.

PET represents the temporal proximity to a crash and has been used as a measure for crash likelihood. PET is the time elapsed between the two vehicles passing a predefined

location on the road stretch. During a cut-in, PET is measured between the cut-in vehicle and neighbouring vehicles $n \in \{f, r, p, t\}$ as shown in Figure 6.6, where f denotes the follower in the target lane; r denotes follower in the current lane; p denotes preceding vehicle in the current lane; and t denotes preceding vehicle in target lane. This results in four measurements. We adopt the method proposed by L. Zheng et al. (2014a) to measure PET of a cut-in. Accordingly, the PET with respect to any n is measured based on the x coordinate of the location at which the closest corner of c crosses the lane boundary (L. Zheng et al., 2014a). In this study, cut-ins with $PET < 0.5$ s are labelled as a conflict (Mullakkal-Babu et al., 2017).

Delta-V is a widely used measure of crash severity, i.e. consequences of the crash in terms of property damage. It is defined as the change in velocity of cut-in vehicle c (See Figure 6.6) between its pre-crash and post-crash trajectories if it crashes with a neighbour n under consideration (Shelby, 2011). Similar to PET, Delta-V is measured between the cut-in vehicle, and neighbouring vehicles n , resulting in four measurements. Among the four measurements, the maximum Delta-V is used as the representative of the manoeuvre. Delta-V is defined for an inelastic crash between c and n , i.e. they stick together after collision and that they have the same mass. Assuming that n does not move laterally at the time of measurement, Delta-V can be defined as

$$\Delta V^c = \sqrt{\left(\frac{v_x^n - v_x^c}{2}\right)^2 + \left(\frac{v_y^c}{2}\right)^2} \quad (6.20)$$

Field theory-based safety metrics represents the driving risk as dynamic variable combining crash likelihood and severity (Mullakkal-Babu et al., 2017). Such a measure would allow a straightforward comparison of manoeuvre safety. Based on field-theory, in Chapter 3, we proposed an approach to assess the driving risk: the risk taken by a vehicle as a result of its interaction with adjacent entities. This approach-Probabilistic Driving Risk Field (PDRF)-can describe the driving risk in interaction with both vehicles and road-side barriers. In this study, we employ this approach solely to quantify the driving risk with respect to f . This approach treats f as an obstacle to c , and models f as a finite scalar risk field formulated in the predicted configuration space of the c . Thereby, the driving risk of c at any given moment is the value of the risk field at the position of its centre of mass.

$$R^c(f) = \frac{M^c \cdot |\mathbf{v}^c - \mathbf{v}^f|^2 \cdot P(f, c)}{8} \quad (6.21)$$

This risk field is formulated as the product of expected crash energy and the collision probability. The term $\frac{M^c \cdot |\mathbf{v}^c - \mathbf{v}^f|^2}{8}$, depicts the expected crash energy if c collides inelastically with f . The second term $P(f, c)$ describes the crash probability between the c and f . The possible states of f at a future time step is estimated from its acceleration distribution. $P(f, c)$ depicts the probability of overlap in the predicted position of c over the possible positions of f at the future time step, which is set as 3 s in our analysis.

6.4 Case study and results

In this section, we present the simulation experiments wherein the ADS and HV models are numerically implemented as time-discrete simulations. The objective of these experiments is to compare the impacts of ADS cut-in handling approaches on the safety and characteristics of HV's lane changes. We simulate a two-lane motorway section of 7.3 km with an on-ramp. The on-ramp merges with the motorway through an acceleration lane of 300 m starting from 5 km. This road geometry allows controlling the number of cut-ins (merges) disturbing the main-lane traffic.

We select two primary input parameters. First, the traffic demand on the on-ramp set as 250 veh/hr/lane (representing low disturbance) and 750 veh/hr/lane (representing high disturbance). Second, the share of ADS-equipped vehicle on the main-lane traffic, set as 0% (reference scenario without ADS-equipped vehicle in traffic), 10% (approximately the current deployment rate of such systems in Europe) (Kyriakidis et al., 2015), 30%, 50% and 90% representing different levels of the mix. Thereby, reactive and predictive cut-in handling approaches are evaluated in two sets of traffic scenarios (varying in the combination of the two input parameters). The resulting scenario matrix consists of 18 scenarios. To improve the statistical reliability of the results, we perform 10 replications of each scenario. The simulations are randomised in terms of the vehicle generation and the desired velocity of HV. To ensure the comparability of the results across the scenarios, the values all the driving model parameters (See Table. 6.1) is fixed across all the simulations. Each scenario is simulated for 30 minutes at a discrete-time step of 0.1 s.

6.4.1 Characteristics of lane changes

We evaluate the change in characteristics of lane changes as an effect of the increasing presence of ADS-equipped vehicles. Figure 6.3 plots the spatial distribution of successful lane changes performed by humans under scenarios with an increasing penetration rate of ADS-equipped vehicle. In all the plots, the distribution peaks in the vicinity of merging section (5000 - 5300 m), where on-ramp vehicle merge into the main lane. It can be seen that HV's perform more lane changes in mixed traffic (See Figure 6.3). In traffic mixed with Reactive ADS, the lane change frequency at the downstream end of the merging section is higher than at the upstream end. This indicates an increase in the number of late merges due to the lack of cooperation by Reactive ADS (See Figure 6.3(a) and (c)). In contrast, such a disparity is not observed in the presence of Predictive ADS; the lane changes occur throughout the merging section (See Figure 6.3(b) and (d)).

Figure 6.4 plots the average velocity at the start of a lane change. The lane changing velocity consistently drops with an increasing presence of reactive ADS. As most of the lane changes are merging manoeuvres, the velocity reduces as vehicles queue up at the on-ramp dead-end, implying an increase in difficulty to find a safe merging gap. In contrast, Predictive ADSs increase the lane-changing velocity at low on-ramp demand. The early yielding by ADS enables smooth merging of the on-ramp vehicle. At the 90 % penetration rate, the difference in the effects of reactive and predictive ADS, as observed by lane change velocity becomes prominent. Interestingly, at 50% penetration rate, the effects (as observed by the lane change velocity) are comparable between the two cut-in handling approach. The reason is that, in 50% mixed traffic, the number of lane changes in the vicinity of the merge

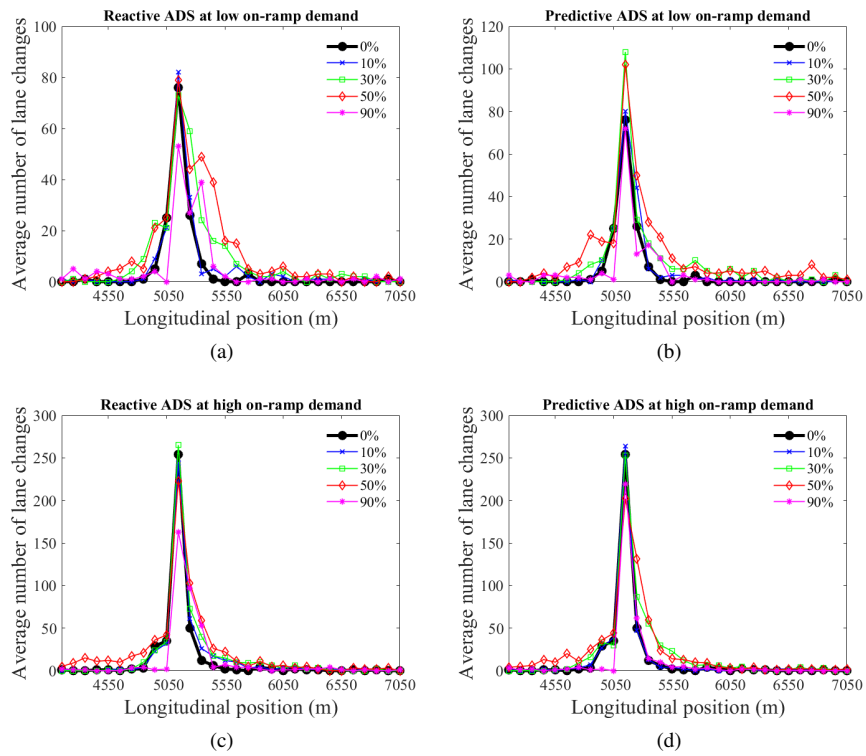


Figure 6.3: Effects of ADS penetration on the spatial distribution of lane changes at low on-ramp demand (a),(b) and high on-ramp demand (c),(d)

Table 6.2: Parameter values in the simulation experiments

Parameter (description)	Value	Parameter (description)	Value
\bar{a} (IDM maximum acceleration)	1 m/s ²	K_1 (ACC parameter)	0.1 1/s ²
b (IDM comfortable braking)	1.5 m/s ²	K_2 (ACC parameter)	5.4 1/s
v^{max} (IDM maximum speed)	160 km/hr	K_3 (ACC parameter)	0.12 1/s ²
v_d (desired velocity)	108 km/hr	Q (ACC parameter)	1
t_d (desired time headway)	1.2 s	J (ACC parameter)	100 m
s_0 (IDM minimum space gap)	2 m	X^l (start of acceleration lane)	5000 m
m (Vehicle mass)	1000 kg	w (Vehicle width)	2 m
W (Lane width)	3.5 m	l (Vehicle length)	5 m
b_{safe} (safe braking limit)	4 m/s ²	a_{min} (maximum braking)	-9 m/s ²
p (MOBIL politeness parameter)	0.5	a_{max} (maximum acceleration)	3 m/s ²
Δa_{th} (MOBIL acceleration threshold)	0.5	Simulation time step	0.1 s

is relatively higher (See Figure 6.3 (c) and (d)), creating congestion on the main lanes. Since the predictive control does not function in a velocity of < 5 m/s, the effect of Predictive ADSs on the merging vehicles is similar to that of Reactive ADSs at this penetration rate.

6.4.2 Aborted lane changes

Figure 6.5 describes the effect of ADS penetration rate on the number of aborted (unsuccessful) lane changes with high on-ramp demand. It can be seen that the aborted lane changes steadily increase with the presence of Reactive ADS. The Reactive ADS cannot respond to the cut-in vehicle during the first half of the cut-in manoeuvre. This creates risky situations, i.e. $\tilde{a}^f(t) < b_{safe}$ in Equation 18, causing c to abort the lane change. On the contrary, aborted lane changes are occasional (< 1) in traffic scenarios with predictive ADS-equipped vehicle, irrespective of their market penetration rate and on-ramp demand. The predictive ADS begins to respond to cut-in at least by the start of the manoeuvre, and therefore risky situations are avoided. Similarly, we observed aborted lane changes with low on-ramp demand in traffic consisting of Reactive ADS: a maximum of six aborted lane changes at 90% penetration rate of Reactive ADS.

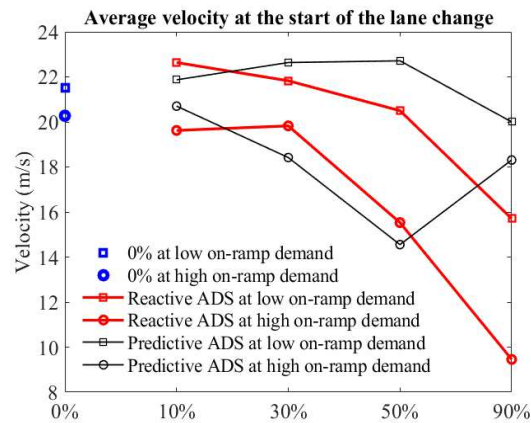


Figure 6.4: Effects of ADS penetration rate on the velocity at the start of lane change

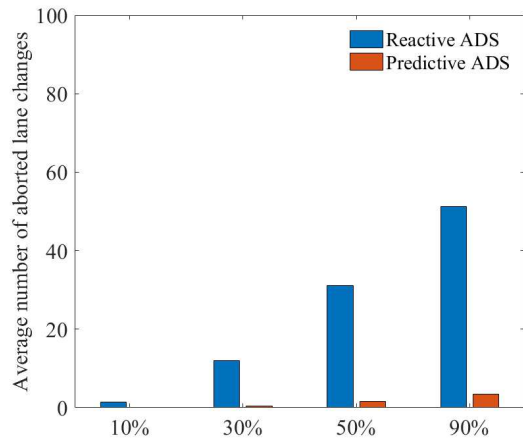


Figure 6.5: Effects of ADS penetration rate on the number of aborted lane changes at high on-ramp demands

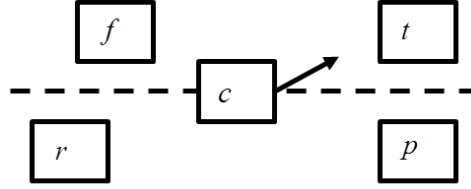


Figure 6.6: Notations for the vehicles in the vicinity of the lane changer c

6.4.3 Conflicts with neighbouring vehicles

We evaluate the conflicts between c and any of its neighbours $n \in \{f, r, p, t\}$ as shown in Figure 6.6. Figure 6.7 describes the effects of the increasing penetration rate of ADS-equipped vehicle on lane-change conflicts. The number of conflicts increases with the market penetration rate of ADS-equipped vehicle irrespective of the cut-in handling approach. It can be seen that Predictive ADS results in fewer conflicts than Reactive ADS. The highest number of conflicts appears between the c and f , following vehicle in the target lane that is handling the cut in, and with an increasing market penetration rate, it is more likely that f is an ADS-equipped vehicle. ADS-equipped vehicle applies a relatively milder acceleration than HV according to their respective control laws, which shortens the PET of the manoeuvre. Therefore the behavioural distinction of ADS-equipped vehicle poorly reflects in the PET metric. In scenarios with high on-ramp demand, the higher number of conflicts appears between the c - r , and c - p . High demand induces queuing in the on-ramp lane, and vehicles are close to each other, resulting in shorter PET. This is in line with the observed drop in lane change velocity (Figure 6.4).

6.4.4 Expected severity of crashes

Figure 6.8 describes the effects of increasing in ADS-equipped vehicle share on the average maximum Delta-V. It can be seen that the impact on the expected crash severity (as estimated by Delta-V) is marginal, except in 90% penetration rate at low on-ramp demand. With lower disturbance from the on-ramp, the main-lane traffic flows at higher speed, resulting in larger Delta-V during cut-in. Delta-V related to Predictive ADS is lower than that of Reactive ADS. The Predictive ADS yields earlier in time allowing it to lower the approach speed.

6.4.5 Driving risk during cut-in

The PDRF incorporates both the crash severity and crash probability and thereby allow straightforward risk comparison. To compare the specific effects of Reactive and Predictive control, we solely analyse cut-ins ahead of ADS-equipped vehicle. Figure 6.9 describes the effects of increasing ADS-equipped vehicle share on the average maximum driving risk as estimated by PDRF strength. It can be seen that cut-in involving Predictive ADS are consistently at a lower risk than those involving Reactive ADS. Besides, the magnitude of risk with cut-in is expected to steadily increase with the share of Reactive ADS in traffic, and

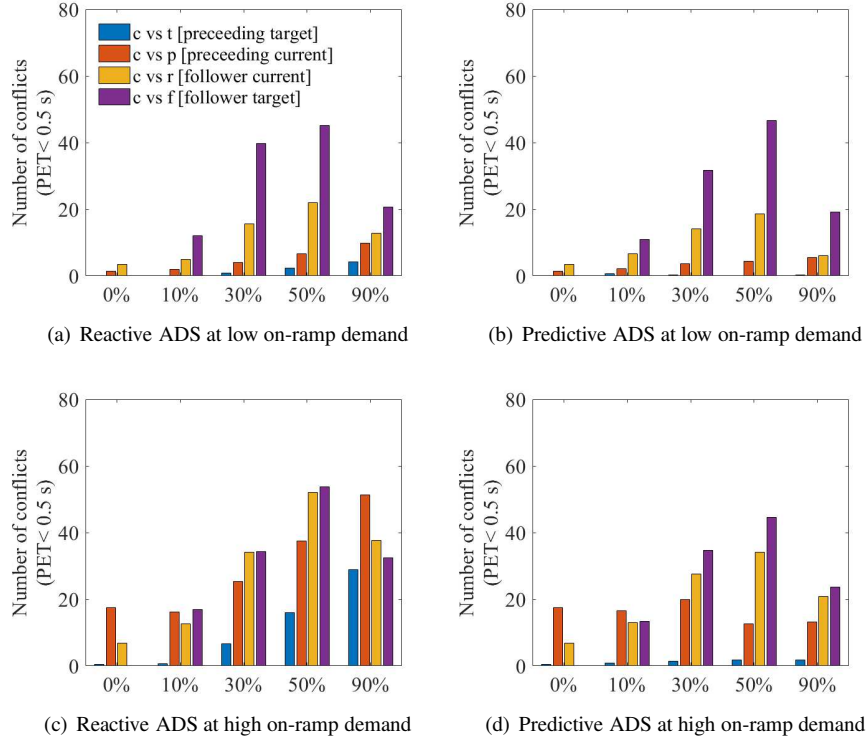


Figure 6.7: Effects of ADS penetration rate on the frequency of conflicts between the c (cut-in vehicle) and each of its neighbours $n \in \{f, r, p, t\}$ at low on-ramp demand (a), (c) and high on-ramp demand (b), (d)

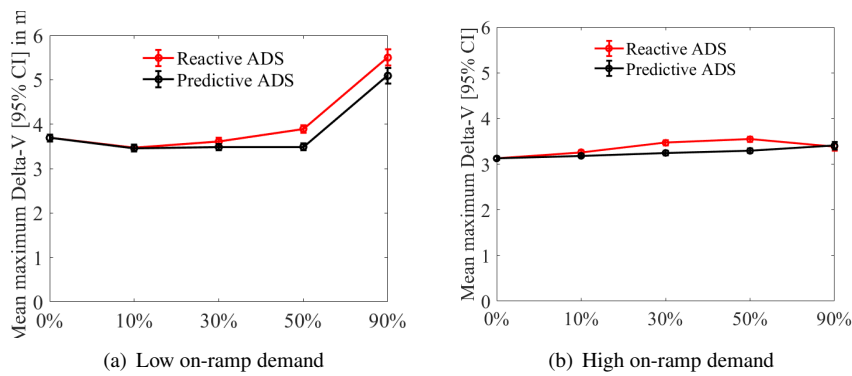


Figure 6.8: Effects of ADS penetration rate on mean Delta-V at low (a) and high on-ramp demands (b)

the variation of risk estimate increases with the penetration rate, suggesting the increasing variability in the risk level of conflicts. In contrast, the magnitude of risk and its variability in cut-ins involving Predictive ADS remain marginal throughout all scenarios.

Figure 6.10 describes the effects of ADS on the risk dynamics during an average cut-in. When the traffic is mixed with Reactive ADS, the driving risk peaks halfway during the manoeuvre, and drops thereafter. This effect can be due to two combining factors: reactive ADS-equipped vehicles cannot respond to the cut-in vehicle during the first half of the cut-in manoeuvre, causing a steep rise in crash probability; the lateral velocity of the lane-changer is highest when halfway through the manoeuvre, implying a peak of expected crash severity. During the second half of cut-in, the follower (Reactive ADS) begins to respond preventing a further rise in risk. On the contrary, when the traffic is mixed with predictive ADS-equipped vehicle, there is no such intermediate peak in driving risk; instead, the risk driving risk remains marginal throughout the manoeuvre. Besides, it can be seen from Figure 6.10 that the magnitude of risk peak increases steadily with the penetration rate of Reactive ADS.

6.5 Sensitivity analysis

In this section, we discuss the implications of the parameter values and model choice on the results. The length of the acceleration lane was set to 300 m in the scenario simulations. To evaluate the implication of this setting, we simulated homogenous HV traffic under high on-ramp demand with a longer acceleration lane of 500 m. In this scenario, we observe that the expected crash severity drops to 2.11 m/s (from 3.12 m/s), whereas the number of conflicts increases to 39 (from 25). The increase in the number of conflicts is a direct effect of increasing the road space available for merging. In traffic mixed with Reactive ADS, larger acceleration lane length can have a positive effect on safety. For instance, in 50% mix of Reactive ADS at high on-ramp demand, the instances of lane change abortion are reduced to 10 from 30 (See Figure 6.5), and average maximum Delta-V reduces by 0.3 m/s. The sensing range of Predictive ADS was set to 200 m. We did not find a considerable improvement in the safety performance of Predictive ADS by increasing their sensing range. For instance, when the sensing range is increased to 300 m, the average maximum Delta-V reduced marginally by 0.1 m/s.

The longitudinal acceleration control of an ADS-equipped vehicle was modelled by a deterministic ACC law (Mullakkal-Babu et al., 2016), and HV was modelled by IDM with the desired velocity as a stochastic parameter. Regarding lateral control, ADS-equipped vehicle model is cannot change lane, whereas HV model can change lane. To check if our comparative findings hold even when the effects of distinct acceleration and lane change models are excluded, we analysed simulations in which longitudinal control of all the vehicles was modelled by IDM (Treiber et al., 2000) (with a fixed desired velocity) and lane-changing decision by MOBIL. We find that our findings hold under such modelling assumptions as well. In traffic scenarios comprising of vehicles with reactive control, we observed 23 (at low on-ramp demand) and 149 (at high on-ramp demand) instances of aborted lane changes, but no aborted lane changes were observed in traffic with predictive control. With low on-ramp demand, in traffic scenarios comprising of vehicles with reactive control, the maximum Delta-V was larger (5.2 m/s) than that of traffic with predictive control (4.4 m/s).

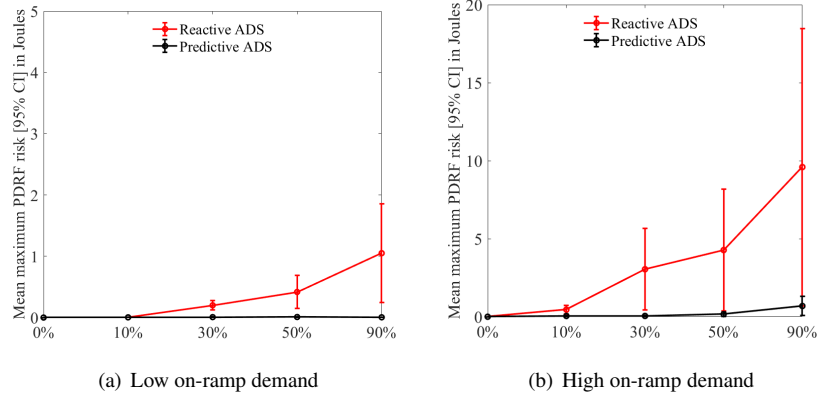


Figure 6.9: Mean maximum PDRF risk with low on-ramp demand (a) and high on-ramp demand (b)

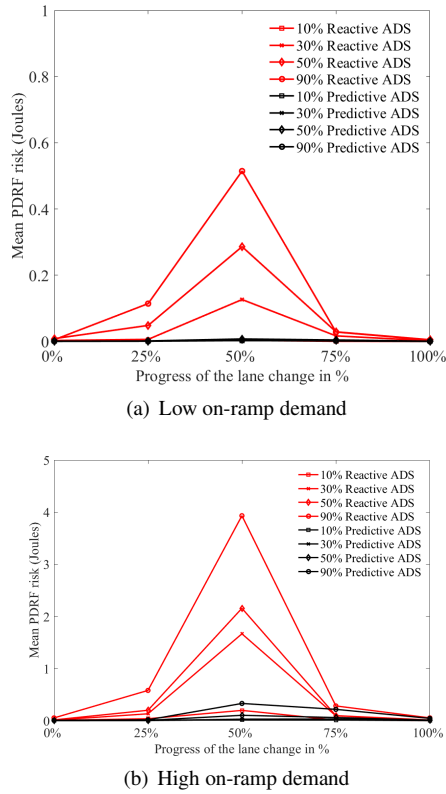


Figure 6.10: Evolution of risk during lane-changing in scenarios with ADS at low (a) and high on-ramp demands (b)

The reactive control resulted in average 62.2 (low on-ramp demand) and 411.3 (high on-ramp demand) conflicts, which is considerably larger than 3.7 (low on-ramp demand) and 6.3 (high on-ramp demand) with the predictive control.

To exclude the effects of the lane-changing decision model, we analysed simulations of IDM controlled traffic fleet with high on-ramp demand. In this case, MOBIL is deactivated and vehicles on the mainline do not change lane. The results further strengthen our finding that predictive control is safer than the reactive one. In traffic scenarios comprising of vehicles with reactive control, we observed 90 (in high on-ramp demand) instances of aborted lane changes, but no aborted lane changes were observed in traffic with predictive control. The reactive control resulted in average 358 conflicts, in contrast, we did not observe any conflict in traffic with predictive control. Similarly, in traffic scenarios comprising of vehicles with reactive control, the maximum Delta-V was larger (5.1 m/s) than that of traffic with predictive control (2.5 m/s).

Models in this study strongly idealise the behaviour of sensors and actuators in the ADS. Similarly, a simple rule-based algorithm was deployed to model the prediction logic of the ADS. Under these assumptions, our results suggest that even a simple prediction scheme could significantly outperform reactive approaches in terms of traffic safety. However, the quantitative accuracy of the results can be improved by relaxing these assumptions and rigorously modelling sophisticated prediction algorithms or other approaches in reactive ADS to improve the robustness of cut-in handling (Xia et al., 2010).

Another assumption underlying the lane change decision model is that human driver can estimate the acceleration gain for the adjacent vehicle (human or equipped), as a consequence of lane change (Kesting et al., 2007). This assumption is not realistic in mixed traffic scenarios with low market penetration, when the human drivers might not be familiar with behaviour of ADS-equipped vehicle. However, we do not expect any influence on the comparative findings, as the assumption applies to both sets of mixed traffic simulations.

6.6 Conclusions and future work

It is well known that ADS equipped vehicles could impact the longitudinal driving behaviour of the non-equipped vehicles and the collective traffic flow properties. Our results suggest the longitudinal functionalities of the ADS could as well impact the lateral manoeuvres of adjacent vehicles (Human-driven vehicles in this study). We find that the presence of ADS-equipped vehicles in traffic could alter the spatial distribution of lane change events in the vicinity of the merging section; Reactive ADS could increase the difficulty for on-ramp vehicles to safely merge onto the motorway, thereby increasing the level of congestion in the on-ramp; and that Reactive ADS could increase the instances of unsuccessful lane changes.

We find that approaches employed by ADS-equipped vehicle to handle a cut-in can impact traffic safety at a motorway discontinuity. The predictive control is the key functionality to improve safety with cut-ins. The predictive control employing a simple rule-based decision provides a safer interaction than reactive control. These two approaches yield distinct risk dynamics during a cut-in. When a vehicle cuts in ahead of Reactive ADS, the risk peaks approximately halfway through the manoeuvre. This is also reflected by the instances of lane change abortions. In contrast, the prediction functionality maintains the risk marginal throughout the encounter. Regarding the variation of safety impact with the mar-

ket penetration rate of ADS equipped vehicles, we find that the negative effects of Reactive ADS become prominent when the penetration rate is greater than 10% and grow stronger with an increase in penetration rate. The level of traffic safety is approximately unaffected by the increasing share of Predictive ADS.

Our results highlight the potential of simulation-based safety assessment in this regard. Our future efforts will be focussed on analysing the safety impacts of a specific ADS feature that is already deployed in passenger vehicles and to provide more concrete estimates such as expected crash rate and related proportion of fatalities.



Chapter 7

Findings, conclusions and recommendations

This final chapter summarises the key findings of this thesis in Section 7.1. The conclusions drawn from the findings are described in Section 7.2. Section 7.3 and Section 7.4 detail the recommendations for practice and future research respectively.

7.1 Findings

In Chapter 1, we established three research objectives. In this section, we reflect on the extent to which these objectives were addressed by the findings of this thesis.

Objective 1: To formulate a metric for driving risk that contains information on crash-severity and crash probability and is sensitive to properties of conflicting on-road entities

To meet this objective, in Chapter 2, we reviewed the literature and selected five metrics with distinct expression of safety. We established a set of qualitative and quantitative properties that a metric should possess in order to describe the crash risk. This study revealed the following: 1) each of the selected safety metrics provides only a partial expression of crash risk, 2) each metric provides a different description of risk dynamics during an encounter in terms of the moment of highest risk, 3) none of them, except safety field force, provides a continuous risk description during the simulated encounters, 4) none of them, except safety field force, can be aggregated in a multi-vehicle scenario, 5) none of them accounts for the uncertainty concerning the driving environment, 6) among the selected metrics, PET and safety field force are the only two which describe the risk dynamics during a lane-changing manoeuvre. In this study, we identified that the safety field force provides the smoothest risk description and contains the highest number of risk contributing factors, revealing the advantages of the field-theoretic paradigm for safety quantification. But the parameters of safety field are not intuitive, and it does not account for the uncertainty concerning the driving environment.

In Chapter 3, we presented a numerical estimate of the crash risk based on artificial field theory. We define a risk estimate that combines the crash probability and expected crash

severity. The uncertainty related to the future evolution of the local traffic environment is modelled by the characteristic acceleration distribution of the ambient vehicles. The acceleration distribution is known to be correlated with safety changes caused by road geometry, traffic state and driver aggressiveness, and can be measured from onboard sensors. The expected crash severity term of the risk estimate factors in the masses and energy dissipation properties of the conflicting entities. The examples in Chapter 3 show that the risk description according to PDRF qualitatively reflects the event narration of the selected near-crash scenarios. The simulation-based case studies show that the PDRF approach can identify the safest manoeuvre among a finite set of alternatives, by factoring the crash severity and probability.

Objective 2: To develop a submicroscopic multi-lane traffic flow simulation framework that is generic to ADS equipped and human-driven vehicles incorporating the respective tactical-level functions, control-level functions, vehicle dynamics, and the interconnections between them.

To achieve this objective, we began with an empirical investigation of lane-changing execution, which is typically oversimplified in traffic simulations. In Chapter 4, we examined empirical lane change trajectories and identified the causal factors and properties of two distinct types of lane changes: continuous and fragmented. The results suggest that the lane-changer exhibits distinct kinematics during a fragmented lane change. Moreover, this manoeuvre induces a distinct effect on the follower in the target lane. We identified a set of factors that is likely to be related to the decision-making process of the type of lane change: an average driver executes a fragmented lane change when the preceding and following vehicles in the target lane are slower, and when the follower in the target lane is closer than those observed during the onset of a continuous lane-changing. The results suggest that fragmented lane-changing is associated with an increased necessity to change lane such as for entering the main lane from an on-ramp. In addition to empirical analysis, Chapter 4 presents two models applicable to traffic simulation: a trajectory model and a transient behaviour model for the target-follower during the two lane change types. This study also highlights that common approaches to simulate lane-changing execution, such as constant manoeuvre duration and linear lane changing trajectory, result in unrealistic trajectory descriptions that differ from actual trajectories by a wide margin.

Chapter 5 presented a generic framework to simulate the two-dimensional motion of both human-driven and ADS-equipped vehicle. This framework consists of two coupled layers, an upper tactical level that generates manoeuvre plans; and a lower operational layer with explicit control module (steering and acceleration control) that operates in a closed loop with a bicycle model of vehicle dynamics. This framework describes trajectories accounting for lateral and longitudinal dynamics and yaw motion, and provide additional variables such as vehicle heading and front road-wheel steering commands. In comparison to typical approaches, the simulation examples show that this framework can simulate more lateral manoeuvres such as curve negotiation, corrective steering, lane change abortion, and fragmented lane-changing. At the macroscopic level, the multi-lane traffic flow simulation can reproduce phenomena such as capacity drop and typical values of traffic properties such as critical density and shockwave velocity. High computational demand has been a major obstacle to the use of sub-microscopic simulators. Chapter 5 shows that the hybrid simulation architecture can improve the computational efficiency.

Objective 3: To demonstrate the application of the proposed risk metric and the traffic simulation framework and to identify the relations between the key ADS design parameters and the safety impacts on multi-lane motorway traffic.

The case study in Chapter 6 presented a comparative safety assessment employing the simulation framework of Chapter 5 and assessment method of Chapter 3. We compare two generic longitudinal strategies of ADS to handle a cut-in: reactive and predictive, and identify their distinctive effects on the safety of cut-in manoeuvres by adjacent human-driven vehicles. Compared to the reactive ADS, the predictive ADS improves safety both at the vehicle level and the traffic level. The changes can be observed in multiple aspects of safety: crash severity, the number of conflicts, frequency of unsuccessful lane changes, and risk dynamics during the lane change. The results suggest that the follower's strategy to handle a cut-in influences safety during the manoeuvre. When the follower is a predictive ADS, the cut-in manoeuvre can be completed without an increase in the crash risk. On the contrary, if the follower is a reactive ADS, an increase in crash-risk is likely to occur. This can detriment the traffic safety at motorway merges and the magnitude of risk increases with an increase in the number of vehicles seeking to merge into the mainline. In addition, we find that reactive ADSs can induce larger traffic disturbances than their predictive counterparts as they do not yield for gap-seeking vehicles on the on-ramp.

7.2 Conclusions

The findings in Chapter 2 suggest that the selected safety metrics are appropriate to assess the chances of rear-end crashes on continuous motorway sections, but are not appropriate to assess the safety of lateral vehicle interactions. Each of the selected metrics provides a different description of risk and, therefore are not comparable. TTC, PICUD, PET and warning index when used as cost index in motion control can lead to a jerky motion (unbounded and discontinuous), and when used as a decision variable in active safety systems can create false negatives. The risk metric based on field-theory, provides a smooth description of risk dynamics during 2D interaction, and possesses mathematical properties to quantify simultaneous risk due to multiple road entities. However, to employ the field-theoretic paradigm to safety assessment, the safety field should be extended to account for uncertainty and should be reformulated with intuitive parameters related to the crash mechanism.

The findings in Chapter 3 show that crash risk can be formulated as a scalar artificial field. The numerical risk estimate, PDRF strength, can quantify the safety impacts of driving strategies employed by ADS. However, the parameters of the estimate should be calibrated to be deployed to predict the crash rate. The examples show that PDRF strength can be employed as a cost index in path planning algorithms, and that it can differentiate the risk levels of different traffic scenes.

Results of Chapter 4 suggest that fragmented lane-changing is a common strategy implemented by human drivers to merge into the main lane. This chapter provides strong evidence that the form of lane-changing trajectory impacts the behaviour of follower in the target lane, particularly in the anticipation phase. We find that the local traffic variables and level of necessity to change lane can influence the lane changing type. Our results suggest that the emergence of fragmented lane change is not related to the aggressiveness of the involved drivers. The modelling results suggest that the accuracy of traffic flow models can

be improved by deploying lane change execution and impact models that are specific to fragmented and continuous lane changes.

Chapter 5 demonstrates the possibility to mathematically formulate a generic framework for 2D vehicle movement in a computationally feasible way. This framework can capture the 2D interaction between road users, which is highly relevant for safety assessment studies. The framework preserves the properties of the component models, and at the same time describe the planar movement of vehicles with realistic nonholonomic constraints. The hybrid scheme is very promising in enabling high-resolution submicroscopic simulations in real-time.

Chapter 6 highlights the potential of simulation-based studies to assess the safety of ADS functionalities. Using an appropriate set of safety metrics and a more realistic simulation of vehicle interactions, simulation-based safety assessment approaches can provide detailed safety predictions. The case study results in this chapter suggest that the predictive-navigation planning is the key functionality that would enable smoother and safer interactions between ADS-equipped and human-driven vehicles. The penetration of ADS-equipped vehicles can also have an impact on the spatial distribution of lane changes, which should be considered in the design of future motorways.

7.3 Recommendations for practice

This thesis provides several practical recommendations regarding design and evaluation of decision-making and control strategies for ADS. Our results show that a predictive strategy to handle cut-in can significantly enhance the driving safety compared to reactive strategies both at the individual and collective traffic level. We find that the ability to detect and monitor the adjacent vehicle are important, particularly near the motorway merges. It may be noted that fragmented lane-changing is an efficient strategy to merge into the congested motorway. This manoeuvre may be included in prediction schemes as they are frequently performed by human drivers. Our findings show that the crash severity is critical information that differentiates the level of safety of candidate path plans and therefore should be accounted for in the risk estimation. The interaction between adjacent follower and the lane changer is a relevant aspect to be considered while developing the test cases to evaluate the performance of ADS.

Policymakers may note the risk of generalising traffic impacts of ADS, since it depends considerably on the functionalities and design specifications of ADS. Therefore, ADSs should be simulated by precise models and their safety impacts should be investigated in terms of both crash probability and crash severity.

Road operators should account for the potential risk caused by ADS-equipped vehicles and their functionalities in mixed traffic while planning for the future infrastructure. Results in Chapter 6 provide an example of how the reactive cut-in handling functionality of the ADS may increase the number of lane changes near the downstream end of the acceleration lane.

7.4 Recommendations for future research

This thesis proposes a theoretical model for collision-risk during driving based on the artificial field paradigm, with proof-of-concept demonstrations. However, this theory has to be tested and validated with empirical data, particularly to be applied for crash predictions. Such an effort requires high resolution trajectory data to estimate the proposed driving risk estimate, to calibrate the model parameters and to examine the correlation with the historic crash frequency. In addition, this model may be extended to incorporate uncertainties arising from factors such as driver behaviour, road surface conditions, lighting and weather conditions, and potential system failures affecting vehicle operation. The uncertainty concerning the behaviour of neighbouring vehicles can be more accurately estimated by modelling the relationship between the distributions of lateral and longitudinal acceleration.

In this thesis, we applied driving risk estimate to compare two distinct strategies employed by ADS. However, there are other potential applications of this model which have not been examined. The risk metric exhibits the potential to describe safety as perceived by a human driver. In Chapter 3, we find that by calibrating the prediction time step, the magnitude of risk visually correlates with the strength of the drivers evasive response. To the best of our knowledge, a dynamic model of perceived safety by the human driver does not exist in the current literature, and applicability of the PDRF in this regard is an interesting direction for future research. Another potential application of PDRF is in trajectory planning algorithms, where the PDRF strength could be employed as the risk cost to identify the safest manoeuvre.

The results in Chapter 4 revealed several distinguishing characteristics and motivating factors of fragmented lane changes. However, the results are related only to cars, and further research is necessary to find if such manoeuvres are performed by other vehicle types as well. Compared to continuous ones, fragmented lane changes are less frequent events and hardly observed in small data sets. The empirical results and models in this chapter can be strengthened by cross-validating them on data sets from different locations.

In Chapter 5, we proposed a hybrid submicroscopic/microscopic simulation framework which was operationalised to simulate a straight motorway road stretch with a merging section. The ultimate aim of the submicroscopic simulation is to enhance the capability of traffic flow models in describing the vehicle motion and interactions. This entails an improvement in the component behavioural models and improvement in the realism of their operationalisation within the numerical traffic simulation scheme. We focus on improving the realism of operationalisation of these behavioural models and their interconnection. Further research is required to calibrate behavioural model parameters and to examine the simulation accuracy of the framework. The required level of calibration depends on the objective of the analysis. In a safety assessment study, the calibration might be restricted to microscopic variables that are used to estimate the safety metrics. On the contrary, if one is interested in the traffic flow impacts of a specific control system, then the parameters related to submicroscopic variables should be calibrated in more detail.

Individual driver behaviour plays a major role in vehicle navigation. The framework can be extended to integrate behavioural parameters characterising the human drivers such as (variable) response time and perception error. A notable work in this direction is by van Lint & Calvert (2018). They proposed a theory to model the perception and response processes at tactical and operational layers. Besides, the vehicular interaction in relation to lane-

changing may begin far ahead of the actual manoeuvre execution, such as during weaving and merging in congested traffic. Such considerations can be incorporated by extending the tactical planning horizon and reformulating the related functions with models such as (Hidas, 2005; Z. Zheng et al., 2013; Schakel et al., 2012).

We applied the simulation framework for safety assessment, but there exist other potential applications. It can be employed to compare the performance of alternative crash-avoidance applications in different vehicle types in uncontrolled traffic situations involving dynamic vehicle interactions. Since the framework provides submicroscopic variables such as front road-wheel steering angle and vehicle heading, it could serve as a test bed to examine the feasibility of decision variables generated by the behavioural sub-models such as the lane-changing decision model.

In Chapter 6, we applied the simulation-based safety assessment approach to compare the traffic safety impacts of two longitudinal strategies employed by ADS to handle cut-ins. This approach can be applied in related subjects, such as to investigate the impacts of lateral manoeuvres by ADSs or to compare the effectiveness of alternative strategies applied by ADS for crash avoidance.

Appendix A

Algorithm and calculations of Chapter 3

Algorithm A.1 Algorithm to calculate kinetic PDRF risk for single time step

- 1: **Data:** Initial states (X, Y, V_X, V_Y) ; geometric parameters (L, W) , motion constraint parameters $()$ of the subject vehicle s and neighbour vehicle n , prediction time step τ , acceleration distribution of n $(\mu_X, \sigma_X, \mu_Y, \sigma_Y)$.
 - 2: **Result:** Kinetic PDRF risk (R_n)
 - 3: **while** n **do**
 - 4: **begin**
 - 5: Calculate the corners of the polygon Q and Z as shown in Table A.1 and Table A.2
 - 6: Calculate the corner of the polygon O whose region is the geometric intersection of Q and Z using computational geometry tools such as the function *intersect* (Q,Z) in Matlab 2017
 - 7: Convert the corners of O (defined in spatial domain) to O^A (acceleration domain) using Eq. 3.7
 - 8: **if** O^A **then**
 - 9: **begin**
 - 10: Solve the integral of joint probability function in Eq.(8) over the area O^A .
 - 11: Calculate the kinetic PDRF risk R_n using Eq.(3.4).
 - 12: **end**
 - 13: **else**
 - 14: $R_n \leftarrow 0$
 - 15: **end**
-

Table A.1: X Coordinate of corners of polygon Q and Z in spatial domain

Corner	X Coordinate
Q1	$X_n + V_{X,n} \cdot \tau + 0.5 \cdot A^{\max} \cdot \tau^2$
Q2	$X_n + V_{X,n} \cdot \tau + 0.5 \cdot \max\left(A^{\min}, \frac{-V_{X,n}}{\tau}\right) \cdot \tau^2$
Q3	$X_n + V_{X,n} \cdot \tau + 0.5 \cdot \max\left(A^{\min}, \frac{-V_{X,n}}{\tau}\right) \cdot \tau^2$
Q4	$X_n + V_{X,n} \cdot \tau + 0.5 \cdot A^{\max} \cdot \tau^2$
Z1	$X_s + V_{X,s} \cdot \tau + L_n$
Z2	$X_s + V_{X,s} \cdot \tau - L_s$
Z3	$X_s + V_{X,s} \cdot \tau - L_s$
Z4	$X_s + V_{X,s} \cdot \tau + L_n$

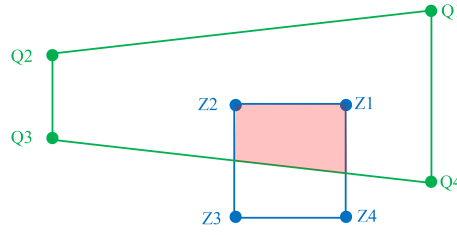


Figure A.1: Geometric representation of the polygons Q, Z and their overlap O (area shaded in pink), used for the crash probability estimation in Algorithm A.1

Table A.2: Y Coordinate of corners of polygon Q and Z in spatial domain

Corner	X Coordinate
Q1	$Y_n + V_{Y,n} \cdot \tau + 0.5 \cdot \min\left(A^{\max}, \frac{0.17 \cdot (V_{Y,n} + A^{\max} \cdot \tau) - V_{Y,n}}{\tau}\right) \cdot \tau^2$
Q2	$Y_n + V_{Y,n} \cdot \tau + 0.5 \cdot \max\left(-A_Y^{\max}, 0.17 \cdot \left(V_{Y,n} + \max\left(A^{\min}, \frac{-V_{Y,n}}{\tau}\right) \cdot \tau\right)\right) \cdot \tau^2$
Q3	$Y_n + V_{Y,n} \cdot \tau - 0.5 \cdot \max\left(-A_Y^{\max}, 0.17 \cdot \left(V_{Y,n} + \max\left(A^{\min}, \frac{-V_{Y,n}}{\tau}\right) \cdot \tau\right)\right) \cdot \tau^2$
Q4	$Y_n + V_{Y,n} \cdot \tau - 0.5 \cdot \min\left(A^{\max}, \frac{0.17 \cdot (V_{Y,n} + A^{\max} \cdot \tau) - V_{Y,n}}{\tau}\right) \cdot \tau^2$
Z1	$Y_s + V_{Y,s} \cdot \tau + W_n$
Z2	$Y_s + V_{Y,s} \cdot \tau + W_n$
Z3	$Y_s + V_{Y,s} \cdot \tau - W_s$
Z4	$Y_s + V_{Y,s} \cdot \tau - W_s$

Bibliography

- Aarts, L., & Van Schagen, I. (2006). Driving speed and the risk of road crashes: A review. *Accident Analysis and Prevention*, 38(2), 215–224.
- Ahn, S., & Cassidy, M. J. (2007). Freeway traffic oscillations and vehicle lane-change maneuvers. *Transportation and Traffic Theory*, 691–710.
- Archer, J. (2005). *Indicators for traffic safety assessment and prediction and their application in micro-simulation modelling: A study of urban and suburban intersections* (Ph.D dissertation). Royal Institute of Technology, Centre for Transport Research.
- Ardelt, M., Coester, C., & Kaempchen, N. (2012). Highly automated driving on freeways in real traffic using a probabilistic framework. *IEEE Transactions on Intelligent Transportation Systems*, 13(4), 1576–1585.
- Azevedo, C. L., & Farah, H. (2015). Using Extreme Value Theory for the Prediction of Head-On Collisions during Passing Maneuvres. In *2015 IEEE 18th International Conference on Intelligent Transportation Systems* (pp. 268–273).
- Bagdadi, O. (2013). Assessing safety critical braking events in naturalistic driving studies. *Transportation Research Part F: Psychology and Behaviour*, 16, 117–126.
- Bagdadi, O., & Várhelyi, A. (2011). Jerky driving - An indicator of accident proneness? *Accident Analysis and Prevention*, 43(4), 1359–1363.
- Bahram, M., Ghandeharioun, Z., Zahn, P., Baur, M., Huber, W., & Busch, F. (2014). Microscopic Traffic Simulation Based Evaluation of Highly Automated Driving on Highways. In *2014 IEEE 17th International Conference on Intelligent Transportation Systems* (pp. 1752–1757).
- Bahram, M., Lawitzky, A., Friedrichs, J., Aeberhard, M., & Wollherr, D. (2016). A Game-Theoretic Approach to Replanning-Aware Interactive Scene Prediction and Planning. *IEEE Transactions on Vehicular Technology*, 65(6), 3981–3992.
- Bahram, M., Wolf, A., Aeberhard, M., & Wollherr, D. (2014). A prediction-based reactive driving strategy for highly automated driving function on freeways. In *2014 IEEE Intelligent Vehicles Symposium* (pp. 400–406).
- Balal, E., Cheu, R. L., & Sarkodie-Gyan, T. (2016). A binary decision model for discretionary lane changing move based on fuzzy inference system. *Transportation Research Part C: Emerging Technologies*, 67, 47–61.

- Balal, E., Cheu, R. L., Sarkodie-Gyan, T., & Miramontes, J. (2014). Analysis of Discretionary Lane Changing Parameters on Freeways. *International Journal of Transportation Science and Technology*, 3, 277–296.
- Bando, M., Hasebe, K., Nakayama, A., Shibata, A., & Sugiyama, Y. (1995). Dynamical model of traffic congestion and numerical simulation. *Physical review. E, Statistical physics, plasmas, fluids, and related interdisciplinary topics*, 51(2), 1035–1042.
- Barcelo, J. (2010). Models, Traffic Models, Simulation, and Traffic Simulation. In Jaume Barceló (Ed.), *International series in operations research and management science: Fundamentals of Traffic Simulation* (pp. 63–95). Springer.
- Ben-Akiva, M., Koutsopoulos, H. N., Toledo, T., Yang, Q., Choudhury, C. F., Antoniou, C., & Balakrishna, R. (2010). Traffic Simulation with MITSIMLab. In *Fundamentals of traffic simulation* (pp. 233–268). Springer, New York, NY.
- Bevrani, K., & Chung, E. (2012). An Examination of the Microscopic Simulation Models to Identify Traffic Safety Indicators. *International Journal of Intelligent Transportation Systems Research*, 10(2), 66–81.
- Brockfeld, E., Kühne, R. D., & Wagner, P. (2004). Calibration and Validation of Microscopic Traffic Flow Models. *Transportation Research Record: Journal of the Transportation Research Board*, No 1876, 62–70.
- Calvert, S., Wilmink, I. R., Soekroella, A. M. G., & van Arem, B. (2016). Considering knowledge gaps for automated driving in conventional traffic. In *Proceedings of the fourth international conference on advances in civil, structural and environmental engineering*.
- Carvalho, A., Williams, A., Lefevre, S., & Borrelli, F. (2016). Autonomous cruise control with cut-in target vehicle detection. In *Advanced Vehicle Control: Proceedings of the 13th International Symposium on Advanced Vehicle Control* (pp. 93–99).
- Casas, J., Ferrer, J. L., Garcia, D., Perarnau, J., & Torday, A. (2010). Traffic Simulation with Aimsun. In *Fundamentals of traffic simulation* (pp. 173–232). Springer, New York, NY.
- Cassidy, M. J., & Bertini, R. L. (1999). Some traffic features at freeway bottlenecks. *Transportation Research Part B: Methodological*, 33B(1), 25–42.
- Cassidy, M. J., & Rudjanakanoknad, J. (2005). Increasing the capacity of an isolated merge by metering its on-ramp. *Transportation Research Part B: Methodological*, 39, 896–913.
- Chan, C. Y. (2017). Advancements, prospects, and impacts of automated driving systems. *International Journal of Transportation Science and Technology*, 6, 208–216.
- Chen, D., Ahn, S., Laval, J., & Zheng, Z. (2014). On the periodicity of traffic oscillations and capacity drop: The role of driver characteristics. *Transportation Research Part B: Methodological*, 59, 117–136.

- Cicchino, J. B. (2017). Effectiveness of forward collision warning and autonomous emergency braking systems in reducing front-to-rear crash rates. *Accident Analysis & Prevention*, 99, 142–152.
- Damerow, F., & Eggert, J. (2014). Predictive risk maps. In *2014 IEEE 17th International Conference on Intelligent Transportation Systems* (pp. 703–710).
- Davis, G. A., Hourdos, J., Xiong, H., & Chatterjee, I. (2011). Outline for a causal model of traffic conflicts and crashes. *Accident Analysis and Prevention*, 43(6), 1907–1919.
- Davis, L. C. (2007). Effect of adaptive cruise control systems on mixed traffic flow near an on-ramp. *Physica A: Statistical Mechanics and its Applications*, 379(1), 274–290.
- Dedes, G., Grejner-Brzezinska, D., Guenther, D., Heydinger, G., Mouskos, K., Park, B., & Toth, C. (2011). Integrated GNSS / INU , vehicle dynamics , and microscopic traffic flow simulator for automotive safety. In *2011 IEEE 14th International Conference on Intelligent Transportation Systems* (pp. 41–53).
- Dunias, P. (1996). *Autonomous robots using artificial potential fields* (Ph.D dissertation). Technical University Eindhoven.
- Duret, A., Ahn, S., & Buisson, C. (2011). Passing rates to measure relaxation and impact of lane-changing in congestion. *Computer-Aided Civil and Infrastructure Engineering*, 26(4), 285–297.
- Edie, L. C. (1961). Car-Following and Steady-State Theory for Noncongested Traffic. *Operations Research*, 9(1), 66–76.
- Evans, L. (1994). Driver injury and fatality risk in two-car crashes versus mass ratio inferred using Newtonian mechanics. *Accident Analysis and Prevention*, 26(5), 609–616.
- Evans, L. C., & Gariepy, R. F. (2015). *Measure theory and fine properties of functions*.
- Fagnant, D. J., & Kockelman, K. (2015). Preparing a nation for autonomous vehicles_ opportunities, barriers and policy recommendations _ Elsevier Enhanced Reader.pdf. *Transportation Research Part A: Policy and Practice*, 167–181.
- Fancher, P. S., & Bareket, Z. (1994). Evaluating Headway Control Using Range Versus Range-Rate Relationships. *Vehicle System Dynamics*, 23(1), 575–596.
- Fancher, P. S., Bareket, Z., & Ervin, R. (2001). Human-Centered Design of an Acc-With-Braking and Forward-Crash-Warning System. *Vehicle System Dynamics*, 36(2-3), 203–223.
- Fellendorf, M., & Vortisch, P. (2010). Microscopic traffic flow simulator VISSIM. In *Fundamentals of traffic simulation* (pp. 63–93). Springer.
- Fraichard, T., & Howard, T. M. (2012). Iterative Motion Planning and Safety Issue. In *Handbook of intelligent vehicles* (pp. 1435–1451).
- Freeman, J. B., & Dale, R. (2013). Assessing bimodality to detect the presence of a dual cognitive process. *Behavior Research Methods*, 45(1), 83–97.

- Gettman, D., & Head, L. (2003). Surrogate Safety Measures from Traffic Simulation Models. *Transportation Research Record: Journal of the Transportation Research Board*, 1840(03-2958), 104–115.
- Gipps, P. G. (1986). A model for the structure of lane-changing decisions. *Transportation Research Part B: Methodological*, 20B(5), 403–414.
- Guériau, M., Billot, R., El Faouzi, N.-E., Monteil, J., Armetta, F., & Hassas, S. (2016). How to assess the benefits of connected vehicles? A simulation framework for the design of cooperative traffic management strategies. *Transportation Research Part C: Emerging Technologies*, 67, 266–279.
- Happee, R., Gold, C., Radlmayr, J., Hergeth, S., & Bengler, K. (2017). Take-over performance in evasive manoeuvres. *Accident Analysis and Prevention*, 106, 211–222.
- Hara, H., Nagalur, S., Knoop, V. L., & van Arem, B. (2018). Rule based control for merges : assessment and case study. In *2018 IEEE 21st International Conference on Intelligent Transportation Systems* (pp. 3006–3013).
- Hatipoglu, C., Özgüner, Ü., & Redmill, K. A. (2003). Automated lane change controller design. *IEEE Transactions on Intelligent Transportation Systems*, 4(1), 13–22.
- Herman, R., Montroll, E. W., Potts, R. B., & Rothery, R. W. (1959). Traffic Dynamics: Analysis of Stability in Car Following. *Operations Research*, 7(1), 86–106.
- Hidas, P. (2005). Modelling vehicle interactions in microscopic simulation of merging and weaving. *Transportation Research Part C: Emerging Technologies*, 13, 37–62.
- Hofmann, P., Rinkenauer, G., & Gude, D. (2010). Preparing lane changes while driving in a fixed-base simulator: Effects of advance information about direction and amplitude on reaction time and steering kinematics. *Transportation Research Part F: Traffic Psychology and Behaviour*, 13(4), 255–268.
- Hoogendoorn, S. P., & Bovy, P. H. L. (2001). State-of-the-art of vehicular traffic flow modelling. In *Proceedings of the Institution of Mechanical Engineers Part 1: Journal Rail and Rapid Transit* (Vol. 215, pp. 283–303).
- Hyden, C. (1987). The development of a method for traffic safety evaluation: The Swedish traffic conflicts technique. *Bulletin Lund Institute of Technology, Department*(70).
- Ibanez-Guzman, J., Laugier, C., Yoder, J.-D., & Sebastian, T. (2010). Autonomous Driving: Context and State-of-the- Art. In A. Eskandarian (Ed.), *Handbook of intelligent vehicles* (2nd ed., pp. 1273–1305). Springer.
- Ioannou, P. A., & Stefanovic, M. (2005). Evaluation of ACC vehicles in mixed traffic: Lane change effects and sensitivity analysis. *IEEE Transactions on Intelligent Transportation Systems*, 6(1), 79–89.
- Jansson, J. (2005). *Collision Avoidance Theory with Application to Automotive Collision Mitigation* (Ph.D dissertation). Linköping University.

- Jeong, E., & Oh, C. (2017). Evaluating the effectiveness of active vehicle safety systems. *Accident Analysis and Prevention*, 100, 85–96.
- Johansson, R. (2009). Vision Zero - Implementing a policy for traffic safety. *Safety Science*, 47(6), 826–831.
- Jones, T. R., & Potts, R. B. (1962). The measurement of acceleration noise-a traffic parameter. *Operations Research*, 10(6), 745–763.
- Jula, H., Kosmatopoulos, E. B., & Ioannou, P. A. (2000). Collision avoidance analysis for lane changing and merging. *IEEE Transactions on Vehicular Technology*, 49(6), 2295–2308.
- Kaths, J., & Krause, S. (2016). Integrated simulation of microscopic traffic flow and vehicle dynamics. In *IPG apply & innovate*.
- Kesting, A., Treiber, M., & Helbing, D. (2007). General Lane-Changing Model MOBIL for Car-Following Models. *Transportation Research Record: Journal of the Transportation Research Board*, 1999, 86–94.
- Keyvan-Ekbatani, M., Knoop, V. L., & Daamen, W. (2016). Categorization of the lane change decision process on freeways. *Transportation Research Part C: Emerging Technologies*, 69, 515–526.
- Khattak, A. J., & Wali, B. (2017). Analysis of volatility in driving regimes extracted from basic safety messages transmitted between connected vehicles. *Transportation Research Part C: Emerging Technologies*, 84, 48–73.
- Kiefer, R. J., Flannagan, C. A., & Jerome, C. J. (2006). Time-to-collision judgments under realistic driving conditions. *Human factors: Journal of the Human Factors and Ergonomics Society*, 48(2), 334–345.
- Kiefer, R. J., Leblanc, D. J., & Flannagan, C. A. (2005). Developing an inverse time-to-collision crash alert timing approach based on drivers' last-second braking and steering judgments. *Accident Analysis and Prevention*, 37(2), 295–303.
- Klauer, S. G., Dingus, T. A., Neale, V. L., Sudweeks, J. D., & Ramsey, D. J. (2006). *The Impact of Driver Inattention On Near Crash/Crash Risk: An Analysis Using the 100-Car Naturalistic Driving Study Data* (Tech. Rep. No. DOT HS 810 594).
- Ko, J., Guensler, R., & Hunter, M. (2010). Analysis of effects of driver/vehicle characteristics on acceleration noise using GPS-equipped vehicles. *Transportation Research Part F: Traffic Psychology and Behaviour*, 13(1), 21–31.
- Ko, W., & Chang, D. E. (2018). Cooperative Adaptive Cruise Control Using Turn Signal for Smooth and Safe Cut-In. In *2018 18th International Conference on Control, Automation and Systems (ICCAS)* (pp. 807–812). Institute of Control, Robotics and Systems - ICROS.

- Kockelman, K., Avery, P., Bansal, P., Stephen, D., Bujanovic, P., Choudhary, T., ... Hutchinson, R. (2016). *Implications of Connected and Automated Vehicles on the Safety and Operations of Roadway Networks : A Final Report* (Vol. FHWA/TX-16; Tech. Rep.). FHWA.
- Krajzewicz, D. (2010). Traffic Simulation with SUMO: Simulation of Urban Mobility. In *Fundamentals of traffic simulation* (pp. 269–293). Springer, New York, NY.
- Kuang, Y., Qu, X., & Wang, S. (2015). A tree-structured crash surrogate measure for freeways. *Accident Analysis and Prevention*, 77, 137–148.
- Kumar, P., Merzouki, R., Conrard, B., Coelen, V., & Bouamama, B. O. (2014). Multilevel Modeling of the Traffic Dynamic. *IEEE Transactions on Intelligent Transport Systems*, 15(3), 1066–1082.
- Kyriakidis, M., de Winter, J. C., Stanton, N., Bellet, T., van Arem, B., Brookhuis, K., ... Happee, R. (2019). A human factors perspective on automated driving. *Theoretical Issues in Ergonomics Science*, 20(3), 223–249.
- Kyriakidis, M., van de Weijer, C., van Arem, B., & Happee, R. (2015). The deployment of Advanced Driver Assistance Systems in Europe. In *22nd ITS World Congress Proceedings*.
- Larsson, A. F. L., Kircher, K., & Hultgren, J. A. (2014). Learning from experience: Familiarity with ACC and responding to a cut-in situation in automated driving. *Transportation Research Part F: Psychology and Behaviour*, 27, 229–237.
- Laureshyn, A., De Ceunynck, T., Karlsson, C., Svensson, Å., Daniels, S., Svensson, A., & Daniels, S. (2017). In search of the severity dimension of traffic events: Extended Delta-V as a traffic conflict indicator. *Accident Analysis and Prevention*, 98, 46–56.
- Laureshyn, A., Olszewski, P., Ceunynck, T. D., Svensson, Å., de Goede, M., Saunier, N., ... Daniels, S. (2016). Review of current study methods for VRU safety. Appendix 6 Scoping review: surrogate measures of safety in site-based road traffic observations: Deliverable 2.1part 4. (635895).
- Laureshyn, A., Svensson, Å., & Hydén, C. (2010). Evaluation of traffic safety, based on micro-level behavioural data: Theoretical framework and first implementation. *Accident Analysis and Prevention*, 42(6), 1637–1646.
- Laval, J., & Leclercq, L. (2008). Microscopic modeling of the relaxation phenomenon using a macroscopic lane-changing model. *Transportation Research Part B: Methodological*, 42(6), 511–522.
- Leclercq, L., Chiabaut, N., Laval, J., & Buisson, C. (2007). Relaxation Phenomenon After Lane Changing: Experimental Validation with NGSIM Data Set. *Transportation Research Record: Journal of the Transportation Research Board*, 1999(January 2007), 79–85.

- Leonard, J., How, J., Teller, S., Berger, M., Campbell, S., Fiore, G., . . . Krishnamurthy, S. (2008). A Perception-Driven Autonomous Urban Vehicle. *Journal of Field Robotics*, 25, 727–774.
- Letter, C., & Elefteriadou, L. (2017). Efficient control of fully automated connected vehicles at freeway merge segments. *Transportation Research Part C: Emerging Technologies*, 80, 190–205.
- Li, L., Lai, G., & Wang, F.-Y. (2005). Safe Steering Speed Estimation and Optimal Trajectory Planning for Intelligent Vehicles. In *Proceedings -2005 IEEE Networking, Sensing and Control* (pp. 722–727).
- Li, L., Lv, C., Cao, D., & Zhang, J. (2018). Retrieving Common Discretionary Lane Changing Characteristics From Trajectories. *IEEE Transactions on Vehicular Technology*, 67(3), 2014–2024.
- Liu, H., Wei, H., Zuo, T., Li, Z., & Yang, Y. J. (2017, mar). Fine-tuning ADAS algorithm parameters for optimizing traffic safety and mobility in connected vehicle environment. *Transportation Research Part C: Emerging Technologies*, 76, 132–149.
- Luo, Y., Xiang, Y., Cao, K., & Li, K. (2016). A dynamic automated lane change maneuver based on vehicle-to-vehicle communication. *Transportation Research Part C: Emerging Technologies*, 62, 87–102.
- Mahmud, S. M. S., Ferreira, L., Hoque, S., Tavassoli, A., Hoque, M. S., & Tavassoli, A. (2017). Application of proximal surrogate indicators for safety evaluation: A review of recent developments and research needs. *IATSS Research*, 41(4), 153–163.
- Menendez-Romero, C., Sezer, M., Winkler, F., Dornhege, C., & Burgard, W. (2018). Courtesy Behavior for Highly Automated Vehicles on Highway Interchanges. In *2018 IEEE Intelligent Vehicles Symposium* (pp. 943–948).
- Michon, J. A. (1985). A critical view of driver behavior models: what do we know, what should we do? *Human behavior and traffic safety*, 485–520.
- Minderhoud, M. M., & Bovy, P. H. L. (2001). Extended time-to-collision measures for road traffic safety assessment. *Accident Analysis and Prevention*, 33(1), 89–97.
- Mohamed, M. G., & Saunier, N. (2013). Motion Prediction Methods for Surrogate Safety Analysis. *Transportation Research Record :Journal of the Transportation Research Board*(2386), 168–178.
- Mondek, M., & Hromcik, M. (2017). Linear analysis of lateral vehicle dynamics. In *21st international conference on process control (pc)* (pp. 240–246).
- Moon, S., Moon, I., & Yi, K. (2009). Design, tuning, and evaluation of a full-range adaptive cruise control system with collision avoidance. *Control Engineering Practice*, 17(4), 442–455.
- Morando, M. M., Tian, Q., Truong, L. T., & Vu, H. L. (2018). Studying the Safety Impact of Autonomous Vehicles Using Simulation-Based Surrogate Safety Measures. *Journal of Advanced Transportation*, 1–11.

- Moridpour, S., Rose, G., & Sarvi, M. (2009). Modelling the heavy vehicle drivers' lane changing decision under heavy traffic conditions. *Road & Transport Research*, 18(4), 49–57.
- Moridpour, S., Sarvi, M., & Rose, G. (2010a). Lane changing models: a critical review. *Transportation Letters*, 2(3), 157–173.
- Moridpour, S., Sarvi, M., & Rose, G. (2010b). Modeling the Lane-Changing Execution of Multiclass Vehicles Under Heavy Traffic Conditions. *Transportation Research Record: Journal of the Transportation Research Board*, 2161, 11–19.
- Mullakkal-Babu, F. A., Wang, M., Farah, H., van Arem, B., & Happee, R. (2017). Comparative assessment of safety indicators for vehicle trajectories on highway. *Transportation Research Record :Journal of the Transportation Research Board*, 2659, 127–136.
- Mullakkal-Babu, F. A., Wang, M., van Arem, B., & Happee, R. (2016). Design and Analysis of Full Range Adaptive Cruise Control with Integrated Collision Avoidance Strategy. In *2016 IEEE 19th International Conference on Intelligent Transportation Systems* (pp. 308–315).
- Najm, W. G., D.Smith, J., & Yanagisawa, M. (2007). *Pre-Crash Scenario Typology for Crash Avoidance Research* (Tech. Rep.).
- Naranjo, J. E., Gonzalez, C., Garrcia, R., & de Pedro, T. (2008). Lane-change fuzzy control in autonomous vehicles for the overtaking maneuver. *IEEE Transactions on Intelligent Transportation Systems*, 9(3), 438–450.
- Neale, V. L., Dingus, T. A., Klauer, S. G., & Goodman, M. (2005). An overview of the 100-car naturalistic study and findings. *National Highway Traffic Safety Administration, Paper*, 5, 0400.
- Ni, D. (2003). 2DSIM: A Prototype of Nanoscopic Traffic Simulation. In *2003 IEEE Intelligent Vehicles Symposium* (pp. 47–52).
- Ni, D. (2013). A Unified Perspective on Traffic Flow Theory, Part I: The Field Theory. *Applied Mathematical Studies*, 7(39), 1929–1946.
- Niezgoda, M., Kaminski, T., & Kruszewski, M. (2012). Measuring Driver Behaviour - Indicators for Traffic Safety. *Journal of KONES Powertrain and Transport*, 19(4), 503–511.
- Nilsson, J., Falcone, P., Ali, M., & Sjoberg, J. (2015). Receding horizon maneuver generation for automated highway driving. *Control Engineering Practice*, 41, 124–133.
- Noon, R. K. (1994). *Engineering Analysis of Vehicular Accidents*. CRC Press.
- Osafune, T., Takahashi, T., Kiyama, N., & Sobue, T. (2016). Analysis of Accident Risks from Driving Behaviors. *International Journal of Intelligent Transportation Systems Research*, 15(3), 192–202.

- Othman, S., & Thomson, R. (2007). Influence Of Road Characteristics On Traffic Safety. In *21st International Technical Conference on the Enhanced Safety of Vehicles Conference (ESV)* (pp. 1–10).
- Papadoulis, A., Quddus, M., & Imprialou, M. (2019). Evaluating the safety impact of connected and autonomous vehicles on motorways. *Accident Analysis and Prevention*, 124, 12–22.
- Park, H., Bhamidipati, C. S., & Smith, B. L. (2011). Development and Evaluation of Enhanced IntelliDrive-Enabled Lane Changing Advisory Algorithm to Address Freeway Merge Conflict. *Transportation Research Record :Journal of the Transportation Research Board*, 2243(1), 146–157.
- Perez, M., Angel, L., Hankey, J., Deering, R., Llaneras, R., Green, C., . . . Antin, J. (2011). *Advanced Crash Avoidance Technologies (ACAT) Program Final Report of the GM-VTTI Backing Crash Countermeasures Project* (Tech. Rep.). U.S. Department of Transportation National Highway Traffic Safety Administration.
- Pipes, L. A. (1953). An Operational Analysis of Traffic Dynamics. *Journal of applied physics*, 24(2), 274–281.
- Qu, X., Jin, S., & Weng, J. (2015). Analysis of the relationship between aggregated traffic volume and traffic conflicts on expressways. *Transportmetrica A: Transport Science*, 11(7), 648–658.
- Rahman, M., Chowdhury, M., Xie, Y., & He, Y. (2013). Review of microscopic lane-changing models and future research opportunities. *IEEE Transactions on Intelligent Transportation Systems*, 14(4), 1942–1956.
- Rahman, M. S., Abdel-Aty, M., Lee, J., & Rahman, M. H. (2019). Safety benefits of arterials' crash risk under connected and automated vehicles. *Transportation Research Part C: Emerging Technologies*(100), 354–371.
- Rahman, M. S., Abdel-Aty, M., Wang, L., & Lee, J. (2018). Understanding the Highway Safety Benefits of Different Approaches of Connected Vehicles in Reduced Visibility Conditions. *Transportation Research Record :Journal of the Transportation Research Board*, 2672(19), 91–101.
- Rajamani, R. (2012). Lateral Vehicle Dynamics. In F. F. Ling (Ed.), *Vehicle dynamics and control* (2nd ed., pp. 12–46). Springer.
- Rakha, H. A., Ahn, K., Faris, W., & Moran, K. S. (2012). Simple Vehicle Powertrain Model for Modeling Intelligent Vehicle Applications. *IEEE Transactions on Intelligent Transportation Systems*, 13(2), 770–780.
- Rehder, T., Koenig, A., Goehl, M., Louis, L., & Schramm, D. (2019). Lane Change Intention Awareness for Assisted and Automated Driving on Highways. *IEEE Transactions on Intelligent Vehicles*, 4(2), 265–276.

- Resende, P., & Nashashibi, F. (2010). Real-time dynamic trajectory planning for highly automated driving in highways. In *2010 IEEE 13th International Conference on Intelligent Transportation Systems* (pp. 653–658).
- Rudin-Brown, C. M., & Parker, H. A. (2004, mar). Behavioural adaptation to adaptive cruise control (ACC): implications for preventive strategies. *Transportation Research Part F: Traffic Psychology and Behaviour*, 7(2), 59–76.
- SAE. (2018). *SAE On-Road Automated Vehicle Standards Committee. "Taxonomy and definitions for terms related to on-road motor vehicles J 3016* (Tech. Rep.).
- Salvucci, D. D., & Gray, R. (2004). A two-point visual control model of steering. *Perception*, 33(10), 1233–1248.
- Salvucci, D. D., & Liu, A. (2002). The time course of a lane change: Driver control and eye-movement behavior. *Transportation Research Part F: Traffic Psychology and Behaviour*, 5(2), 123–132.
- Samiee, S., Azadi, S., Kazemi, R., & Eichberger, A. (2016). Towards a Decision-Making Algorithm for Automatic Lane Change Manoeuvre Considering Traffic Dynamics. *PROMET Traffic&Transportation*, 28(2), 91–103.
- Saunier, N., & Sayed, T. (2009). Probabilistic Framework for Automated Analysis of Exposure to Road Collisions. *Transportation Research Record: Journal of the Transportation Research Board*, 2083, 96–104.
- Saunier, N., Sayed, T., & Ismail, K. (2010). Large-Scale Automated Analysis of Vehicle Interactions and Collisions. *Transportation Research Record: Journal of the Transportation Research Board*, 2147(2147), 42–50.
- Savitzky, A., & Golay, M. J. (1964). Smoothing and Differentiation of Data by Simplified Least Square Procedures. *Analytical Chemistry*, 36(8), 1627–1639.
- Schakel, W. J., Knoop, V. L., & van Arem, B. (2012). Integrated Lane Change Model with Relaxation and Synchronization. *Transportation Research Record: Journal of the Transportation Research Board*, 2316, 47–57.
- Schakel, W. J., van Arem, B., van Lint, H., & Tamminga, G. (2013, oct). A modular approach for exchangeable driving task models in a microscopic simulation framework. In *2013 IEEE 16th International Conference on Intelligent Transportation Systems* (pp. 565–571).
- Schlechtriemen, J., Wedel, A., Hillenbrand, J., Breuel, G., & Kuhnert, K.-d. (2014). A Lane Change Detection Approach using Feature Ranking with Maximized Predictive Power. In *2014 IEEE Intelligent Vehicles Symposium proceedings* (pp. 108–114).
- Schneider, W., Savolainen, P., & Zimmerman, K. (2009). Driver Injury Severity Resulting from Single-Vehicle Crashes Along Horizontal Curves on Rural Two-Lane Highways. *Transportation Research Record: Journal of the Transportation Research Board*, 2102, 85–92.

- Shelby, S. G. (2011). Delta-V As a Measure of Traffic Conflict Severity. In *3rd International Conference on Road Safety and Simulation*.
- Shladover, S. E. (2007). PATH at 20 History and Major Milestones. *IEEE Transactions on Intelligent Transport Systems*, 8(4), 584–592.
- Shladover, S. E. (2018). Connected and automated vehicle systems: Introduction and overview. *Journal of Intelligent Transportation Systems*, 22(3), 190–200.
- Sivak, M., & Schoettle, B. (2015). *Road safety with self-driving vehicles: General limitations and road sharing with conventional vehicles* (Tech. Rep.). The University of Michigan Transportation Research Institute.
- Smith, D. E., & Starkey, J. M. (1995). Effects of Model Complexity on the Performance of Automated Vehicle Steering Controllers: Model Development, Validation and Comparison. *Vehicle System Dynamics: International Journal of Vehicle Mechanics and Mobility*, 24(2), 163–181.
- So, J., Motamedidehkordi, N., Wu, Y., Busch, F., & Choi, K. (2018). Estimating emissions based on the integration of microscopic traffic simulation and vehicle dynamics model. *International Journal of Sustainable Transportation*, 12(4), 286–298.
- So, J., Park, B., Wolfe, S. M., & Dedes, G. (2015). Development and Validation of a Vehicle Dynamics Integrated Traffic Simulation Environment Assessing Surrogate Safety. *Journal of Computing in Civil Engineering*, 29(5), 04014080.
- Songchitruksa, P., & Tarko, A. P. (2006). The extreme value theory approach to safety estimation. *Accident Analysis and Prevention*, 38(4), 811–822.
- Soudbakhsh, D., Eskandarian, A., & Chichka, D. (2013). Vehicle Collision Avoidance Maneuvers With Limited Lateral Acceleration Using Optimal Trajectory Control. *Journal of Dynamic Systems, Measurement, and Control*, 135, 1–12.
- Spalanzani, A., Rios-Martinez, J., Laugier, C., & Lee, S. (2012). Risk Based Navigation Decisions. In *Handbook of intelligent vehicles* (pp. 1460–1475).
- Staubach, M. (2009). Factors correlated with traffic accidents as a basis for evaluating Advanced Driver Assistance Systems. *Accident Analysis and Prevention*, 41(5), 1025–1033.
- St-Aubin, P., Miranda-Moreno, L., & Saunier, N. (2011). Analysis of Driver Behaviour and Collision Risks for Protected Freeway Entrance and Exit Ramps: Trajectories and Surrogate Safety Measures. In *Proc. CMRSC-XXI* (Vol. 1, p. 15).
- Svensson, Å. (1998). *A method for analysing the traffic process in a safety perspective* (Ph.D dissertation). Lund University.
- Sykes, P. (2010). Traffic Simulation with Paramics. In *Fundamentals of traffic simulation* (pp. 131–171). Springer, New York, NY.

- Thiemann, C., Treiber, M., & Kesting, A. (2008). Estimating acceleration and lane-changing dynamics from next generation simulation trajectory data. *Transportation Research Record :Journal of the Transportation Research Board*, 2088, 90–101.
- Toledo, T., Koutsopoulos, H. N., & Ben-Akiva, M. (2007). Integrated driving behavior modeling. *Transportation Research Part C: Emerging Technologies*, 15(2), 96–112.
- Toledo, T., & Zohar, D. (2007). Modeling Duration of Lane Changes. *Transportation Research Record :Journal of the Transportation Research Board*, 1999, 71–78.
- Treiber, M., Hennecke, A., & Helbing, D. (2000). Congested Traffic States in Empirical Observations and Microscopic Simulations. *Physical Review E*, 62(2), 1805–1824.
- Treiber, M., & Kesting, A. (2013). *Traffic Flow Dynamics*.
- Treiber, M., Kesting, A., & Helbing, D. (2006). Delays, inaccuracies and anticipation in microscopic traffic models. *Physica A: Statistical Mechanics and its Applications*, 360(1), 71–88.
- Urmson, C., Anhalt, J., Bagnell, D., Baker, C., Bittner, R., Clark, M. N., ... Taylor, M. (2008). Autonomous Driving in Urban Environments : Boss and the Urban Challenge. *Journal of Field Robotics*, 25, 425–466.
- van Arem, B., de Vos, A. P., & Vanderschuren, M. J. W. A. (1997). *The microscopic traffic simulation model MIXIC 1.3* (Tech. Rep.). TNO.
- van Beinum, A., Farah, H., Wegman, F., & Hoogendoorn, S. P. (2016). A critical assessment of methodologies for operations and safety evaluations of freeway turbulence. *Transportation Research Record: Journal of the Transportation Research Board*, 31(2556), 39–48.
- Vanholme, B., Gruyer, D., Lusetti, B., Glaser, S., & Mammar, S. (2013). Highly automated driving on highways based on legal safety. *IEEE Transactions on Intelligent Transportation Systems*, 14(1), 333–347.
- van Lint, J. W., & Calvert, S. C. (2018). A generic multi-level framework for microscopic traffic simulation: Theory and an example case in modelling driver distraction. *Transportation Research Part B: Methodological*, 117, 63–86.
- van Winsum, W., de Waard, D., & Brookhuis, K. (1999). Lane change manoeuvres and safety margins. *Transportation Research Part F: Traffic Psychology and Behaviour*, 2(3), 139–149.
- Wagner, P., Nippold, R., Gabloner, S., & Margreiter, M. (2015). *Analyzing human driving data an approach motivated by data science methods* (Vol. 90).
- Wang, J., Wu, J., & Li, Y. (2015). The Driving Safety Field Based on Driver - Vehicle - Road Interactions. *IEEE Transactions on Intelligent Transportation Systems*, 16(4), 2203–2214.

- Wang, J., Wu, J., Zheng, X., Ni, D., & Li, K. (2016). Driving safety field theory modeling and its application in pre-collision warning system. *Transportation Research Part C: Emerging Technologies*, 72, 306–324.
- Wang, M. (2018). Infrastructure assisted adaptive driving to stabilise heterogeneous vehicle strings. *Transportation Research Part C: Emerging Technologies*, 91, 276–295.
- Wang, M., Hoogendoorn, S. P., Daamen, W., van Arem, B., & Happee, R. (2015). Game theoretic approach for predictive lane-changing and car-following control. *Transportation Research Part C: Emerging Technologies*, 58, 73–92.
- Wang, Q. I., Li, Z., & Li, L. I. (2014). Investigation of Discretionary Lane-Change Characteristics Using Next-Generation Simulation Data Sets. *Journal of Intelligent Transportation Systems*, 18(3), 246–253.
- Wang, S., & Li, Z. (2019). Exploring the mechanism of crashes with automated vehicles using statistical modeling approaches. *PLoS ONE*, 14(3), 1–16.
- Wang, W., Jiang, X., Xia, S., & Cao, Q. (2010). Incident tree model and incident tree analysis method for quantified risk assessment: An in-depth accident study in traffic operation. *Safety Science*, 48(10), 1248–1262.
- Wei, J., Dolan, J. M., & Litkouhi, B. (2013). Autonomous Vehicle Social Behavior for Highway Entrance Ramp Management. In *2013 IEEE Intelligent Vehicles Symposium* (pp. 201–207).
- Wilmink, I. R., Klunder, G., & van Arem, B. (2007). Traffic flow effects of Integrated full-Range Speed Assistance (IRSA). In *2007 IEEE Intelligent Vehicles Symposium* (pp. 1204–1210).
- World Health Organization. (2015). *Global status report on road safety* (Tech. Rep.). World Health Organisation.
- World Health Organization. (2018). *Global status report on road safety* (Tech. Rep.). World Health Organisation.
- Xia, T., Yang, M., Yang, R., & Wang, C. (2010). CyberC3 : A Prototype Cybernetic Transportation System for Urban Applications. *IEEE Transactions on Intelligent Transportation Systems*, 11(1), 142–152.
- Xiao, L., & Gao, F. (2010). A Comprehensive Review of the Development of Adaptive Cruise Control Systems. *Vehicle System Dynamics*, 48(10), 1167–1192.
- Yang, D., Zhu, L., Ran, B., Pu, Y., & Hui, P. (2016). Modeling and Analysis of the Lane-Changing Execution in Longitudinal Direction. *IEEE Transactions on Intelligent Transportation Systems*, 17(10), 2984–2992.
- Yang, D., Zhu, L., Yang, F., & Pu, Y. (2015). Modeling and Analysis of Lateral Driver Behavior in Lane-Changing Execution. *Transportation Research Record: Journal of Transportation Research Board*, 2490, 127–137.

- Yao, W., Zhao, H., Davoine, F., & Zha, H. (2012). Learning lane change trajectories from on-road driving data. In *2012 IEEE Intelligent Vehicles Symposium* (pp. 885–890).
- Young, W., Sobhani, A., Lenné, M. G., & Sarvi, M. (2014). Simulation of safety: A review of the state of the art in road safety simulation modelling. *Accident Analysis and Prevention*, 66, 89–103.
- Yue, L., Abdel-Aty, M., Wu, Y., & Wang, L. (2018). Assessment of the safety benefits of vehicles' advanced driver assistance, connectivity and low level automation systems. *Accident Analysis and Prevention*, 117, 55–64.
- Zhao, D., Lam, H., Peng, H., Bao, S., Leblanc, D. J., Nobukawa, K., & Pan, C. S. (2017). Accelerated Evaluation of Automated Vehicles Safety in Lane-Change Scenarios Based on Importance Sampling Techniques. *IEEE Transactions on Intelligent Transportation Systems*, 18(3), 595–607.
- Zheng, L., Ismail, K., & Meng, X. (2014a). Freeway safety estimation using extreme value theory approaches: A comparative study. *Accident Analysis & Prevention*, 62, 32–41.
- Zheng, L., Ismail, K., & Meng, X. (2014b). Traffic conflict techniques for road safety analysis: open questions and some insights. *Canadian Journal of Civil Engineering*, 41(7), 633–641.
- Zheng, Z. (2014). Recent developments and research needs in modeling lane changing. *Transportation Research Part B: Methodological*, 60, 16–32.
- Zheng, Z., Ahn, S., Chen, D., & Laval, J. (2013). The effects of lane-changing on the immediate follower: Anticipation, relaxation, and change in driver characteristics. *Transportation Research Part C: Emerging Technologies*, 26, 367–379.
- Zheng, Z., Ahn, S., & Monsere, C. M. (2010). Impact of traffic oscillations on freeway crash occurrences. *Accident Analysis and Prevention*, 42(2), 626–636.
- Zhou, B., Wang, Y., Yu, G., & Wu, X. (2017). A lane-change trajectory model from drivers' vision view. *Transportation Research Part C: Emerging Technologies*, 85, 609–627.
- Zou, Y., Tarko, A. P., Chen, E., & Romero, M. A. (2014). Effectiveness of cable barriers, guardrails, and concrete barrier walls in reducing the risk of injury. *Accident Analysis and Prevention*, 72, 55–65.

Samenvatting

Modellering van de veiligheidseffecten van geautomatiseerde rijssystemen in verkeer met meerdere rijstroken

In de afgelopen drie decennia zijn er verschillende automobieltoepassingen ontwikkeld die de rijtaak verduurzaam en overnemen. De meest geavanceerde klasse van dergelijke toepassingen staat bekend als Automated Driving Systems (ADS). ADS kunnen het voertuig zelfstandig besturen op wegen die onder zijn operationele bereik vallen, zonder menselijke tussenkomst. Industrie en overheden geven aan dat dergelijke systemen binnenkort technologisch haalbaar zijn en dat het verkeer zal bestaan uit zowel geautomatiseerde als door mensen bestuurde voertuigen. Hoewel voertuigen uitgerust met ADS een impact hebben op de verkeersveiligheid, is er geen duidelijkheid of zij de verkeersveiligheid zullen verbeteren of benadelen. Een mens en een ADS gebruiken fundamenteel verschillende processen om informatie te verzamelen, beslissingen te nemen en het voertuig te besturen. Daarom zijn onze huidige inzichten in de relatie tussen rijgedrag en veiligheid niet voldoende om de mogelijke gevolgen van ADS-systemen te voorspellen. Hierdoor is er een dringende behoefte om de effecten van ADS-functionaliteiten en ontwerpfactoren op verkeersveiligheid te bestuderen.

Van de verschillende alternatieven is de op simulatie gebaseerde aanpak een proactief en kosteneffectief middel om de verkeersveiligheidseffecten van met ADS uitgeruste voertuigen te bestuderen. In deze benadering wordt de verkeersstroom bestaande uit door mensen bestuurde voertuigen (HV's) en met ADS uitgeruste voertuigen gesimuleerd met een hoge resolutie. De gegenereerde voertuigtrajecten worden nabewerkt om statistieken over de veiligheid van voertuiginteracties te kwantificeren. Conclusies over verkeersveiligheid worden getrokken door deze statistieken te analyseren. Deze op simulatie gebaseerde veiligheids-evaluatie kan autofabrikanten in een vroeg stadium van de ontwikkeling van ADS ontwerpfeedback geven en inzichten bieden om een weloverwogen beleid met betrekking tot ADS-technologie te formuleren. De veiligheidsmaatstaven en simulatiehulpmiddelen die momenteel worden gebruikt in veiligheidsstudies zijn meestal gericht op door mensen bestuurde voertuigen. In de context van gemengd en meerstrooksverkeer zien simulatiegebaseerde benaderingen meerdere uitdagingen, waaronder het nauwkeurig modelleren van voertuigdynamiek en -functionaliteit van ADS en het volledig kwantificeren van het ongeval-lenrisico.

Dit proefschrift adresseert deze uitdagingen door een nieuwe veiligheidsmaatstaf te ontwikkelen op basis van veldtheorie en door een simulatiemethode te ontwikkelen die

een realistischere weergave van het rijproces biedt, en compatibel is met bekende ADS-architecturen. Met behulp van de ontwikkelde maatstaaf en simulatiemethode evalueert dit proefschrift verschillende case studies die de potentie van de op simulatie gebaseerde aanpak aantonen om onderscheid te maken tussen ADS-functionaliteiten in termen van verkeersveiligheid en om hun impact op verkeersveiligheid te identificeren.

Een nieuwe aanpak voor veiligheidsbeoordeling

Betreffende de veiligheidsmaatstaf, evalueert hoofdstuk 2 van dit proefschrift de bestaande veiligheidsmaatstaven om hun sterktepunten en beperkingen te identificeren bij het bestuderen van gemengd verkeer. De beoordeling concludeert dat maatstaven op basis van veldtheorie verschillende voordelen hebben in vergelijking met bestaande alternatieven. Een dergelijke maatstaaf kan de risicodynamica tijdens tweedimensionale voertuigontmoetingen beschrijven en kan numeriek worden gecombineerd om het risico van meerdere weg en verkeersaspecten te omvatten. Dit hoofdstuk benadrukt ook dat de resultaten op basis van verschillende veiligheidsmaatstaven onvergelykbaar en onvolledig zijn, omdat ze zijn afgeleid van een unieke en onvolledige definitie van risico.

Hoofdstuk 3 geeft een definitie van rijrisico die wordt toegeschreven aan het voertuig en een numerieke schatting op basis van veldtheorie. Elk obstakel (naburige entiteit op de weg) voor het betreffende voertuig wordt behandeld als een eindig scalair risicoveld: PDRF dat is geformuleerd in de voorspelde configuratieruimte van het betreffende voertuig. Dit risicoveld is geformuleerd als het product van twee factoren: verwachte botsingsenergie (als een benadering van de gevolgen) en de botsingskans. De botsingskans wordt numeriek geschat op basis van de karakteristieke versnellingsverdeling van de wegentiteiten en in hoeverre deze conflicteren met het betreffende voertuig. De crashkans wordt geschat op de discrete toekomstige tijdstappen en het aantal stappen wordt op de toepassing afgestemd. Om de veiligheid van interacties te analyseren, wordt voor de risico-inschatting een ongevalskans geschat in een enkele stap. De analyse werd uitgevoerd op voertuigtrajecten tijdens drie bijna-ongeval situaties die werden vastgelegd met camera's aan boord. De PRR-gebaseerde risicobeschrijving kwamen kwalitatief overeen met de beschrijvingen van de gebeurtenis. Vervolgens pasten we de risico-inschatting toe met een geschatte ongevalskans in een reeks tijdstappen op een realtime voertuignavigatieprobleem. De PRR-benadering werd gebruikt om het risico van vier kandidaat-manoeuvrepunten in een complexe verkeerssituatie te schatten. Onze aanpak kon objectief het veiligste plan identificeren. Vergeleken met Surrogate Measures of Safety afgeleid van een gedeeltelijke uitdrukking van risico, is het voordeel van de PRR-methode zoals gedemonstreerd in de casestudy's dat deze de ernst- en waarschijnlijkheidsaspecten van risico combineert en daardoor de kans verkleint om het rijrisico te onderschatten.

Nieuwe inzichten in het handmatig veranderen van rijstrook

Dit proefschrift biedt empirische inzichten in de handmatige rijstrookverandering en de impact ervan op aangrenzende voertuigen. Bestaande microscopische verkeersmodellen simuleren het veranderen van rijstrook als een continue en ononderbroken zijwaartse beweging van het voertuig van de oorspronkelijke naar de doel rijstrook. We noemen deze weergave Continuous Lane -Changing (CLC). Hoofdstuk 4 van dit proefschrift richt zich

op de minder onderzochte Fragmented Lane-Changing (FLC), waarbij de rijstrookwisselaar zijn zijwaartse beweging tijdens de manoeuvre pauzeert. We karakteriseren het traject en identificeren de effecten van FLC. We zien dat tijdens het uitvoeren van een FLC de rijbaanwisselaar verschillende kinematica vertoont en het langer duurt om de rijbaanwisseling te voltooien. Bovendien identificeren we een aantal factoren die mogelijk verband houden met het besluitvormingsproces achter FLC: een gemiddelde bestuurder voert een FLC uit wanneer de voorgaande en volgende voertuigen in de doelstrook langzamer zijn en wanneer het volgende voertuig in de doelstrook dichterbij is dan waargenomen tijdens het begin van een CLC, en bij hogere noodzaak om van rijstrook te veranderen, zoals tijdens een verplichte rijstrookverandering. Bovendien zien we dat FLC een duidelijk microscopisch effect op de volger in de doelstrook induceert. In het licht van de empirische bevindingen bieden we modellen voor de uitvoering en impact van rijstrookverandering, door bestaande modellen te herzien en opnieuw te kalibreren. De modelleringsresultaten suggereren dat de nauwkeurigheid van verkeersstroommodellen kan worden verbeterd door uitvoering van rijstrookverandering en impactmodellen die specifiek zijn voor FLC en CLC.

Een uitgebreid verkeerssimulatiekader

Hoofdstuk 5 van dit proefschrift presenteert een verkeerssimulatiekader dat voertuigtrajectoriën kan genereren die geschikt zijn voor veiligheidsevaluatie op een hoger detailniveau dan huidige simulatoren voor verkeersveiligheidsevaluatie. Het raamwerk is hybride van structuur en bestaat uit een expliciet voertuigmodel en geeft de hiërarchische beslissings- en besturingsstructuur van de voertuigbediening weer. De resulterende trajectoriën vertegenwoordigen rotatie dynamica en extra variabelen zoals voertuig richting en voorwiel uitslag. Het kader hanteert een modulaire architectuur om onafhankelijke modellen te kunnen implementeren en testen die specifiek zijn voor verschillende subtaken. Het resulterende raamwerk bestaat uit twee gekoppelde lagen, een hoger tactisch niveau dat manoeuvreplannen genereert; en een lagere operationele laag met expliciete besturingsmodule (stuur- en versnellingsregeling) die in een gesloten lus werkt met de voertuigdynamiek van het zogenaamde fietsmodel. De simulatieresultaten tonen de kracht van het voorgestelde raamwerk om laterale manoeuvres te beschrijven, zoals bochnavigatie, corrigerende besturing, afbreken van rijstrookverandering en gefragmenteerde rijstrookverandering. Uit macroscopische verkeersfenomenen die door de simulator worden gereproduceerd, blijkt ook dat de eigenschappen van de voorgestelde rij subtaakmodellen in het kader zijn behouden.

Toepassing van op simulatie gebaseerde veiligheidsevaluatie

In hoofdstuk 6 passen we de voorgestelde veiligheidsbeoordelingsmethode en simulatie-tool toe op een case study met gemengd verkeer. Hier vergelijken we twee generieke longitudinale functionaliteiten van ADS om een cut-in af te handelen: reactief en voorspellend. Deze studie onthult dat deze functionaliteiten zich tijdens snijdingsmanoeuvres van aangrenzende door mensen bestuurde voertuigen onderscheiden in termen van veiligheid en kinematische kenmerken van de manoeuvre. We zien dat de aanwezigheid van voertuigen uitgerust met ADS in het verkeer de ruimtelijke verdeling van rijstrookwisselingen in de buurt van samenvoegende rijstroken zou kunnen veranderen; en dat het reactieve ADS het aantal mislukte rijstrookwisselingen zou kunnen verhogen. Resultaten suggereren dat

zelfs een eenvoudig voorspellingsschema aanzienlijk beter zou kunnen presteren dan reactieve benaderingen in aspecten zoals temporale nabijheid tot ongevallen en verwachte ernst van ongevallen, evenals in termen van rijrisico (combinatie van de twee aspecten). De negatieve veiligheidseffecten van met reactief ADS uitgeruste voertuigen worden duidelijk wanneer deze $> 10\%$ van het verkeer omvat. In tegendeel, de voorspellende ADS maakt een relatief veiligere inschakeling mogelijk, met een marginale impact op de veiligheid bij grotere proporties. Bovendien zien we dat risicodynamiek een cruciale factor is die de ADS-functionaliteiten onderscheidt. Wanneer een voertuig voor Reactive ADS inschakelt, piekt het risico ongeveer halverwege de manoeuvre. Daarbij benadrukt dit werk het potentieel van een op simulatie gebaseerde veiligheidsevaluatie om relevante dimensies van de veiligheidsimpact van automatiseringsfunctionaliteiten in een vroeg stadium van productontwikkeling te voorspellen.

Implicaties en aanbevelingen

Dit proefschrift stelt een nieuwe veiligheidsmaatstaf voor en een uitgebreid simulatiekader voor het beoordelen van de veiligheid van verkeer bestaande uit door mensen bestuurde en systeemgestuurde voertuigen. De effecten van met ADS uitgeruste voertuigen kunnen niet worden gegeneraliseerd en zijn afhankelijk van de inherente functionaliteiten en operationele strategieën. Onze resultaten suggereren dat voorspellende strategieën die rekening houden met het gedrag van aangrenzende voertuigen, zowel de individuele als de collectieve verkeersveiligheid kunnen verbeteren. We vinden dat de ernst van ongevallen en de evolutie van het risico kritieke veiligheidsaspecten zijn die de effectiviteit van ontwijkende acties in verkeersconflicten onderscheiden. De functionaliteit van ADS kan van invloed zijn op het gedrag van aangrenzende voertuigen, omdat onze resultaten aantonen dat de reactieve afhandeling van snijmanoeuvres van met ADS uitgerust voertuigen het aantal rijstrookwisselingen nabij het einde van de invoegstrook kan verhogen. De empirische inzichten in dit proefschrift kunnen een heronderzoek van de rijstrookveranderende modellen en hun operationalisering in een simulatiekader faciliteren. De auto-industrie en de beleidsmakers van de overheid moeten rekening houden met het risico van generalisatie van de verkeersimpact van ADS, omdat dit sterk afhankelijk is van de functionaliteiten en ontwerpspecificaties van ADS. Om sluitende inzichten te verkrijgen, moet een ADS worden gesimuleerd door een nauwkeurig model en de veiligheidseffecten ervan moeten worden onderzocht in termen van zowel crashkans als ernst van de crash.

F.A. Mullakkal-Babu

Summary

Modelling Safety Impacts of Automated Driving Systems in Multi-Lane Traffic

The past three decades have witnessed the emergence of several automotive applications that take over the task of vehicle driving on a sustained basis. The most advanced class of such applications is known as Automated Driving Systems (ADSs). ADS can autonomously operate the vehicle on road stretches that fall under its operational design domain. Industry and governments expect that such systems will be technologically feasible shortly and the traffic will be mixed with system-driven and human-driven vehicles. Even though ADS-equipped vehicles will have an impact on traffic safety, there is no clarity on if they would enhance or detriment traffic safety and at what conditions and magnitude. A human and an ADS apply fundamentally different processes to acquire information, make decisions, and operate the vehicle. Therefore, our current insights on the relationship between driving behaviour and safety may not be sufficient to predict the possible impacts of ADS systems. Hence there is an urgent need to study the impacts of ADS functionalities and design factors on traffic safety.

Among the several alternatives, the simulation-based approach is a proactive and cost effective means to study the traffic safety impacts of ADS-equipped vehicles. In this approach, the traffic flow comprising of Human-driven Vehicles (HVs) and ADS-equipped vehicles are simulated at a high resolution. The generated vehicle trajectories are post-processed to extract metrics that quantify the safety of vehicle interactions. Conclusions on traffic safety are drawn by statistically analysing these metrics. This simulation-based safety assessment approach could provide design-feedback to automakers at an early stage of ADS development and insights to formulate deliberate policies and regulations related to ADS technology. The safety metrics and traffic simulation tools that are currently employed in safety studies are mostly targeted towards human-driven vehicles. In the context of mixed and multi-lane traffic, simulation-based approaches see multiple challenges, including accurately modelling vehicle dynamics and functionalities of ADS and in comprehensively quantifying the crash-risk.

This thesis addresses these challenges by developing a novel safety metric based on field theory and by creating a submicroscopic simulation framework that provides a more realistic depiction of the driving process which is also compatible with the known ADS architectures. Using the developed metric and tool, this thesis provides several case studies that demonstrate the potential of the simulation-based approach to differentiate between

ADS functionalities in terms of traffic safety and to identify their impact on traffic safety.

A new approach for safety assessment

Regarding the safety metric, Chapter 2 of this thesis reviews the existing safety metrics to identify their strengths and limitations to study mixed traffic. The review identifies that metrics based on field-theory possess several advantages compared to existing alternatives. Such a metric can describe the risk dynamics during two-dimensional vehicle encounters and can be numerically aggregated to combine the risk posed by multiple road-entities. This chapter also highlights that the results based on existing safety metrics are incomparable and incomplete as they are derived from a unique and partial definition of risk.

Chapter 3 provides a definition of driving-risk that is attributed to the subject vehicle, and a numerical estimate based on field theory. Any obstacle (neighbouring entity on the road) to the subject vehicle is treated as a finite scalar risk field: Probabilistic Driving Risk Field that is formulated in the predicted configuration space of the subject vehicle. This risk field is formulated as the product of two factors: expected crash energy (as an approximation of consequences) and the collision probability. The collision probability is numerically estimated based on the characteristic acceleration distribution of the road-entities that conflict with the subject. The crash probability is estimated at discrete future time-steps, and the number of the steps is determined based on the application requirement. To analyse the safety of on-road interactions, we employ the risk estimate with crash probability estimated at a single time-step. The analysis was performed on vehicle trajectories during three near-crash situations which were recorded from on-board cameras. It was seen that the PDRF based risk description qualitatively matches the event narration. Next, we applied the risk estimate with crash probability estimated in a series of time-steps in the context of a real-time vehicle navigation problem. The PDRF approach was employed to estimate the risk of four candidate manoeuvre plans in a complex traffic situation. It was seen that our approach could objectively identify the safest plan. Compared to the surrogate metrics of safety, which are mostly derived from a partial expression of risk, one of the advantages of the PDRF method as demonstrated in the case studies is that it combines the severity and probability aspects of risk, and therefore reduces the chances of underestimating driving risk. Moreover PRDF combines longitudinal and lateral interaction in a continuous metric.

New insights on manual lane changing

This thesis provides empirical insights into the manual lane-changing execution and its impacts on adjacent vehicles. Existing microscopic traffic models represent the lane-changing manoeuvre as a continuous and uninterrupted lateral movement of the vehicle from its original to the target lane. We term this representation as Continuous lane-changing (CLC). Chapter 4 of this thesis focusses on a less studied Fragmented lane-changing (FLC), where the lane-changer pauses its lateral movement during the manoeuvre. We characterise the FLC trajectory and identify its impacts on local traffic. We find that during the execution of an FLC, the lane-changer exhibits distinct kinematics and takes a longer duration to complete the lane-change. Besides, we identify a set of factors that might be related to the

decision-making process behind FLC: an average driver executes an FLC when the preceding and following vehicles in the target lane are slower, and when the follower in the target lane is closer than those observed at the onset of a CLC, and when there is a higher necessity to change lane such as during a mandatory lane change. Besides, we find that FLC induce a distinct microscopic effect on the follower in the target lane. Considering the empirical findings, we provide models for the lane change execution and impact, by revising and recalibrating existing models. The modelling results suggest that the accuracy of traffic flow models can be improved by deploying lane change execution and impact models that are specific to FLC and CLC.

An extended traffic simulation framework

Chapter 5 of this thesis presents a traffic simulation framework that can generate vehicle trajectories suitable for safety assessment at a higher level of detail than current microscopic traffic simulators. The framework is hybrid in structure, consisting of an explicit vehicle model and depicting the hierarchical decision and control structure of vehicle operation. The resulting trajectories account for yaw dynamics and provide additional variables such as vehicle heading and front wheel steering angle. The framework adopts a modular architecture to allow implementing and testing of independent models specific to various driving sub-tasks. The resulting framework consists of two coupled layers, an upper tactical level that generates manoeuvre plans; and a lower operational layer with explicit control module (steering and acceleration control) that operates in a closed loop with a bicycle model of vehicle dynamics. The simulation results demonstrate the power of the proposed framework to describe lateral manoeuvres such as curve negotiation, corrective steering, lane change abortion, and fragmented lane changing. Besides, the macroscopic traffic phenomena reproduced by the simulator, show that the properties of the featured driving subtask models are preserved in the framework. The framework shifts the modelling paradigm from discrete-lane-based traffic simulation to continuous-trajectory-based simulation.

Application of simulation-based safety assessment

In chapter 6, we apply the proposed safety assessment method and simulation tool for a mixed traffic case study. Here, we compare two generic longitudinal functionalities of ADS to handle a cut-in: reactive and predictive. This study reveals the distinctive effects of these functionalities on the cut-in manoeuvres of adjacent human-driven vehicles in terms of the safety and kinematic characteristics of the manoeuvre. We find that the presence of ADS equipped vehicles in traffic could alter the spatial distribution of lane change events in the vicinity of the merging section; and that the reactive ADS could increase the instances of unsuccessful lane changes. Results suggest that even a simple prediction scheme could significantly outperform reactive approaches in aspects such as temporal proximity to crash and expected crash severity, and PRDF representing driving risk (combining the two aspects). The negative safety impacts of reactive ADS-equipped vehicles become prominent at penetration $>10\%$. The predictive approach enables a relatively safer cut-in handling, with a marginal safety impact at increased penetrations. Besides, we find that risk dynamics is a crucial factor that differentiates the ADS functionalities. When a vehicle cuts-in ahead

of Reactive ADS, the risk peaks approximately halfway through the manoeuvre. Thereby, this work highlights the potential of simulation-based safety assessment approach to predict relevant dimensions of the safety impact by automation functionalities at an early stage of product development.

Implications and recommendations

This thesis proposes a new safety metric and a submicroscopic simulation framework for assessing the safety of traffic comprising of human-driven and system-driven vehicles. The impacts of ADS equipped vehicles depend on the inherent functionalities and operational strategies. Our results suggest that predictive strategies that account for the convenience of adjacent vehicles can improve both ego and collective traffic safety. We find that crash severity and risk evolution are critical safety aspects that differentiate the effectiveness of evasive actions in traffic conflicts. The functionality of ADS can impact the behaviour of adjacent vehicles since our results show that the reactive cut-in handling functionality of ADS-equipped vehicles may increase the number of lane changes near the downstream end of the acceleration lane. The empirical insights presented in this thesis can facilitate a re-examination of the lane-changing models and their operationalisation in a simulation framework. Automotive industry and the government policy makers must note the risk of generalising the traffic impacts of ADS, since it depends considerably on the functionalities and design specifications of ADS. In order to draw conclusive insights, an ADS should be simulated by precise model and its safety impacts should be investigated in terms of both crash probability and crash severity.

F.A. Mullakkal-Babu

About the Author

Freddy Antony Mullakkal Babu was born in Kerala, India on the 31st of October 1989. After finishing his high school in 2007, he pursued a bachelors degree at National Institute of Technology Calicut, where he studied Civil Engineering. He completed his B Tech in 2011.

He started his MTech in Civil Engineering at Indian Institute of Technology- Mumbai, where he specialised in Transportation Systems Engineering. He conducted his Master thesis research in Karlsruhe Institute of Technology, Germany. He obtained his M Tech in 2014. His thesis focused on microscopic modelling of motorcyclists in traffic stream with weak lane-discipline.

In May 2015, he joined the Transport and Planning group at Delft University of Technology for PhD studies. His research interests include traffic simulation, road safety, design and analysis of driving automation systems. He currently works as a simulation engineer at Siemens PLM software.



List of Publications

Peer-reviewed Journal and Conference Articles

- **Mullakkal-Babu, F. A.**, Wang, M., Farah, H., van Arem, B., & Happee, R. (2017). Comparative assessment of safety indicators for vehicle trajectories on highways. *Transportation Research Record*, 2659(1), 127-136.
- Stapel, J., **Mullakkal-Babu, F. A.**, & Happee, R. (2019). Automated driving reduces perceived workload, but monitoring causes higher cognitive load than manual driving. *Transportation research part F: traffic psychology and behaviour*, 60, 590-605.
- Farah, H., Bhusari, S., van Gent, P., **Mullakkal Babu, F.A.**, Morsink, P., Happee, R., & van Arem, B. An Empirical Analysis to Assess the Operational Design Domain of Lane Keeping System Equipped Vehicles Combining Objective and Subjective Risk Measures. *IEEE Transactions on Intelligent Transportation Systems*

Journal articles under review

- **Mullakkal-Babu, F. A.**, Wang, M., van Arem, B., Shyrokau, B., & Happee, R. (under review) A hybrid submicroscopic-/microscopic traffic flow simulation framework
- **Mullakkal-Babu, F. A.**, Wang, M., van Arem, B., & Happee, R. (under review) Probabilistic field approach for motorway driving risk assessment
- **Mullakkal-Babu, F. A.**, Wang, M., van Arem, B., & Happee, R. (under review) Empirics and models of fragmented lane changes
- **Mullakkal-Babu, F. A.**, Wang, M., van Arem, B., & Happee, R. (under review) Comparative safety assessment of automated driving strategies at highway merges in mixed traffic

Conference contributions

- **Mullakkal-Babu, F. A.**, Wang, M., van Arem, B., & Happee, R. (2016). Design and analysis of full range adaptive cruise control with integrated collision avoidance strategy. In *2016 IEEE 19th International Conference on Intelligent Transportation Systems (ITSC)* (pp. 308-315). IEEE.
- **Mullakkal-Babu, F. A.**, Wang, M., Farah, H., van Arem, B., & Happee, R. Comparative assessment of safety indicators for vehicle trajectories on highways. *Proceedings of the 96th Transportation Research Board Annual Meeting*, January 2017, Washington DC, USA
- **Mullakkal-Babu F. A.**, Wang, M., van Arem, B., & Happee, R. Probabilistic Field Approach for Highway Driving Risk Assessment in Mixed Traffic with Conventional and Automated Vehicles *Poster at Automated Vehicle Symposium*, July 2017, San Francisco, USA
- **Mullakkal-Babu F. A.**, Wang, M., van Arem, B., & Happee, R. Probabilistic field approach for driving risk assessment in mixed highway traffic. *Presented at Road Safety & Simulation Conference*, October 2017, Hague, The Netherlands

- **Mullakkal-Babu F. A.**, Wang, M., van Arem, B., & Happee, R. Sub-microscopic framework to model mixed highway traffic- *Presented at 2nd Symposium on Management of Future Motorway and Urban Traffic Systems*, June 2018, Ispra, Italy.
- **Mullakkal-Babu, F. A.**, Wang, M., van Arem, B., & Happee, R. A hybrid submicroscopic-/microscopic traffic flow simulation framework. *Proceedings of the 98th Transportation Research Board Annual Meeting*, January 2019, Washington DC, USA
- **Mullakkal-Babu, F. A.**, Vortisch, P., & Mathew, T. V. (2014). Modelling of motorcycle movements in mixed traffic conditions. In 94th Annual Meeting Transportation Research Board, Washington, DC.

TRAIL Thesis Series

The following list contains the most recent dissertations in the TRAIL Thesis Series. For a complete overview of more than 250 titles see the TRAIL website: www.rsTRAIL.nl. The TRAIL Thesis Series is a series of the Netherlands TRAIL Research School on transport, infrastructure and logistics.

Mullakkal-Babu, F.A., *Modelling Safety Impacts of Automated Driving Systems in Multi-Lane Traffic*, T2020/6, March 2020, TRAIL Thesis Series, the Netherlands

Krishnakumari, P.K., *Multiscale Pattern Recognition of Transport Network Dynamics and its Applications: A birds eye view on transport*, T2020/5, February 2020, TRAIL Thesis Series, the Netherlands

Yap, M.D., *Measuring, Predicting and Controlling Disruption Impacts for Urban Public Transport*, T2020/3, February 2020, TRAIL Thesis Series, the Netherlands

Luo, D., *Data-driven Analysis and Modeling of Passenger Flows and Service Networks for Public Transport Systems*, T2020/2, February 2020, TRAIL Thesis Series, the Netherlands

Erp, P.B.C. van, *Relative Flow Data: New opportunities for traffic state estimation*, T2020/1, February 2020, TRAIL Thesis Series, the Netherlands

Zhu, Y., *Passenger-Oriented Timetable Rescheduling in Railway Disruption Management*, T2019/16, December 2019, TRAIL Thesis Series, the Netherlands

Chen, L., *Cooperative Multi-Vessel Systems for Waterborne Transport*, T2019/15, November 2019, TRAIL Thesis Series, the Netherlands

Kerkman, K.E., *Spatial Dependence in Travel Demand Models: Causes, implications, and solutions*, T2019/14, October 2019, TRAIL Thesis Series, the Netherlands

Liang, X., *Planning and Operation of Automated Taxi Systems*, T2019/13, September 2019, TRAIL Thesis Series, the Netherlands

Ton, D., *Unravelling Mode and Route Choice Behaviour of Active Mode Users*, T2019/12, September 2019, TRAIL Thesis Series, the Netherlands

Shu, Y., *Vessel Route Choice Model and Operational Model Based on Optimal Control*, T2019/11, September 2019, TRAIL Thesis Series, the Netherlands

Luan, X., *Traffic Management Optimization of Railway Networks*, T2019/10, July 2019,

TRAIL Thesis Series, the Netherlands

Hu, Q., *Container Transport inside the Port Area and to the Hinterland*, T2019/9, July 2019, TRAIL Thesis Series, the Netherlands

Andani, I.G.A., *Toll Roads in Indonesia: transport system, accessibility, spatial and equity impacts*, T2019/8, June 2019, TRAIL Thesis Series, the Netherlands

Ma, W., *Sustainability of Deep Sea Mining Transport Plans*, T2019/7, June 2019, TRAIL Thesis Series, the Netherlands

Alemi, A., *Railway Wheel Defect Identification*, T2019/6, January 2019, TRAIL Thesis Series, the Netherlands

Liao, F., *Consumers, Business Models and Electric Vehicles*, T2019/5, May 2019, TRAIL Thesis Series, the Netherlands

Tamminga, G., *A Novel Design of the Transport Infrastructure for Traffic Simulation Models*, T2019/4, March 2019, TRAIL Thesis Series, the Netherlands

Lin, X., *Controlled Perishable Goods Logistics: Real-time coordination for fresher products*, T2019/3, January 2019, TRAIL Thesis Series, the Netherlands

Dafnomilis, I., *Green Bulk Terminals: A strategic level approach to solid biomass terminal design*, T2019/2, January 2019, TRAIL Thesis Series, the Netherlands

Feng, Fan, *Information Integration and Intelligent Control of Port Logistics System*, T2019/1, January 2019, TRAIL Thesis Series, the Netherlands

Beinum, A.S. van, *Turbulence in Traffic at Motorway Ramps and its Impact on Traffic Operations and Safety*, T2018/12, December 2018, TRAIL Thesis Series, the Netherlands

Bellsol Olba, X., *Assessment of Capacity and Risk: A Framework for Vessel Traffic in Ports*, T2018/11, December 2018, TRAIL Thesis Series, the Netherlands

Knapper, A.S., *The Effects of using Mobile Phones and Navigation Systems during Driving*, T2018/10, December 2018, TRAIL Thesis Series, the Netherlands

Varotto, S.F., *Driver Behaviour during Control Transitions between Adaptive Cruise Control and Manual Driving: empirics and models*, T2018/9, December 2018, TRAIL Thesis Series, the Netherlands

Stelling-Konczak, A., *Cycling Safe and Sound*, T2018/8, November 2018, TRAIL Thesis Series, the Netherlands

Essen, van M.A., *The Potential of Social Routing Advice*, T2018/7, October 2018, TRAIL Thesis Series, the Netherlands

Su, Zhou, *Maintenance Optimization for Railway Infrastructure Networks*, T2018/6, September 2018, TRAIL Thesis Series, the Netherlands